



Novel technologies to study single-cell response to environmental stimuli

Volume 1 of 2

Submitted by **Ashley Andrew Smith** to the University of Exeter
as a thesis for the degree of
Doctor of Philosophy in Biological Sciences (SWBio)
In September 2019

This thesis is available for Library use on the understanding that it is copyright material and that no quotation from the thesis may be published without proper acknowledgement.

I certify that all material in this thesis which is not my own work has been identified and that no material has previously been submitted and approved for the award of a degree by this or any other University.

Signature:

Abstract

Antibiotic tolerant phenotypes, such as persister and viable but non culturable cells (VBNC), are known to be present in isogenic bacterial populations. These phenotypes are now recognised as an important factor in the recalcitrance of infections and the development of antibiotic resistance; which itself is currently a major global health crisis. However, despite their clinical importance, we still know little about the mechanisms behind their formation and the relationship between the two phenotypes. Due to the relatively low abundance of the two phenotypes within the population and, in the case of VBNC cells, their ability to remain dormant for extended periods of time, high throughput single cell approaches currently provide the best opportunities for investigating them; in particular microfluidics has emerged as an exciting platform for investigating phenotypic heterogeneity at the single cell level due to the control it allows of the extracellular environment.

Using antibiotic persistence as a proxy, we identify temporal windows in which a growing *E. coli* population exhibits significant changes in phenotypic heterogeneity and determine highly regulated genes and pathways at the population level. We then develop a high throughput microfluidic protocol, based on the pre-existing Mother Machine device, to investigate persister and VBNC cells before, during and after antibiotic exposure at the single cell level. We then developed the first fully automated image analysis pipeline that is capable of analysing Mother Machine images acquired in both bright field and phase contrast imaging modalities. The combination of our protocol and image analysis software allowed us to investigate the role of the previously identified genes in the formation of antibiotic persister and VBNC cells, where we identify potential biomarkers for these phenotypes before exposure to antibiotic. We then used the microfluidic set up to investigate the relationship between protein aggregation and antibiotic persister and VBNC cells. We find that protein aggregation can be correlated to the expression of exogenous proteins and that cells containing visible protein aggregates are, in turn, more likely to be persister or VBNC cells; providing further evidence that these phenotypes are not distinct and are instead part of one physiological continuum.

Acknowledgements

This thesis would not have been possible without the support and guidance of so many people. You have all been an integral part of the process which has shaped me, both as a scientist and as a person, and I will always be grateful to every one of you for your help, however big or small, throughout my time at the University of Exeter.

I would first like to thank my supervisor, Dr. Stefano Pagliara, who encouraged me to pursue my PhD after I spent my undergraduate project working with him. Not only is this thesis testament to the faith he had in me, but none of this research would have been possible without his guidance. Above all though, I have thoroughly enjoyed working with him over the last 5 years since we met and I now consider him a friend as well as a mentor. I will forever be in his debt.

I would also like to thank my secondary supervisor, Prof. Rick Titball, whose years of microbiological experience were invaluable, particular during the first year or two of my studies.

Although I only worked with Dr. Rosie Bamford for the first half of my PhD, her influence on this thesis and my time at Exeter can't be underestimated. She was the only other member of the Pagliara lab when I first started my PhD and as a result we spent a lot of time working together. She is an incredibly talented scientist and she helped me with all aspects of my research from the offset. However, perhaps most importantly, her brilliant sense of humour meant working with her was always enjoyable.

A major part of my PhD was the development of an automated image analysis program and none of this could have been achieved without the guidance of Dr. Jeremy Metz. He was incredibly patient throughout and I am so proud of what I managed to achieve with his support. In fact, this experience in particular has played a major role in deciding what I want to pursue in my future career, so for this I can't thank him enough.

As is the nature with scientific research, the Pagliara group has seen faces come and go and everyone who has been part of the team, regardless of how long for, has had an impact on me and the work reported in this thesis. However, there are a few people that deserve extra thanks. In no particular order:

Dr. Zehra Kahveci, joined the group as Rosie was leaving and although her research field was different to mine we spent a lot of time together and I feel lucky to call her my friend. I can't wait to visit her in Spain and hopefully some of our Spanish conversations (by that I mean her speaking and me replying "Sí"), come in handy!

I first met Agnes when she was doing a summer project, before she returned as a master's student and went on to become a laboratory technician. Not only does she have an incredible work ethic and an attention to detail that is second to none, but she is one of the nicest people I have ever met.

Since they joined the group within 4 months of each other, George, Erin and Liv have had a massive impact. Whether we are discussing politics or the entertaining forensic science report we've just marked, our lunch time chats are always fun, particularly when Liv catches up! On a serious note, they have all been extremely supportive both as friends and as fellow researchers. The last 2 years since they joined the lab have been perhaps the hardest of my whole PhD and without them I am not sure if I would have made it through, I honestly can't thank them enough! I can only hope I have in some way helped them as much as they have helped me and I wish them all the best of luck with the rest of their PhDs!

Outside of the Pagliara group, a big thank you needs to be said to the BBSRC SWBio DTP for their funding and training throughout the last 4 years. I've met some amazing people during my time with the DTP and some of my best memories are from times I spent with members of my cohort; from Pablo's infamous night in Cardiff to realising Gareth and I become an odd looking father and son duo when using face swap. There are too many people in the cohort to mention individually but you all know who you are and I've enjoyed spending

time with all of you over the last few years. A special mention though, to my fellow Exeter members of the intake; Connor, James and Gareth, without whom, I don't know if I would have even made it through the first year.

Obviously undertaking a PhD is a huge commitment and I couldn't have done it without the support of my family and friends.

I'll start with my girlfriend, Kimberley. Words can't do justice to how grateful I am to you for everything you have done for me over the last 4 years. Although we started living between parents houses, we took the step of getting our own house last year and after 6 months of hard work it was finally habitable! Here I am now, sat in that very house (getting incredibly frustrated whilst our newest addition, Flick, continues to put her tennis ball in the fireplace!!!) writing up my thesis! Although my PhD journey ends shortly, ours is still only just beginning and I can't wait to see where it goes.

My family have always been incredibly supportive and I wouldn't change them for the world. My Mum and Dave provided a roof over my head for the first 3 years of my PhD (and obviously a fair few more years prior to that) and then gave up a lot of their own time to help renovate our new house – although I am sure some of that was also to get me out of their hair!! My Dad and Fiona always had an open door and provided me with a bed and food slightly closer to the university when I had experiments with late finishes and early starts – this seems like something small but the difference it made was massive. Thank you all.

My Nan, Liz, has always been there for me and will ask how my PhD is going every time I see her, even if it was only the day before! It really is the little things that count, for instance when she planted some courgettes in our new vegetable patch as they were the easiest to maintain and she knew we were busy with everything else (although we have yet to find it in our hearts to tell her we don't really like courgettes)! My Grandad, Stuart who ensured that I would double check I'd prepared my lunch for the next day after he decided to eat my sandwiches for dinner one evening! Unfortunately, I lost both my grandparents

on my Dad's side, Anne and Robert, during my PhD studies, but I know they would both be extremely proud to see how far I have come.

One of the biggest thank yous has to go to my sister, Zoe. She is always one of the first people I speak to when I have exciting news or want advice and has always been there when I need her. How times have changed since she kicked me head first into a radiator (for once I didn't deserve it!). She really is the best sister anyone could ask for and although I can still be her annoying big brother at times, I really do appreciate everything she's done for me.

Auntie Tina, Uncle Neville, Joley, Olivia all deserve a special thank you as well, even it is for simply making me laugh at family gatherings, helping with our house or going for days out watching some random 13th tier football team.

I would also like to thank Kimberley's mum, Sheena, for providing us with a roof over our heads, particularly when we were renovating our own house. I know we weren't the easiest to live with but we couldn't have done it without you.

There are many other people that deserve a thank you, far too many to mention individually, but you all know who you are.

Contents

Please note: As the papers for chapters 2, 3 and 4 are included in their published format, the numbering and referencing within them will not align with the rest of the thesis.

ABSTRACT	1
ACKNOWLEDGEMENTS	2
CONTENTS	6
CONTRIBUTION TO PAPERS STATEMENT	8
CHAPTER 1: INTRODUCTION	10
1.1 <i>Phenotypic heterogeneity</i>	10
1.2 <i>Antibiotic persister and VBNC cells</i>	14
1.2.1 Defining antibiotic persister and VBNC cells	14
1.2.2 Persister and VBNC cells and their role in the recalcitrance of infections	17
1.2.3 Antibiotic persistence and cellular stress	17
1.2.3.1 Metabolic stress	18
1.2.3.2 Extrinsic cellular stress.....	18
1.2.4 Antibiotic persistence in biofilms	19
1.2.5 Potential mechanisms of antibiotic persistence.....	19
1.2.6 Growth stage dependence of antibiotic persistence.....	20
1.2.7 Viable but non-culturable cells and the relationship with persistence.....	22
1.3 <i>Single cell analysis for investigating population heterogeneity</i>	23
1.3.1 The need for single cell analysis	23
1.3.2 Microfluidics for single cell analysis.....	24
1.3.3 The microfluidic “Mother Machine”	27
1.3.4 Investigating antibiotic persistence with microfluidics.....	28
1.4 <i>Current image analysis platforms</i>	31
1.5 <i>Gaps in the knowledge</i>	33
CHAPTER 2: THE CULTURE ENVIRONMENT INFLUENCES BOTH GENE REGULATION AND PHENOTYPIC HETEROGENEITY IN ESCHERICHIA COLI	36
2.1 <i>Introduction</i>	36
2.2 <i>Supplementary material</i>	52
2.3 <i>Conclusion</i>	62
CHAPTER 3: INVESTIGATING THE PHYSIOLOGY OF VIABLE BUT NON-CULTURABLE BACTERIA BY MICROFLUIDICS AND TIME-LAPSE MICROSCOPY	64
3.1 <i>Introduction</i>	64
3.2 <i>Supplementary materials</i>	79
3.3 <i>Conclusion</i>	86
CHAPTER 4: MMHELPER: AN AUTOMATED FRAMEWORK FOR THE ANALYSIS OF MICROSCOPY IMAGES ACQUIRED WITH THE MOTHER MACHINE.....	89
4.1 <i>Introduction</i>	89
4.2 <i>Supplementary material</i>	104
4.3 <i>Conclusion</i>	116
CHAPTER 5: HETEROLOGOUS PROTEIN EXPRESSION FAVOURS THE FORMATION OF INCLUSION BODIES IN PERSISTENT AND SLEEPER ESCHERICHIA COLI	118
5.1 <i>Introduction</i>	118

5.2 Manuscript.....	121
5.3 Supplementary figures.....	142
5.4 Conclusion.....	146
CHAPTER 6: CONCLUSIONS AND OUTLOOK.....	148
6.1 Population level transcriptome and the need for single cell analysis.....	148
6.2 The dormancy continuum and cellular ageing	149
6.3 Identification of potential biomarkers.....	150
6.4 Adaptability of the protocol.....	152
6.4.1 Potential for investigating cellular pH	152
6.5 Future development of the protocol and microfluidic setup	153
6.6 Future development of MMHelper	154
6.7 Concluding remarks.....	155
BIBLIOGRAPHY.....	157

Contribution to papers statement

Chapter two

Chapter two contains a paper entitled: "*The culture environment influences both gene regulation and phenotypic heterogeneity in Escherichia coli*" that was published in *Frontiers in Microbiology* in 2018.

For this paper I:

- Performed the CFU assays that provided us with the persister fractions throughout the different phases of growth.
- Performed the RNA extractions for all but two of the time points.
- Performed the transcriptomic analysis (i.e. KEGG) once we received the read numbers back from the sequencing department.
- Wrote the full first version of the manuscript and was responsible for editing future iterations upon reviewer feedback.

Chapter three

Chapter three contains a paper entitled: "*Investigating the physiology of viable but non-culturable bacteria by microfluidics and time-lapse microscopy*" that was published in *BMC Biology* in 2017.

For this paper I:

- Performed approximately 50 % of the experiments and analysed these accordingly.
- Was heavily involved in the development of the image analysis program that was used (see chapter four)
- Involved in the initial writing of the manuscript and figure production as well as future iterations

Chapter four

Chapter four contains a paper entitled: “*MMHelper: An automated framework for the analysis of microscopy images acquired with the mother machine*” that was published in Nature Scientific Reports in 2019.

For this paper I:

- Wrote and developed the code alongside Jeremy Metz.
- Wrote the full first version of the manuscript and produced the figures.
- Was responsible for editing future iterations upon reviewer feedback.

Chapter five

Chapter five contains a paper entitled: “*Heterologous protein expression favours the formation of inclusion bodies in persister and sleeper Escherichia coli*” that will soon be submitted for publication.

For this paper I:

- Performed approximately 50 % of the experiments
- Analysed all of the experiments
- Wrote the full first version of the manuscript and produced the figures.

Chapter 1: Introduction

1.1 Phenotypic heterogeneity

Phenotypic heterogeneity is the term used to describe the variation between cells within an isogenic population and has been observed across multiple domains of life. For instance, non-hereditary variation in protein expression is known to increase the rate of evolution in mammalian cancer cells¹ and virulence of the fungi *Candida glabrata*². Population heterogeneity has also been observed in a wide range of bacterial species, from motility in *S. putrefaciens*³, to biofilm formation in *B. subtilis*⁴ and Quorum sensing in *V. harveryi*⁵. Heterogeneity occurs as a result of the inherent random nature of biochemical reactions; for instance the likelihood of cellular components coming together to initiate processes, such as RNA polymerase and ribosomes in translation, is heavily influenced by the cellular concentration of the components. Two factors control this cellular concentration; the number of cellular components, such as ribosomes, and the size of the cell itself. In fact, in one study, researchers managed to reduce heterogeneity during the initiation of sporulation by genetically modifying the bacterium *Bacillus subtilis* to create a population with larger than normal cell size⁶. The size of individual cells can be affected by multiple factors, for instance asymmetrical bacterial division will result in old-pole and new-pole daughter cells having different levels of cellular components, with even small variations in cell size resulting in potentially significant differences in the two cells. A good example of this is efflux activity, for instance Bergmiller *et al.* showed that the multi drug efflux pump AcrB-TolC forms a ternary complex which becomes immobilised within the bacterial membrane and therefore undergoes biased partitioning, with the old-pole daughter cell retaining, on average, 58% of AcrB-TolC complexes⁷. Furthermore, Bergmiller *et al.* showed that the old-pole daughter cells had significantly lower levels of a fluorescent intercellular dye, Hoechst (H) 33342, as a result of their higher efflux activity⁷. They also showed that not only did the old-pole daughter cells have increased efflux activity, but they also had an increased growth rate in the presence of a bacteriostatic substrate; tetracycline⁷.

The difference in growth rate observed by Bergmiller, *et al.* was a result of heterogeneity providing a subpopulation with an advantage when the extracellular environment becomes unfavourable (in this case the presence of $\leq 0.75 \mu\text{g ml}^{-1}$ of tetracycline). However, heterogeneity in population growth rates has been observed in non-stressful conditions⁸. For example, older cells within a population were shown to have increased filamentation and reduced division rates by Wang *et al.*⁸. Similarly, work on cellular ageing has shown that as bacteria divide, the cell which retains the old cell pole have lower growth rates than the daughter cells who gain a new cell pole⁹. This has been observed regularly in studies of protein aggregation where, during growth, aggregates are localised at the cell poles and, therefore, are often retained in the old-pole daughter cell upon cell division^{9,10}. As a result, the toxic aggregates are concentrated within small subpopulations that are slower growing. Furthermore, by removing these aggregates from the majority of the population, the population can as a whole maintain a higher average growth rate¹¹⁻¹³. This is an example of where some of the population exhibit a phenotype which is non-optimal in favourable environments, but benefits the population as a whole. For instance, Nikolic *et al.* used fluorescent reporters of metabolic genes, such as the glucose specific transporter *ptsG* and *acs* which is co-transcribed with an acetate permease, to show that two subpopulations are present in a glucose rich environment; one which utilizes glucose and excretes acetate as a by-product and a second that uptakes and utilizes the acetate¹⁴.

Some of the best studied examples of cellular heterogeneity are in terms of cellular metabolism. Metabolism can be broken down into three sub-processes: taking up substrates from the extracellular environment (substrate uptake), breaking these down to basic building blocks (catabolism) and using these building blocks to construct macromolecules (anabolism)¹⁵. Given that these macromolecules are often components used for important cellular functions, heterogeneity in any of the previously mentioned sub-processes could result in the emergence of phenotypic diversity within the population¹⁵. As previously discussed, heterogeneity has been observed in glucose uptake in *Escherichia coli*¹⁴, however, it has also been observed in the N₂-fixing bacteria *Klebsiella oxytoca*¹⁶. Schreiber *et al.* found that heterogeneity in N₂-fixation increased as a result of transcriptional noise in the nitrogen fixing nitrogenase, *nifH*, when the

supply of NH_4 increased¹⁶. On a similar note, a study by Veening *et al.* showed only a small subpopulation of *Bacillus subtilis* express *aprE*, the gene encoding subtilisin E which degrades proteins outside of the cell, in nutrient limiting conditions¹⁷. Subtilisin E is secreted from the bacterium and breaks down extracellular proteins that can then be utilised by the whole population¹⁷; this being another example of a small portion of the population exhibiting a phenotype which is costly to themselves, but benefits the wider population.

Heterogeneity has often been discussed as a type of bet-hedging strategy within a population, whereby some of the population are able to rapidly adjust when the environment becomes unfavourable¹⁸⁻²¹. In fact, in normal conditions these subpopulations are not significant, but they are able to dominate the population behaviour when the extracellular environment changes²²; this is particularly obvious when we look at the population response to a nutrient shift^{16,19,23,24}. Acar *et al.* showed this by genetically modifying the galactose utilisation pathway of *Saccharomyces cerevisiae* to stochastically switch between “On” and “Off” at different rates²⁵. Interestingly, they found that when they grew the populations in fluctuating environments, for instance fluctuations in pH, temperature and nutrient availability, the fast switching phenotype grew faster than the slower switching phenotype²⁵. A similar study on the same organism by van Heerden *et al.* showed that, upon a nutrient shift, variation in metabolic flux within the glycolysis pathway resulted in the generation of two subpopulations with distinct growth phenotypes²⁶. Kotte *et al.* had similar findings in *E. coli*, whereby they observed the population responsively diversifying into growing and non-growing phenotypes depending on their level of metabolic flux when the nutrient source was shifted from glucose to gluconeogenic²³.

As previously mentioned, heterogeneity allows a population to rapidly adapt to fluctuating environments. Interestingly, Bódi *et al.* showed that population heterogeneity accelerates adaptive evolution in the face of extracellular stress by using a synthetically generated gene circuit that expressed an anti-fungal resistance gene with varying levels of heterogeneity²⁷. They found that strains with a bimodal distribution (more heterogeneity) due to a positive feedback loop survived better than those with a normal distribution (less heterogeneity) when exposed to an antifungal agent²⁷. However, what was perhaps more interesting,

was that both strains evolved to have more heterogeneity (bimodal distributions) but this evolution was particularly prominent in the strain which had an initial normal distribution²⁷. Furthermore, heterogeneity can be amplified or dampened if a feedback loop is present for the mechanism generating the phenotype. For example, negative feedback on gene regulation has been shown to reduce phenotypic heterogeneity²⁸, whereas positive feedback can increase heterogeneity by turning stochastic fluctuations into multiple phenotypes^{23,29}.

Throughout the above I have discussed how populations adapt over time to increase their heterogeneity and how this allows an isogenic population to rapidly adjust to fluctuating environments. A key example of this is phenotypic heterogeneity allowing a subpopulation to survive high concentrations of antibiotics; such as antibiotic persister or viable but non-culturable (VBNC) cells³⁰⁻³⁷. Importantly, increased exposure to otherwise lethal stresses can increase the likelihood of adaptive mutations^{27,38}; therefore persister and VBNC cells can provide a reservoir for the development of antibiotic resistant strains.

Table 1: A summary of the different sources of heterogeneity covered in 1.1, what they cause and how they may affect the formation of different phenotypes.

Source of heterogeneity	Causes and effects	Potential phenotypes
Cellular metabolism / nutrient utilisation	<ul style="list-style-type: none"> • Nutrient transitions have been shown to result in the formation of different phenotypes within bacteria, growing and non-growing, as a result of metabolic flux causing bistability in carbon metabolism. • Similarly, even in glucose (preferred carbon source) rich environments, some cells will utilise the acetate by-product of their kin. This will result in two growth phenotypes within the 	<ul style="list-style-type: none"> • Reduced growth rate / dormancy • Formation of antibiotic tolerant phenotypes

	<p>population, with the slower growing phenotype potentially acting as a bet-hedging strategy if the extracellular environment rapidly becomes unfavourable.</p>	
<p>Asymmetric cell division</p>	<ul style="list-style-type: none"> • Proteins can become immobilised in the bacterial membrane resulting in them being divided asymmetrically between daughter cells. In the case of efflux pumps, this can result in increased antibiotic survival. • As daughter cells will not be identical in size they will contain different levels of cellular components such as ribosomes and as a result, there will be inherent heterogeneity in biochemical reactions • The movement of protein aggregates is often restricted by the nucleoids, resulting in polar localisation. This means only one daughter cell will inherit the aggregate and have a reduced amino acid pool; triggering the stringent response and increased cellular dormancy/reduced growth rate. 	<ul style="list-style-type: none"> • Reduced growth rate / dormancy • Visible protein aggregates • Formation of antibiotic tolerant phenotypes

1.2 Antibiotic persister and VBNC cells

1.2.1 Defining antibiotic persister and VBNC cells

Antibiotic resistance is where a bacterium acquires a genetic mutation that allows it to continue growing and dividing in the presence of a given antibiotic³⁹. Antibiotic resistance is a major global health threat, particularly due to the emergence of multi-drug resistant (MDR) strains³⁹. MDR strains are emerging at a rate faster than ever, as a result of the over use of antibiotics, both in humans and in animals^{39,40}. Furthermore, the use of antibiotics is currently projected to continue, with estimations suggesting that its use in livestock may increase by up to 67 % over the next 10 years⁴⁰.

In comparison, persister and VBNC cells remain genetically identical to their susceptible kin but are able to survive exposure to otherwise lethal doses of antibiotic (Fig. 1). Although first discovered by Hobby *et al.* in 1942⁴¹, the term “persister” was first used to describe drug tolerant cells two years later by Bigger two years later when he observed that penicillin was often unable to fully sterilise a flask of *Staphylococcus aureus*⁴². However, recently interest in antibiotic persister and VBNC cells has increased; in fact, such is the current levels of interest, that several leading experts in the field recently published a consensus statement in order to ensure the different phenotypes were being correctly defined⁴³. They discuss how several factors can be used to distinguish between resistance and persistence; 1) in persistence not all cells are killed at the same rate, 2) the progeny of persister cells remain susceptible to antibiotics, 3) the size of the persister population is not dependent on antibiotic concentration and 4) persister cells are unable to replicate whilst in the presence of antibiotics⁴³. They continue by discussing how tolerance and persistence are often interchangeable terms, with the difference being tolerance is a population level phenomenon, whereas persistence is an attribute that only affects a subpopulation⁴³. As a result, mechanisms that allow tolerant cells to survive antibiotics can be investigated with respect to both tolerance and persistence, unless such survival is a result of population heterogeneity, in which case it is limited to persistence⁴³. Interestingly, some cells are able to survive antibiotic treatment but remain dormant and can only resuscitate after a long and specific treatment^{36,44,45}. In fact, as a result of their increased dormancy, although they are still an example of antibiotic tolerant cells, these VBNC cells are considered separate from the persistence phenotype³⁶. As persister and VBNC cells are able survive in the presence of antibiotics for

extended periods of time, they have regularly been associated with the recalcitrance of chronic infections, such as cystic fibrosis^{33,46}, and proposed to be a stepping stone to antibiotic resistance³⁸.

Despite first being observed in bacterium^{41,42}, antibiotic persistence is not restricted to bacteria. LaFleur *et al.* observed multi drug persistence in biofilms of the major human pathogen *Candida albicans*⁴⁷. Furthermore, heterogeneity in metabolic activity and nutrient utilisation has been suggested to be involved in *C. albicans* persistence⁴⁸. Interestingly, in *C. albicans*, persistence has only been observed in biofilms and not in planktonic cultures^{47,48} however, they were discovered in both biofilms and planktonic cultures in the yeast *Saccharomyces cerevisiae*⁴⁹. LaCrue *et al.* reported a dormant state in the parasite *Plasmodium falciparum* that they propose contribute to the recurrence of infections⁵⁰. Drug tolerant persister cells have also been observed in human tumour cell lines^{51,52}. For example, Sharma *et al.* found approximately 0.3 % of a population in a lung cancer derived cell line survived treatment with EGFR (epidermal growth factor receptor) inhibitors as a result of phenotypic heterogeneity within the population⁵².

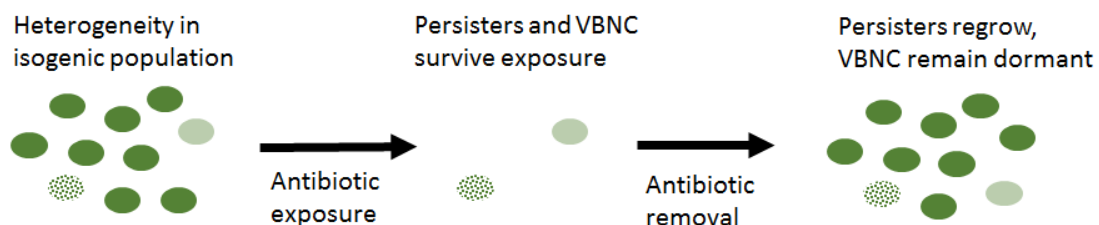


Figure 1. A summary of the difference between susceptible, persisters and VBNC cells. The population is isogenic both before and after exposure to antibiotics, however susceptible cells (solid green circles) are killed during antibiotic exposure, persister cells (pale green circles) survive and regrow upon removal of antibiotic removal to form a new, mainly susceptible, population and VBNC cells (dotted green circle) survive the exposure but remain in a dormant non culturable state after antibiotic removal. As a result, persisters and VBNC are currently only identifiable after exposure to antibiotics.

1.2.2 Persister and VBNC cells and their role in the recalcitrance of infections

As previously mentioned, antibiotic persistence has been linked to recalcitrance of chronic infections and proposed to act as a stepping stone in the development of antibiotic resistance^{38,46}. In *Pseudomonas aeruginosa* isolates taken from patients, such as those suffering with cystic fibrosis, persister levels are up to 100 fold higher, indicating that persister cells are mainly responsible for our inability to treat these chronic infections⁵³. There are multiple factors involved in the development of antibiotic resistance; one is the initial likelihood the mutation occurs and the other is the likelihood of the mutation surviving antibiotic exposure³⁸. Therefore, given that persister cells can survive in the presence of antibiotics for long periods of time before resuscitating, they provide a reservoir for the establishment of resistance. However, increasing the reservoir of viable cells during treatment is not the only way in which persistence has been proposed to increase the development of resistance⁵⁴. Persistence has also been associated with the stress response pathway^{55,56}, as well as pathways which have been linked to promoting both adaptive mutations and horizontal gene transfer⁵⁷. Windels, *et al.* found a positive correlation between antibiotic persistence and the probability cells became resistant in *E. coli*⁵⁴. Furthermore, they used a strain that had evolved to exhibit a higher level of persistence than wild type *E. coli*, *hipA7*, and found a higher mutation rate compared to their low persister, *oppB**, counterparts, suggesting that mutations are more likely to occur in persister cells⁵⁴. Petrosino *et al.* showed that nutrient stress can increase mutations in *ampD*, an enzyme involved in the regulation of β -lactamase production, and result in an increase in resistance to β -lactams⁵⁸. Furthermore, they found the mutagenic response was controlled by the general stress response controller, RpoS⁵⁸. Similarly, when using strains lacking in a stress response, Nguyen *et al.* found a decrease in persistence in *P. aeruginosa* biofilms compared to the wild type strains⁵⁹. Interestingly, they also found that when they exposed the strain to conditions promoting adaptive resistance it was unable to generate ofloxacin resistant mutants⁵⁹.

1.2.3 Antibiotic persistence and cellular stress

1.2.3.1 Metabolic stress

Stress has also been shown to have a direct effect on antibiotic persistence, with populations that are pre-stressed exhibiting higher levels of persister cells^{60,61}. Metabolic stress as a result of nutrient shifts is perhaps the most well studied example of this^{56,60,62,63}. By growing *E. coli* in minimal media supplemented with either a single carbon source or a combination of carbon sources, Amato *et al.* were able to show that the populations grown in the presence of multiple different carbon sources had an approximately 50 fold increase in antibiotic persistence as a result of the diauxic shift⁶³. Using autotrophic mutants of *E. coli*, Bernier *et al.* were able to starve biofilms of individual amino acids and found that they contained significantly more persister cells in response to treatment with ofloxacin⁶⁴. Similarly, Fung *et al.* performed survival assays on *E. coli* grown in different combinations of nutrients and amino acids⁶⁵. Interestingly, they found 8 combinations, all of which lacked glucose and some amino acids, in which the populations showed increased persistence to ampicillin, ofloxacin and gentamicin, respectively⁶⁵.

1.2.3.2 Extrinsic cellular stress

Metabolic stress, however, isn't the only stress that can increase levels of antibiotic persistence; oxidative stress, heat shock, DNA damaging agents and pre-treatment with antibiotics have also shown to have an effect^{35,55,61,66,67}. Working with *Streptococcus mutans*, a common contributor to tooth decay, Leung and Lévesque showed that they could increase ofloxacin persister levels by pre-stressing the population through acid treatment, oxidative stress, amino acid starvation and heat shock, respectively⁵⁵. Wu *et al.* induced oxidative stress by pre-treating *E. coli* with paraquat and found it significantly increased persister levels in response to the fluoroquinolone ofloxacin⁶¹. Interestingly, by using a Δ *acrB* strain, they also identified that this was a result of the superoxidise response gene, *SoxRS*, inducing the expression of the multi drug efflux pump AcrAB-TolC⁶¹. A similar phenomenon was observed in exponential phase *Pseudomonas aeruginosa*, which typically has lower levels of persisters than *E. coli*, where paraquat again increased persister levels⁶⁷. Exposure to sub-minimum inhibitory concentration (MIC) antibiotic levels, the lowest concentration of antibiotic required to prevent bacterial growth, can increase the size of the persister population in response to a future higher antibiotic

concentration. For instance, pre-treatment of an *E. coli* culture with 0.1 $\mu\text{g ml}^{-1}$ of ciprofloxacin for 3h increased the persister fraction by more than 10 fold⁶⁶.

1.2.4 Antibiotic persistence in biofilms

Biofilms are often a source of antibiotic persistence^{59,64}. Biofilms form physical barriers to parts of the body and although the majority of bacterium within the biofilm itself are highly susceptible to antibiotics⁶⁸, a small proportion of cells survive⁶⁹⁻⁷¹. Furthermore, the exposure to antibiotics within the biofilm can vary, with some bacterium experiencing sub-MIC concentrations, as a result of variations in tissue location and biofilm size⁷². Adding to this, although persistence is not a genetic trait, there is evidence to show that adaptive evolution, through continued exposure to antibiotics, can result in increased persistence⁴⁶. For instance, the previously mentioned *Pseudomonas aeruginosa* isolates that had up to 100 fold higher levels of persister cells⁵³. Similarly, through periodic treatment with antibiotics, Moyed and Bertrand identified a mutant strain that had the same MIC as the wild-type strain but had increased levels of persisters, which they found this to be a result of the *HipA* (*high persistence*) allele⁷³. This adaptive evolution is not limited to bacteria however, LaFleur *et al.* tested 150 isolates of *Candida* species from cancer patients who had received daily treatment⁷⁴. Interestingly, they found isolates from patients that had been receiving prolonged treatment had higher persister levels of the fungal pathogen⁷⁴.

1.2.5 Potential mechanisms of antibiotic persistence

Despite the obvious importance of persister cells to health and the recalcitrance of infections, a single conclusive mechanism for antibiotic persistence has yet to be identified, however several different mechanisms have been proposed to play a role. For example, the previously mentioned high persistence (*hip*) strains suggested that persistence was related to toxin/antitoxin (TA) modules which act as a maintenance mechanism³². Toxins inhibit important cellular functions but plasmid encoded antitoxins act as a down regulator by binding them in an inactive complex³². If a daughter cell fails to receive the plasmid encoding the antitoxin, then the toxin remains active and the bacterium is killed or further replication is prevented³². In a previously discussed study where the authors found ciprofloxacin to induce persister formation, they also found that

the deletion of the TA module *tisAB* significantly reduced persister formation, but the phenotype could be recovered with complementation⁶⁶. Similarly, overexpression of the toxins *MazEF* and *RelBE* in *S. mutans*, resulted in an increase in persistence relative to wild type⁵⁵. Keren, *et al.* treated an *E. coli* population with ampicillin in order to lyse all susceptible cells, they then pelleted the surviving cells and performed transcriptional analysis⁷⁵. Interestingly, they found chromosomal TA module proteins RelBE, MazEF, and DinJ/YafQ were all overexpressed however, it is important to note that they still observed susceptible unlysed cells which may contaminate these readings⁷⁵. Furthermore, their method of isolation required antibiotic treatment which is likely to affect the transcriptome as well as being performed on a *hip* strain of *E. coli*. To try and negate the issue of using antibiotics to isolate the persister population, Shah *et al.* used a fluorescent reporter to sort an *E. coli* population based on their level of dormancy³⁴. Using DNA microarrays, they found the most induced gene in the dormant cells to be the toxin gene *mqsR*³⁴ however, how accurately this reflects the persister phenotype is questionable as less than 40 % of this population were persisters.

TA modules aren't the only genes associated with increased persistence⁷⁶; Shan *et al.* developed a transposon sequencing experiment that identified 142 genes/promoter regions whose deletions resulted in a 5 fold or higher change in persister levels to gentamicin treatment from that of the wild type (WT) in stationary phase cultures. Although some of these genes coded for TA modules, there was also 39 genes involved in flagella synthesis and 13 genes related to amino acid biosynthesis⁵³. Again, indicating the lack of a distinct mechanism that results in persister formation. A potential reason could have been attributed to the variety in identification methods of these persister genes; from different types of drugs and different strains of organisms, to different organisms' altogether. Wu *et al.* sought to rectify this by ranking the response of candidate genes to multiple drugs within a single organism⁷⁶. Their results showed that persistence often still varied depending on the stage of growth and the drug used⁷⁶. Their results were not unusual, growth phase dependent persistence has been observed in multiple organisms to multiple drugs⁷⁷⁻⁷⁹.

1.2.6 Growth stage dependence of antibiotic persistence

The growth stage dependence can be linked to the metabolic activity of bacteria. As previously discussed, metabolic heterogeneity within a bacterial population can generate multiple phenotypes, particularly in terms of dormancy^{44,80}. Additionally, external stressors, such as metabolism, heat shock and oxidative stress can induce the bacterial stringent response⁸¹. The effector molecule of the stringent response is the “alarmone” ppGpp, which in turn stimulates the production of RpoS⁸¹. Similarly, overexpression of Obg, a conserved GTPase which measures the cellular energy status to control entry into dormant spores in *Bacillus subtilis*, increased persistence in response to ofloxacin in both *P. aeruginosa* and *E. coli*, with the latter being increased 54 fold relative to wild type²⁰. However, this increase in persistence was lost in a $\Delta relA \Delta spoT$ mutant, indicating the effect of Obg was dependent on ppGpp²⁰. Amato, *et al.* used the $\Delta relA \Delta spoT$ mutant to investigate nutrient transitions in planktonic cultures and found that upon glucose exhaustion persister levels increased 20 fold in the wild type strain but only 1.8 fold in the mutant, further suggesting a role for ppGpp⁶³. Similarly, Radzikowski *et al.* switched *E. coli* from growth on glucose to fumarate and found that a slow/non-growing subpopulation arose which was antibiotic tolerant and accumulated higher levels of ppGpp⁵⁶.

Aside from ppGpp, other signalling molecules and quorum sensing have been associated with antibiotic persistence. In the *P. aeruginosa* strain PAO1, Möker *et al.* found exposure to acyl-homoserine lactone, a quorum sensing related signalling molecule, significantly increased persisters⁶⁷. Leung and Lévesque showed quorum sensing also affects persistence in *S. mutans*, albeit using a slightly different approach⁵⁵. They looked at the expression of *comC*, a CSP pheromone gene, and found it to be upregulated in response to multiple environmental stressors⁵⁵. Furthermore, they showed that a mutant strain, $\Delta comE$, which couldn't respond to the CSP pheromone, no longer produced an increase number of persisters in response to environmental stress⁵⁵. Another signalling molecule which is produced by a variety of gram negative and gram positive bacteria is indole^{35,82-85}. Indole is produced during the breakdown of tryptophan by tryptophanase^{86,87} and has been shown to control many bacterial functions, such as spore and biofilm formation⁸². Furthermore, during the transition from exponential to stationary phase growth in *E. coli*, a substantial

intracellular indole “pulse” has been observed and proposed to inhibit growth^{84,85}. Interestingly, despite a general consensus amongst researchers that indole appears to play a role in persistence, whether it promotes or reduces it is still disputed^{35,83,88,89}. For example, Hu *et al.* reported that *E. coli* persister fractions in response to ampicillin decreased when cells were pre-incubated with increasing concentrations of indole⁸⁸ however, this doesn't take VBNC bacterium into consideration. In comparison, when Vega *et al.* incubated *E. coli* with indole, they reported an increase in survival³⁵, but they used a shorter incubation time. Interestingly, in a later study, Vega *et al.* found that a co-culture of *salmonella typhimurium*, which is unable to produce indole, with wild type *E. coli* produced higher levels of persister cells compared to when it was co-cultured with a $\Delta tnaA$ *E. coli* strain which also didn't produce indole⁸³.

1.2.7 Viable but non-culturable cells and the relationship with persistence

So far I have mainly focused on persister cells however VBNC cells can also be considered an antibiotic tolerant phenotype^{36,44}. Like persisters, they have been linked to the recalcitrance of infections and they constitute a major threat to human health, in fact they have been observed in 51 human pathogens⁹⁰. Despite this, most of the knowledge about persister and VBNC cells is focused on that of persister cells with even less known about VBNC. Although the two were originally thought to be two different distinct tolerant phenotypes, there is increasing evidence to suggest they are part of one continuum³⁶. For example, I previously discussed the role of the stringent response, particularly *relA* and ppGpp, in persistence and both of these have also been linked to the VBNC state. For instance, Mishra *et al.* incubated *Vibrio cholerae* at 4 °C for 23 days in order to induce the VBNC state and using qPCR found *relA* to be upregulated by over 60 fold⁹¹. In another study, cells were able to enter the VBNC state more efficiently than wild type cells in strains overproducing ppGpp and less efficiently in strains unable to produce ppGpp⁹². Similarly, the VBNC state has also been associated with TA modules. For example, Korch and Hill showed that although they were unable to grow some cells after long term induction of the *hipA* toxin, the majority of these cells remained viable according to a LIVE/DEAD stain, suggesting induction of the VBNC state⁹³. In an interesting study by Ayrapetyan *et al.*, the group that first proposed persister and VBNC states to be part of a continuum³⁶, they found that in *Vibrio vulnificus* a persister

population was able to enter the VBNC faster than a wild type logarithmic population³⁷. Furthermore, they also found that activation with human serum was able to induce both persister and VBNC states³⁷. Pu *et al.* hypothesised that if the VBNC state is simply a more dormant state along the continuum than persisters, then increased exposure to factors, such as nutrient starvation, that induce dormancy would result in more of the population transitioning from the persister to VBNC state⁹⁴. By leaving an *E. coli* population in stationary phase for a prolonged period of time, they observed that the number of VBNC bacteria increased with time⁹⁴. Adding to this, the persister fraction initially increased before beginning to decrease, suggesting they became VBNC⁹⁴.

Despite all of the above, the mechanisms behind the formation of persister and particularly VBNC cells and the potential continuum that defines them, are still not well understood. As discussed above, the majority of research in to the phenotypes is at the population level using traditional microbiological methods, such as CFU, but these methods often fail to characterise individual subpopulations and, in fact, in the case of VBNC, fail to detect them altogether. Therefore, to help further characterise the persister and VBNC phenotypes, further research should be carried out with single cell resolution.

1.3 Single cell analysis for investigating population heterogeneity

1.3.1 The need for single cell analysis

As previously discussed, multiple sub phenotypes can exist within bacterial populations, for instance in terms of growth rate, metabolic activity and resistance to stress^{7,14,23,24,72,95,96}. These sub phenotypes arise as a result of variations at the single cell level⁹⁶⁻⁹⁸. Therefore, many traditional microbiological assays, such as colony forming units (CFU), are unable to effectively determine the mechanisms behind their appearance. For example, if a population were to be split into two phenotypes in a bimodal distribution, bulk analysis of the entire population would result in an average value and would incorrectly identify the whole population to have one intermediate phenotype²².

Cell to cell heterogeneity exists within microbial populations, but research has shown that less than a few percent of a population is more than two fold

different than the population average²². However, as discussed earlier, when the environmental conditions allow it, these small subpopulations are able to dominate population behaviour²². In these circumstances, the population behaviour can be interpreted incorrectly if studies are performed at the population level (Fig. 2). This is particularly important, when considering heterogeneity in response to antibiotics, such as the ability of a persister cell to survive antibiotic treatment and its role in recalcitrance of infections^{33,45,46,72}. In order to collect single cell measurements, researchers have performed single-cell microscopy in order to study cellular growth and infection⁹⁹. Similarly, single cell measurements, such as cell size and fluorescence intensity, can be acquired using flow cytometry^{14,100}. However, although both of these techniques allow researchers to acquire measurements on single cells, they don't allow the control and manipulation of the extracellular environment so are not suitable for investigating temporal changes, for instance population heterogeneity in response to extracellular stimuli.

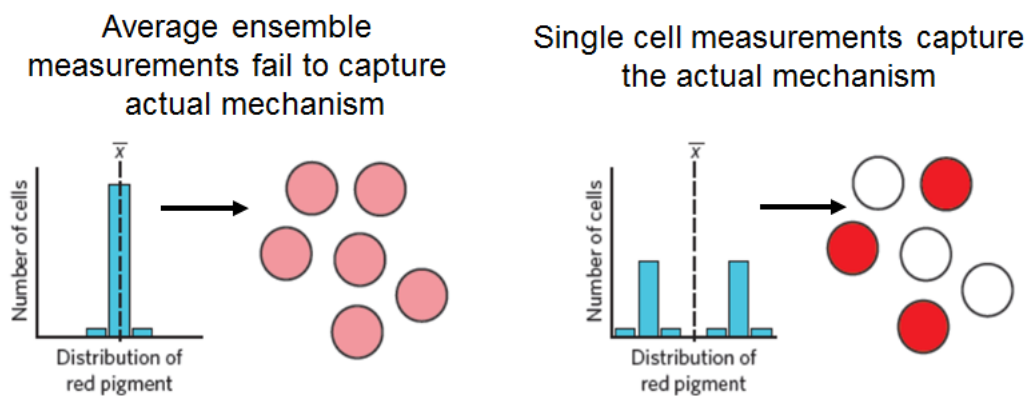


Figure 2. The importance of single cell analysis for identifying population heterogeneity. The above figure, taken from *Lidstrom and Konopka 2010*²², really nicely illustrates how ensemble measurements (such as CFU assays or plate reader analysis of fluorescence) will result in an average population level response, whereas single cell approaches (such as microfluidic assays and flow cytometry) can help illicit the true distribution of phenotypes within a population

1.3.2 Microfluidics for single cell analysis

An important technological advance which has been adopted by researchers in order to investigate cellular heterogeneity in microbial populations is microfluidics^{7,30,101–105}. Microfluidics allows the control and manipulation of fluids

within devices that are purpose built with submillimetre precision¹⁰⁶. The introduction of polydimethylsiloxane (PDMS) by Duffy *et al.* in 1998, as a compound that could be used to rapidly fabricate microfluidic devices was a major contributing factor to the growth of the microfluidic field¹⁰⁷. Adding to this, the relatively low cost of PDMS and speed of fabrication means microfluidics is more accessible than ever and is being utilised for research into a wide variety of biological functions across all domains of life^{103,104,106}.

In eukaryotes, microfluidics has been used to investigate the physical properties. For instance, Pagliara *et al.* showed pluripotent embryonic stem cells had auxetic nuclei, meaning they contracted when compressed, when they experienced extracellular pressure as a result of being forced through a microfluidic channel that was slightly narrower than their cellular diameter; these auxetic properties could be involved in converting mechanical stimuli to a cellular response, for instance deciding how the stem cell differentiates¹⁰⁸. Similarly, Irimia and Toner confined cancer cell lines within a microfluidic device and found all the cells migrated in the same direction even in the absence of a chemical gradient¹⁰⁹. Furthermore, they found when they treated the cells with drugs which target microtubules that the speed at which this migration occurred was drastically reduced¹⁰⁹. In bacteria Yu *et al.* used a microfluidic device to compress single *E. coli* cells; by measuring the cells shortly after compression and before they can respond biochemically, it allowed them to focus on the physical properties¹¹⁰. Using fluorescently tagged loci, they used their approach to show the importance of nucleoid organisation and DNA elasticity in loci subdiffusion¹¹⁰. Nobs and Maerkl developed a microfluidic platform which allowed them to characterise the growth and division rates in the yeast *Schyzosaccharomyces pombe*, during both a steady temperature and during temperature changes¹⁰⁹. Furthermore, by performing single cell analysis, they were able to correlate the growth and division rates to the cells lineage¹⁰⁹. In another study, fluorescence microscopy was utilised within a microfluidic device in order to perform high throughput screening to identify 10 out of over 50 000 compounds which improved the efficacy of amphotericin B by over 30 % when treating *C. albicans*¹¹¹. In bacteria, microfluidics has been used to investigate multiple cellular functions, such as growth rate, chemotaxis^{103,112}, gene expression¹⁰⁵ and response to antibiotics³⁰.

Due to its ability to allow tight control and manipulation of the extracellular environment, microfluidics has proved an extremely useful tool for studying bacterial chemotaxis. Park *et al.*, designed a maze like microfluidic device and used it to show for the first time that both *E. coli* and *Vibrio harveyi* populations aggregate to form quorums¹¹³. In a similar study, using a cleverly designed device, Cho *et al.* found that over time bacterial populations organised themselves spatially to try and optimise nutrient access and waste removal, further highlighting their ability to self-organise¹¹⁴. Microfluidic approaches have allowed increased sensitivity in chemotaxis assays, this was epitomised in a study by Mao *et al.*, who observed chemo-attraction at a level nearly 3 orders of magnitude lower than observed in capillary assays by using a specially designed device to investigate the attraction of *E. coli* to the amino acid attractant L-aspartate¹¹⁵. Interestingly, the fact the bacteria responded to such low levels of L-aspartate highlighted how sensitive bacteria are to extracellular stimuli. Stocker *et al.*, investigated how chemotaxis can allow bacteria to exploit nutrient rich regions in a marine setting by using a microfluidic device that simulated the settling of dissolved organic matter within the oceans¹¹⁶. Using this, they found that the motile bacteria, *Pseudoalteromonas haloplanktis*, were able to accumulate in the nutrient rich areas and, as a result, were 4 times more likely to be exposed to nutrients than non-motile bacteria¹¹⁶; again highlighting how bacteria can react to extracellular stimuli.

Exposure to nutrients or nutrient depletion can affect population growth rates and, as previously discussed, this can be a result of population heterogeneity^{14,23,24}. Therefore, microfluidics has emerged as a useful tool for investigating growth dynamics within a population. An early example of this was by Elfving *et al.* who trapped single bacterium to the surface of a microfluidic device and optimised the flow rate to wash away any daughter cells, allowing for the long term tracking of the mother cell¹¹⁷. Using this set up, they found that heterogeneity in lag time increased with increasing concentration of salt in *E. coli*¹¹⁷, indicating the extracellular salt content can affect cellular dormancy. In a similar study, Long *et al.* used a microfluidic chemostat device to track individual cellular parameters, such as growth rate, cell size and GFP expression, for an *E. coli* population during continuous growth and upon nutrient shifts, highlighting how microfluidics can be utilised for investigating cellular dynamics¹¹⁸. Using a

microfluidic agarose channel, Choi *et al.* tracked the growth rate of single bacterium in response to different concentrations of antibiotics, allowing them to rapidly identify the MIC; a method which can improve efficiency for diagnosis and treatment of clinical isolates¹¹⁹. Norman *et al.* investigated the ability of individual *B. subtilis* to switch between two different states during exponential growth; a bet hedging strategy in nature to allow the population to “settle down” and colonise an environment with favourable conditions¹²⁰. In this study, they used an early version of what is now a widely adopted microfluidic set up; the “Mother Machine”⁸.

1.3.3 The microfluidic “Mother Machine”

The Mother Machine device was first developed by Wang *et al.* in 2010⁸. It consists of an inlet tube, which allows the manipulation of the extracellular environment, and an outlet tube, for the removal of waste products or unwanted cells. However, its most important feature is the thousands of miniature side channels which were designed to trap a single “Mother” cell whilst its progeny divide towards the centre channel and are eventually washed away⁸. After developing the Mother Machine device, Wang *et al.* used it to show that the “Mother” cell accumulated the same pole over hundreds of generations and the damages that it accumulates as a consequence, ultimately result in cell death⁸. The previously discussed work by Bergmiller *et al.* used a mother machine device to investigate the distribution of the multi-drug efflux pump AcrB-TolC and found it was more prominent in old-pole compared to new-pole daughter cells after cellular division⁷. Kaiser *et al.* utilised a Mother Machine device to investigate the single cell response of *E. coli* cells during a nutrient switch from glucose to lactose¹⁰⁵. Interestingly, they found that growth arrest during this transition was deterministic and not stochastic as previously believed¹⁰⁵. Also in *E. coli*, Uphoff used DNA alkylation to inflict DNA damage and visualise mutation dynamics in real time, finding that mutagenesis was modulated by stochasticity in the expression of DNA repair mechanisms¹²¹. Furthermore, exposure to the alkylating agent resulted in a variety of cell fates, including sudden growth arrest and lysis¹²¹. Roberts *et al.* further investigated the mutational dynamics in *E. coli* by fluorescently tagging the mismatch repair system, by using the Mother Machine device they developed a micro mutation accumulation experiment that allowed them to characterise lethal mutations that

are overlooked in similar bulk assays¹²². Moolman *et al.* used a slightly modified version of a mother machine device to investigate the loading and unloading of β_2 -clamps, which in turn allow the binding of DNA Polymerase III to the DNA template, during DNA replication, finding they can remain on the DNA to provide a docking platform for other enzymes¹²³. Chait *et al.* combined optogenetics and the Mother Machine to develop a fully integrated platform that allowed them to control the gene expression of hundreds of individual bacteria using light responsive transcription¹⁰¹. Their approach dynamically combines mathematical simulation with experimental results to provide a new platform for investigating population behaviour¹⁰¹. Finally, the mother machine has also been used to investigate response to antibiotics in *S. typhimurium*¹²⁴. Arnoldini *et al.* induced the bistable expression of the virulence factor *ttss-1*, resulting in the production of two phenotypes one expressing *ttss-1* and one not. Interestingly, the bacterium expressing the virulence factor also exhibited a reduced growth rate which, in turn, made them more likely to survive exposure to the fluoroquinolone ciprofloxacin¹²⁴.

1.3.4 Investigating antibiotic persistence with microfluidics

The Mother Machine is not the only microfluidic device that has been used for investigating antibiotic persistence. Gefen *et al.* used a device that allowed micro-colonies to grow in microscopic chambers whilst their extracellular environment was tightly controlled by diffusion through a cellulose membrane that separated these chambers from larger flow channels¹²⁵. Using this device, they investigated the level of dormancy in persister cells that are found in cultures leaving stationary phase¹²⁵. Using a *hip* mutant strain of *E. coli* they induced mCherry expression with a synthetic promoter and expected to observe little or no fluorescence in persister cells to reflect a level of complete dormancy¹²⁵. In contrast, they found the persister cells exhibited the same initial fluorescence response as their susceptible kin, suggesting the persister cells were perhaps not in a dormant state in stationary phase but developed upon leaving¹²⁵. Vega *et al.* suggested that persistence could be induced in *E. coli* in response to the cell-cell signalling molecule indole³⁵. They developed a device with a subsection that was the same height as a single monolayer of *E. coli* and would therefore allow individual bacterium to be trapped; once the bacteria were seeded in this area the flow could be reversed and the extracellular

environment controlled through the “switching” of integrated elastomeric valves³⁵. They found an increase in the expression of the *tnaC* fluorescence reporter when they incubated the bacterium with indole and showed that the indole induced fluorescence was higher in those bacteria that went on to survive ampicillin treatment³⁵. In a device that shared some similarities to both the mother machine and the one previously described for Gefen *et al.*, Balaban *et al.* trapped cells in micro channels and the diffusion of media through a cellulose membrane allowed the tight control of the extracellular environment³⁰. Using this device, they were able to track single cells after exposure to ampicillin and determined that those that persist cells had a slower growth rate than their susceptible kin prior to antibiotic exposure³⁰. Importantly, however, due to limitations with throughput on their device, they had to perform their experiment on a *hip* mutant in order to generate enough persisters. Finally, Pu *et al.* designed a device that had 12 channels alongside each other that were each 150 μm wide and 20 μm deep and imaged cells that stuck to the channel surface¹²⁶. They used BOCILLINTM, a fluorescent β -lactam antibiotic, to investigate whether persister cells had lower intracellular accumulation of antibiotics¹²⁷. Interestingly, they found by fluorescently tagging the multi drug efflux pump, *toIC*, that persisters had a higher level of fluorescence, and therefore increased efflux activity, than their susceptible counterparts¹²⁷. However, they also found that in a Δ *toIC* strain persisters and susceptible cells showed the same level of BOCILLINTM fluorescence¹²⁷, which raises the question if intracellular drug levels do play a role in persistence.

Although microfluidics has provided researchers with a tool for investigating heterogeneity at the single cell level, a lot is still left to be determined, particularly with respect to antibiotic persister and VBNC cells. For example, many of the investigations into antibiotic persistence have still required the use of *hip* mutants in order to generate sufficient numbers of persister cells. Furthermore, with VBNC cells believed to be even less frequently occurring, they still remain difficult to investigate. However, as these high throughput devices become more readily available and researchers are rapidly producing vast amounts of data, it is the analysis steps that are becoming the limiting factor.

Table 2. A summary of the microfluidic experiments discussed in 1.3 and the respective cellular / population attributes being investigated.

Attributes being measured	Examples
Mechanical / physical properties	<ul style="list-style-type: none"> • Auxetic properties of nuclei in stem cells¹⁰⁸ • Physical response of <i>E. coli</i> to mechanical pressure before they could respond biochemically¹¹⁰
Chemotaxis / motility	<ul style="list-style-type: none"> • Migration of cancer cells¹²⁸ • Self-organisation of bacteria to improve population efficiency, for instance with respect to nutrient utilisation^{113–116}
Growth rate	<ul style="list-style-type: none"> • Effect of temperature on growth rate of <i>S. pombe</i>¹⁰⁹ • Rapidly identifying MIC of bacteria in response to different antibiotics¹¹⁹ • Switching between growth phenotypes^{117,118,120} • Growth dynamics of the mother cell over time and in response to different extracellular environments^{8,105}
Mutation dynamics	<ul style="list-style-type: none"> • Stochasticity in the expression of DNA repair mechanisms¹²¹ • Characterising lethal mutations overlooked in bulk assays¹²²
Antibiotic persistence	<ul style="list-style-type: none"> • Effect of indole exposure³⁵ • Level of dormancy of persister cells leaving stationary phase¹²⁵ • Growth rate of persister cells prior to antibiotic exposure³⁰ • Efflux activity in persister cells¹²⁶

1.4 Current image analysis platforms

The development of new high throughput technologies in microbiological research, including microfluidics, means researchers are now accumulating data faster than ever. In terms of microscopy images, this means that it now often takes longer for researchers to analyse their images than it does to initially acquire them. As a result, the development of image analysis technologies has been described as “lagging behind the adoption of high-throughput imaging technologies”¹²⁹. As a result, groups are now often spending time developing their own automated or semi-automated image analysis tools^{101,105,118,124,130–133}. However, this is often time consuming and if the imaging platform is very specific, they are unlikely to be used by other groups.

One of the first open source image analysis packages available for biological applications was ImageJ¹³⁴. However, despite its relative success, ImageJ is designed for single images and therefore programming knowledge is required to develop macros if a researcher wished to adapt it for use on larger, more complex datasets. That being said, some groups have developed freely available plugins which can be utilised by the scientific community, for example MicrobeJ¹³⁵. MicrobeJ was utilised by Simsek and Kim to detect single bacterium trapped under an agar pad whilst investigating single cell metabolic heterogeneity¹⁵. Haugan *et al.* used it to detect single bacteria and fluorescent foci in *E. coli* whilst investigating growth during host infection¹³⁶. However, MicrobeJ is limited to phase contrast or fluorescence images and is not fully automated as it still requires some level of manual input.

In a similar approach, the Broad institute developed CellProfilerTM, a freely available open source platform¹³⁷. CellProfilerTM allows researchers with limited computer vision experience to develop their own pipelines through combining multiple individual modules. Rees *et al.* used CellProfilerTM to detect the nucleus and nanoparticle loaded vesicles whilst investigating heterogeneity in nanoparticle uptake in lung carcinoma cells¹³⁸. In contrast, Inamine, *et al.* used it to detect gut bacteria in fecal samples¹³⁹. However, although Long *et al.* used CellProfilerTM for image analysis, they required additional custom scripts in order to segment the channels and track images across frames¹¹⁸ as

CellProfiler™ is mainly focused on problems surrounding colonies and colony growth.

Table 3. A comparison summary of the current image analysis softwares designed specifically for mother machine images; highlighting the need for a fully automated platform for images acquired in bright field.

	Current analysis softwares		
Functionality	<i>mmJ</i>	<i>MoMA</i>	<i>Molyso</i>
Level of automation	Semi	Almost fully	Fully
Language	ImageJ plugin	ImageJ plugin	Python
Additional issues	Requires Gurobi	-	-
Phase contrast	✓	✓	✓
Bright field	✗	✗	✗

Similar to the previously discussed MicrobeJ, some Mother Machine specific plugins have been developed for ImageJ. The first plugin, *mmj*, was developed by Arnoldini *et al.* and was used by their research group to investigate the expression of virulence factors in *S. typhimurium*¹²⁴. However, the plugin is semi-automatic and, therefore, due to the level of pre-processing required, it remains relatively inefficient and has not been adopted by the wider community. A second, more automated, imageJ plugin, *MoMA*, has since been developed by Kaiser *et al.*¹⁰⁵. They used it to analyse images of *E. coli* during a nutrient shift between glucose and lactose and claim to have achieved unprecedented levels of accuracy¹⁰⁵. However, *MoMA* requires a license for Gurobi, which is only free for academics, therefore limiting its accessibility within the scientific community. Furthermore, its detection pipeline is designed specifically for phase contrast images, so its ability to cope with bright-field images remains to be determined. To my knowledge, the only other, freely available Mother Machine specific image analysis platform is *Molyso*¹³⁰. *Molyso* is a fast and efficient software developed in python by Sachs *et al.*¹³⁰. However, like *MoMA*, it is also limited to phase contrast images. As a result, despite the now widespread

adoption of the Mother Machine^{7,101,105,130–132}, there are still very few image analysis platforms available specifically for Mother Machine images. In fact, to the best of my knowledge, there are no platforms available for Mother Machine images acquired using bright field microscopy.

1.5 Gaps in the knowledge

The fact that antibiotic persister and VBNC cells are involved in the recalcitrance of infection^{33,46} and can act as a stepping stone for antibiotic resistance³⁸ has resulted in a heightened interest in the phenotypes. However, despite this, still very little is known about the two phenotypes, or the relationship between them. Researchers have found that pre-stressing a population, for example exposure to sub-MIC levels of antibiotic, oxidative stress and nutrient transitions^{35,55,61,66,67}, has been shown to increase the level of persistence, but in all of these examples the stress has been deliberately added by the researchers. Furthermore, it is known that persister fractions, the number of persister cells within a population divided by the total population size, vary at different stages of the bacterial growth cycle and in response to different antibiotics⁷⁹. However, what remains unclear is how bacteria populations may shape their extracellular environment during the growth cycle and how this, in turn may affect persister formation.

One reason why persisters and VBNC cells are particularly difficult to investigate is that they exist in a temporary state and are genetically identical to their susceptible kin. As a result, traditional microbiological methods have struggled to elucidate the mechanisms behind their appearance. For instance, colony forming units (CFU) assays can give an indication of the persister fraction within a population, but fail to consider VBNC bacteria. Furthermore, persister fraction is the only information that can be gained from CFU assays, as new populations formed from the persisters are genetically identical to the original population and remain susceptible to future antibiotic exposure. As a result, new high throughput technologies, such as microfluidics, are rapidly being adopted by researchers in order to generate measurements, such as shape and transcriptional activity, at the single cell level^{105,140,141}.

Although microfluidics has provided a platform for investigating antibiotic persister cells, many of the devices that have been used thus far are still limited. For example, some groups don't confine individual bacterium and therefore face the difficulty of having to track cells within micro colonies¹²⁷. As a result, they have to remain focused on a small area of their device, which in turn limits their throughput. Others have realised the importance of confining the bacteria in order to make tracking much easier and, as a result, increase throughput³⁰. However, in many examples, the devices used still didn't have sufficient throughput in order to effectively analyse persister formation in wild type strains, so were often forced to investigate high persistence (*hip*) mutants^{30,71}.

Despite this, to the best of my knowledge, until this thesis work there are no reports of VBNC cells being investigated using single cell microfluidics. Furthermore, some researchers have proposed that VBNC and persister cells are part of one physiological continuum^{36,37}. Therefore, a carefully designed, single cell microfluidic platform that would allow the investigation of VBNC and persister cells in unison may prove extremely useful for investigating this hypothesis.

I previously discussed how protein aggregation has been linked to reduced growth rate and increased efflux activity within bacterium^{7,9}; similar characteristics as to those that have been observed in persister and VBNC cells^{127,142}. However, the link between the persister cells, VBNC cells and protein aggregation has yet to be determined. Therefore, a microfluidic protocol, such as the one discussed above, could also be utilised to investigate the relationship between cellular stress, protein aggregation and the formation of persister and VBNC cells.

As previously discussed, persister and VBNC cells are genetically identical and only survive antibiotic exposure as a result of entering a transient state. Interestingly, although this temporary state is one of the characteristics that make persisters and VBNC so unique; it also makes them extremely difficult to investigate. To date, there is no way to isolate persisters or VBNC prior to exposure to antibiotics. In fact, it is still not completely clear if persister and VBNC cells exists within a population prior to exposure, or if it is the exposure itself that causes them to enter the persister or VBNC state. In order to decipher

this, it is important for researchers to be able to investigate and track the response to antibiotics before, during and after exposure, all within a single experiment.

The above gaps in knowledge could all be investigated with a well-designed microfluidic device and accompanying protocol. However, the issue still remains that persister and VBNC cells only make up a small proportion of a population. Therefore, thousands of cells will need to be included in each assay in order to gather enough information on each phenotype. As a result, any such protocol would generate vast amounts of data, of which the respective analysis could become the limiting step. Therefore, the development of a fully automated image analysis software would allow the protocol to maintain sufficient throughput. To date, no such programs exist for the analysis of Mother Machine images acquired using bright field microscopy.

Chapter 2: The culture environment influences both gene regulation and phenotypic heterogeneity in *Escherichia coli*

2.1 Introduction

In this chapter, we investigate population heterogeneity by using antibiotic persistence as a proxy. This approach allows us to identify temporal windows in which significant changes, with respect to the size of the antibiotic persister population, occur. Therefore, by investigating the population transcriptome, we can identify genes and pathways which are highly regulated during the aforementioned temporal windows; genes and pathways which can be further investigated at the single cell level using the protocol developed in chapters 3 and 4, respectively.

Genetically identical bacterial populations can exhibit cell to cell variations that result in the formation of multiple sub populations with different phenotypes^{95,98}. This phenotypic heterogeneity can be generated in response to a variety of factors, such as pH and metabolic stress^{35,55,61,66,67}. Nikolic, *et al.* investigated heterogeneity in metabolic rate and nutrient uptake using fluorescence based transcriptional reporters and observed heterogeneity in the expression of the two glucose transporters, *ptsG* and *MglBAC*, when cells were grown with glucose as their only nutrient source¹⁴. Furthermore, they found that there was heterogeneity in the expression of *acs*, encoding acetyl-CoA synthetase, when the culture was provided with high concentrations of glucose¹⁴. *acs* is co transcribed with the acetate permease, *ActP*, so there results also suggested heterogeneity in utilisation of acetate¹⁴. In a similar study, Kotte *et al.* used flow cytometry and theory to investigating the response of individual bacteria within an *E. coli* population during a switch from glucose to gluconeogenic substrates²³. By staining the cellular membranes with a fluorescent dye, they could determine a cells growth history as its fluorescence halved with each division. Their results showed that during the shift from glucose to

gluconeogenic substrates, the population diversified in response, with some bacterium growing on the gluconeogenic substrates and others entering a dormant, non-growing state²³. Finally, using the fluorescently labelled glucose molecule (2-NBDG), Şimşek and Kim investigated metabolic uptake and activity in response to nutrient upshifts, minimal media to rich LB medium, in *E. coli*¹⁵. They found that 3 different phenotypes existed when they categorised the cells based on metabolic activity and viability; a metabolically active and growing phenotype, a partially metabolically active and non-growing phenotype and a metabolically inactive and non-viable phenotype¹⁵. However, what was perhaps most interesting was that the distribution of these sub populations changed during starvation or exposure to extracellular stress, in this case oxidative¹⁵. Despite this heterogeneity, physiological variations that are more than 2 % different than the population average are often only observed in less than a few percent of the population²². This means it is extremely difficult to study such sub populations, however one possible option is to use a proxy, such as persistence, to study phenotypic heterogeneity⁹⁸.

Interestingly, nutrient shifts have also been associated with an increase in antibiotic persistence; Amato and Brynildsen showed that a shift in carbon source, such as glucose to fumarate, can generate persister formation in response to the β -lactam ampicillin and the fluoroquinolone ofloxacin⁶². One hypothesis as to how starvation can cause increased antibiotic survival is that the growth arrest associated with starvation can reduce the efficacy of antibiotics on their targets¹⁴³. However, Nguyen *et al.* showed that, upon serine starvation, persistence only increased 34 fold in a mutant strain of *Pseudomonas aeruginosa* that was unable to generate a stringent response compared to a 2300 fold increase in the parent strain; suggesting the stringent response plays a major role in the increased persistence we observe upon nutrient starvation. Nutrient starvation, however, is not the only source of stress that has been linked to an increase in antibiotic persistence, for instance Leung and Lévesque witnessed an increase in ofloxacin persistence after pre-exposure to acid⁵⁵.

All of the above examples of extracellular stress, be it metabolic or acidic, that have been externally applied to a culture by the researchers. However, Keren *et al.* showed that the number of persisters increased for an *E. coli* population

growing in LB broth between lag and stationary phase in response to ofloxacin and ampicillin⁷⁹. This suggests that increases in antibiotic persistence can result from a population's self-generated stress and is not reliant on external stressors. For example, the extracellular environment of a growing planktonic *E. coli* population will be constantly changing as a result of the uptake of nutrients and excretion of waste products. Furthermore, the nutrients being utilised will change over the growth cycle, for instance as the favoured nutrient source, glucose, runs out²⁴. On top of this, the excretion of waste products, such as acetate, will affect the extracellular pH which, in turn, has been shown to affect the regulation of genes involved in catabolism and transport¹⁴⁴.

The gene expression profile has been characterised for exponential and stationary phase *E. coli* O157 in minimal media supplemented with glucose¹⁴⁵. However, until this thesis, no one has characterised the relationship between the extracellular environment and the population transcriptome of *E. coli* K12 growing in lysogeny broth, despite it being a regularly used model experimental system. In the following chapter, we characterise the extracellular pH and sugar levels throughout the growth cycle and investigate how this is reflected in the population transcriptome. We then use the formation of antibiotic persister cells in response to the β -lactam ampicillin, the fluoroquinolone ofloxacin and the aminoglycoside gentamicin, as a proxy for population heterogeneity in order to identify temporal windows where the population shows substantial phenotypic diversification. Finally, we explored the population transcriptome during these temporal windows, in order to identify candidate genes and pathways that could be further investigated using the single cell approach we discuss later in this thesis.



The Culture Environment Influences Both Gene Regulation and Phenotypic Heterogeneity in *Escherichia coli*

Ashley Smith^{1,2}, Agnieszka Kaczmar^{1,2}, Rosemary A. Bamford^{1,2}, Christopher Smith², Simona Frustaci¹, Andrea Kovacs-Simon², Paul O'Neill², Karen Moore², Konrad Paszkiewicz², Richard W. Titball² and Stefano Pagliara^{1,2*}

¹ Living Systems Institute, University of Exeter, Exeter, United Kingdom, ² Biosciences, University of Exeter, Exeter, United Kingdom

OPEN ACCESS

Edited by:

Daniela De Biase,
Sapienza Università di Roma, Italy

Reviewed by:

Bei-Wen Ying,
University of Tsukuba, Japan
Peter Adrian Lund,
University of Birmingham,
United Kingdom

*Correspondence:

Stefano Pagliara
s.pagliara@exeter.ac.uk

Specialty section:

This article was submitted to
Microbial Physiology and Metabolism,
a section of the journal
Frontiers in Microbiology

Received: 11 March 2018

Accepted: 11 July 2018

Published: 15 August 2018

Citation:

Smith A, Kaczmar A, Bamford RA, Smith C, Frustaci S, Kovacs-Simon A, O'Neill P, Moore K, Paszkiewicz K, Titball RW and Pagliara S (2018) The Culture Environment Influences Both Gene Regulation and Phenotypic Heterogeneity in *Escherichia coli*. *Front. Microbiol.* 9:1739. doi: 10.3389/fmicb.2018.01739

Microorganisms shape the composition of the medium they are growing in, which in turn has profound consequences on the reprogramming of the population gene-expression profile. In this paper, we investigate the progressive changes in pH and sugar availability in the medium of a growing *Escherichia coli* (*E. coli*) culture. We show how these changes have an effect on both the cellular heterogeneity within the microbial community and the gene-expression profile of the microbial population. We measure the changes in gene-expression as *E. coli* moves from lag, to exponential, and finally into stationary phase. We found that pathways linked to the changes in the medium composition such as ribosomal, tricarboxylic acid cycle (TCA), transport, and metabolism pathways are strongly regulated during the different growth phases. In order to quantify the corresponding temporal changes in the population heterogeneity, we measure the fraction of *E. coli* persisters surviving different antibiotic treatments during the various phases of growth. We show that the composition of the medium in which β -lactams or quinolones, but not aminoglycosides, are dissolved strongly affects the measured phenotypic heterogeneity within the culture. Our findings contribute to a better understanding on how the composition of the culture medium influences both the reprogramming in the population gene-expression and the emergence of phenotypic variants.

Keywords: phenotypic heterogeneity, *Escherichia coli*, persisters, metabolism, bacterial physiology, antibiotics, gene-expression profiling, KEGG pathways

INTRODUCTION

Within isogenic populations there may be substantial cell-to-cell heterogeneity in terms of metabolic activity (Nikolic et al., 2013; Şimşek and Kim, 2018), growth rate (Kotte et al., 2014), substrate assimilation (Sheik et al., 2016), compound secretion (Veening et al., 2008), virulence (Arnoldini et al., 2014), and resistance to stress (Balaban et al., 2004). This heterogeneity has been observed across all the domains of life and arises from the inherent random nature of biochemical reactions (Elowitz et al., 2002; Kaern et al., 2005; Lidstrom and Konopka, 2010). Phenotypic heterogeneity may allow some individual cells to survive shifts in the environmental conditions,

and thus permitting the population to withstand fluctuating environments (Balaban et al., 2004; Ackermann, 2015; Venturelli et al., 2015; Schreiber et al., 2016; Bódi et al., 2017). It has also been suggested that phenotypic heterogeneity can accelerate evolutionary adaptation to different environmental challenges (Beaumont et al., 2009; New et al., 2014). The culture environment in turn affects the population transcriptome. For instance, pH has been shown to regulate genes involved in catabolism and transport (Hayes et al., 2006), whereas glucose-lactose diauxie induces the downregulation of amino acid biosynthesis and aerobic metabolism genes (Chang et al., 2002). Additionally, changes in gene-expression levels in response to nutritional changes are strongly linked to growth rate and cell size (Weart et al., 2007; Scott et al., 2010; Chien et al., 2012; Yao et al., 2012). Moreover, it has been suggested that a reduction in cell size increases the heterogeneity in gene-expression within the population (Kaern et al., 2005).

However, only a small subpopulation of bacteria shows observable physiological variations, such as growth rate that is more than twofold different than the remainder of the population (Lidstrom and Konopka, 2010). Therefore, the identification and study of such small subpopulations can be challenging but can be simplified by analyzing the functional consequences of a given case of phenotypic heterogeneity (Ackermann, 2015).

For example, persister cells are a small proportion of a clonal microbial population that can survive otherwise lethal doses of antibiotics and resume growth shortly after removing the antibiotic (Hansen et al., 2008; Lewis, 2010; Maisonneuve et al., 2013), but without acquiring genetic changes that confer antibiotic resistance. In this paper we used persister cell formation as a proxy for phenotypic heterogeneity. Persister cells have been observed across all the domains of life (Lewis, 2010; Hangauer et al., 2017; Megaw and Gilmore, 2017) and are believed to contribute to the survival of bacteria in biofilms exposed to antibiotics (LaFleur et al., 2006; Lewis, 2010) and to chronic infections in immunosuppressed hosts (Mulcahy et al., 2010; Maisonneuve and Gerdes, 2014).

Persisters can form stochastically as a result of fluctuations in gene-expression (Amato et al., 2013). However, a variety of environmental factors favor persister formation, including subinhibitory concentrations of antibiotics (Amato et al., 2013), nutrient limitation (Vega et al., 2012), intra-species interactions (Bernier et al., 2013), starvation (Fung et al., 2010), and in the case of pathogens, interactions with the host (Helaine et al., 2014). Amato et al. (2013) showed that diauxic growth contributes to persister cell formation, whereas another study by the same group showed that nutrient transitions contributed to persister formation within bacterial biofilms (Amato and Brynildsen, 2014). Keren et al. reported that the number of ampicillin or ofloxacin persisters increased from lag to stationary phase (Keren et al., 2004a). However, the temporal windows when there are substantial increases in the formation of persisters to different antibiotics during growth of *Escherichia coli* (*E. coli*) on lysogeny broth (LB) have yet to be defined. Moreover, gene-expression profiling has been carried out on both exponential and stationary phase *E. coli* O157 growing on 3-(*N*-morpholino)propanesulfonic acid (MOPS) minimal medium

supplemented with 0.1% glucose (Bergholz et al., 2007). However, the changes in the transcriptome throughout the growth cycle of *E. coli* K12 growing in LB remain to be determined, despite this being an experimental model system employed in microbiology, biotechnology, and molecular biology.

In this paper, we report the changes in sugar levels and pH and the associated reprogramming in gene-expression during the transitions between the different phases of *E. coli* growth. We then investigate the phenotypic heterogeneity within the *E. coli* population throughout the growth cycle by using persister formation, in response to ampicillin, gentamicin, or ofloxacin as a proxy for studying cellular heterogeneity. Our findings will be instrumental for investigations into the mechanisms underlying microbial survival in transitioning environments and provide key transcriptomic data for a commonly used model in many bacterial studies.

MATERIALS AND METHODS

Chemicals and Culture Preparation

All chemicals were purchased from Fisher Scientific or Sigma-Aldrich unless otherwise stated. LB medium (10 g/L tryptone, 5 g/L yeast extract, and 10 g/L NaCl, Melford) and LB agar plates (LB with 15 g/L agar) were used for planktonic growth and enumeration of colony-forming units (CFUs), respectively. *E. coli* BW25113 was purchased from Dharmacon (GE Healthcare). A single colony of *E. coli* BW25113 was grown in 200 ml fresh LB in a shaking incubator at 200 rpm and 37°C for 17 h (**Supplementary Figure S1A**). After 17 h incubation, the culture was diluted 1:1000 in fresh LB and growth was measured hourly by taking three aliquots that were then centrifuged (13,000 g for 5 min), the supernatant was removed, the pellet was resuspended in phosphate-buffered saline (PBS), and serial dilutions were plated on LB agar for CFU counts (**Supplementary Figures S1B,C,H**). This experiment allowed us to determine that the culture was in stationary phase at $t = 17$ h (left axis in **Supplementary Figure S2**). In order to avoid introducing any bias in our measurements (Luidalepp et al., 2011), we used the same LB autoclaving conditions in all our assays. The relatively small error bars in our measurements and in other recent reports (Orman and Brynildsen, 2016; Radzikowski et al., 2016) demonstrate the suitability of autoclaved LB for these microbiological assays.

Characterizing the Bacterial Environment

A culture was prepared as described above and eighty-one 100 μ l aliquots were added to individual wells of a 96-well plate (three technical replicates in biological triplicates for each of the nine time points were investigated). The remaining wells were filled with fresh LB for blank measurements. The plate was placed in a preheated (37°C) Infinite[®] 200 PRO plate reader (TECAN) shaking at 200 rpm. To quantify bacterial growth in this assay, optical density at 595 nm (OD₅₉₅) was measured hourly in nine selected wells for each time point. Bacterial growth measured via the plate reader method (right axis in **Supplementary Figure S2**) was comparable to that measured via

CFU counts in cultures growing in 200 ml flasks (left axis in **Supplementary Figure S2**). To quantify the amount of reducing sugars, preheated (100°C) Benedict's reagent (Sigma-Aldrich) was then added to the same wells according to the manufacturer's instructions and absorbance at 490 nm was measured after 15 min incubation. The absolute sugar concentration was determined by extrapolation through a standard curve of known glucose concentration (**Supplementary Figure S3**). This was obtained by adding glucose in MilliQ water at concentrations of 125, 250, 500, or 1000 μM in triplicate in a 96-well plate. Preheated (100°C) Benedict's reagent was then added to the same wells and the absorbance at 490 nm was measured after a 15 min incubation. The average reading from three wells containing only MilliQ water was subtracted from the readings of the glucose containing wells. These blank subtracted readings are reported in **Supplementary Figure S3** together with a linear regression fitting of the experimental data. In order to measure the culture pH, the probe of a PH-100 ATC pH meter (with an accuracy of pH 0.01, Voltcraft) was immersed in a separate culture prepared as described above and the pH was recorded hourly. The measurements were taken in at least three biological replicates.

Transcriptomic and qPCR Analysis

A culture was prepared as described above. Immediately after dilution (0 h), 500 μl aliquots were taken from the overnight (17 h) culture and 1, 2, 3, 3.5, 4, 4.5, 5, 6, or 7 h after dilution in fresh LB (1:1000) and were incubated at 200 rpm and 37°C as described above. The RNA of the cells contained in each aliquot was stabilized using RNeasy Protect Bacteria Reagent (Qiagen). Extraction was performed with RNeasy Mini Kit (Qiagen) and DNA removal with DNase I (RNase-free, Ambion), using the recommended protocols. RNA concentration and purity were determined using a 2100 Bioanalyzer (Agilent). cDNA libraries from all samples with an RNA integrity number (RIN) greater than eight were prepared and then sequenced using Illumina HiSeq 2500. The paired reads were trimmed and sequencing adaptors were removed using fastq-mcf. RNA ERCC spike-in control sequences were removed using bowtie version 1.0.0, and the remaining reads were aligned to the reference genome using tophat2 version 2.1.0. The gene-expression was quantified using HTseq-count. DESeq2 v1.6.3 was used to normalize the raw transcript reads for all genes by using the median-ratio normalization method and for library size (Love et al., 2014). To reduce the number of false-positive results, the \log_2 fold changes were shrunk toward zero for lowly expressed genes and the adjusted p -values were calculated using a false discovery rate (FDR) of 0.1. We then determined the \log_2 fold change in the normalized transcript reads for each gene at different time points, relative to the normalized transcript reads in the overnight stationary phase sample ($t = 17$ h). In order to identify the variables that best differentiate the data, as well as to determine how well-clustered the replicates were, we performed principal component analysis (PCA) using DESeq2 and a built-in R method (prcomp) on the top 500 expressed genes. These genes were normalized using a regularized log transform prior to PCA to allow better visualization of the trends and clusters that

may otherwise remain hidden. The data shown represent the first (PC1) and second principal components (PC2). The clustering of the time point replicates indicates a high level of reproducibility in our data. During the three different growth phases the top 10% of upregulated and downregulated genes, based on their \log_2 fold change, were identified and goseq was used to identify overrepresented pathways in the Kyoto Encyclopedia of Genes and Genomes (KEGG) (Ogata et al., 1999; Kanehisa et al., 2016, 2017). In order to check the results, qPCR was performed on the same aliquots on a StepOnePlus™ Real-Time PCR System for selected genes. Both RNA-seq and qPCR measurements were performed in biological triplicates.

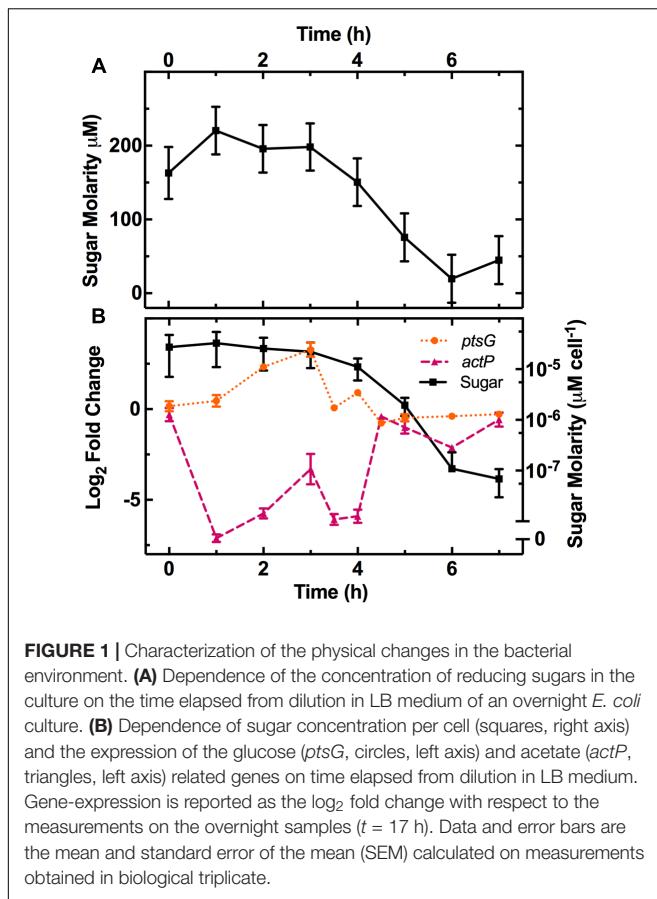
MIC Determination

The minimum inhibitory concentration (MIC) of the employed antibiotics against *E. coli* BW25113 was determined using a 96-well plate method. *E. coli* was grown for 17 h in LB containing different concentrations of ampicillin (0.5–512 $\mu\text{g ml}^{-1}$), ofloxacin (0.0625–64 $\mu\text{g ml}^{-1}$), or gentamicin (0.125–128 $\mu\text{g ml}^{-1}$) and the OD₅₉₅ was measured hourly. The MICs were measured as the lowest concentrations at which the OD₅₉₅ was the same as the control (bacteria-free LB) and were determined as 5, 4, and 0.125 $\mu\text{g ml}^{-1}$ for ampicillin, gentamicin, and ofloxacin, respectively.

Persister Enumeration

A culture was prepared as described above and during mid-exponential phase ($t = 3$ h after dilution) the respective antibiotics were added to the culture to reach a concentration of $25 \times \text{MIC}$, with persister levels typically not varying above this concentration of antibiotics (Johnson and Levin, 2013). Every 30 min an aliquot was taken from the treated culture, centrifuged (13,000 g for 5 min), re-suspended in PBS, and plated on LB agar plates. The plates were incubated and CFUs were determined the following day. For each antibiotic, the fraction of persister cells plateaued after 3 h of treatment, as previously reported (Johnson and Levin, 2013), confirming that we were studying persister subpopulations rather than antibiotic-tolerant populations (Brauner et al., 2016).

In order to enumerate persisters based on the effect of different antibiotics during the various phases of growth, a culture was prepared as described above (**Supplementary Figures S1A,B**). Nine 500 μl aliquots were withdrawn from the growing culture hourly (**Supplementary Figures S1C,E**). Three of them were used for untreated controls, the aliquots were centrifuged (13,000 g for 5 min), supernatant was removed, the pellet was resuspended in PBS, and serial dilutions were plated on LB agar (**Supplementary Figure S1H**). Three aliquots were supplied with 500 μl LB (1:1 dilution) containing $50 \times \text{MIC}$ of one of the three above specified antibiotics (final concentration $25 \times \text{MIC}$) and were returned to the shaking incubator (**Supplementary Figure S1F**). After 3 h, these aliquots were centrifuged, the supernatant was removed, and the pellet was re-suspended in PBS. Serial dilutions were then performed and plated on LB agar (**Supplementary Figure S1I**). Three aliquots were injected with 10 μl of one of the three above specified antibiotics to reach a final concentration of $25 \times \text{MIC}$ and returned to the shaking



incubator (**Supplementary Figure S1G**). After 3 h these aliquots were centrifuged, the supernatant was removed, the pellet was re-suspended in PBS, serially diluted and plated on LB agar (**Supplementary Figure S1J**).

RESULTS

Nutritional and Chemical Environment of a Growing *E. coli* Culture

We investigated how the sugar content and the pH of the growth medium changed over time. Notably, both quantities are known to affect the outcome of antibiotic treatment (Allison et al., 2011; Cama et al., 2014). The measured concentration of fermentable sugars in the LB medium we employed was $163 \pm 35 \mu\text{M}$. A previous study found that LB contained less than $100 \mu\text{M}$ fermentable sugars by using a genetic approach based on a *hemA* deletion mutant unable to grow in the absence of fermentable sugars (Sezonov et al., 2007). This discrepancy could be due to the different sources of LB and the different techniques used to quantify the sugar concentrations. This further emphasizes the added value of carrying out the simple assay described in Section 3.2 to quantify the concentration of fermentable sugars during bacterial growth.

After *E. coli* inoculation into LB medium, we measured the remaining sugar concentration at various intervals throughout

the growth cycle (**Figure 1A**). We calculated the corresponding concentration of sugar available per bacterium (squares in **Figure 1B**) by dividing the measured sugar concentration by the measured number of bacteria in the culture (full symbols in **Supplementary Figure S2**, left axis). This revealed a one order of magnitude decrease in the sugar available per bacterium between 3 and 6 h after inoculation, when the culture transitioned from exponential to stationary growth-phase.

We also measured the pH of the culture throughout the growth cycle (**Supplementary Figure S4**). The pH decreased from 6.8 and reached its most acidic value of 6.2 during the exponential phase at $t = 4$ h, then rose up to a maximum of 7.0 during the stationary phase at $t = 7$ h. We explain this finding by considering that the culture environment is acidified by the excretion of acetate during aerobic fermentation, resulting from bacterial growth on carbohydrates during exponential phase (Kleman and Strohl, 1994). However, upon exhaustion of these carbohydrates, the bacteria use alternative carbon sources such as amino acids and other gluconeogenic substrates (Sezonov et al., 2007), resulting in the production and excretion of ammonia that increases the culture pH. Losen et al. (2004) did not observe the same growth-phase dependence for the pH of a growing *E. coli* culture. However, their assay was performed using a different *E. coli* strain (ATCC 53323) and different culture conditions including a different LB supplier, a one order of magnitude smaller LB volume and a one order of magnitude higher inoculum concentration. All together, our data complement our existing knowledge on the changes occurring in the medium composition during *E. coli* growth in LB (Losen et al., 2004; Sezonov et al., 2007).

Changes in Gene-Expression During the Growth Cycle

The gene-expression profile of bacterial populations is profoundly affected by changes in the culture (Hua et al., 2004; Bergholz et al., 2007; Klumpp and Hwa, 2015; Vital et al., 2015). However, to the best of our knowledge, this is the first study reporting the progressive reprogramming of the gene-expression profile of *E. coli* growing in LB throughout the different phases of growth.

In order to study the effect of the changing nutritional or chemical environment of the culture on the population transcriptome, we measured gene-expression profile in aliquots taken at different stages of growth in biological triplicates. **Supplementary Table S1** reports, for each gene, the mean and SEM of the normalized transcript reads measured in the samples taken at $t = 17$ h post inoculation. **Supplementary Table S1** also reports the mean and SEM of the \log_2 fold change in normalized transcript reads in the samples taken at $t = 0, 1, 2, 3, 3.5, 4, 4.5, 5, 6, \text{ or } 7$ h post inoculation relative to the $t = 17$ h sample. The mean relative error, averaged on the relative errors for the transcript reads of all genes at $t = 17$ h, is 24%, thus confirming good reproducibility across biological replicates. Indeed, this corresponds to a \log_2 fold change of 0.31, whereas in comparison, the average absolute \log_2 fold change in gene-expression at $t = 2$ h relative to $t = 17$ h is 1.9. We further confirmed the changes in

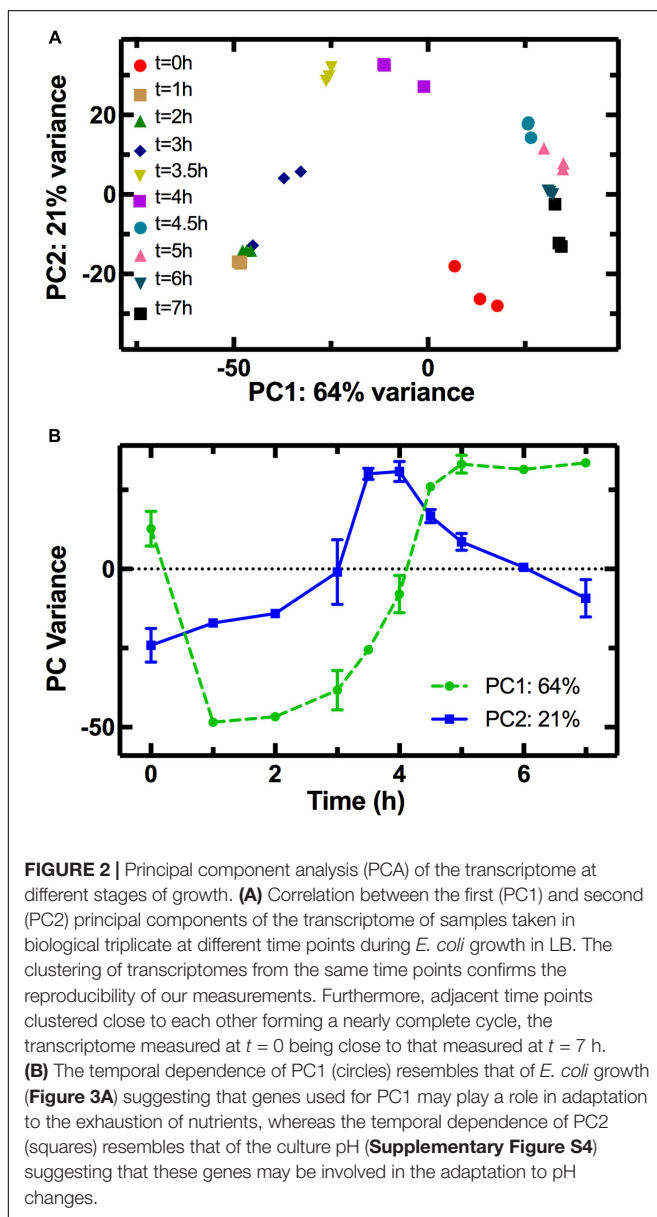
gene-expression of selected genes using qPCR (**Supplementary Figure S5**).

The PCA allowed clustering of the transcriptome profiles measured from the different biological replicates at each time point (**Figure 2A**), demonstrating good reproducibility of our cultures grown in shake flasks without the need for fermenter cultivation (Chang et al., 2002). The transcriptomes from adjacent time points clustered close to each other forming a nearly complete cycle, with the transcriptome measured at $t = 0$ being close to that measured at $t = 7$ h. Similarly, a cyclic transcriptional response of *E. coli* to acid adaptation was previously reported (Stincone et al., 2011). Furthermore, the transcriptomes measured at $t = 0$ and $t = 1$ h are simultaneously similar in terms of PC2 but different in terms of PC1 (**Figure 2B**), suggesting that part of the transcriptome

rapidly adapts to changes in the nutritional environment. The population transcriptome then becomes increasingly different in PC1 (circles in **Figure 2B**). This suggests that the regulation of the genes used for PC1 analysis allows the culture to progressively adapt to an environment unfavorable for growth, as explained in the discussion below. On the other hand, the PC2 variance reveals that the transcriptomes at $t = 3.5$ and $t = 4$ h differ the most from the transcriptome at $t = 0$ h. The PC2 variance for the $t = 0$ h transcriptome is instead similar to that of the $t = 7$ h transcriptome, a trend similar to the temporal dependence of the average division rate (**Supplementary Figure S6**) and a mirror image of the trend in pH (**Supplementary Figure S4**). This suggests that the regulation of the genes used in the PC2 analysis governs the cell division and metabolism machineries, which in turn drive the changes in the environmental pH. This is, to the best of our knowledge, the first time PCA is carried out on the transcriptome of an *E. coli* culture throughout its growth cycle.

The decrease in sugar levels in the medium parallels the regulation of a set of genes including *ptsG*, a glucose-specific phosphotransferase (Luli and Strohl, 1990), and the dedicated acetate uptake system *actP* (Luli and Strohl, 1990; **Figure 1B**). Expression of *ptsG* increases during the lag phase (circles in **Figure 1B**) when fresh medium is added to the culture and then decreases as the sugar concentration per bacterium decreases after $t = 3$ h (squares in **Figure 1B**). Bergholz et al. did not investigate gene-expression profile during lag phase but reported a similar downregulation of *ptsG* with a $-3 \log_2$ fold change between 4.5 and 5 h growth. In comparison, *actP* expression rapidly decreases between $t = 0$ h to $t = 1$ h as fresh medium is added to the culture before increasing at $t = 4$ h as sugars are metabolized and acetate becomes available in the environment (triangles in **Figure 1B**) as previously reported (Bergholz et al., 2007).

The growth curve in **Figure 3A** shows the three characteristic phases of growth: lag phase between $t = 0$ h and $t = 2$ h, exponential phase from $t = 2$ h to $t = 5$ h, and stationary phase from $t = 5$ h onward. We considered gene regulation during each of these phases based on the \log_2 fold change in transcript levels at $t = 2$ h relative to $t = 0$ h, $t = 5$ h relative to $t = 2$ h, and $t = 7$ h relative to $t = 5$ h, respectively. Furthermore, for each growth phase we grouped the top 10% of upregulated genes, from the 4313 genes analyzed. Then for each KEGG pathway we determined the number of genes that were in the top 10% group. We then used goseq to calculate the probability of this number occurring when compared to the total number of genes in the pathway (p -value in **Figure 3**). For example, the KEGG pathway “Microbial metabolism in diverse environments” has 201 associated genes. Therefore, in the top 10% group of the upregulated genes from all pathways one would expect to find 20 genes associated to this KEGG pathway. However, in the top 10% group of upregulated genes during exponential phase, we identified 54 genes from the “Microbial metabolism in diverse environments” pathway. Therefore, this pathway was overrepresented in the 10% group of upregulated genes during exponential phase with a p -value



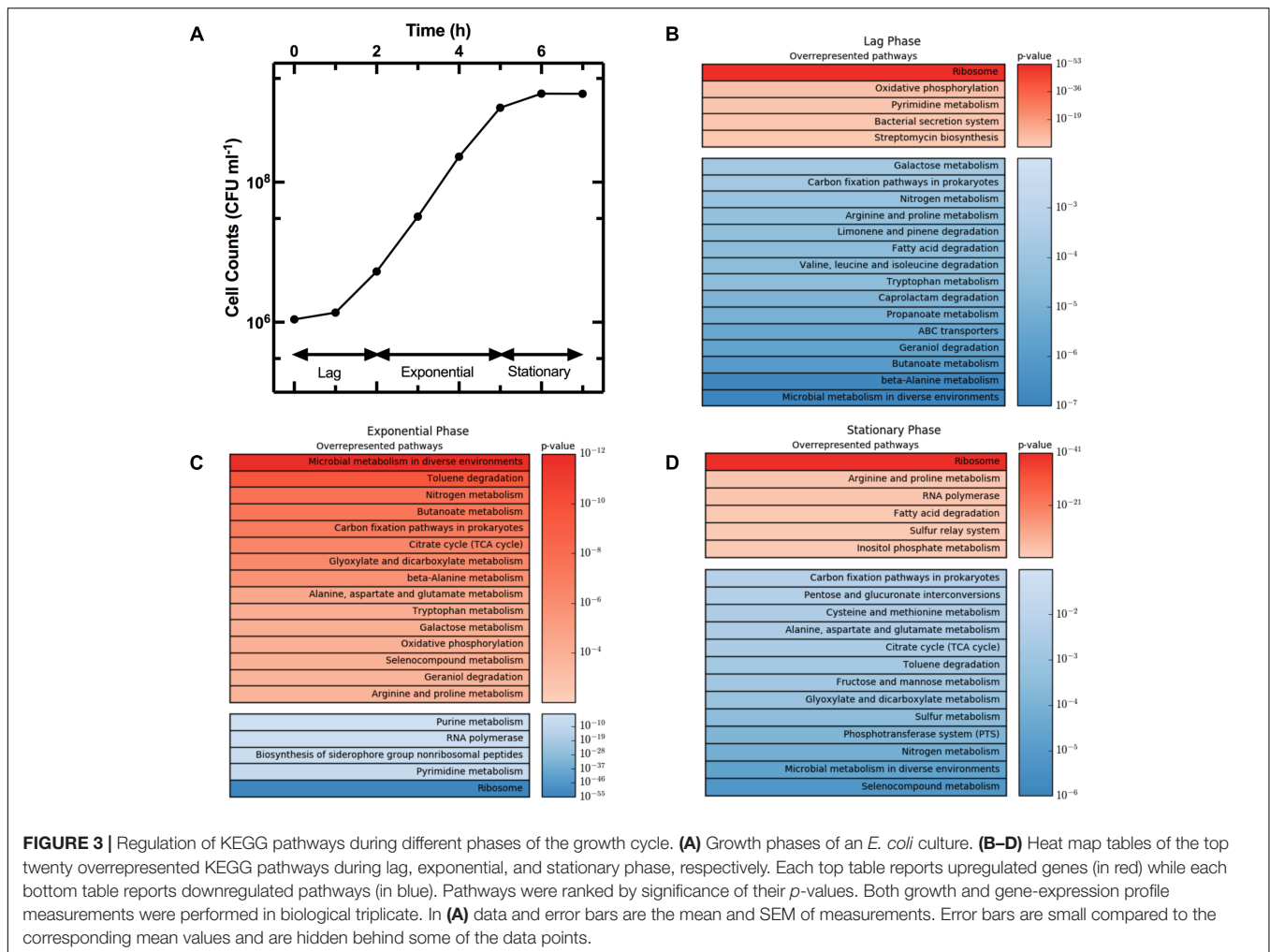


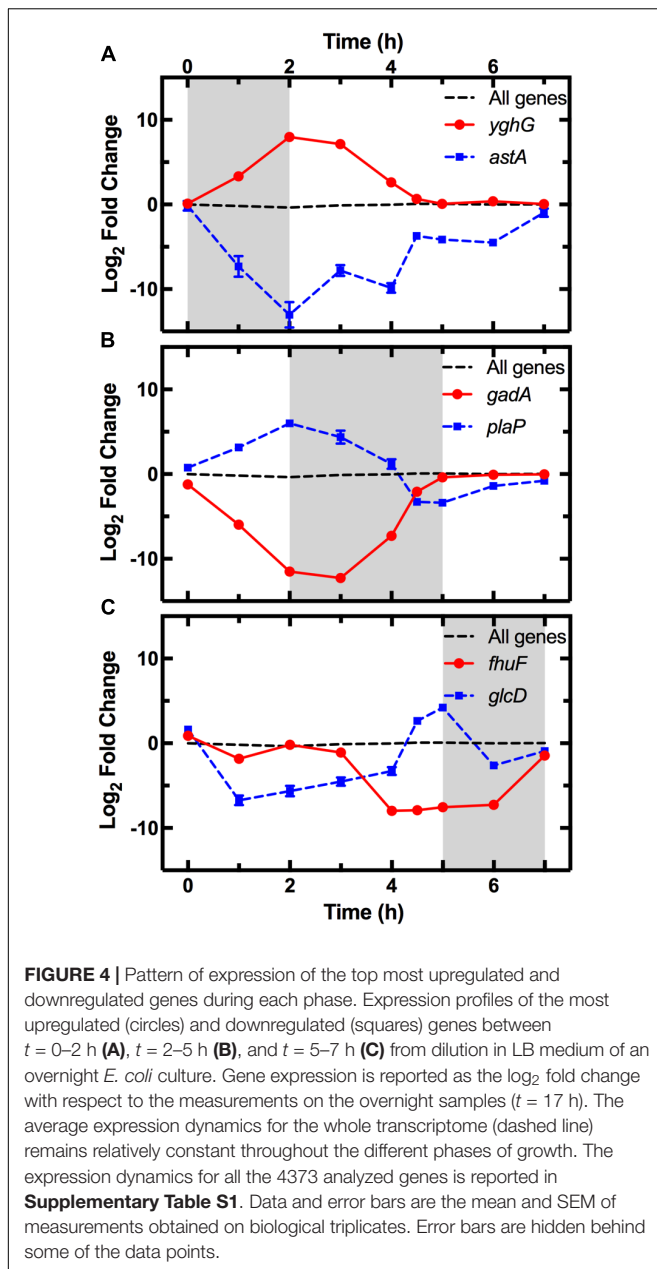
FIGURE 3 | Regulation of KEGG pathways during different phases of the growth cycle. **(A)** Growth phases of an *E. coli* culture. **(B–D)** Heat map tables of the top twenty overrepresented KEGG pathways during lag, exponential, and stationary phase, respectively. Each top table reports upregulated genes (in red) while each bottom table reports downregulated pathways (in blue). Pathways were ranked by significance of their *p*-values. Both growth and gene-expression profile measurements were performed in biological triplicate. In **(A)** data and error bars are the mean and SEM of measurements. Error bars are small compared to the corresponding mean values and are hidden behind some of the data points.

of 1.12×10^{-12} . We repeated this process for the top 10% downregulated genes, before ranking all the KEGG pathways by *p*-value, and reported the top 20 overrepresented pathways for the up- and downregulated genes (in red and blue, respectively, in **Figure 3**) during lag phase (**Figure 3B**), exponential phase (**Figure 3C**), and stationary phase (**Figure 3D**). **Supplementary Table S2** reports the *p*-value and number of genes in each of these pathways for lag, exponential, and stationary phase. We could not directly compare our results with previously reported datasets (Weber et al., 2005; Bergholz et al., 2007) because these studies did not employ the KEGG database. Therefore, we report below the expression of strongly regulated genes for each growth phase and discuss our findings in the context of data reported in previous studies investigating either persists or the influence of the medium composition on gene regulation.

The average expression dynamics for the whole transcriptome (dashed line in **Figure 4**) remained relatively constant throughout the different phases of growth. However, unlike previous reports (Chang et al., 2002), we found significant changes in the expression of several pathways during the lag phase ($t = 0$

$t = 2$ h). Metabolism pathways were strongly downregulated (**Figure 3B** bottom table and **Supplementary Table S2**) and in particular the most overrepresented of these KEGG pathways was “Microbial metabolism in diverse environments.” This pathway was previously found to play a key role in *Klebsiella pneumoniae* adaptation to cold or heat shocks (Tripathy et al., 2014). Among the 10 most downregulated genes, we found *astA* ($-13.0 \log_2$ fold change, squares in **Figure 4A**), *astB*, and *astC* in the AST pathway controlling arginine degradation; *gadA* and *gadB* controlling glutamate decarboxylase activity (De Biase et al., 1999); the biofilm regulator *bssR*; and the aldehyde dehydrogenase *aldB*. These genes were then all strongly induced during the exponential phase (between 8 and 10 \log_2 fold).

Among the upregulated pathways (**Figure 3B** top table and **Supplementary Table S2**), “Ribosome” was the most overrepresented indicating induction of the translation machinery. Furthermore, among the 10 most upregulated genes, we found *yghG* ($7.9 \log_2$ fold change, circles in **Figure 4A**) and *yghF* that were induced at $t = 1$ h and have previously been linked to type II secretion (Kim et al., 2017); *borD* encoding a



prophage lipoprotein; *proV*, *proW*, and *proX* also induced at $t = 1$ h, encoding parts of an ABC transporter for the uptake of glycine, betaine, and proline; *iraM* induced at $t = 1$ h and encoding an anti-adaptor protein that inhibits RpoS proteolysis; and *stpA* encoding a DNA-binding protein. *yghG*, *yghF*, *borD*, *iraM*, and *stpA* were then strongly downregulated (between -6 and $-8 \log_2$ fold) during exponential phase. Notably, gene-expression profiling during the lag phase was not reported in a previous transcriptomic study carried out on *E. coli* O157 (Bergholz et al., 2007).

During the exponential growth phase ($t = 2$ h to $t = 5$ h) there was an extensive reprogramming of gene-expression. The “Ribosome” pathway was the most overrepresented in the

top 10% downregulated genes, indicating repression of the translation machinery at the transition between exponential and stationary phase ($t = 5$ h) in response to the depletion of nutrients in the culture conditions. This was reflected in the measured division rate (**Supplementary Figure S6**). Among the 10 most downregulated genes, we found *plaP* ($-9.4 \log_2$ fold change, squares in **Figure 4B**) encoding a putrescine importer required for the induction of pili-driven motility, in accordance with the reported low motility of exponentially growing *E. coli* (Amsler et al., 1993); *cspA* encoding a cold shock protein; *fhuF* encoding an iron reductase protein; *lpxT* encoding the lipid A 1-diphosphate synthase; *fecA* encoding an outer membrane receptor in the Fe^{3+} dicitrate transport system; and the above discussed *yghF*, *fhuF* and *plaP* were then upregulated by a factor of 6 and 2 \log_2 fold, respectively, during stationary phase.

Metabolism related pathways were upregulated with “Microbial metabolism in diverse environments” now being the most overrepresented KEGG pathway (**Figure 3C** top table). Among the 10 most upregulated genes, we found *gadA* ($11.1 \log_2$ fold change, circles in **Figure 4B**), *gadB*, *gadC*, and *gadE* that were induced at $t = 4$ h and whose upregulation at the transition between exponential and stationary phase have previously been reported (De Biase et al., 1999; Weber et al., 2005; Bergholz et al., 2007); *glcD* and *glcE* induced at $t = 3.5$ h, encoding a subunit of the glycolate oxidase; *narU* induced at $t = 3$ h, encoding a nitrate and nitrite inner membrane transporter; *aldB* already discussed above; and *tnaC* discussed below. *glcD*, *glcE*, and *tnaC* were then downregulated during the stationary phase. The *tnaC* gene is part of the *tnaCAB* operon that regulates tryptophan catabolism and is comprised of a 24 residue upstream peptide TnaC, the tryptophanase TnaA, and the low affinity tryptophan permease TnaB (Konan and Yanofsky, 1997). TnaA is responsible for the breakdown of tryptophan, which is utilized by *E. coli* as an energy source to produce pyruvate, ammonia, and indole (Luli and Strohl, 1990). Interestingly, as the sugars were depleted in the culture, we observed an increase in expression of the *tnaCAB* operon (**Supplementary Table S1**). This was in accordance with a previous proteomic study carried out on *E. coli* K12 BW25113 growing on minimal medium (Soufi et al., 2015), suggesting a correlation between tryptophan related gene and protein expression. Furthermore, Gaimster and Summers (2015) observed an increase in *tnaA* expression in a growing *E. coli* culture, correlating this to an increase in the concentration of extracellular indole (Gaimster et al., 2014). Finally, we also observed an upregulation of transport genes including *ompF* and *lamB* encoding two of the major *E. coli* outer membrane porins (**Supplementary Table S1**), which was not previously observed (Bergholz et al., 2007).

Metabolism related pathways were downregulated as the population entered stationary phase ($t = 5$ h to $t = 7$ h) with “Microbial metabolism in diverse environments” now being the most overrepresented KEGG pathway (**Figure 3D** bottom table). This coincided with the previously mentioned reduction in sugar availability (**Figure 1B**). Almost all of the genes in the phosphoenolpyruvate (PEP)-dependent phosphotransferase system (PTS) pathway, a major bacterial mechanism for the accumulation of carbohydrates (Shimizu, 2013), were

downregulated as the bacteria moved from late-exponential to stationary phase (**Figure 3D**). The downregulation of the PTS pathway may cause reduced levels of glycolysis intermediates such as fructose 1,6-bisphosphate (FDP), which in *E. coli* results in the activation of *cra* and the subsequent transcriptional repression of *pfkA* and *pykF* (Shimizu, 2013). Both *pykF* and *pfkA* were downregulated as the culture transitioned from exponential to stationary phase (**Supplementary Figure S7**) resulting in the downregulation of the TCA cycle (**Figure 3D**). This is in agreement with a previous transcriptomic study carried out on *E. coli* O157, reporting a downregulation of the tricarboxylic acid (TCA) cycle pathway after $t = 4.5$ h compared to $t = 3$ h growth on minimal medium (Bergholz et al., 2007). Similarly, we found agreement between Bergholz's data and ours on the downregulation of the sulfur metabolism pathway, sulfur being present in LB and instrumental for the biosynthesis of the amino acids cysteine and methionine (Sekowska et al., 2000).

Among the 10 most downregulated genes were *glcD* (-5.1 \log_2 fold change, squares in **Figure 4C**), *glcE*, *glcA*, and *glcB*; *ansB* encoding L-asparaginase 2; *fumB* encoding a fumarate hydratase; and *adiY* encoding a transcriptional regulator. *glcD*, *glcE*, *glcA*, and *glcB* were further downregulated during the lag phase. Finally, genes encoding transporters including *ompF* and *lamB*, were also downregulated as previously reported (Chang et al., 2002).

The "Ribosome" pathway was the most overrepresented in the top 10% upregulated genes. However, the mean expression of all the 48 genes in this pathway was downregulated by a factor of 2.8 \log_2 fold at $t = 7$ h compared to $t = 2$ h. Among the 10 most upregulated genes, we identified *fhuF* (6.1 \log_2 fold change, circles in **Figure 4C**); *astA*, *astC*, and *astE* in the AST pathway, that were induced at $t = 6$ h; *prpB* induced at $t = 4$ h, encoding the 2-methylisocitrate lyase; *bfd* encoding bacterioferritin-associated ferredoxin; *rmf* induced at $t = 4$ h, encoding a ribosome modulation factor; *ynfM* encoding an inner membrane transporter; *sodA* induced at $t = 6$ h, encoding a superoxide dismutase, previously associated with the emergence of metabolic heterogeneity during nutrient starvation (Şimşek and Kim, 2018); and *obgE* encoding the essential GTPase ObgE/CgtA. In the AST pathway, *rmf*, *ynfM*, and *prpB* were then strongly downregulated (between -5 and -10 \log_2 fold) during lag phase. Furthermore, a major regulator of the stress response in bacteria, particularly their entry into stationary phase, is the sigma factor *rpoS* controlling the expression of approximately 10% of genes in *E. coli* (Weber et al., 2005). Our data shows that *rpoS* expression increases rapidly as the culture enters stationary phase (**Supplementary Figure S8**), in accordance with previously reported data (2.4 and 2.8 \log_2 fold change, respectively, between $t = 4$ h and 5 h from inoculation) (Bergholz et al., 2007). Bergholz, et al. also reported that the most highly upregulated gene during the transition to stationary phase was *acs*, which encodes acetyl CoA synthetase, confirming the data reported in a separate study on *E. coli* MG1655 (Baev et al., 2006). Similarly, between $t = 4$ h and $t = 4.5$ h from inoculation, we observe a 7.4 \log_2 fold change in the expression of *acs* and 4.7 \log_2 fold change of *aceB* expression,

in accordance with Bergholz, et al. who reported a 5.4 \log_2 fold change for *aceB* during the same temporal window. These data suggest that at least some *E. coli* responses to changes in growth medium are conserved across evolutionary distance and are not specific to the growth medium employed. All together, our data on the reprogramming of the culture gene-expression during the transitions between the different growth phases (**Figures 3, 4** and **Supplementary Tables S1, S2**) will be relevant for studying the responses of microbial communities to environmental changes.

Growth Stage Dependent Persister Formation

We then studied the growth cycle dependence of phenotypic heterogeneity within the population by measuring persistence to antibiotics as a phenotypic proxy. We used three antibiotics with distinct modes of action: ampicillin, gentamicin, and ofloxacin. Specifically, ampicillin is a β -lactam that binds to the penicillin-binding proteins located inside the bacterial cell wall. It inhibits the last stage of bacterial cell wall synthesis leading to lysis mediated by autolytic enzymes. Gentamicin is an aminoglycoside that works by irreversibly binding to the 30S subunit of the bacterial ribosome, thereby interrupting protein synthesis. Ofloxacin is a second-generation fluoroquinolone that acts on DNA gyrase and topoisomerase IV, and thus altering the control of DNA supercoiling and inhibiting normal cell division (Aldred et al., 2014).

To investigate the growth-dependent heterogeneity of the response to each antibiotic, we performed two different treatments (see **Supplementary Figure S1**): three culture aliquots were injected with antibiotic and fresh LB (**Supplementary Figure S1F**), while three other aliquots were injected with antibiotic only (**Supplementary Figure S1G**). In both cases, the final antibiotic concentration was 25 \times the antibiotic MIC. For each time point and each antibiotic treatment, we then calculated the ratio between the measured number of persisters in the culture relative to the total number of bacteria in the culture (**Figure 3A**), defining this as the persister fraction. We finally normalized each persister fraction dataset to their maximum values.

When gentamicin was added to the culture aliquots with fresh LB, the fraction of persisters showed a 3.4 \log_{10} fold increase between $t = 3$ h and $t = 4$ h, before remaining relatively constant for the remainder of the growth cycle (**Figure 5A**). When only gentamicin was added to the culture aliquots the fraction of persisters showed a similar pattern, except for a shift of 1 h, with a 3.6 \log_{10} fold increase between $t = 2$ h and $t = 3$ h (**Figure 5B**).

When ofloxacin was added to the culture aliquots with fresh LB, there was a small increase in the persister fraction during the lag phase (**Figure 5C**). However, the persister fraction showed a 2.6 \log_{10} fold increase during the exponential phase (between $t = 2$ h and $t = 4$ h) when only ofloxacin was added to the culture aliquots (**Figure 5D**).

When ampicillin was added to the culture aliquots with fresh LB, we measured a 2 \log_{10} fold increase in the persister fraction

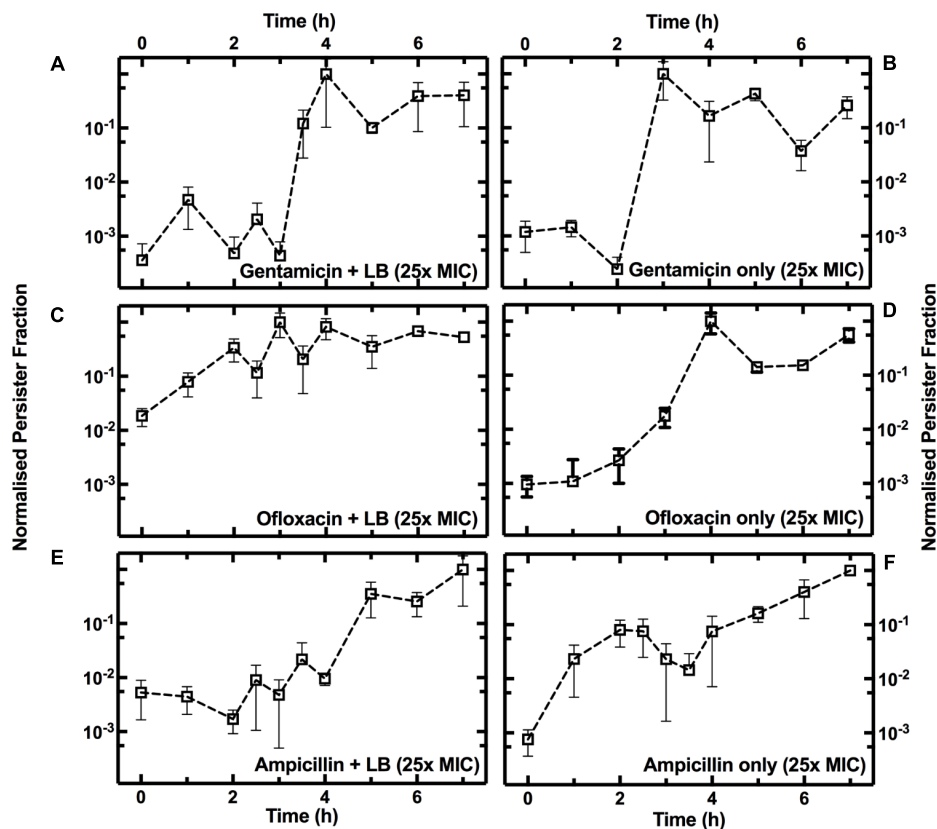


FIGURE 5 | Growth phase dependence of the fraction of persisters to gentamicin, ofloxacin, or ampicillin. Temporal dependence of the normalized fraction of persisters to treatment either with gentamicin (A), ofloxacin (C), or ampicillin (E), with the addition of fresh LB, or with antibiotics only [(B,D,F), respectively]. At $t = 0$ an overnight *E. coli* culture was diluted 1:1000 in LB medium and the culture growth started. Each data set is normalized to its maximum persister fraction. Data and error bars are the mean and SEM of measurements obtained at least on biological and technical triplicates.

during the stationary phase (Figure 5E). When only ampicillin was added to the culture aliquots, we measured a 1.5 log₁₀ fold increase in the fraction of persister cells during the lag phase ($t = 1$ h, Figure 5F).

Growth-dependent bacterial susceptibility has recently been reported (Greulich et al., 2015). Here, we demonstrate that as the composition of the medium in the culture environment changes, the microbial population becomes increasingly heterogeneous in response to the treatment to antibiotics with different modes of action.

Furthermore, antibiotic susceptibility and persister assays are often carried out by supplementing antibiotics with fresh LB medium (Wu et al., 2015; Orman and Brynildsen, 2016). We demonstrate that in the case of gentamicin, the addition of fresh LB medium does not substantially affect the dependence of persister fraction on growth phase. Indeed, it has recently been demonstrated that nutrient-rich environments do not increase susceptibility to antibiotics that irreversibly bind to the 30S subunit of the bacterial ribosome (Greulich et al., 2015). On the contrary, we observed that the formation of persisters to β -lactams and quinolones is strongly affected by the medium composition, suggesting that this should be carefully considered when screening for antibiotics against persister cells.

DISCUSSION

Within an isogenic population, there is inherent phenotypic heterogeneity which allows an adaptive response to an ever-changing extracellular environment (Balaban et al., 2004; Ryall et al., 2012; Nikolic et al., 2013; Kotte et al., 2014). For example, within a growing isogenic population of bacteria there are multiple growth phenotypes present, from exponentially growing to slow growing, or dormant bacteria (Ryall et al., 2012; Kotte et al., 2014). Persister cells are an example of a phenotype which differs from the majority of cells in a clonal population in terms of growth rate (Lewis, 2010; Maisonneuve et al., 2013), motility, gene expression, and cell size (Ryall et al., 2012). Furthermore, persister cells can be generated in response to a number of environmental conditions (Keren et al., 2004b; Vega et al., 2012; Bernier et al., 2013; Helaine et al., 2014), including nutrient limitation (Fung et al., 2010; Maisonneuve and Gerdes, 2014) and nutrient transitions (Amato et al., 2013) that also generate a variety of other bacterial responses (Lidstrom and Konopka, 2010).

Therefore, we utilized the persister phenotype as a proxy for changes in population-wide heterogeneity throughout the *E. coli* growth cycle where the environmental conditions are

constantly changing. We observed homogeneity in response to all antibiotics during lag phase with very few persisters to any of the tested antibiotics. However, the different persister fractions observed in response to the different antibiotics further emphasize the phenotypic heterogeneity within the population during the exponential and stationary phases. In fact, population based heterogeneity allows rapid response to alterations in the nutritional environment; it is only when the environment becomes favorable to a given subpopulation that they are able to dominate the whole population-level response (Lidstrom and Konopka, 2010). Indeed, within the growth cycle we observed changes in both nutrient availability (**Figure 1**) and pH (**Supplementary Figure S4**).

These changes in the culture medium also influenced the population transcriptome during the same temporal windows where we measured notable increases in the fraction of persisters. We observed upregulation of carbon fixation pathways and tryptophan metabolism (**Figure 3C**), potentially as a result of an increase in the concentration of extracellular indole (Gaimster et al., 2014). Indole has also been linked to persister cell formation (Vega et al., 2012, 2013) and the induced expression of a variety of drug exporters (Meng and Bennett, 1992; Balaban et al., 2004). Moreover, *ompF* and *lamB*, encoding two of the major outer membrane porins that have been associated with drug uptake (Ziervogel and Roux, 2013; Lin et al., 2014; Cama et al., 2015) were also upregulated at the whole population level during exponential phase (**Supplementary Table S1**).

In comparison, during stationary phase we observed a clear downregulation of metabolism related pathways (**Figure 3D**). The downregulation of the TCA cycle as the population moves from exponential to stationary phase (**Figure 3D**) results in the excretion of acetate into the extracellular environment and its subsequent utilization (**Figure 1**; Luli and Strohl, 1990; Shimizu, 2013). Kotte et al. (2010) modeled population adaptation to different nutrients *in silico*, showing that as glucose levels reduce, cells are predicted to utilize their natively produced acetate. This ability to adapt to nutrient availability appears to be a result of metabolic flux at the single-cell level (Kotte et al., 2010; Kochanowski et al., 2013) and results in the diversification of growing and non-growing phenotypes, such as persisters (Kotte et al., 2014). Indeed, we measured an increase in persister fraction in response to all three antibiotics as the available sugars become limited (**Figure 1**). However, each type of antibiotic reveals different levels of heterogeneity suggesting that different biological pathways underlie persistence to different antibiotics.

We also found that the outcome of antibiotic treatment is strongly influenced by the composition of the medium containing the antibiotic. In fact, the addition of antibiotics and fresh LB alters the native culture environment and causes a reduction in the number of persisters (**Figure 5**), reducing phenotypic heterogeneity within the *E. coli* community.

One of the current limitations within our knowledge of persister bacteria is that their transcriptome has been examined only after treatment with antibiotics (Keren et al., 2004b) owing to the lack of biomarkers to isolate persisters from the majority of susceptible cells before antibiotic challenge. However, antibiotic treatment is known to alter the bacterial transcriptome (Lewis,

2010). Our current study identifies molecular pathways that are strongly regulated at the whole population level when the environment changes and, coincidentally, the fraction of persisters within the population increases. Some of the identified pathways such as tryptophan metabolism and TCA cycle (Vega et al., 2012; Kotte et al., 2014), have indeed previously been associated with persisters. However, it is noteworthy that our approach measures the mean transcriptomic response of the whole population. Therefore, our measurements do not allow us to determine whether the pathways that we have identified are also strongly regulated in the minority of persister cells. Indeed, the differential response of persisters could be masked by that of the majority of susceptible cells. Considering that cell-to-cell variation increases with increasing mean gene-expression (Silander et al., 2012), these comprehensive data sets provide well defined culturing time points, medium compositions, and putative pathways that could be investigated with single-cell approaches (Henry and Brynildsen, 2016; Bamford et al., 2017) to determine molecular pathways that are differentially regulated in persisters compared to the majority of susceptible cells.

Our approach could easily be extended to investigate the dynamics of phenotypic heterogeneity in different microbial communities such as bacterial biofilms (Domka et al., 2007), natural yeast and fungal populations (LaFleur et al., 2010; Holland et al., 2014), or cancer cells (Hangauer et al., 2017) responding to a variety of environmental cues.

AUTHOR CONTRIBUTIONS

SP developed the project and designed the research. AS, AK, RB, CS, SF, and AK-S performed the experiments. PO, KM, and KP carried out sequencing. All authors analyzed and discussed the data. AS and SP wrote the paper.

FUNDING

This work was supported by a Royal Society Research Grant (RG140203), a Wellcome Trust Strategic Seed Corn Fund (WT097835/Z/11/Z), and a start up Grant from the University of Exeter awarded to SP. AS acknowledges support from the BBSRC through a SWBio-DTP studentship (BB/M009122/1). KP, KM, and PO would like to acknowledge support from the following awards: Wellcome Trust Institutional Strategic Support Fund (WT097835MF), Wellcome Trust Multi User Equipment Award (WT101650MA), and Medical Research Council Clinical Infrastructure Funding (MR/M008924/1). This work was partly supported by BBSRC award BB/1024631/1 to RT.

SUPPLEMENTARY MATERIAL

The Supplementary Material for this article can be found online at: <https://www.frontiersin.org/articles/10.3389/fmicb.2018.01739/full#supplementary-material>

REFERENCES

- Ackermann, M. (2015). A functional perspective on phenotypic heterogeneity in microorganisms. *Nat. Rev. Microbiol.* 13, 497–508. doi: 10.1038/nrmicro3491
- Aldred, K. J., Kerns, R. J., and Osheroff, N. (2014). Mechanism of quinolone action and resistance. *Biochemistry* 53, 1565–1574. doi: 10.1021/bi5000564
- Allison, K. R., Brynildsen, M. P., and Collins, J. J. (2011). Metabolite-enabled eradication of bacterial persisters by aminoglycosides. *Nature* 473, 216–220. doi: 10.1038/nature10069
- Amato, S. M., and Brynildsen, M. P. (2014). Nutrient transitions are a source of persisters in *Escherichia coli* biofilms. *PLoS One* 9:e93110. doi: 10.1371/journal.pone.0093110
- Amato, S. M., Orman, M. A., and Brynildsen, M. P. (2013). Metabolic control of persister formation in *Escherichia coli*. *Mol. Cell* 50, 475–487. doi: 10.1016/j.molcel.2013.04.002
- Amsler, C. D., Cho, M., and Matsumura, P. (1993). Multiple factors underlying the maximum motility of *Escherichia coli* as cultures enter post-exponential growth. *J. Bacteriol.* 175, 6238–6244. doi: 10.1128/jb.175.19.6238-6244.1993
- Arnoldini, M., Vizcarra, I. A., Peña-Miller, R., Stocker, N., Diard, M., Vogel, V., et al. (2014). Bistable expression of virulence genes in *Salmonella* leads to the formation of an antibiotic-tolerant subpopulation. *PLoS Biol.* 12:e1001928. doi: 10.1371/journal.pbio.1001928
- Baev, M. V., Baev, D., Radek, A. J., and Campbell, J. W. (2006). Growth of *Escherichia coli* MG1655 on LB medium: determining metabolic strategy with transcriptional microarrays. *Appl. Microbiol. Biotechnol.* 71, 323–328. doi: 10.1007/s00253-006-0392-8
- Balaban, N. Q., Merrin, J., Chait, R., Kowalik, L., and Leibler, S. (2004). Bacterial persistence as a phenotypic switch. *Science* 305, 1622–1625. doi: 10.1126/science.1099390
- Bamford, R. A., Smith, A., Metz, J., Glover, G., Titball, R. W., and Pagliara, S. (2017). Investigating the physiology of viable but non-culturable bacteria by microfluidics and time-lapse microscopy. *BMC Biol.* 15:121. doi: 10.1186/s12915-017-0465-4
- Beaumont, H. J. E., Gallie, J., Kost, C., Ferguson, G. C., and Rainey, P. B. (2009). Experimental evolution of bet hedging. *Nature* 462, 90–93. doi: 10.1038/nature08504
- Bergholz, T. M., Wick, L. M., Qi, W., Riordan, J. T., Ouellette, L. M., and Whittam, T. S. (2007). Global transcriptional response of *Escherichia coli* O157:H7 to growth transitions in glucose minimal medium. *BMC Microbiol.* 7:97. doi: 10.1186/1471-2180-7-97
- Bernier, S. P., Lebeaux, D., DeFrancesco, A. S., Valomon, A., Soubigou, G., Coppée, J. Y., et al. (2013). Starvation, together with the SOS response, mediates high biofilm-specific tolerance to the fluoroquinolone ofloxacin. *PLoS Genet.* 9:e1003144. doi: 10.1371/journal.pgen.1003144
- Bódi, Z., Farkas, Z., Nevozhay, D., Kalapis, D., Lázár, V., Csörgő, B., et al. (2017). Phenotypic heterogeneity promotes adaptive evolution. *PLoS Biol.* 15:e2000644. doi: 10.1371/journal.pbio.2000644
- Brauner, A., Fridman, O., Gefen, O., and Balaban, N. Q. (2016). Distinguishing between resistance, tolerance and persistence to antibiotic treatment. *Nat. Rev. Microbiol.* 14, 320–330. doi: 10.1038/nrmicro.2016.34
- Cama, J., Bajaj, H., Pagliara, S., Maier, T., Braun, Y., Winterhalter, M., et al. (2015). Quantification of fluoroquinolone uptake through the outer membrane channel ompf of *Escherichia coli*. *J. Am. Chem. Soc.* 137, 13836–13843. doi: 10.1021/jacs.5b08960
- Cama, J., Chimere, C., Pagliara, S., Javer, A., and Keyser, U. F. (2014). A label-free microfluidic assay to quantitatively study antibiotic diffusion through lipid membranes. *Lab Chip* 14, 2303–2308. doi: 10.1039/c4lc00217b
- Chang, D., Smalley, D. J., and Conway, T. (2002). Gene expression profiling of *Escherichia coli* growth transitions: an expanded stringent response model. *Mol. Microbiol.* 45, 289–306. doi: 10.1046/j.1365-2958.2002.03001.x
- Chien, A.-C., Hill, N. S., and Levin, P. A. (2012). Cell size control in bacteria. *Curr. Biol.* 22, R340–R349. doi: 10.1016/j.cub.2012.02.032
- De Biase, D., Tramonti, A., Bossa, F., and Visca, P. (1999). The response to stationary-phase stress conditions in *Escherichia coli*: role and regulation of the glutamic acid decarboxylase system. *Mol. Microbiol.* 32, 1198–1211. doi: 10.1046/j.1365-2958.1999.01430.x
- Domka, J., Lee, J., Bansal, T., and Wood, T. K. (2007). Temporal gene-expression in *Escherichia coli* K-12 biofilms. *Environ. Microbiol.* 9, 332–346. doi: 10.1111/j.1462-2920.2006.01143.x
- Elowitz, M., Levine, A., Siggia, E., and Swain, P. (2002). Stochastic gene expression in a single cell. *Science* 297, 1183–1186. doi: 10.1126/science.1070919
- Fung, D. K. C., Chan, E. W. C., Chin, M. L., and Chan, R. C. Y. (2010). Delineation of a bacterial starvation stress response network which can mediate antibiotic tolerance development. *Antimicrob. Agents Chemother.* 54, 1082–1093. doi: 10.1128/AAC.01218-09
- Gaimster, H., Cama, J., Hernández-Ainsa, S., Keyser, U. F., and Summers, D. K. (2014). The indole pulse: a new perspective on indole signalling in *Escherichia coli*. *PLoS One* 9:e93168. doi: 10.1371/journal.pone.0093168
- Gaimster, H., and Summers, D. (2015). Regulation of indole signalling during the transition of *E. coli* from exponential to stationary phase. *PLoS One* 10:e0136691. doi: 10.1371/journal.pone.0136691
- Greulich, P., Scott, M., Evans, M. R., and Allen, R. J. (2015). Growth-dependent bacterial susceptibility to ribosome-targeting antibiotics. *Mol. Syst. Biol.* 11:796. doi: 10.15252/msb.20145949
- Hangauer, M. J., Viswanathan, V. S., Ryan, M. J., Bole, D., Eaton, J. K., Matov, A., et al. (2017). Drug-tolerant persister cancer cells are vulnerable to GPX4 inhibition. *Nature* 551, 247–250. doi: 10.1038/nature24297
- Hansen, S., Lewis, K., and Vulić, M. (2008). Role of global regulators and nucleotide metabolism in antibiotic tolerance in *Escherichia coli*. *Antimicrob. Agents Chemother.* 52, 2718–2726. doi: 10.1128/AAC.00144-08
- Hayes, E. T., Wilks, J. C., Sanfilippo, P., Yohannes, E., Tate, D. P., Jones, B. D., et al. (2006). Oxygen limitation modulates pH regulation of catabolism and hydrogenases, multidrug transporters, and envelope composition in *Escherichia coli* K-12. *BMC Microbiol.* 6:89. doi: 10.1186/1471-2180-6-89
- Helaine, S., Cheverton, A., Watson, K., Faure, L., Matthews, S., and Holden, D. (2014). Internalization of *Salmonella* by macrophages induces formation of nonreplicating persisters. *Science* 343, 204–208. doi: 10.1126/science.1244705
- Henry, T. C., and Brynildsen, M. P. (2016). Development of persister-FACSeq: a method to massively parallelize quantification of persister physiology and its heterogeneity. *Sci. Rep.* 6:25100. doi: 10.1038/srep25100
- Holland, S. L., Reader, T., Dyer, P. S., and Avery, S. V. (2014). Phenotypic heterogeneity is a selected trait in natural yeast populations subject to environmental stress. *Environ. Microbiol.* 16, 1729–1740. doi: 10.1111/1462-2920.12243
- Hua, Q., Yang, C., Oshima, T., Mori, H., and Shimizu, K. (2004). Analysis of gene expression in *Escherichia coli* in response to changes of growth-limiting nutrient in chemostat cultures. *Appl. Environ. Microbiol.* 70, 2354–2366. doi: 10.1128/AEM.70.4.2354-2366.2004
- Johnson, P. J. T., and Levin, B. R. (2013). Pharmacodynamics, population dynamics, and the evolution of persistence in *Staphylococcus aureus*. *PLoS Genet.* 9:e1003123. doi: 10.1371/journal.pgen.1003123
- Kaern, M., Elston, T. C., Blake, W. J., and Collins, J. J. (2005). Stochasticity in gene expression: from theories to phenotypes. *Nat. Rev. Genet.* 6, 451–464. doi: 10.1038/nrg1615
- Kanehisa, M., Furumichi, M., Tanabe, M., Sato, Y., and Morishima, K. (2017). KEGG: new perspectives on genomes, pathways, diseases and drugs. *Nucleic Acids Res.* 45, D353–D361. doi: 10.1093/nar/gkx1092
- Kanehisa, M., Sato, Y., Kawashima, M., Furumichi, M., and Tanabe, M. (2016). KEGG as a reference resource for gene and protein annotation. *Nucleic Acids Res.* 44, D457–D462. doi: 10.1093/nar/gkv1070
- Keren, I., Kaldalu, N., Spoering, A., Wang, Y., and Lewis, K. (2004a). Persister cells and tolerance to antimicrobials. *FEMS Microbiol. Lett.* 230, 13–18. doi: 10.1016/S0378-1097(03)00856-5
- Keren, I., Shah, D., Spoering, A., Kaldalu, N., and Lewis, K. (2004b). Specialized persister cells and the mechanism of multidrug tolerance in *Escherichia coli*. *J. Bacteriol.* 186, 8172–8180.
- Kim, S., Jeong, H., Kim, E. Y., Kim, J. F., Lee, S. Y., and Yoon, S. H. (2017). Genomic and transcriptomic landscape of *Escherichia coli* BL21(DE3). *Nucleic Acids Res.* 45, 5285–5293. doi: 10.1093/nar/gkx228
- Kleman, G. L., and Strohl, W. R. (1994). Acetate metabolism by *Escherichia coli* in high-cell-density fermentation. *Appl. Environ. Microbiol.* 60, 3952–3958.

- Klumpp, S., and Hwa, T. (2015). Bacterial growth: global effects on gene expression, growth feedback and proteome partition. *Curr. Opin. Biotechnol.* 28, 96–102. doi: 10.1016/j.copbio.2014.01.001
- Kochanowski, K., Volkmer, B., Gerosa, L., Haverkorn van Rijsewijk, B. R., Schmidt, A., and Heinemann, M. (2013). Functioning of a metabolic flux sensor in *Escherichia coli*. *Proc. Natl. Acad. Sci. U.S.A.* 110, 1130–1135. doi: 10.1073/pnas.1202582110
- Konan, K. V., and Yanofsky, C. (1997). Regulation of the *Escherichia coli* tna operon: nascent leader peptide control at the tnaC stop codon. *J. Bacteriol.* 179, 1774–1779. doi: 10.1128/jb.179.5.1774-1779.1997
- Kotte, O., Volkmer, B., Radzikowski, J. L., and Heinemann, M. (2014). Phenotypic bistability in *Escherichia coli*'s central carbon metabolism. *Mol. Syst. Biol.* 10:736. doi: 10.15252/msb.20135022
- Kotte, O., Zaugg, J. B., and Heinemann, M. (2010). Bacterial adaptation through distributed sensing of metabolic fluxes. *Mol. Syst. Biol.* 6, 1–9. doi: 10.1038/msb.2010.10
- LaFleur, M. D., Kumamoto, C. A., and Lewis, K. (2006). *Candida albicans* biofilms produce antifungal-tolerant persister cells. *Antimicrob. Agents Chemother.* 50, 3839–3846. doi: 10.1128/AAC.00684-06
- LaFleur, M. D., Qi, Q., and Lewis, K. (2010). Patients with long-term oral carriage harbor high-persister mutants of *Candida albicans*. *Antimicrob. Agents Chemother.* 54, 39–44. doi: 10.1128/AAC.00860-09
- Lewis, K. (2010). Persister cells. *Annu. Rev. Microbiol.* 64, 357–372. doi: 10.1146/annurev.micro.112408.134306
- Lidstrom, M. E., and Konopka, M. C. (2010). The role of physiological heterogeneity in microbial population behavior. *Nat. Chem. Biol.* 6, 705–712. doi: 10.1038/nchembio.436
- Lin, X. M., Yang, M. J., Li, H., Wang, C., and Peng, X. X. (2014). Decreased expression of LamB and Odp1 complex is crucial for antibiotic resistance in *Escherichia coli*. *J. Proteomics* 98, 244–253. doi: 10.1016/j.jpro.2013.12.024
- Losen, M., Frölich, B., Pohl, M., and Büchs, J. (2004). Effect of oxygen limitation and medium composition on *Escherichia coli* fermentation in shake-flask cultures. *Biotechnol. Prog.* 20, 1062–1068. doi: 10.1021/bp034282t
- Love, M. I., Huber, W., and Anders, S. (2014). Moderated estimation of fold change and dispersion for RNA-seq data with DESeq2. *Genome Biol.* 15, 1–21. doi: 10.1186/s13059-014-0550-8
- Luidalepp, H., Joers, A., Kaldalu, N., and Tenson, T. (2011). Age of inoculum strongly influences persister frequency and can mask effects of mutations implicated in altered persistence. *J. Bacteriol.* 193, 3598–3605. doi: 10.1128/JB.00085-11
- Luli, G. W., and Strohl, W. R. (1990). Comparison of growth, acetate production, and acetate inhibition of *Escherichia coli* strains in batch and fed-batch fermentations. *Appl. Environ. Microbiol.* 56, 1004–1011.
- Maisonneuve, E., Castro-Camargo, M., and Gerdes, K. (2013). (p)ppGpp controls bacterial persistence by stochastic induction of toxin-antitoxin activity. *Cell* 154, 1140–1150. doi: 10.1016/j.cell.2013.07.048
- Maisonneuve, E., and Gerdes, K. (2014). Molecular mechanisms underlying bacterial persisters. *Cell* 157, 539–548. doi: 10.1016/j.cell.2014.02.050
- Megaw, J., and Gilmore, B. F. (2017). Archaeal persisters: persister cell formation as a stress response in *Haloferax volcanii*. *Front. Microbiol.* 8:1589. doi: 10.3389/fmicb.2017.01589
- Meng, S. Y., and Bennett, G. N. (1992). Nucleotide sequence of the *Escherichia coli* cad operon: a system for neutralization of low extracellular pH. *J. Bacteriol.* 174, 2659–2669. doi: 10.1128/jb.174.8.2659-2669.1992
- Mulcahy, L. R., Burns, J. L., Lory, S., and Lewis, K. (2010). Emergence of *Pseudomonas aeruginosa* strains producing high levels of persister cells in patients with cystic fibrosis. *J. Bacteriol.* 192, 6191–6199. doi: 10.1128/JB.01651-09
- New, A. M., Cerulus, B., Govers, S. K., Perez-Samper, G., Zhu, B., Boogmans, S., et al. (2014). Different levels of catabolite repression optimize growth in stable and variable environments. *PLoS Biol.* 12:e1001764. doi: 10.1371/journal.pbio.1001764
- Nikolic, N., Barner, T., and Ackermann, M. (2013). Analysis of fluorescent reporters indicates heterogeneity in glucose uptake and utilization in clonal bacterial populations. *BMC Microbiol.* 13:258. doi: 10.1186/1471-2180-13-258
- Ogata, H., Goto, S., Sato, K., Fujibuchi, W., Bono, H., and Kanehisa, M. (1999). KEGG: Kyoto encyclopedia of genes and genomes. *Nucleic Acids Res.* 27, 29–34. doi: 10.1093/nar/27.1.29
- Orman, M. A., and Brynildsen, M. P. (2016). Persister formation in *Escherichia coli* can be inhibited by treatment with nitric oxide. *Free Radic. Biol. Med.* 93, 145–154. doi: 10.1016/j.freeradbiomed.2016.02.003
- Radzikowski, J. L., Vedelaar, S., Siegel, D., Ortega, Á.D., Schmidt, A., and Heinemann, M. (2016). Bacterial persistence is an active σ S stress response to metabolic flux limitation. *Mol. Syst. Biol.* 12:882. doi: 10.15252/msb.20166998
- Ryall, B., Eydallin, G., and Ferenci, T. (2012). Culture history and population heterogeneity as determinants of bacterial adaptation: the adaptomics of a single environmental transition. *Microbiol. Mol. Biol. Rev.* 76, 597–625. doi: 10.1128/MMBR.05028-11
- Schreiber, F., Littmann, S., Lavik, G., Escrig, S., Meibom, A., Kuypers, M. M. M., et al. (2016). Phenotypic heterogeneity driven by nutrient limitation promotes growth in fluctuating environments. *Nat. Microbiol.* 1, 1–7. doi: 10.1038/nmicrobiol.2016.55
- Scott, M., Gunderson, C. W., Mateescu, E. M., Zhang, Z., and Hwa, T. (2010). Interdependence of cell growth origins and consequences. *Science* 330, 1099–1102. doi: 10.1126/science.1192588
- Sekowska, A., Kung, H., and Danchin, A. (2000). Sulfur metabolism in *Escherichia coli* and related bacteria: facts and fiction. *J. Mol. Microbiol. Biotechnol.* 2, 145–177.
- Sezonov, G., Joseleau-Petit, D., and D'Ari, R. (2007). *Escherichia coli* physiology in Luria-Bertani broth. *J. Bacteriol.* 189, 8746–8749. doi: 10.1128/JB.01368-07
- Sheik, A. R., Muller, E. E. L., Audinot, J. N., Lebrun, L. A., Grysan, P., Guignard, C., et al. (2016). In situ phenotypic heterogeneity among single cells of the filamentous bacterium *Candidatus Microthrix parvicella*. *ISME J.* 10, 1274–1279. doi: 10.1038/ismej.2015.181
- Shimizu, K. (2013). Regulation systems of bacteria such as *Escherichia coli* in response to nutrient limitation and environmental stresses. *Metabolites* 4, 1–35. doi: 10.3390/metabo4010001
- Silander, O. K., Nikolic, N., Zaslaver, A., Bren, A., Kikoin, I., Alon, U., et al. (2012). A genome-wide analysis of promoter-mediated phenotypic noise in *Escherichia coli*. *PLoS Genet.* 8:e1002443. doi: 10.1371/journal.pgen.1002443
- Şimşek, E., and Kim, M. (2018). The emergence of metabolic heterogeneity and diverse growth responses in isogenic bacterial cells. *ISME J.* 12, 1199–1209. doi: 10.1038/s41396-017-0036-2
- Soufi, B., Krug, K., Harst, A., and Macek, B. (2015). Characterization of the *E. coli* proteome and its modifications during growth and ethanol stress. *Front. Microbiol.* 6:103. doi: 10.3389/fmicb.2015.00103
- Stincone, A., Daudi, N., Rahman, A. S., Antczak, P., Henderson, I., Cole, J., et al. (2011). A systems biology approach sheds new light on *Escherichia coli* acid resistance. *Nucleic Acids Res.* 39, 7512–7528. doi: 10.1093/nar/gkr338
- Tripathy, S., Sen, R., Padhi, S. K., Mohanty, S., and Maiti, N. K. (2014). Upregulation of transcripts for metabolism in diverse environments is a shared response associated with survival and adaptation of *Klebsiella pneumoniae* in response to temperature extremes. *Funct. Integr. Genomics* 14, 591–601. doi: 10.1007/s10142-014-0382-3
- Veening, J. W., Igooshin, O. A., Eijlander, R. T., Nijland, R., Hamoen, L. W., and Kuipers, O. P. (2008). Transient heterogeneity in extracellular protease production by *Bacillus subtilis*. *Mol. Syst. Biol.* 4, 1–15. doi: 10.1038/msb.2008.18
- Vega, N. M., Allison, K. R., Khalil, A. S., and Collins, J. J. (2012). Signaling-mediated bacterial persister formation. *Nat. Chem. Biol.* 8, 431–433. doi: 10.1038/nchembio.915
- Vega, N. M., Allison, K. R., Samuels, A. N., Klempner, M. S., and Collins, J. J. (2013). *Salmonella typhimurium* intercepts *Escherichia coli* signaling to enhance antibiotic tolerance. *Proc. Natl. Acad. Sci. U.S.A.* 110, 14420–14425. doi: 10.1073/pnas.1308085110
- Venturelli, O. S., Zuleta, I., Murray, R. M., and El-Samad, H. (2015). Population diversification in a yeast metabolic program promotes anticipation of environmental shifts. *PLoS Biol.* 13:e1002042. doi: 10.1371/journal.pbio.1002042

- Vital, M., Chai, B., Østman, B., Cole, J., Konstantinidis, K. T., and Tiedje, J. M. (2015). Gene expression analysis of *E. coli* strains provides insights into the role of gene regulation in diversification. *ISME J.* 9, 1130–1140. doi: 10.1038/ismej.2014.204
- Weart, R. B., Lee, A. H., Chien, A. C., Haeusser, D. P., Hill, N. S., and Levin, P. A. (2007). A metabolic sensor governing cell size in bacteria. *Cell* 130, 335–347. doi: 10.1016/j.cell.2007.05.043
- Weber, H., Polen, T., Heuveling, J., Wendisch, V. F., and Hengge, R. (2005). Genome-wide analysis of the general stress response network in *Escherichia coli*: σ^S -dependent genes, promoters, and sigma factor selectivity. *J. Bacteriol.* 187, 1591–1603. doi: 10.1128/JB.187.5.1591-1603.2005
- Wu, N., He, L., Cui, P., Wang, W., Yuan, Y., Liu, S., et al. (2015). Ranking of persister genes in the same *Escherichia coli* genetic background demonstrates varying importance of individual persister genes in tolerance to different antibiotics. *Front. Microbiol.* 6:1003. doi: 10.3389/fmicb.2015.01003
- Yao, Z., Davis, R. M., Kishony, R., Kahne, D., and Ruiz, N. (2012). Regulation of cell size in response to nutrient availability by fatty acid biosynthesis in *Escherichia coli*. *Proc. Natl. Acad. Sci. U.S.A.* 109, E2561–E2568. doi: 10.1073/pnas.1209742109
- Ziervogel, B. K., and Roux, B. (2013). The binding of antibiotics in OMPF porin. *Structure* 21, 76–87. doi: 10.1016/j.str.2012.10.014
- Conflict of Interest Statement:** The authors declare that the research was conducted in the absence of any commercial or financial relationships that could be construed as a potential conflict of interest.
- Copyright © 2018 Smith, Kaczmar, Bamford, Smith, Frustaci, Kovacs-Simon, O'Neill, Moore, Paszkiewicz, Titball and Pagliara. This is an open-access article distributed under the terms of the Creative Commons Attribution License (CC BY). The use, distribution or reproduction in other forums is permitted, provided the original author(s) and the copyright owner(s) are credited and that the original publication in this journal is cited, in accordance with accepted academic practice. No use, distribution or reproduction is permitted which does not comply with these terms.

2.2 Supplementary material

The culture environment influences both gene regulation and phenotypic heterogeneity in *Escherichia coli*

Ashley Smith^{1,2}, Agnieszka Kaczmar^{1,2}, Rosemary A. Bamford^{1,2}, Christopher Smith², Simona Frustaci¹, Andrea Kovacs-Simon², Paul O'Neill², Karen Moore², Konrad Paszkiewicz², Richard W. Titball², Stefano Pagliara^{1,2*}

¹Living Systems Institute, University of Exeter, Exeter, UK

²Biosciences, University of Exeter, Exeter, UK

* **Correspondence:**

Stefano Pagliara

s.pagliara@exeter.ac.uk

Supplementary Figures and Tables

Supplementary Tables –

Please note: the tables are deposited online at:

<https://www.frontiersin.org/articles/10.3389/fmicb.2018.01739/full#supplementary-material>

Table S1. A comprehensive data set of gene expression profiling at the different phases of growth. Columns A-D report each gene b, JWID, and ID number and name, respectively. DESeq2 was used to normalize the raw transcript reads using the median of ratios method and correcting for library size. Columns E and F report the mean, and standard error of the mean, calculated by averaging measurements of normalized transcript reads obtained from three t=17 h culture aliquots. Columns G-Z report the mean, and standard error of the mean, of the \log_2 fold change in normalized transcript reads on the samples at t=0, 1, 2, 3, 3.5, 4, 4.5, 5, 6, and 7h post dilution, respectively, relative to the normalized transcript reads of the t=17h sample.

Table S2. Overrepresented pathways during each growth phase. The table reports the top 20 overrepresented KEGG pathways. The top 10% of up or down differentially expressed genes were selected and goseq used to identify the overrepresented KEGG pathways for each phase of growth. Column A reports if these pathways were up or down regulated. Column B reports the name of the pathway. Column C gives the calculated p value. Column D shows the number of genes that were differentially expressed (number of genes that were in the top 10% of up or down regulated genes, respectively). Column E reports the total number of genes in the pathway.

Supplementary Figures

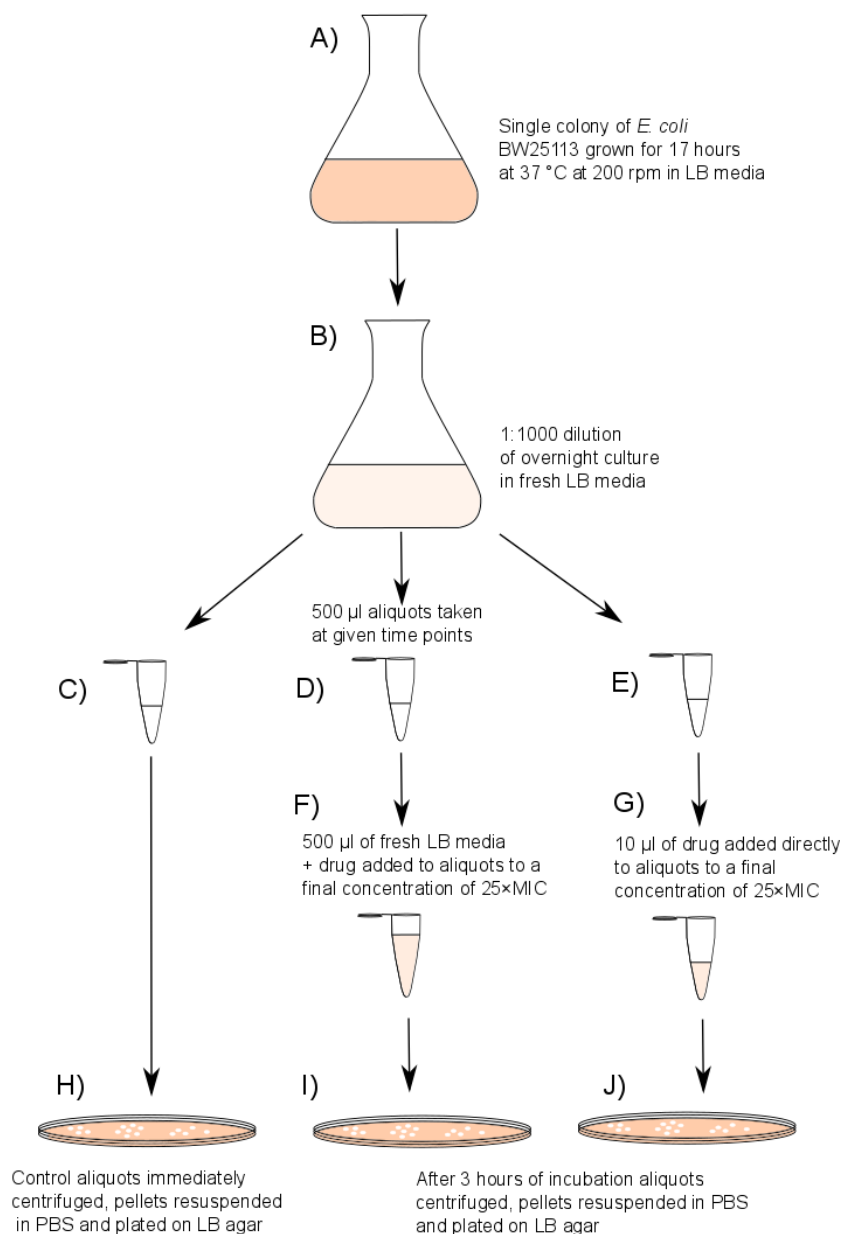


Figure S1. Schematic illustrating the persister assay. A single colony of *E. coli* was grown at 37 °C and 200 rpm in 200ml LB for 17 hours (A). We defined $t=0$ the time at which this culture was diluted 1:1000 in LB and growth at 37 °C and 200 rpm was restarted (B). Nine aliquots were taken from the growing culture hourly (C-E). Three aliquots were centrifuged immediately (13,000 g , 5 minutes) (C), serially diluted and plated on LB agar (H). The other six were treated for 3 hours, three supplemented with 500 µl of fresh LB (F) and three directly to the aliquot (G). In both cases the final concentration was 25×MIC. The treated aliquots were incubated for 3 hours, centrifuged, re-suspended in PBS and plated on LB agar(I-J).

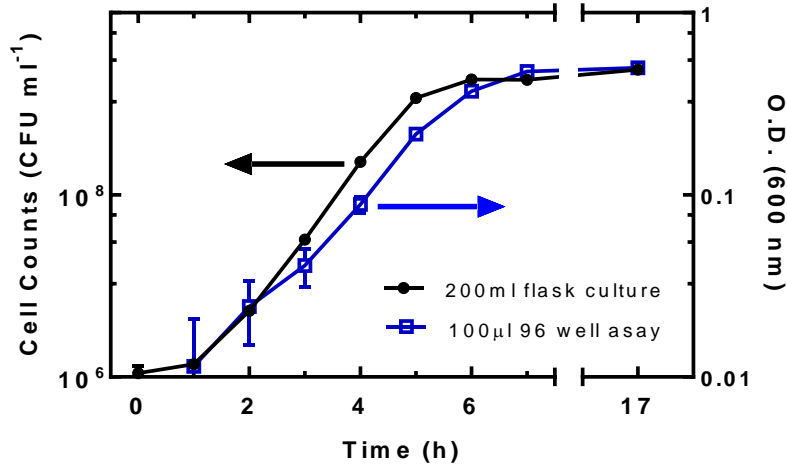


Figure S2. Comparison of *E. coli* growth in a conical flask and in a 96 well plate. Three overnight cultures of *E. coli* were diluted 1:1000 in fresh LB. Three 200 mL aliquots of these solutions were placed in three glass conical flasks whereas eighty-one 100 µl aliquots were added to individual wells of a 96 well plate (3 technical replicate in biological triplicate for each of the 9 time points investigated). The remaining wells were filled with fresh LB for blank measurements. Growth was measured hourly via CFU counts on LB agar plated with technical triplicate taken hourly from each flask (left axis) and via O.D. 600 measurements of 9 selected wells on a plate reader (right axis). All data represent mean and standard error of the mean of biological and technical triplicates. Some error bars are small compared to the corresponding mean values and are hidden behind the data.

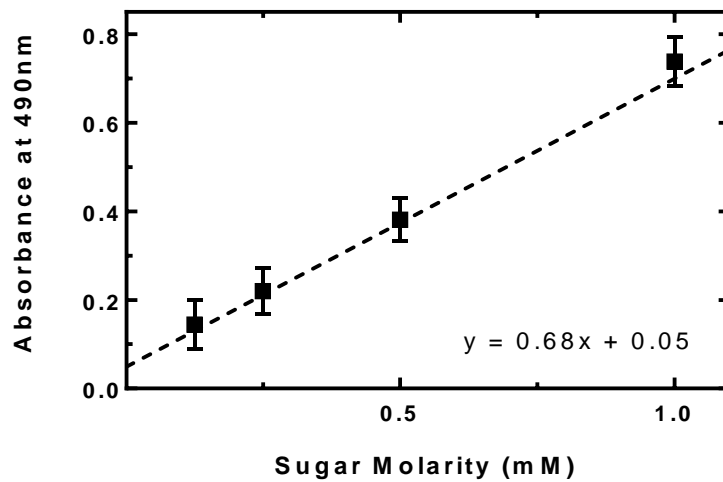


Figure S3. Standard curve for glucose detection using Benedict's reagent. The absorbance at 490 nm was measured for known glucose concentrations of 125, 250, 500 and 1000 μ M, respectively. The background was determined as the average of a triplicate measure of milliQ water. Triplicate readings were taken for each concentration, the background subtracted and the mean and SEM plotted. A linear regression was fitted to these points and the resulting function used to extrapolate sugar concentrations through the growth cycle of *E. coli*.

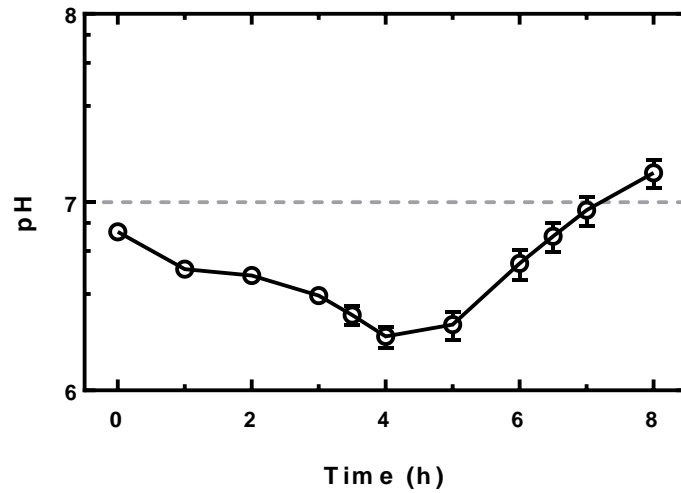


Figure S4. The growing culture shapes the extracellular environment pH. An overnight culture of *E. coli* was diluted 1:1000 in fresh LB and the pH of the culture measured through the resulting growth cycle. The pH decreases during lag and early exponential phase reaching a minimum of 6.2, then increases during late-exponential phase and up to 7 after 7h of growth. Data and error bars are the mean and SEM of at least 3 biological replicates.

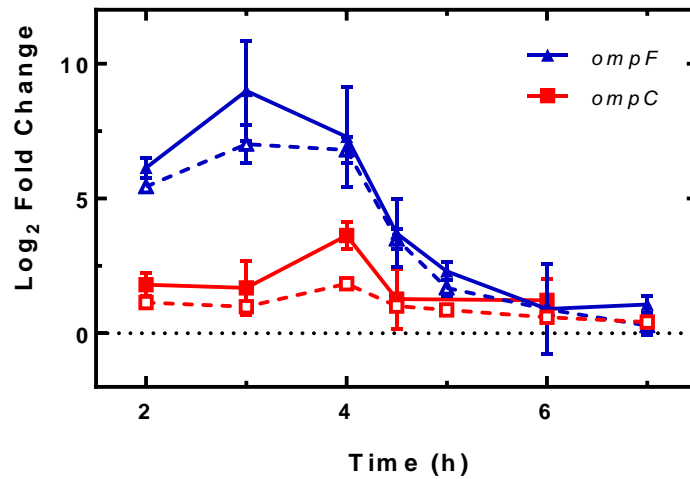


Figure S5. qPCR measurements confirm reliability of RNA-seq. In order to confirm the reliability of the RNA-seq data we performed quantitative PCR (qPCR) on the same samples for selected genes. The open symbols and dashed lines represent the transcriptomic results, whereas the filled symbols and lines represent those values obtained from qPCR. The results clearly indicate a similar pattern in the expression profiles for both methods.

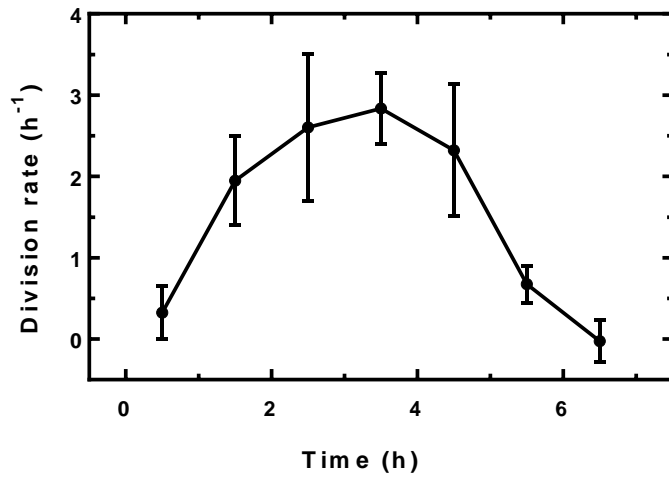


Figure S6. The bacterial division rate throughout the different stages of growth. An overnight culture of *E. coli* BW25113 was diluted 1:1000 in fresh LB. We measure division rate as the \log_2 fold change between the bacterial CFU at consecutive hourly intervals throughout the bacterial growth cycle reported in Fig. 2A. Means and SEM are calculated from at least 3 biological and technical replicates.

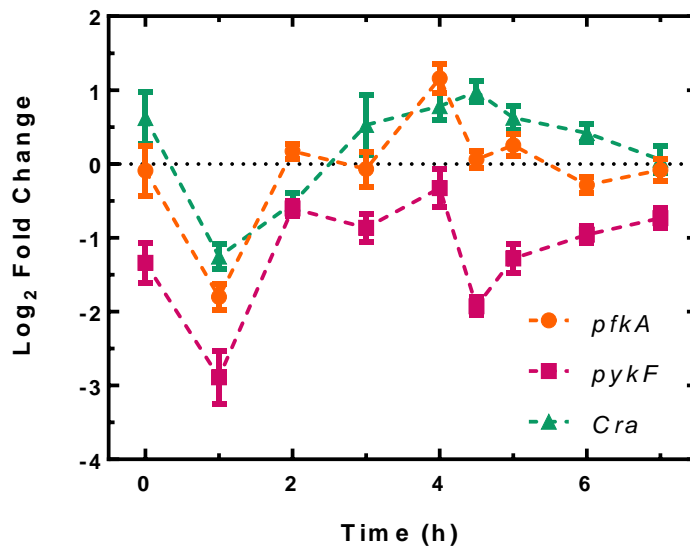


Figure S7. Regulation of glycolysis related genes. Carbon starvation results in increased expression of the transcription factor *Cra* (green triangles) which represses glycolysis enzymes *pfkA* (orange circles) and *pykF* (purple squares). During carbon starvation in *E. coli* levels of the glycolysis intermediate phosphoenol pyruvate (PEP) increases and inhibits the enzyme *pfkA*, which catalyzes an earlier step of glycolysis where GF6P is converted to FDP. The resulting increase in FDP activates the transcription factor *cra* which subsequently represses both *pykF* and *pfkA*.

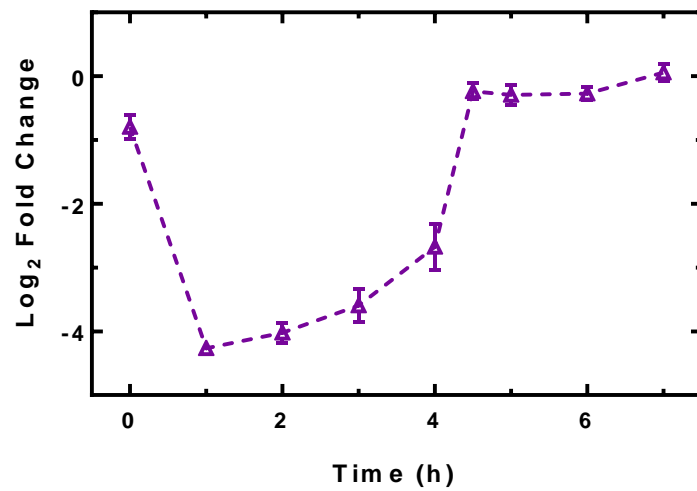


Figure S8. The regulation of the sigma factor *rpoS* through the growth cycle. *rpoS* is a sigma factor that is heavily associated with adaptation to stress and the onset of stationary phase. The graph above shows how upon dilution into fresh, nutrient rich, LB media, *rpoS* is downregulated. As the growth cycle progresses, it is gradually upregulated before a sharper rise is observed at the onset of stationary phase, where it then plateaus.

2.3 Conclusion

During growth in LB media, a planktonic population of *E. coli* transitions through multiple phases of growth, resulting in the easily recognisable bacterial growth curve⁷⁹. These phases are typically referred to as lag phase, exponential phase and stationary phase⁷⁹. However, even during these phases, the population will be continuously adapting to its extracellular environment. For instance, during lag phase, the population is gradually adjusting to the nutrient rich environment. Despite this, until this thesis, the changes to the extracellular environment and how these affect the population transcriptome, had yet to be determined for a planktonic *E. coli* population growing in LB medium, despite it being an experimental model system^{79,85,146,147}.

Using the data on pH, sugar content and population transcriptome, we were able to paint a picture of how bacteria were adapting to different nutrient sources. We found that the concentration of sugar was initially high (~200 μ M) but declined through the growth cycle, with a rapid decline during exponential growth. As a result, the sugar concentration essentially mirrored the growth curve, indicating the importance of sugar availability for the population to maintain its maximal growth rate. The pH, in comparison, became more acidic during the lag and early exponential phases of the growth cycle before increasing as the population entered stationary phase. We hypothesised that this was a result of the population initially utilising the sugars and excreting acetate during aerobic fermentation increasing the acidity of the extracellular environment. Then, upon exhaustion of these preferred nutrient sources the population would switch to gluconeogenic substrates, such as the aforementioned acetate, resulting in the extracellular environment becoming more basic from the excretion of ammonia as a waste product. By investigating the population level transcriptome, we were able to support this hypothesis by showing that the temporal expression of the glucose permease, *ptsG*, initially increased and peaked at approximately the same time as the pH was at its most acidic. In comparison, *actP* almost mirrored this expression, with a sharp increase after 4 hours of growth, coinciding with an increase in pH. Interestingly, both nutrient availability and pH have been shown to affect antibiotic survival^{56,60,62–65}, therefore we used persister formation as a proxy to identify

temporal windows within the growth cycle where we could observe drastic changes in phenotypic heterogeneity.

We investigated persister formation in response to three different classes of antibiotics; aminoglycosides, fluoroquinolones and β -lactams, respectively. All three showed similar responses during lag phase, however the response to the three antibiotics was different depending on the stage of growth. This variation highlighted the population heterogeneity, particularly during exponential and stationary phase. We then investigated the population level transcriptome during the temporal windows where we observed large increases in persister formation in response to our respective drugs. This approach allowed us to identify genes and pathways that were highly regulated during the temporal windows in which we observed increases, for instance the upregulation of the *tna* operon during the transition from exponential to stationary phase. However, it is important to note that these genes and pathways are a reflection of the entire population, so may not be representative of the sub populations that harbour persister cells. Therefore, it is important to develop a high throughput approach, like the one we introduce in chapter three, that will allow us to further investigate genes or pathways at the single cell level. In fact, using the data from this chapter, we identified *tnaC* in chapter three as a potential biomarker for VBNC and persister cells prior to antibiotic exposure.

Chapter 3: Investigating the physiology of viable but non-culturable bacteria by microfluidics and time-lapse microscopy

3.1 Introduction

Although genetically identical to their susceptible kin, persister and VBNC cells are able to survive otherwise lethal doses of antibiotics. Both of these phenotypes have been proposed as stepping stones for the development of antibiotic resistance^{32,38} and have also been linked to the recalcitrance of chronic infections^{32,70}. Despite this, as researchers, we still know very little about both phenotypes, in particular VBNC cells. One reason for this is it is currently not possible to isolate a persister or VBNC population for further analysis, such as transcriptomic, without using antibiotic exposure to identify them. Therefore, given that such exposure is also likely to affect the cells transcriptome, a non-invasive biomarker that would allow the identification and isolation of persister cells prior to antibiotic exposure would be a major breakthrough for the research field.

We previously showed in chapter two how we could use antibiotic survival, in particular persister cell formation, as a proxy for investigating phenotypic heterogeneity at the population level. By coupling this with transcriptomic analysis we were able to identify potential genes and pathways which were highly regulated at the population level during more than 10 fold increases in persister formation. However, as previously discussed in chapter two, this approach provided us with the mean transcriptome of the whole population rather than that of the persister subpopulation; highlighting the importance of single cell measurements. For instance, by using an “on/off” bimodal distribution (i.e. red cells and white cells) of a population as an example, Lidstrom and Konopka elegantly explained how population level averages would result in the phenotype being incorrectly as an intermediate (i.e. pink cells) state²².

Microfluidics has emerged as an excellent tool for investigating phenotypic heterogeneity and has, in fact, been utilised by some researchers to investigate persister formation^{30,127}. However, to the best of our knowledge, until this thesis, no one has utilised microfluidics to investigate the VBNC phenotype. This seems surprising, as there is increasing evidence to suggest that the two phenotypes, persister and VBNC cells, are not physiologically distinct but are, in fact, part of one dormancy continuum³⁶.

As a result of the above and as highlighted in chapter one, there is a need for a cleverly designed microfluidic device that would allow the tracking of individual bacterium before, during and after antibiotic exposure. Such a device would provide a useful research tool for investigating the expression of single genes or pathways, such as the ones identified using our method in chapter two, to help decipher the mechanisms behind the formation of persister and VBNC cells. Furthermore, this approach may also allow potential biomarkers to be identified for the isolation of persister and VBNC cells before antibiotic exposure. Finally, if such a device were to allow the simultaneous analysis of persister and VBNC cells, it would prove extremely useful for further investigating the relationship between both phenotypes.

Wang *et al.* first introduced their Mother Machine device to investigate heterogeneity in growth rate within an *E. coli* population⁸. The device is cleverly designed so that the side channels are narrow enough to confine individual bacterium, whilst the larger main channel can be used for the careful manipulation of the extracellular environment⁸. With that in mind, we identified the Mother Machine as a perfect platform for us to analyse antibiotic persister and VBNC cells at the single cell level.

In the following chapter, we report the protocol we developed and how we utilised it alongside plasmid-encoded fluorescent reporters to investigate the expression of 3 genes (*ptsG*, *tnaC* and *tolC*) in persister and VBNC cells before, during and after exposure to ampicillin. *tolC* and *tnaC* were chosen as a result of their previous links to antibiotic persistence, as discussed in chapter one. Furthermore, *tnaC* was also chosen as a result of the population level transcriptomic analysis we reported in chapter two. In short, *tolC* has been shown to increase persistence as a result of enhanced efflux activity¹²⁶.

Whereas the tryptophanase (*tna*) operon was highly regulated during a temporal window identified by an increase in persistence in chapter two and the role of indole, a product of tryptophanase, in persistence has been debated by multiple researchers^{35,83,88,89}. In comparison, *ptsG* has not previously been linked with persisters or VBNC cells so was chosen as a control.

METHODOLOGY ARTICLE

Open Access



Investigating the physiology of viable but non-culturable bacteria by microfluidics and time-lapse microscopy

Rosemary A. Bamford^{1,2†}, Ashley Smith^{1,2†}, Jeremy Metz^{1,2}, Georgina Glover^{1,2}, Richard W. Titball¹ and Stefano Pagliara^{1,2*} 

Abstract

Background: Clonal microbial populations often harbor rare phenotypic variants that are typically hidden within the majority of the remaining cells, but are crucial for the population's resilience to external perturbations. Persister and viable but non-culturable (VBNC) cells are two important clonal bacterial subpopulations that can survive antibiotic treatment. Both persister and VBNC cells pose a serious threat to human health. However, unlike persister cells, which quickly resume growth following drug removal, VBNC cells can remain non-growing for prolonged periods of time, thus eluding detection via traditional microbiological assays. Therefore, understanding the molecular mechanisms underlying the formation of VBNC cells requires the characterization of the clonal population with single-cell resolution. A combination of microfluidics, time-lapse microscopy, and fluorescent reporter strains offers the perfect platform for investigating individual cells while manipulating their environment.

Methods: Here, we report a novel single-cell approach to investigate VBNC cells. We perform drug treatment, bacterial culturing, and live/dead staining in series by using transcriptional reporter strains and novel adaptations to the mother machine technology. Since we track each cell throughout the experiment, we are able to quantify the size, morphology and fluorescence that each VBNC cell displayed before, during and after drug treatment.

Results: We show that VBNC cells are not dead or dying cells but share similar phenotypic features with persister cells, suggesting a link between these two subpopulations, at least in the *Escherichia coli* strain under investigation. We strengthen this link by demonstrating that, before drug treatment, both persister and VBNC cells can be distinguished from the remainder of the population by their lower fluorescence when using a reporter strain for *tnaC*, encoding the leader peptide of the *tnaCAB* operon responsible for tryptophan metabolism.

Conclusion: Our data demonstrates the suitability of our approach for studying the physiology of non-growing cells in response to external perturbations. Our approach will allow the identification of novel biomarkers for the isolation of VBNC and persister cells and will open new opportunities to map the detailed biochemical makeup of these clonal subpopulations.

Keywords: Viable but non-culturable cells, Microfluidics, *Escherichia coli*, Persisters, Single-cell, Antibiotic tolerance, Non-growing cells

* Correspondence: s.pagliara@exeter.ac.uk

†Equal contributors

¹Biosciences, University of Exeter, Exeter, Devon EX4 4QD, UK

²Living Systems Institute, University of Exeter, Exeter, Devon EX4 4QD, UK



Background

Clonal bacterial populations show cell-to-cell differences in physiological parameters, including responses to external perturbations [1]. For example, under drug treatment, the majority of a clonal bacterial population is susceptible to the drug, whereas at least two subpopulations – persister cells and viable but non-culturable (VBNC) cells – are able to survive high doses of antibiotics. Persister cells survive the antibiotic challenge and resume growth on nutrient-rich media shortly after removing the drug [2, 3], whereas VBNC cells survive the antibiotic challenge but may regrow only after a long and specific treatment [4]. Therefore, VBNC cells are difficult to detect and study via standard microbiology assays.

Persister and VBNC cells are in a transient state and are often, but not always [5], associated with dormancy [2, 6]. It has been suggested that they form stochastically as a result of fluctuations in gene and protein expression [6, 7]. However, deterministic components of persister and VBNC formation have also been documented [8–13]. Persister and VBNC cells pose a serious threat to human health since they may be recalcitrant to drug treatment [2], and thus can contribute to the relapse of diseases such as tuberculosis, cystic fibrosis-associated lung infections, candidiasis, cholera, septicemia, and gastroenteritis [4]. Furthermore, these subpopulations may constitute a reservoir for the development of antibiotic resistance mechanisms [14].

The recent advances in single-cell microfluidic analysis [15] have greatly enriched our understanding of persister cells, highlighting the contributions from toxin-antitoxin modules [6], the alarmone guanosine tetraphosphate pathway [7, 16, 17], efflux activity [18], the catalase-peroxidase enzyme [19], respiration [20], and protein production [21, 22]. However, single-cell microfluidic analysis has not yet been implemented to investigate VBNC cells due to the difficulty in distinguishing these cells from dead or dying cells, and the requirement to image and track thousands of individual cells. Nevertheless, VBNC cells constitute a major public health concern, since they have been observed in 51 human pathogens [3] and are difficult to eradicate via standard sterilization treatments such as heat, acid, ethanol, antibiotic or osmotic stress [23]. Therefore, there is an urgent to develop methodologies to study and combat bacteria in the VBNC state [4].

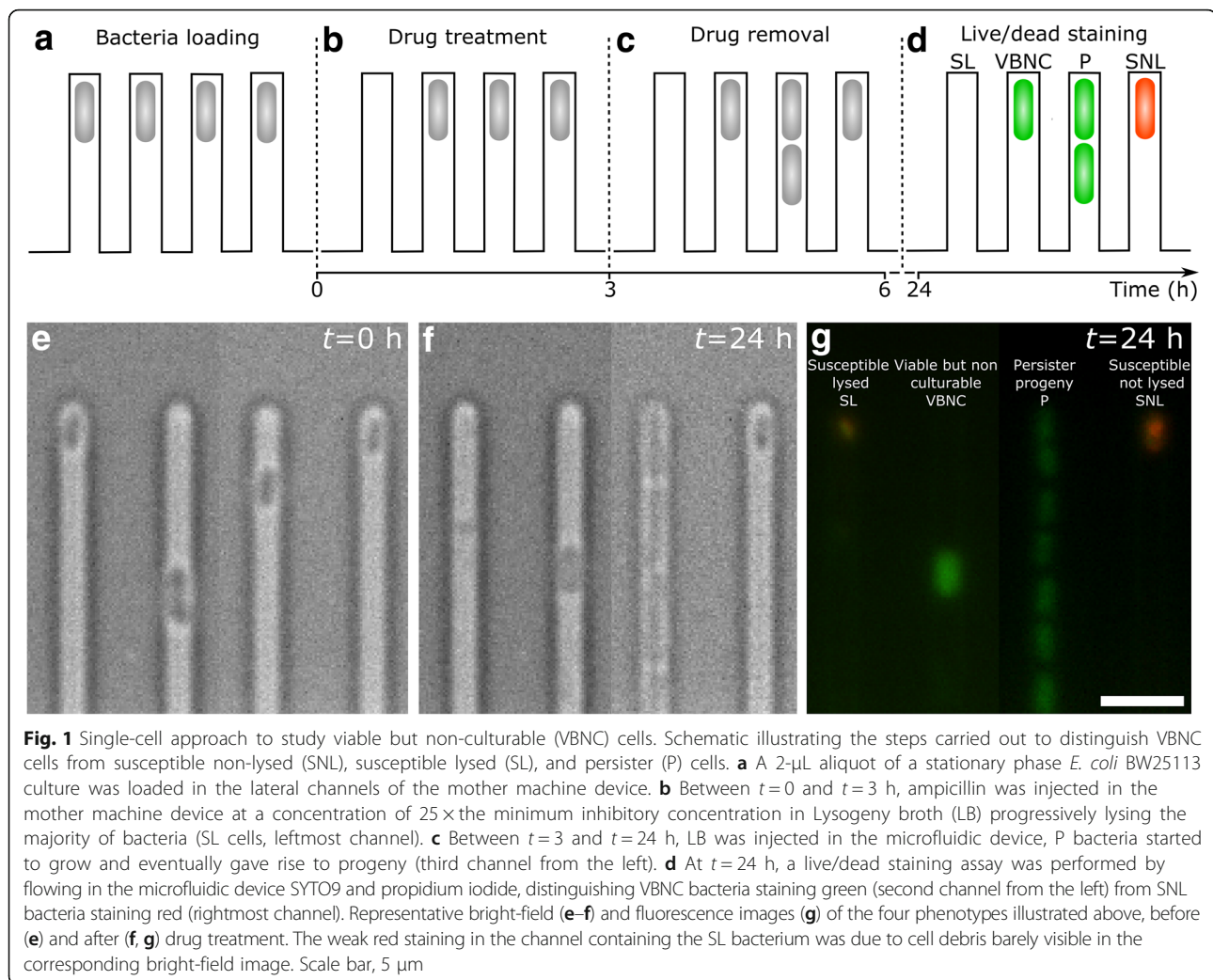
Here, we introduce a novel single-cell approach allowing, for the first time, the investigation of the changes in size, morphology and promoter activity in VBNC cells responding to drug treatment (Fig. 1). We take advantage of the well-established mother machine device [24, 25], designed to investigate the growth of a large number of individual *E. coli* cells. This device is equipped with thousands of microfluidic channels with cross section comparable to the size

of individual *E. coli* cells and connected to a large microfluidic chamber where the medium is continuously exchanged via pressure-driven microfluidics. In this paper, we use this technology to perform drug treatment, bacterial culturing, and live/dead staining in series, while imaging and tracking individual cells, thus permitting the identification of single VBNC cells alongside persister or susceptible cells. This new methodology allows us to obtain the following crucial information that will advance our understanding of VBNC cells. (1) We demonstrate that ampicillin-treated stationary phase *E. coli* cultures contain more VBNC than persister cells. (2) We show that, before drug treatment, VBNC cells exhibit cell length and levels of fluorescence for selected reporter strains similar to the ones measured in persister cells, supporting the hypothesis that these two phenotypes are part of a shared physiological continuum at least in the investigated *E. coli* strain [4]. (3) We demonstrate that, after drug treatment, VBNC cells are distinct from dead or dying cells and display fluorescence levels comparable to persister cells. (4) We identify the fluorescence of the *tnaC* reporter strain as a new biomarker for distinguishing persister and VBNC bacteria from the remainder of the population before drug treatment. Our novel single-cell approach will facilitate unraveling the molecular mechanisms underlying the formation of non-growing subpopulations and their capabilities to survive environmental changes. As such, our methodology represents a powerful tool for researchers investigating phenotypic or genotypic heterogeneity.

Results

Identification of VBNC cells

We chose to apply our novel single-cell approach to stationary phase *E. coli* cultures because the fraction of VBNC and persister cells in this growth phase is in the range 10^{-3} – 10^{-1} [18, 20, 26, 27]. This suggested that these phenotypes could be investigated with our proposed approach since it allows manipulating and tracking of approximately 2000 individual cells. In order to do so, we first loaded a 2- μ L aliquot of a stationary phase *E. coli* culture into the microfluidic mother machine device [24] and confined the bacteria in the lateral channels of the device ($t = 0$, Fig. 1a, e). We then treated the bacteria with a high dose of ampicillin, 25 \times minimum inhibitory concentration (MIC), dissolved in Lysogeny broth (LB; $0 < t < 3$ h, Fig. 1b). Since ampicillin targets cell wall synthesis, we identified susceptible lysed cells that die and lyse either during or after drug treatment and comprise the majority of the population (leftmost channel in Fig. 1) [28]. We then exchanged the drug-containing medium for LB ($3 < t < 24$ h, Fig. 1c) and identified intact persister cells that survived the antibiotic challenge and could regrow upon restoring favorable conditions



(third channel from the left in Fig. 1), similarly to previously reported microfluidic approaches [6, 7, 18, 19]. However, these methodologies did not allow the study of VBNC cells. In order to overcome this limitation, we performed live/dead staining as a last step in the series of our on-chip assays [5, 29, 30]. This step allowed us to identify two further phenotypes of susceptible non-lysed cells that died but did not lyse during nor after drug treatment (rightmost channel in Fig. 1) and VBNC cells that survived the antibiotic challenge but did not regrow upon restoring favorable conditions (second channel from the left in Fig. 1). Since we imaged and tracked each single cell throughout this series of assays, we were able to measure the size and morphology of each single cell before, during and after drug treatment and to assign each cell to a specific phenotype at the end of the experiment. This is, to the best of our knowledge, the first methodology allowing for the study of VBNC cells, alongside persister and susceptible cells, before, during, and after drug treatment.

Size and morphology of VBNC cells before, during, and after ampicillin treatment

Before ampicillin treatment ($t=0$), the four phenotypes (persister, VBNC, susceptible lysed, and susceptible non-lysed cells) had similar average lengths (Fig. 2a), calculated as the mean and standard error of the mean of single-cell measurements for the different phenotypes. Persister cells survived the 3-h ampicillin treatment and began dividing within 2 hours of exposure to LB (Additional file 1: Figure S1a); forming microcolonies and reaching an average length of $3.8 \pm 0.2 \mu\text{m}$ by $t=24$ h. In contrast, after exposure to ampicillin and subsequent incubation in LB, VBNC cells were smaller ($2.3 \pm 0.2 \mu\text{m}$) in average length, (squares in Fig. 2a) and more rounded compared to persister cells. Indeed, both cell dwarfing and rounding have been observed in VBNC cells of many species [31, 32]. In separate control experiments we measured the growth of bacteria confined in the lateral channels of the mother machine device and exposed to LB, but without the addition of

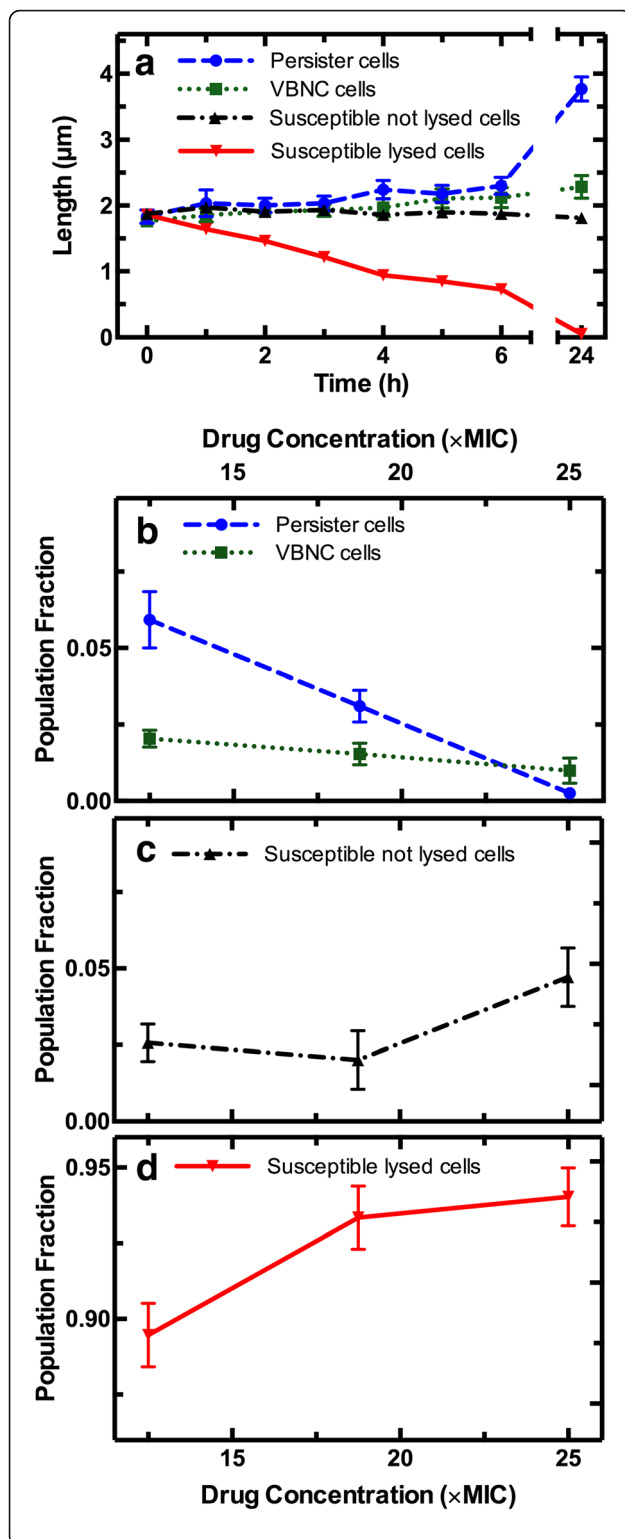


Fig. 2 Dimension and fraction of viable but non-culturable (VBNC) cells. **a** Average length of VBNC cells (green squares), alongside persister (blue circles), susceptible non-lysed (black upward triangles), and susceptible lysed cells (red downward triangles) before ($t = 0$), during ($0 < t < 3$ h), and after treatment ($3 < t < 24$ h) with ampicillin at a concentration of $25 \times$ minimum inhibitory concentration in Lysogeny broth. We assigned a length value of zero to cells that became undetectable with our code upon cell lysis. This explains the decrease in the average length of susceptible lysed cells. Lengths of untreated cells in control experiments are reported in Additional file 1: Figure S1a. Bacterial width did not significantly change throughout the experiment for the different phenotypes but for susceptible lysed cells (data not shown). Data and error bars are mean and standard error of the mean obtained by averaging single-cell values ($n_{SL} = 1651$, $n_P = 33$, $n_{VBNC} = 48$, $n_{SNL} = 87$) measured in the microfluidic experiment illustrated in Fig. 1 performed on biological triplicates ($N = 3$). We did not observe any significant difference between the results obtained from different biological replica. Due to the large sample sizes, error bars are small compared to the corresponding mean values and are hidden behind some of the data points. Ampicillin concentration dependence of the fraction of **(b)** VBNC and persister cells surviving the antibiotic challenge, of **(c)** susceptible non-lysed cells, and of **(d)** susceptible lysed cells killed by the antibiotic challenge. Data and error bars are obtained by averaging each phenotype frequency measured at least in biological triplicate

ampicillin (Additional file 1: Figure S1b, c). As expected, these bacteria exhibited similar initial average length to the bacteria measured in the ampicillin treatment experiments. However, they began dividing within 2 hours of exposure to LB (Additional file 1: Figure S1b) and at $t = 24$ h exhibited an average length close to that measured for the persister cell progenies (diamonds in Additional file 1: Figure S1c).

VBNC cells constitute the majority of cells surviving ampicillin treatment in a stationary phase *E. coli* culture

We enumerated the bacteria belonging to the four phenotypes and defined f_{SL} , f_{SNL} , f_P and f_{VBNC} as the fractions given by the number of counts for susceptible lysed, susceptible non-lysed, persister, or VBNC cells, respectively, divided by the number of total cells imaged in our assay before drug treatment. When we used a high dose of ampicillin ($25 \times$ MIC), we measured $f_{VBNC} = 0.01$ and $f_P = 0.003$ (Fig. 2b). Therefore, we provide direct evidence that VBNC cells, rather than persister cells as recently reported [18], constitute the majority of cells surviving ampicillin treatment in a stationary phase *E. coli* culture [27]. These cells possibly entered the VBNC state during nutrient starvation in stationary phase [32] or during the successive antibiotic treatment [23]. These findings suggest the need for investigating the VBNC phenotype in concert with persister cells [4]. We also found that susceptible cells that did not lyse were another small fraction, while the majority of bacteria lysed as a result of drug treatment ($f_{SNL} = 0.047$ and $f_{SL} = 0.94$, Fig. 2c and d, respectively).

We confirmed the reliability of our assay by performing bulk ampicillin treatment and colony forming unit (CFU) assays on separate aliquots of the same *E. coli* cultures. Through these bulk assays we obtained a measured f_P similar to that measured via our novel single-cell assay (Additional file 2: Figure S2) and to previously reported f_P values [33]. The CFU method does not, however, allow distinction between the VBNC and susceptible phenotypes. In contrast, our novel methodology provides a powerful tool to identify and study VBNC cells. Moreover, we found that f_P and f_{VBNC} decreased with ampicillin concentration (Fig. 2b and Additional file 2: Figure S2), whereas f_{SNL} and f_{SL} increased (Fig. 2c, d). It is worth noting that, at high ampicillin concentration ($25 \times \text{MIC}$) we measured four times as many VBNC as persister cells, whereas at a lower ampicillin concentration ($12.5 \times \text{MIC}$) this ratio was reversed, with f_P being three times higher than f_{VBNC} (Fig. 2b). These findings suggest the importance of employing the same standardized dose of drug when studying rare phenotypes within a clonal population.

Tracking promoter activity in individual VBNC cells

In order to further investigate the VBNC state, we used the approach illustrated in Fig. 1 in combination with green fluorescent protein (GFP) transcriptional reporter strains [34]. Each strain carried a low copy number plasmid with the promoter region of a gene of interest inserted upstream of a gene for a fast-folding GFP with an average lifetime of 8 h. GFP expression levels in individual strains of this library have been used to measure the corresponding promoter activity both at the population and single cell levels [34, 35]. We used this approach to measure single-cell GFP fluorescence levels as a proxy for the activity of the promoters that initiate the transcription of the genes *tolC*, *tnaC*, and *ptsG*. The *tolC* gene encodes part of the multidrug efflux pump AcrAB-TolC, and *E. coli* persister cells have previously been shown to exhibit higher *tolC* expression than untreated cells [18]. The *tnaC* gene encodes the leader peptide of the *tnaCAB* operon responsible for tryptophan transport and catabolism, including the enzyme TnaA, which converts tryptophan to indole, pyruvate, and ammonia. Indole has previously been shown to regulate the formation of *E. coli* persister cells [9, 36]. The role of these putative persister genes in VBNC cells remains to be investigated. The *ptsG* gene encodes part of the glucose permease transporter, and was chosen as a control gene as it has not been previously associated with persister nor with VBNC cells.

Figure 3a–c shows a representative set of images displaying GFP fluorescence of a persister cell, a VBNC cell (dashed and dotted contours, respectively), and five susceptible lysed cells of the *tolC* reporter strain. Figure 3d–g

shows the corresponding single-cell fluorescence throughout the different steps of the experiment, which are before ($t = 0$), during ($0 < t < 3$ h), and after ($3 < t < 24$ h) ampicillin treatment. We found that the VBNC cell exhibited a level of GFP fluorescence similar to the persister cell before and during drug treatment. After drug removal and 21 h exposure to LB, the VBNC cell was distinguishable from susceptible lysed or susceptible non-lysed cells even before performing the live/dead staining. In fact, whereas susceptible cells did not show any GFP fluorescence, the VBNC cell exhibited a high level of GFP fluorescence, being more than two times brighter than the persister cell progeny. This suggests that the non-growing VBNC phenotype maintains an active *tolC* promoter.

We also found that susceptible non-lysed and susceptible lysed cells showed similar patterns of fluorescence for the three investigated reporter strains and henceforth refer to them as susceptible cells. However, we identified two further subgroups within the susceptible subpopulation in the *tolC* reporter strain, namely cells that displayed increasing fluorescence levels during drug treatment (filled triangles in Fig. 3a–c, f and Additional file 3: Figure S3b) and cells that showed decreasing levels of fluorescence (open triangles in Fig. 3a–c, g and Additional file 3: Figure S3b).

VBNC cells can be distinguished from susceptible cells before antibiotic treatment

In order to investigate the patterns of GFP fluorescence in VBNC cells of the three reporter strains, we imaged, tracked, and analyzed approximately 2000 individual bacteria for each reporter strain.

Before ampicillin treatment, VBNC cells exhibited fluorescence levels similar to those measured in persister cells for all the investigated reporter strains (Fig. 4a–c). This further supports the hypothesis that the persister and VBNC phenotypes are part of a shared physiological continuum [4]. Furthermore, persister and VBNC cells of the *tolC* reporter strain exhibited only slightly higher fluorescence levels than susceptible cells (Fig. 4a). This suggests that persister and VBNC cells may not rely on antibiotic efflux to survive the antibiotic challenge in disagreement with previously reported findings [18]. This disagreement, however, could also be ascribed to the use of different antibiotic treatment conditions. Remarkably, fluorescence levels in persister and VBNC cells in the *tnaC* reporter strain were half of those measured in susceptible cells, possibly because the former are in a less active metabolic state [27]. This contradicts a previous study that suggested that persister cells exhibit higher levels of *tnaC* promoter activity with respect to susceptible cells [9]; however, in that study, 0.5 mM indole had been added to an exponentially growing *E. coli* culture. Furthermore, a different study suggested a link between reduction of *tnaCAB* operon expression and the formation of persister cells [36],

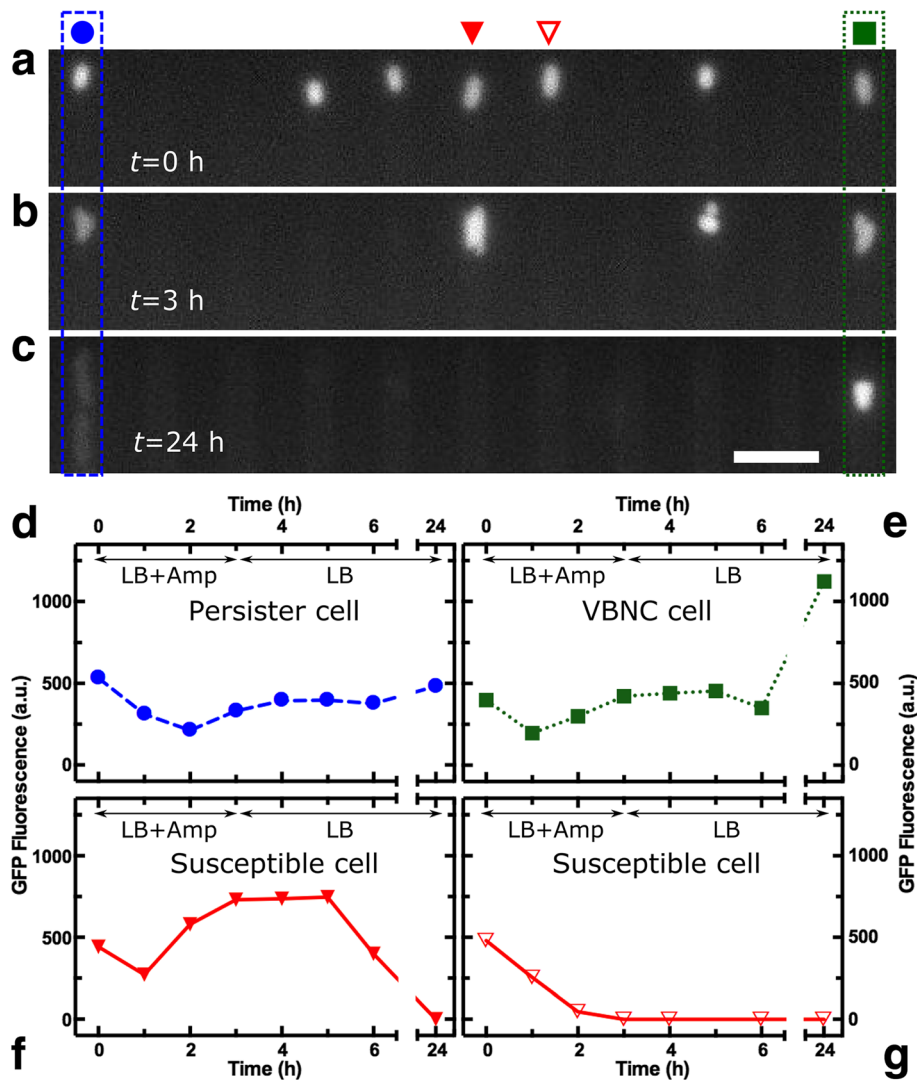
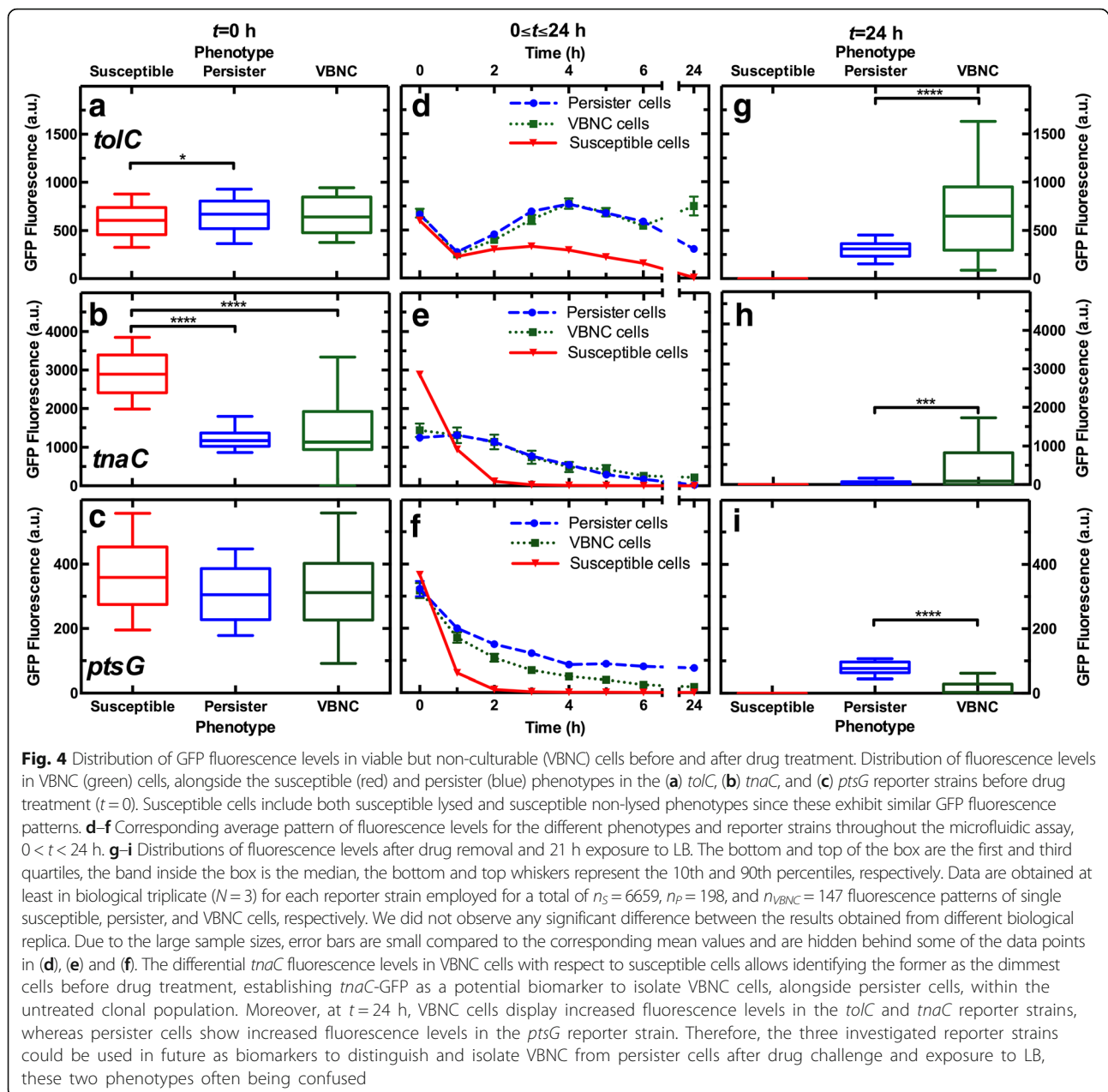


Fig. 3 GFP fluorescence patterns in single viable but non-culturable (VBNC) cells. Fluorescence images reporting GFP expression levels, as a proxy for the activity of the promoter of *tolC*, in a single VBNC cell (green square), alongside a persister cell (blue circle) and five susceptible cells (a) before, (b) during, and (c) after drug treatment. Scale bar, 5 μ m. Corresponding fluorescence patterns for the (d) persister, (e) VBNC, and (f, g) the two selected susceptible cells in the images above. The VBNC cell exhibited a fluorescence pattern similar to the one of the persister cell throughout the entire assay, but the VBNC cell was much brighter and easily distinguishable at $t = 24$ h. This suggests that the fluorescence associated to the *tolC* reporter strain could be used to isolate VBNC cells from the remainder of the population after ampicillin treatment and 21 h exposure to LB. The two susceptible cells displayed very different responses to the antibiotic treatment. For the cell in (f) (marked with a filled triangle in Fig. 3a), fluorescence levels increased during and immediately after drug treatment but decreased after $t = 5$ h, with the cell eventually lysing by $t = 24$ h. For the cell in (g) (marked with an open triangle in Fig. 3a), fluorescence levels decreased during drug treatment, with the cell lysing by $t = 3$ h. This suggests that besides the four phenotypes introduced in Figs. 1 and 2, there are at least two further subgroups of susceptible cells (Additional file 3: Figure S3)

corroborating our findings. Our data suggests that the persister and VBNC cells found in a stationary phase *E. coli* culture constitute subpopulations existing before exposure to ampicillin, confirming previous findings [6]. However, this is still under debate since other studies suggest that exposure to antibiotics itself underlies persister cell formation [12]. We anticipate that our new methodology will be crucial for identifying further phenotypic differences between VBNC, persister, and susceptible cells prior to drug treatment.

During ampicillin treatment, VBNC and persister cells maintained similar fluorescence levels in the *tolC* and *tnaC* reporter strains, but VBNC cells displayed lower fluorescence levels in the *ptsG* reporter strain compared to persister cells (circles and squares in Fig. 4d–f, $0 < t < 3$ h). On the contrary, susceptible cells very quickly lost their fluorescence in all three employed reporter strains (triangles in Fig. 4d–f) but not in a subpopulation of the *tolC* reporter strain (Fig. 4d and Additional file 3: Figure S3).



After ampicillin treatment and 21 h exposure to LB, VBNC cells displayed markedly different fluorescence levels for all the investigated strains compared to persister cells. VBNC cells maintained higher fluorescence levels in the *tolC* and *tnaC* reporter strains, and exhibited different fluorescence levels with respect to susceptible cells (Additional file 4: Figure S4). This is consistent with the hypothesis that, whereas dead cells do not express genes, VBNC cells continue producing mRNA [37]. Therefore, we unambiguously demonstrated that VBNC cells can be distinguished from susceptible non-lysed cells before, during, and after drug treatment. Persister cells instead showed higher fluorescence levels in the

ptsG reporter strain (Fig. 4g–i) compared to VBNC cells, suggesting that the former were utilizing a higher amount of sugars after drug treatment.

In separate control experiments we measured the changes in GFP fluorescence of bacteria confined in the lateral channels of the mother machine device, exposing them to LB without the addition of ampicillin. As expected, these bacteria exhibited similar fluorescence levels to susceptible cells at $t = 0$ (Additional file 5: Figure S5). Moreover, during exposure to LB, these bacteria exhibited similar patterns of fluorescence levels as persister cells (Additional file 6: Figure S6, $3 < t < 24$ h), further suggesting that persister cells had reverted to a normally growing state.

Discussion

Progress in our understanding of VBNC cells since their discovery in 1982 [38] has been slow and incremental. Our approach represents a general tool to measure the physiological state of VBNC cells, alongside persister cells, before antibiotic treatment. Moreover, this approach, as well as other recently introduced methods [27], can serve to bridge the gap between VBNC and persister states that are rarely studied in the same context [4]. Specifically, in this paper we quantitatively compare persister and VBNC fractions in a stationary phase *E. coli* culture, and characterize the size, morphology, and activity of selected promoters in persister and VBNC cells exposed to the same microenvironment. However, our approach could easily be adapted to measure other physiological parameters previously linked to the formation of VBNC and persister cells such as uptake and efflux of nutrients and drugs [18, 39], metabolic activity [5], and mRNA metabolism [40].

Little is known about the genetic control underlying the VBNC state and the gene expression profile in VBNC *E. coli* [3, 41, 42]. Indeed, transcriptome analysis has been reported only for *V. cholerae* VBNC cells [43]. Furthermore, gene expression profiling is typically carried out on VBNC cells isolated after exposure to drugs [27] or other stressful environments such as cold seawater or low pH [3, 43], which affect the VBNC state [44]. Our approach instead allows investigating VBNC cells, alongside persister cells, before drug treatment and in a microenvironment that we can accurately control via microfluidics. In this respect, our approach is likely to change the way we investigate non-growing subpopulations within clonal or mixed microbial populations.

It is worth noting that, if VBNC cells are present in microbiological quality control samples from the food industry, water distribution systems, or hospitals, the number of viable bacteria in the sample will be underestimated via the widely employed CFU count method. Therefore, the inability to detect VBNC cells can pose a risk to human health [3]. Our platform represents a rapid and reliable tool to detect VBNC cells in bacterial populations. This allowed us to unambiguously demonstrate that VBNC cells are not in a transitory stage in the degeneration of bacteria leading to cell death [45, 46]. On the contrary, our data proves that, even after drug treatment, at least the *tolC* promoter remained active in VBNC cells and thus supports the hypothesis that VBNC cells are in a transitional state awaiting for suitable conditions to resuscitate [44]. In this respect, our single-cell approach represents an ideal tool for the future investigation of the mechanisms underlying VBNC resuscitation, which remain largely unknown [3, 47].

Our microfluidic system can be adapted to investigate other bacterial pathogens and cell types, including cancer populations where drug-tolerant cells have been identified [48]. More generally, our platform will allow the investigation of how non-growing subpopulations within clonal or mixed microbial populations respond to changes in the environmental pH, temperature, and nutrient content. Furthermore, we are currently working on scaling up our microfluidic system to investigate persister and VBNC phenotypes occurring at frequencies below 10^{-3} . Specifically, we plan to apply our approach to bacterial cultures transitioning from the exponential to the stationary phase when the fraction of persister, and possibly VBNC cells, monotonously increases from 10^{-5} to 10^{-2} [26], thus suggesting that the changes occurring in the culture environment might favor the formation of these phenotypes. Such a higher throughput system will also allow investigating candidate VBNC cell formation mechanisms involving multiple genes through the simultaneous investigation of several reporter strains [4]. In this respect, a recent study investigated the expression of up to 100 genes in persister cells, but not in VBNC cells, by using fluorescence-activated cell sorting, sequencing, and a library of promoter reporters [33]. However, this approach also relies on the use of antibiotics to identify persister cells and does not allow measurements of gene expression on the same cell before, during, and after drug treatment.

Conclusion

There is currently a lack of biomarkers that can be used to segregate VBNC cells from the majority of S cells before antibiotic treatment [33]. Our single-cell approach allowed us to establish that, when using the *tnaC* reporter strain, stationary phase persister and VBNC *E. coli* were significantly less fluorescent than susceptible *E. coli* and will allow future identification of other genes that are differentially regulated in VBNC cells before antibiotic treatment. The associated reporter strains could be used to isolate natively formed VBNC cells via fluorescence-activated cell sorting for downstream transcriptomic and proteomic analysis. As such, our novel single-cell approach provides a new opportunity to unravel the molecular mechanisms underlying the capability of microbial pathogens to survive drug treatment and remain non-growing.

Methods

Chemicals and cell culture

All chemicals were purchased from Fisher Scientific or Sigma-Aldrich unless otherwise stated. LB medium (10 g/L tryptone, 5 g/L yeast extract, and 10 g/L NaCl) and LB agar plates (LB with 15 g/L agar) were used for planktonic growth and enumeration of CFUs, respectively. *E. coli* BW25113 were purchased from Dharmacon

(GE Healthcare). *tolC*, *tnaC*, and *ptsG* reporter strains of an *E. coli* K12 MG1655 promoter library [34] were purchased from Dharmacon (GE Healthcare). Plasmids were extracted and transformed into chemically competent *E. coli* BW25113 as previously reported [33]. We verified that these reporter strains exhibit similar growth rates and levels of f_P and f_{VBNC} compared to wild-type *E. coli* BW25113. Overnight cultures were prepared by picking a single colony of *E. coli* BW25113 from a streak plate and growing it in 200 mL fresh LB medium in a shaking incubator at 200 rpm and 37 °C for 17 h.

Fabrication of the microfluidic devices

The mold for the mother machine microfluidic device [24] was obtained by pouring epoxy onto a polydimethylsiloxane (PDMS, Dow Corning) replica of the original mold containing 12 independent microfluidic chips (kindly provided by S. Jun). Each of these chips is equipped with approximately 6000 lateral microfluidic channels with width and height of approximately 1 μm each and a length of 25 μm . These lateral channels are connected to a main microfluidic chamber that is 25 and 100 μm in height and width, respectively. PDMS replicas of this device were realized as previously described [49]. Briefly, a 9:1 (base:curing agent) PDMS mixture was cast on the mold and cured at 70 °C for 120 min in an oven. The cured PDMS was peeled from the epoxy mold and cut into individual chips. Fluidic accesses were created by using a 0.75 mm biopsy punch (Harris Uni-Core, WPI). The PDMS chip was irreversibly sealed on a glass coverslip by exposing both surfaces to oxygen plasma treatment (10 s exposure to 30 W plasma power, Plasma etcher, Diener, Royal Oak, MI, USA). This treatment temporarily rendered the PDMS and glass hydrophilic, so within 5 min after bonding the chip was filled with 2 μL of a 50 mg/mL bovine serum albumin solution and incubated at 37 °C for 1 h, thus passivating the device's internal surfaces and preventing subsequent cell adhesion.

Microfluidics-microscopy assay to identify and study VBNC cells

An overnight culture was prepared as described above. Spent LB broth and bacteria were prepared by centrifuging the overnight culture (10 min at 3000 g and 20 °C). The supernatant was filtered twice (Medical Millex-GS Filter, 0.22 μm , Millipore Corp.) and used to re-suspend the bacteria in their spent LB to an optical density of 50 at 595 nm. Bovine serum albumin was added to the bacterial suspension at a concentration of 0.5 mg/mL. A 2- μL aliquot of this suspension was injected in the above described microfluidic device and incubated at 37 °C. The high bacterial concentration favors bacteria entering the narrow lateral channels from the main microchamber of the mother machine (Fig. 1a, e) [24]. We found

that an incubation time of 20 min allowed filling of the lateral channels with, typically, between one and three bacteria per channel. An average of 60% of lateral channels of the mother machine device were filled with bacteria and 50% of the filled channels contained single bacteria. This facilitated tracking each single bacterium throughout the different phases of our assay (Fig. 1). The microfluidic device was completed by the integration of fluorinated ethylene propylene tubing (1/32" \times 0.008"). The inlet tubing was connected to a flow-rate measuring device (Flow Unit S, Fluigent, Paris, France) controlling the pressure applied by a computerized pressure-based flow control system (MFCS-4C, Fluigent) on the inlet reservoir feeding the flow rate device itself. This instrumentation was controlled by MAESFLO software (Fluigent). At the end of the 20 min incubation period, the chip was mounted on an inverted microscope (IX73 Olympus, Tokyo, Japan) and the bacteria remaining in the main microchamber of the mother machine were washed into the outlet tubing and reservoir by flowing spent LB at 300 $\mu\text{L}/\text{h}$ for 8 minutes. At this point (Fig. 1a, e) we acquired our first set of images in bright-field and fluorescence mode (the latter were acquired only when using reporter strains). Images were collected via a 60 \times , 1.2 NA objective (UPLSAPO60XW, Olympus) and a sCMOS camera (Zyla 4.2, Andor, Belfast, UK). The region of interest of the camera was adjusted to visualize 23 lateral channels per image. Upon acquiring each bright-field image the microscope was switched to fluorescent mode and FITC filter using custom built Labview software and a fluorescence image was acquired by exposing the bacteria to the blue excitation band of a broad-spectrum LED (CoolLED pE300white, Andover, UK) at 100%, 20%, and 20% of its intensity and for 0.05, 0.03, and 0.05 s for *tolC*, *tnaC*, and *ptsG* imaging, respectively. These parameters were adjusted in order to maximize the signal to noise ratio. The device was moved by two automated stages (M-545.USC and P-545.3C7, Physik Instrumente, Karlsruhe, Germany, for coarse and fine movements, respectively) to image the next set of lateral channels and these steps were repeated until approximately 2000 bacteria were imaged (average of 1943 ± 316 bacteria per experiment). After acquiring the first set of images, the microfluidic environment was changed by flowing LB containing ampicillin at 25 \times MIC at 300 $\mu\text{L}/\text{h}$ for 8 minutes and then at 100 $\mu\text{L}/\text{h}$ for 3 h ($t = 0$, Fig. 1b). Imaging was carried out hourly for $0 < t < 6$ h and at $t = 24$ h. After 3 h, the antibiotic was removed and LB medium was flowed in the chip at 300 $\mu\text{L}/\text{h}$ for 8 minutes and then at 100 $\mu\text{L}/\text{h}$ for 21 h (Fig. 1c). Crucially, at $t = 24$ h live/dead staining [27] was performed by flowing SYTO9 and propidium iodide (PI, Thermo Fisher Scientific) into the microfluidic device for 25 and 10 min, respectively, at a concentration of 3.34 and 30 μM , respectively, according to the

manufacturer's specifications. To the best of our knowledge, this is the first time that live/dead staining is implemented in the mother machine approach and it is crucial for distinguishing VBNC cells from susceptible non-lysed cells. Indeed, these fluorescent dyes differ in their ability to penetrate the bacterial membrane and stain live and dead bacterial cells, respectively [50]. Bright-field and fluorescence images were acquired to determine whether each bacterium was dead or alive. SYTO9 and PI staining were imaged by using 60% blue and 100% green LED intensity, FITC and TRITC filters, respectively, and an exposure time of 0.01 s. PI only was used imaging reporter strains. The entire assay was carried out at room temperature.

Image and data analysis

Microfluidics confinement and time-lapse microscopy allow the tracking of each individual bacterium and its eventual progeny throughout the entire assay. All image processing was performed using a custom Python module [51]. Briefly, channels and bacteria were detected by using automated thresholding algorithms. Each channel within a frame and each bacterium within a channel were assigned unique numeric labels. Each bacterium was tracked by taking into account all of the possible combinations for cell death or division and the most likely calculated depending on several factors, including each cell location and area. Once bacterial lineage was established, the corresponding masks were used to extract information about each bacterium such as width, length, area and fluorescence intensity from the corresponding fluorescence image. The fluorescence background was determined as the average fluorescence for the areas of the channels that did not contain bacteria and subtracted from the fluorescence intensity measured on each bacterium. For each bacterium, the measured GFP signal was normalized by cell size to account for variations in expression due to the cell cycle [52]. The final output images showed each detected bacterium with its unique numeric label. The measurements for all bacteria within a frame across the different time points were written to .csv files. The detection and label assignment was visually verified and each bacterium classified as persister, VBNC, susceptible lysed, or susceptible non-lysed phenotype as defined in Fig. 1. Further details of this framework will be reported in a separate publication currently in preparation. Semi-automated measurements were performed on randomly selected pools of images using ImageJ and the accuracy of the above automated framework verified. All data reported in GraphPad Prism 7 represent mean and standard error of the mean of at least biological triplicates. Due to the large sample sizes, error bars are small compared to the corresponding mean values and are hidden behind the data

points in some of the graphs (Fig. 4d–f, Additional file 1: Figure S1a, Additional file 3: Figure S3b, and Additional file 4: Figure S4). Statistical significance was tested by unpaired *t* test with Welch's correction.

MIC determination and persister enumeration via CFU assay

The MIC of ampicillin against *E. coli* strain BW25113 was determined using a 96-well plate method. *E. coli* was grown in LB medium for 17 h at varying concentrations of ampicillin ($0.5\text{--}512\ \mu\text{g mL}^{-1}$) and the absorbance measured at 595 nm. The MIC was defined as the lowest concentration at which the absorbance was the same as the control (bacteria-free LB) and determined as $5\ \mu\text{g mL}^{-1}$. In order to measure the fraction of persister cells to ampicillin in the culture, six 500- μL aliquots were withdrawn from the overnight culture. Three were used for untreated controls, centrifuged (12,000 *g* for 5 minutes), the supernatant removed, the pellet re-suspended in phosphate-buffered saline, serially diluted, plated on LB agar, and CFU counted after overnight growth in an incubator at 30 °C. Three aliquots were supplied with 500 μL LB containing ampicillin at $50 \times$ MIC (resulting in a final concentration of $25 \times$ MIC) and returned to the shaking incubator. After 3 h, these aliquots were centrifuged, the supernatant removed, the pellet re-suspended in phosphate-buffered saline, serially diluted, plated on LB agar, and CFU counted after overnight growth in an incubator at 30 °C. The persister cell fraction f_p was defined as the number of CFUs obtained from the treated aliquots divided by the number of CFUs obtained from the untreated aliquots.

Additional files

Additional file 1: Figure S1. Bacterial growth in the microfluidic device. a) Fractional distributions of time elapsed to first cell division for persister cells. b) Fractional distributions of time elapsed to first cell division for untreated cells in separate control experiments where LB but without ampicillin was added in the mother machine device. $n \geq 3$, $n_p = 134$ and $n_c = 1274$ persister and untreated control cells, respectively. c) Corresponding average length of persister cells (circles) before ($t = 0$), during ($0 < t < 3$ h), and after treatment ($3 < t < 24$ h) with ampicillin at a concentration of $25 \times$ MIC in LB and of untreated control cells (diamonds). Data and error bars are mean and standard error of the mean obtained by averaging single-cell values obtained on $n_p = 33$ and $n_c = 592$ persister and untreated control cells, respectively, in biological triplicate. We did not observe any significant differences between the results obtained from different biological replica. Due to the large sample sizes, error bars are small compared to the corresponding mean values and are hidden behind some of the data points in (c). (PNG 1509 kb)

Additional file 2: Figure S2. Bulk and single-cell persister enumeration. Dependence of the frequency of persister cells on ampicillin concentration as measured via the single-cell microfluidics-microscopy assay (full circles) illustrated in Fig. 1 and the colony forming unit assay (open circles). The two assays are performed on aliquots withdrawn from the same *E. coli* overnight culture. Data and error bars are mean and standard error of the mean of measurements obtained in biological triplicate ($N = 3$). Data agreement within experimental error confirms the validity of the newly developed microfluidic assay. (PNG 226 kb)

Additional file 3: Figure S3. Subgroups in the subpopulation of susceptible cells. a) Distribution of GFP fluorescence levels in susceptible cells of the *tolC* reporter strain after ampicillin treatment ($t = 3$ h). b) Temporal dependence of average fluorescence levels for susceptible cells that fluoresce (filled triangles) and do not fluoresce (open triangles) at $t = 3$ h, resembling the two susceptible cells reported in Fig. 3. Data and error bars are the mean and standard error of $n = 623$ (filled triangles) and $n = 754$ (open triangles) susceptible cells measured in biological triplicate ($N = 3$). We did not observe any significant difference between the results obtained from different biological replica. Due to the large sample sizes, error bars are small compared to the corresponding mean values and are hidden behind the data points in (b). (PNG 365 kb)

Additional file 4: Figure S4. Viable but non-culturable (VBNC) cells are different from susceptible non-lysed cells (SNL). Average pattern of GFP fluorescence levels of the VBNC (green squares) and SNL (black triangles) phenotypes throughout the microfluidic assay for the a) *tolC*, b) *tnaC*, and c) *ptsG* reporter strains. The two phenotypes are already distinguishable during drug treatment. Data and error bars are obtained as the mean and standard error of single-cell measurements in biological triplicate ($N = 3$) for each reporter strain for a total of $n_{VBNC} = 147$ and $n_{SNL} = 335$ VBNC and SNL cells, respectively. We did not observe any significant difference between the results obtained from different biological replica. Due to the large sample sizes, error bars are small compared to the corresponding mean values and are hidden behind some of the data points. (PNG 568 kb)

Additional file 5: Figure S5. Susceptible cells are indistinguishable from untreated cells before drug treatment. Distribution of fluorescence levels in the susceptible phenotype before drug treatment ($t = 0$) and in untreated control cells before regrowth in LB ($t = 0$) in the a) *tolC*, b) *tnaC*, and c) *ptsG* reporter strain. The two populations are not statistically different, an unpaired t test with Welch's correction yielding a P value of 0.07, 0.7, and 0.9, respectively. The bottom and top of the box are the first and third quartiles, the band inside the box is the median, the bottom and top whiskers represent the 10th and 90th percentiles, respectively. Data are obtained at least in biological triplicate ($N = 3$) for each reporter strain employed for a total of $n_S = 6659$ and $n_C = 3076$ susceptible and control cells, respectively. We did not observe any significant difference between the results obtained from different biological replica. (PNG 423 kb)

Additional file 6: Figure S6. Persister and untreated control cells have similar patterns of fluorescence levels during regrowth on LB. Average pattern of fluorescence levels in persister (circles) and untreated control (diamonds) cells throughout the microfluidic assay in the a) *tolC*, b) *tnaC*, and c) *ptsG* reporter strains. Persister and untreated control cells exhibit similar patterns of fluorescence levels during regrowth on LB ($3 < t < 24$ h and $0 < t < 24$ h for persister and control cells, respectively) demonstrating that persister cells revert back to a normally growing state after removal of the antibiotic drug. Data and error bars are obtained as the mean and standard error of the mean of single-cell measurements in biological triplicate ($N = 3$) for each reporter strain for a total of $n_P = 132$ and $n_C = 3076$ persister and control cells, respectively. We did not observe any significant difference between the results obtained from different biological replica. Due to the large sample sizes, error bars are small compared to the corresponding mean values and are hidden behind the data points. (PNG 585 kb)

Acknowledgements

We thank S. Jun for providing the original mother machine and C. Schwall for training on handling this device.

Funding

This work was supported by a Royal Society Research Grant (RG140203), a Wellcome Trust ISSF (WT097835/Z/11/Z) and a Start up Grant from the University of Exeter awarded to SP. AS acknowledges support from the BBSRC through a SWBio-DTP studentship (BB/M009122/1). JM was generously supported by a Wellcome Trust Institutional Strategic Support Award (WT097835MF). This work was partly supported by BBSRC award BB/1024631/1 to RWT.

Availability of data and materials

The Python code for single-bacterium detection, tracking, and analysis is available in the Github repository [51]. All the data used in this work are available in the Figshare repository [53–56].

Authors' contributions

SP developed the project and designed the research. RB, AS, GG, and SP performed the experiments. RB, AS, JM, GG, RT, and SP analyzed and discussed the data. AS and JM wrote the Python code. RB, AS, RT, and SP wrote the paper. All authors read and approved the final manuscript.

Competing interests

The authors declare no competing financial interests.

Publisher's Note

Springer Nature remains neutral with regard to jurisdictional claims in published maps and institutional affiliations.

Received: 15 September 2017 Accepted: 30 November 2017

Published online: 21 December 2017

References

- Lidstrom ME, Konopka MC. The role of physiological heterogeneity in microbial population behavior. *Nat Chem Biol.* 2010;6:705–12.
- Lewis K. Persister cells. *Annu Rev Microbiol.* 2010;64:357–72.
- Li L, Mendis N, Trigui H, Oliver JD, Faucher SP. The importance of the viable but non-culturable state in human bacterial pathogens. *Front Microbiol.* 2014;5:1–1.
- Ayrapetyan M, Williams TC, Oliver JD. Bridging the gap between viable but non-culturable and antibiotic persistent bacteria. *Trends Microbiol.* 2015;23:7–13.
- Orman MA, Brynildsen MP. Dormancy is not necessary or sufficient for bacterial persistence. *Antimicrob Agents Chemother.* 2013;57:3230–9.
- Balaban NQ, Merrin J, Chait R, Kowalik L, Leibler S. Bacterial persistence as a phenotypic switch. *Science.* 2004;305:1622–5.
- Maisonneuve E, Castro-Camargo M, Gerdes K. (p)ppGpp controls bacterial persistence by stochastic induction of toxin-antitoxin activity. *Cell.* 2013;154:1140–50.
- Amato SM, Orman MA, Brynildsen MP. Metabolic control of persister formation in *Escherichia coli*. *Mol Cell.* 2013;50:475–87.
- Vega NM, Allison KR, Khalil AS, Collins JJ. Signaling-mediated bacterial persister formation. *Nat Chem Biol.* 2012;8:431–3.
- Day AP, Oliver JD. Changes in membrane fatty acid composition during entry of *Vibrio vulnificus* into the viable but nonculturable state. *J Microbiol.* 2004;42:69–73.
- Wu Y, Vulić M, Keren I, Lewis K. Role of oxidative stress in persister tolerance. *Antimicrob Agents Chemother.* 2012;56:4922–6.
- Dörr T, Vulić M, Lewis K. Ciprofloxacin causes persister formation by inducing the TisB toxin in *Escherichia coli*. *PLoS Biol.* 2010;8:29–35.
- Helaine S, Cheverton AM, Watson KG, Faure LM, Matthews SA, Holden DW. Internalization of *Salmonella* by macrophages induces formation of nonreplicating persisters. *Science.* 2014;343:204–8.
- Levin-Reisman I, Ronin I, Gefen O, Braniss I, Shores N, Balaban NQ. Antibiotic tolerance facilitates the evolution of resistance. *Science.* 2017;350:1–10.
- Sackmann EK, Fulton AL, Beebe DJ. The present and future role of microfluidics in biomedical research. *Nature.* 2014;507:181–9.
- Germain E, Castro-Roa D, Zenkin N, Gerdes K. Molecular mechanism of bacterial persistence by HipA. *Mol Cell.* 2013;52:248–54.
- Germain E, Roghanian M, Gerdes K, Maisonneuve E. Stochastic induction of persister cells by HipA through (p)ppGpp-mediated activation of mRNA endonucleases. *Proc Natl Acad Sci U S A.* 2015;112:5171–6.
- Pu Y, Zhao Z, Li Y, Zou J, Ma Q, Zhao Y, et al. Enhanced efflux activity facilitates drug tolerance in dormant bacterial cells. *Mol Cell.* 2016;62:284–94.
- Wakamoto Y, Dhar N, Chait R, Schneider K, Signorino-Gelo F, Leibler S, et al. Dynamic persistence of antibiotic-stressed mycobacteria. *Science.* 2013;339:91–5.
- Orman MA, Brynildsen MP. Inhibition of stationary phase respiration impairs persister formation in *E. coli*. *Nat Commun.* 2015;6:7983.
- Gefen O, Gabay C, Mumcuoglu M, Engel G, Balaban NQ. Single-cell protein induction dynamics reveals a period of vulnerability to antibiotics in persister bacteria. *Proc Natl Acad Sci U S A.* 2008;105:6145–9.

22. Gefen O, Fridman O, Ronin I, Balaban NQ. Direct observation of single stationary-phase bacteria reveals a surprisingly long period of constant protein production activity. *Proc Natl Acad Sci*. 2014;111:556–61.
23. Nowakowska J, Oliver JD. Resistance to environmental stresses by *Vibrio vulnificus* in the viable but nonculturable state. *FEMS Microbiol Ecol*. 2013;84:213–22.
24. Wang P, Robert L, Pelletier J, Dang WL, Taddei F, Wright A, et al. Robust growth of *Escherichia coli*. *Curr Biol*. 2010;20:1099–103.
25. Bergmiller T, Andersson AMC, Tomasek K, Balleza E, Kiviet DJ, Hauschild R, et al. Biased partitioning of the multidrug efflux pump AcrAB-TolC underlies long-lived phenotypic heterogeneity. *Science*. 2017;356:311–5.
26. Keren I, Kaldalu N, Spoering A, Wang Y, Lewis K. Persister cells and tolerance to antimicrobials. *FEMS Microbiol Lett*. 2004;230:13–8.
27. Orman MA, Brynildsen MP. Establishment of a method to rapidly assay bacterial persister metabolism. *Antimicrob Agents Chemother*. 2013;57:4398–409.
28. Keren I, Shah D, Spoering A, Kaldalu N, Lewis K. Specialized persister cells and the mechanism of multidrug tolerance in *Escherichia coli*. *J Bacteriol*. 2004;186:8172–80.
29. Cunningham E, O'Byrne C, Oliver JD. Effect of weak acids on *Listeria monocytogenes* survival: Evidence for a viable but nonculturable state in response to low pH. *Food Control*. 2009;20:1141–4.
30. Roostalu J, Jöers A, Luidalepp H, Kaldalu N, Tenson T. Cell division in *Escherichia coli* cultures monitored at single cell resolution. *BMC Microbiol*. 2008;8:68.
31. Adams BL, Bates TC, Oliver JD. Survival of *Helicobacter pylori* in a Natural freshwater environment. *Appl Environ Microbiol*. 2003;69:7462–6.
32. Cook KL, Bolster CH. Survival of *Campylobacter jejuni* and *Escherichia coli* in groundwater during prolonged starvation at low temperatures. *J Appl Microbiol*. 2007;103:573–83.
33. Henry TC, Brynildsen MP. Development of Persister-FACSeq: a method to massively parallelize quantification of persister physiology and its heterogeneity. *Sci Rep*. 2016;6:25100.
34. Zaslaver A, Bren A, Ronen M, Itzkovitz S, Kikoin I, Shavit S, et al. A comprehensive library of fluorescent transcriptional reporters for *Escherichia coli*. *Nat Methods*. 2006;3:623–8.
35. Silander OK, Nikolic N, Zaslaver A, Bren A, Kikoin I, Alon U, et al. A genome-wide analysis of promoter-mediated phenotypic noise in *Escherichia coli*. *PLoS Genet*. 2012;8(1), e1002443.
36. Hu Y, Kwan BW, Osbourne DO, Benedik MJ, Wood TK. Toxin YafQ increases persister cell formation by reducing indole signalling. *Environ Microbiol*. 2015;17:1275–85.
37. Del Mar LM, Pierobon S, Tafi MC, Signoretto C, Canepari P. mRNA detection by reverse transcription-PCR for monitoring viability over time in an *Enterococcus faecalis* viable but nonculturable population maintained in a laboratory microcosm. *Appl Environ Microbiol*. 2000;66:4564–7.
38. Xu H-S, Roberts N, Singleton FL, Attwell RW, Grimes DJ, Colwell RR. Survival and viability of nonculturable *Escherichia coli* and *Vibrio cholerae* in the estuarine and marine environment. *Microb Ecol*. 1982;8:313–23.
39. Nikolic N, Barner T, Ackermann M. Analysis of fluorescent reporters indicates heterogeneity in glucose uptake and utilization in clonal bacterial populations. *BMC Microbiol*. 2013;13:258.
40. Sugimoto S, Arita-Morioka KI, Mizunoe Y, Yamanaka K, Ogura T. Thioflavin T as a fluorescence probe for monitoring RNA metabolism at molecular and cellular levels. *Nucleic Acids Res*. 2015;43:1–12.
41. Hansen S, Lewis K, Vulić M. Role of global regulators and nucleotide metabolism in antibiotic tolerance in *Escherichia coli*. *Antimicrob Agents Chemother*. 2008;52:2718–26.
42. Maisonneuve E, Gerdes K. Molecular mechanisms underlying bacterial persisters. *Cell*. 2014;157:539–48.
43. Asakura H, Ishiwa A, Arakawa E, Makino SI, Okada Y, Yamamoto S, et al. Gene expression profile of *Vibrio cholerae* in the cold stress-induced viable but non-culturable state. *Environ Microbiol*. 2007;9:869–79.
44. Del Mar LM, Benedetti D, Tafi MC, Signoretto C, Canepari P. Inhibition of the resuscitation from the viable but non-culturable state in *Enterococcus faecalis*. *Environ Microbiol*. 2007;9:2313–20.
45. Nyström T. Nonculturable bacteria: programmed survival forms or cells at death's door? *Bioessays*. 2003;25:204–11.
46. Thomas C, Hill D, Mabey M. Culturability, injury and morphological dynamics of thermophilic *Campylobacter* spp. within a laboratory-based aquatic model system. *J Appl Microbiol*. 2002;92:433–42.
47. Epstein SS. Microbial awakenings. *Nature*. 2009;457:1083.
48. Sharma SV, Lee DY, Li B, Quinlan MP, Takahashi F, Maheswaran S, et al. A chromatin-mediated reversible drug-tolerant state in cancer cell subpopulations. *Cell*. 2010;141:69–80.
49. Pagliara S, Chimere C, Langford R, Aarts DG, Keyser UF. Parallel sub-micrometre channels with different dimensions for laser scattering detection. *Lab Chip*. 2011;11:3365–8.
50. Berney M, Weilenmann HU, Egli T. Flow-cytometric study of vital cellular functions in *Escherichia coli* during solar disinfection (SODIS). *Microbiology*. 2006;152:1719–29.
51. Smith A, Metz J, Pagliara S. Alpha Version of Momanalysis. <https://doi.org/10.5281/zenodo.1063990>. Accessed 21 Nov 2017.
52. Taniguchi Y, Choi PJ, Li GW, Chen H, Babu M, Hearn J, et al. Quantifying *E. coli* proteome and transcriptome with single-molecule sensitivity in single cells. *Science*. 2010;329:533–8.
53. Bamford R, Smith A, Metz J, Glover G, Titball R, Pagliara S. Distributions of Times to First Division for Persister and Untreated Control Cells. https://figshare.com/articles/Distributions_of_times_to_first_division_for_persister_and_untreated_control_cells/5584492. Accessed 22 Nov 2017.
54. Bamford R, Smith A, Metz J, Glover G, Titball R, Pagliara S. Fraction of Persister, Viable but Non-culturable, Susceptible Lysed, and Susceptible Non Lysed Cells. https://figshare.com/articles/Fraction_of_persister_viable_but_non-culturable_susceptible_lysed_and_susceptible_non_lysed_cells/5579941. Accessed 22 Nov 2017.
55. Bamford R, Smith A, Metz J, Glover G, Titball R, Pagliara S. Length of Persister, Viable but Non-culturable, Susceptible Lysed, Susceptible Not Lysed, and Untreated Control *E. coli*. https://figshare.com/articles/Length_of_persister_viable_but_non-culturable_susceptible_lysed_susceptible_not_lysed_and_untreated_control_E_coli/5577367. Accessed 22 Nov 2017.
56. Bamford R, Smith A, Metz J, Glover G, Titball R, Pagliara S. Patterns of GFP Fluorescence for Viable but Non-culturable, Persister, Susceptible, Susceptible not lysed, and Untreated Control Cells. https://figshare.com/articles/Patterns_of_GFP_fluorescence_for_viable_but_non-culturable_persister_susceptible_susceptible_not_lysed_and_untreated_controlcells/5576923. Accessed 22 Nov 2017.

Submit your next manuscript to BioMed Central and we will help you at every step:

- We accept pre-submission inquiries
- Our selector tool helps you to find the most relevant journal
- We provide round the clock customer support
- Convenient online submission
- Thorough peer review
- Inclusion in PubMed and all major indexing services
- Maximum visibility for your research

Submit your manuscript at
www.biomedcentral.com/submit



3.2 Supplementary materials

Investigating the physiology of viable but non culturable cells by microfluidics and time-lapse microscopy

Rosemary Bamford,^{1,2,†} Ashley Smith,^{1,2,†} Jeremy Metz,¹ Georgina Glover,^{1,2}
Richard Titball,¹ and Stefano Pagliara^{1,2,*}

¹ Biosciences and ²Living Systems Institute, University of Exeter, Exeter, Devon
EX4 4QD, UK.

*Correspondence to E-mail: s.pagliara@exeter.ac.uk

†Authors contributed equally to this work

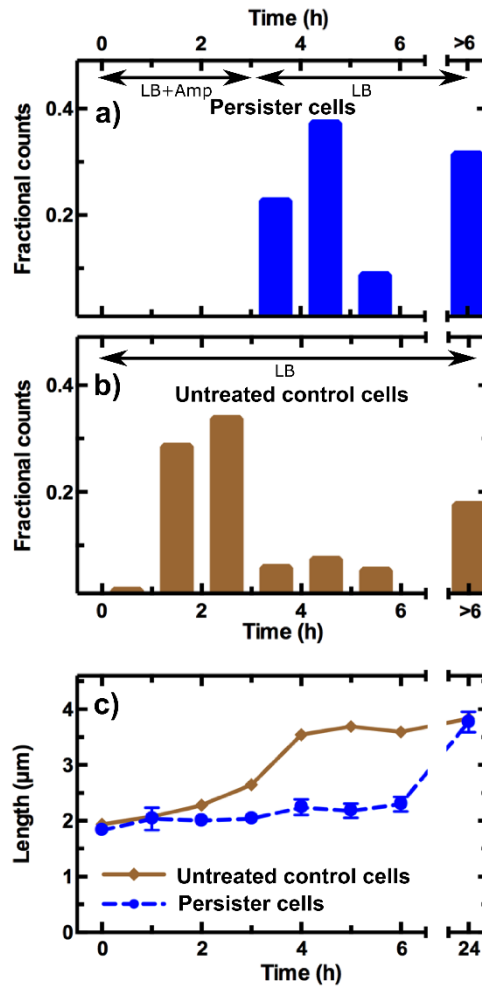


Fig. S1. Bacterial growth in the microfluidic device. a) Fractional distributions of time elapsed to first cell division for persister cells. b) Fractional distributions of time elapsed to first cell division for untreated cells in separate control experiments where LB but without ampicillin was added in the mother machine device. $n \geq 3$, $n_P = 134$ and $n_C = 1274$ persister and untreated control cells, respectively. c) Corresponding average length of persister cells (circles) before ($t=0$), during ($0 < t < 3$ h), and after treatment ($3 < t < 24$ h) with ampicillin at a concentration of $25 \times \text{MIC}$ in LB and of untreated control cells (diamonds). Data and error bars are mean and standard error of the mean obtained by averaging single-cell values obtained on $n_P = 33$ and $n_C = 592$ persister and untreated control cells, respectively, in biological triplicate. We did not observe any significant differences between the results obtained from different biological replica. Due to the large sample sizes, error bars are small compared to the corresponding mean values and are hidden behind some of the data points in (c).

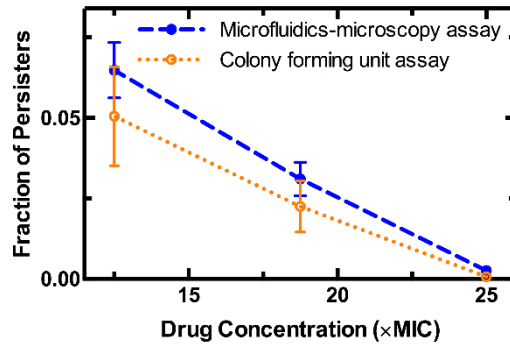


Fig. S2. Bulk and single-cell persister enumeration. Dependence of the frequency of persister cells on ampicillin concentration as measured via the single-cell microfluidics-microscopy assay (full circles) illustrated in Fig. 1 and the colony forming unit assay (open circles). The two assays are performed on aliquots withdrawn from the same *E. coli* overnight culture. Data and error bars are mean and standard error of the mean of measurements obtained in biological triplicate ($N=3$). Data agreement within experimental error confirms the validity of the newly developed microfluidic assay.

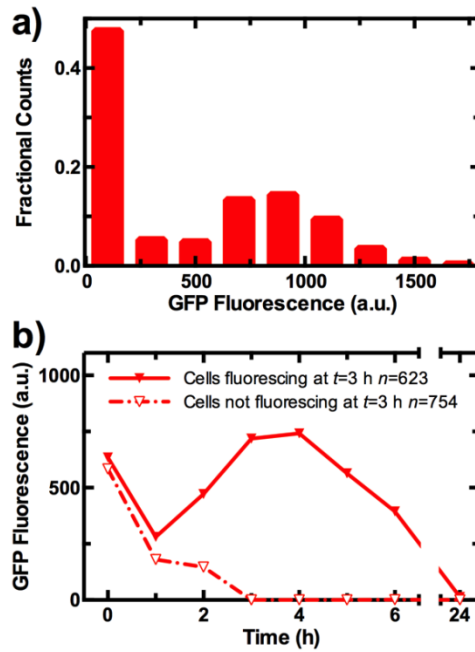


Fig. S3. Subgroups in the subpopulation of susceptible cells. a) Distribution of GFP fluorescence levels in susceptible cells of the *toIC* reporter strain after ampicillin treatment ($t=3$ h). b) Temporal dependence of average fluorescence levels for susceptible cells that fluoresce (filled triangles) and do not fluoresce (open triangles) at $t=3$ h, resembling the two susceptible cells reported in Fig. 3. Data and error bars are the mean and standard error of $n=623$ (filled triangles) and $n=754$ (open triangles) susceptible cells measured in biological triplicate ($N=3$). We did not observe any significant difference between the results obtained from different biological replica. Due to the large sample sizes, error bars are small compared to the corresponding mean values and are hidden behind the data points in (b).

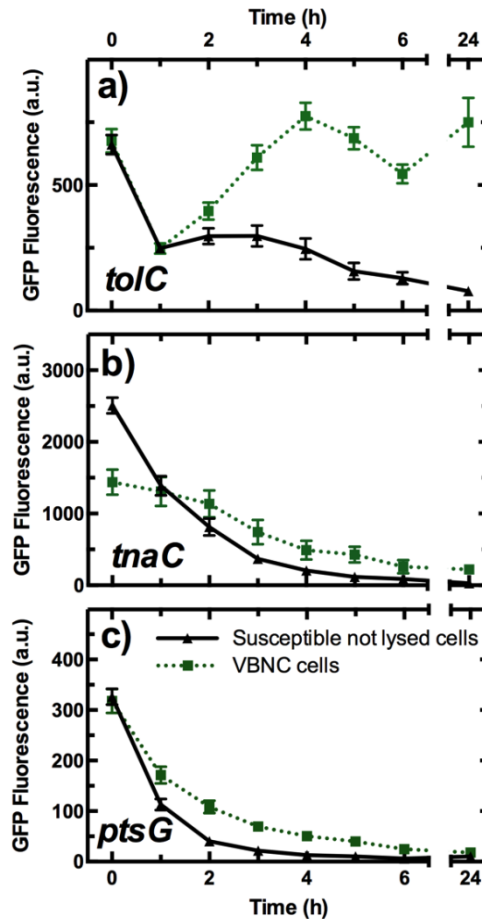


Fig. S4. Viable but non culturable (VBNC) cells are different from susceptible non lysed cells (SNL). Average pattern of GFP fluorescence levels of the VBNC (green squares) and SNL (black triangles) phenotypes throughout the microfluidic assay for the a) *tolC*, b) *tnaC*, and c) *ptsG* reporter strains. The two phenotypes are already distinguishable during drug treatment. Data and error bars are obtained as the mean and standard error of the mean of single-cell measurements in biological triplicate ($N=3$) for each reporter strain for a total of $n_{VBNC} = 147$ and $n_{SNL} = 335$ VBNC and SNL cells, respectively. We did not observe any significant difference between the results obtained from different biological replica. Due to the large sample sizes, error bars are small compared to the corresponding mean values and are hidden behind some of the data points.

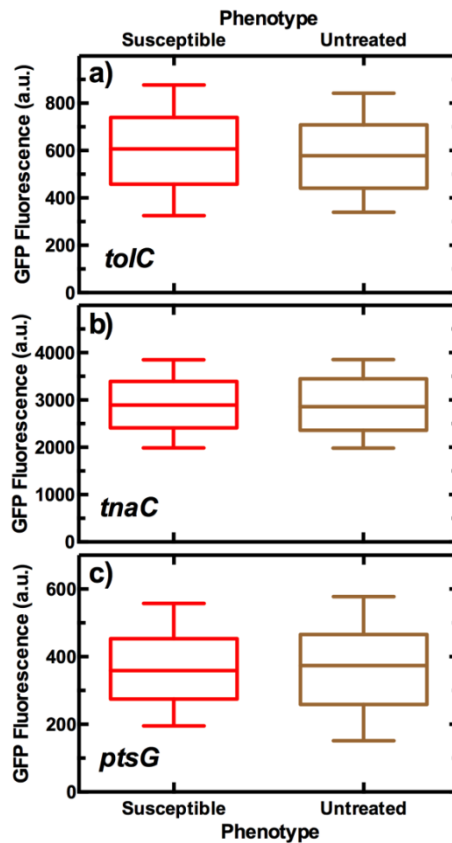


Fig. S5. Susceptible cells are indistinguishable from untreated cells before drug treatment. Distribution of fluorescence levels in the susceptible phenotype before drug treatment ($t=0$) and in untreated control cells before regrowth in LB ($t=0$) in the a) *tolC*, b) *tnaC*, and c) *ptsG* reporter strain. The two populations are not statistically different, an unpaired t test with Welch's correction yielding a P value of 0.07, 0.7, and 0.9, respectively. The bottom and top of the box are the first and third quartiles, the band inside the box is the median, the bottom and top whiskers represent the 10th and 90th percentiles, respectively. Data are obtained at least in biological triplicate ($N=3$) for each reporter strain employed for a total of $n_S = 6659$ and $n_C = 3076$ susceptible and control cells, respectively. We did not observe any significant difference between the results obtained from different biological replica.

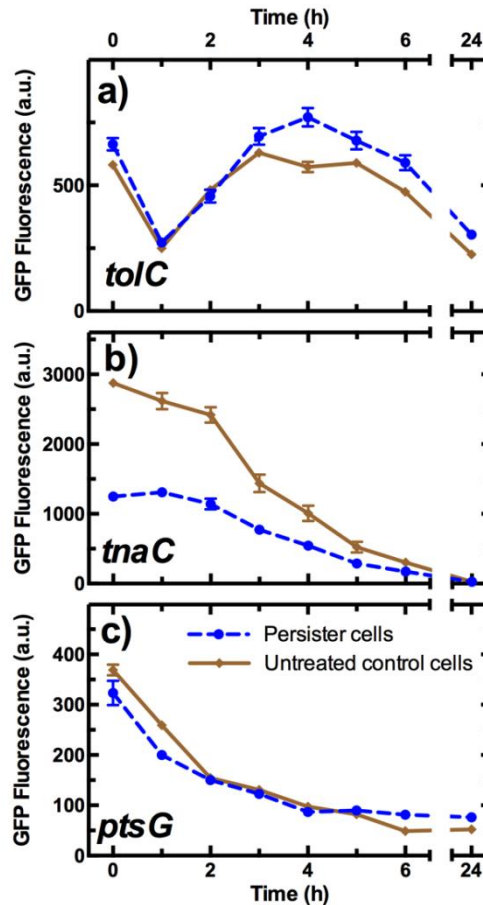


Fig. S6. Persister and untreated control cells have similar patterns of fluorescence levels during regrowth on LB. Average pattern of fluorescence levels in persister (circles) and untreated control (diamonds) cells throughout the microfluidic assay in the a) *tolC*, b) *tnaC*, and c) *ptsG* reporter strains. Persister and untreated control cells exhibit similar patterns of fluorescence levels during regrowth on LB ($3 < t < 24$ h and $0 < t < 24$ h for persister and control cells, respectively) demonstrating that persister cells revert back to a normally growing state after removal of the antibiotic drug. Data and error bars are obtained as the mean and standard error of the mean of single-cell measurements in biological triplicate ($N=3$) for each reporter strain for a total of $n_P = 132$ and $n_C = 3076$ persister and control cells, respectively. We did not observe any significant difference between the results obtained from different biological replica. Due to the large sample sizes, error bars are small compared to the corresponding mean values and are hidden behind the data points.

3.3 Conclusion

Using the protocol reported in this chapter, we identified that both persister and VBNC cells had significantly lower expression of a plasmid based fluorescent reporter for the precursor of the tryptophanase operon; *tnaC*. As a result, we propose low fluorescence in this reporter strain for stationary phase cultures to be a potential biomarker for the isolation of persister and VBNC cells before exposure to antibiotics. Furthermore, using a similar reporter for the multidrug efflux pump *toxC*, we showed that VBNC continue to have a significantly higher level of expression than their persister kin. The continued efflux activity could indicate a higher level of damage in VBNC cells and that persister cells recover quicker upon removal of antibiotics. This provides evidence that VBNC are not cells that are “at death’s door”¹⁴⁸, but are in fact still in an active state and are awaiting favourable conditions in order to resuscitate. In fact, VBNC cells actually exhibited significantly different fluorescence levels compared to persister cells in all 3 of the reporter strains used after 21 hours of regrowth in fresh media. Again, VBNC fluorescence was significantly higher than persisters in *tnaC*, however it was significantly lower in the glucose specific permease *ptsG*. The latter suggesting some level of reduced metabolic activity remaining in the VBNC cells; consistent with literature findings that they remain metabolically active, albeit at a significantly reduced rate^{37,44,149,150}. In fact, as discussed in a recent paper by Ayrapetyan *et al.* our protocol can be used to investigate the transition of cells into the dormant state, particularly under exposure to stressful conditions, such as antibiotics or the pH levels identified in chapter two; an approach which may be crucial for testing the dormancy continuum hypothesis⁴⁴.

Importantly, this protocol can allow for the simultaneous screening of multiple genes through the use of different fluorescent reporters. For instance, in chapter two we hypothesise that cells first use glucose before switching to acetate and show that the population level transcriptome reflects this hypothesis through the expression of *ptsG* and *actP*. By switching the main nutrient source from glucose to acetate prior to antibiotic exposure, reporters for both of these genes could be simultaneously measured to determine if the cells response to the switch allows it to enter the persister or VBNC state. Furthermore, our system is not limited to the reporter strains we used or to antibiotic response mechanisms,

it could easily be utilised for investigating how microbial populations adapt to changes in their extracellular environment, such as the changes in pH levels measured in chapter two.

As mentioned above, our protocol also allowed us to analyse persister and VBNC cells prior to exposure to antibiotics. Using this information, we were able to show that VBNC and persister cells shared similar levels of fluorescence and similar morphological attributes (i.e. cell size) for all 3 reporter strains prior to antibiotic exposure. This supports the hypothesis that VBNC and persister cells are not distinct entities but exist as part of one physical continuum³⁷. Our evidence that VBNC cells had higher fluorescence levels than persister cells after 21 hours of regrowth in the *toIC* reporter strain, suggests that VBNC are more damaged than their persister counterparts, perhaps as a result of added intracellular stress. Interestingly, the protocol discussed in this chapter provides an exciting platform to further investigate this.

In chapter one I discussed how indole has been associated with antibiotic persistence, but whether it decreased or increased survival was still up for debate. In chapter two, we then showed that *tnaC*, the precursor to the *tna* operon, was one of the 10 most upregulated genes during the exponential phase of growth when we also witnessed increases in the persister fraction within the population. However, as discussed above, we showed in this chapter that the fluorescence level in the *tnaC* reporter strain was significantly lower in the persister and VBNC phenotypes. As a result, we propose it to be a potential non-invasive biomarker and aim to use it for the isolation of persister and VBNC cells prior to antibiotic exposure. Furthermore, once isolated transcriptomic analysis can help elucidate the mechanisms involved in their formation such as their metabolic state. Therefore, this shows that the approach we took in chapter one can be useful for identifying potential genes and mechanisms involved in phenotypic heterogeneity, and again highlights the importance that these need to be investigated at the single cell level.

In this chapter we report the protocol we developed, based on the pre-existing Mother Machine technology⁸, for the analysis of single antibiotic persister and VBNC cells. To the best of my knowledge, this is the only protocol developed that allows the simultaneous analysis of persister and VBNC cells before, during

and after, exposure to antibiotics.. However, we discussed in chapter one how modern single cell technologies are often limited by the time required to perform the data analysis. This protocol is no different, despite producing a vast amount of data on single bacteria, the throughput was limited by the time required to analyse all the images. As a result, I developed an automated python program that would allow the analysis of the images acquired using the mother machine; *MMHelper*. *MMHelper* was discussed briefly in this chapter and it was utilised for the data analysis of the experiments reported. However, a more detailed overview can be found in chapter four.

Chapter 4: MMHelper: An automated framework for the analysis of microscopy images acquired with the mother machine

4.1 Introduction

In the previous chapters we have discussed and shown the importance of single cell approaches, particularly microfluidics, for investigating phenotypic heterogeneity. Due to their ability to allow manipulation of both the extracellular environment and extracellular space, microfluidic devices have already been used for investigating single cell characteristics in multiple domains of life^{104,115,151}. Pagliara *et al.* used microfluidics to discover pluripotent embryonic stem cells had auxetic properties¹⁰⁸. In bacteria, Norman *et al.* investigated the ability of cells to switch between growth states in *B. subtilis*¹²⁰. Similarly, single cell growth and division rates were characterised in the yeast *S. pombe*¹⁰⁹. However, perhaps the most commonly adapted microfluidic device to date has been the Mother Machine⁸.

The mother machine was first developed by Wang *et al.* to investigate heterogeneity in growth rates in an *E. coli* population⁸. It has since been used by a variety of research groups, for example to discover that *S. typhimurium* cells that express the virulence factor *ttss-1* were more inclined to survive exposure to a fluoroquinolone¹²⁴ and that multi-drug efflux pump AcrB-TolC is more prominent in mother cells after *E. coli* cellular division⁷. In chapter three I introduced our high throughput protocol for investigating antibiotic persister and VBNC cells in bacterial populations using the mother machine technology. Furthermore, in chapter one and chapter three, we discussed how the throughput of microfluidic devices, such as the mother machine, can be limited by the analysis steps and therefore the need for automated analysis systems to compliment them.


To this end, multiple research groups who have utilised the mother machine have developed custom image analysis programs^{8,105,124,130}. In fact, Wang *et al.*

themselves realised the importance of automated analysis as they would typically be analysing $\sim 10^7$ cells per time lapse experiment⁸. However, the program they developed using C++, required a fluorescence channel in order to detect the bacterium⁸. As a result, this limits the ability of researchers to utilise fluorescence channels for researching other cellular mechanisms. Other groups have produced custom analysis programs for Mother Machine and these have been discussed in more detail in Chapter one. Briefly, Arnoldini, *et al.* developed an ImageJ plugin (*MMJ*) and used it for the previously discussed research into *S. typhimurium* virulence¹²⁴. However, this plugin is only semi-automatic and the level of pre-processing that is required makes it non feasible for use on large datasets¹²⁴. Kaiser *et al.* used the mother machine to investigate gene regulation at the single cell level in *E. coli* and similarly developed a ImageJ plugin (*MoMA*) to analyse their images, although *MoMA* is more automated than the previously discussed *MMJ* plugin^{105,152}. Sachs, *et al.* developed a fully automated python module (*Molyso*) and showed they could utilise it to investigate heterogeneity in the production of L-valine during a nutrient switch in an engineered strain of *Corynebacterium glutamicum*¹³⁰. Importantly, however both of the two fully automated approaches, *MoMA*¹⁰⁵ and *Molyso*¹³⁰, were developed for the analysis of images acquired in phase contrast. Therefore, until this thesis, there was no automated analysis software available for Mother Machine images that can be applied to multiple imaging modalities, particularly images that are acquired in bright field.

With that in mind, we developed *MMHelper*, a fully automated python program that is able to detect bacteria in a Mother Machine device in multiple imaging modalities (phase contrast and bright field). We have already briefly discussed *MMHelper* and how we used it to investigate antibiotic persister and VBNC in over 10 000 cells in chapter three. However, in this chapter we discuss the analysis pipeline in more detail and compare the performance of *MMHelper* against the other freely available automated Mother Machine analysis tool *Molyso*. We show how *MMHelper* outperforms *Molyso* in both modalities. Furthermore, we extract cellular information on shape and fluorescence and directly compare the results from *MMHelper* to those acquired through manual analysis, showing *MMHelper* to return similar values. As a result, we show

MMHelper can be reliably used for the high throughput analysis of mother machine images tackling a variety of biological problems.

SCIENTIFIC REPORTS



OPEN

MMHelper: An automated framework for the analysis of microscopy images acquired with the mother machine

Ashley Smith^{1,2}, Jeremy Metz^{1,2} & Stefano Pagliara^{1,2}

Live-cell imaging in microfluidic devices now allows the investigation of cellular heterogeneity within microbial populations. In particular, the mother machine technology developed by Wang *et al.* has been widely employed to investigate single-cell physiological parameters including gene expression, growth rate, mutagenesis, and response to antibiotics. One of the advantages of the mother machine technology is the ability to generate vast amounts of images; however, the time consuming analysis of these images constitutes a severe bottleneck. Here we overcome this limitation by introducing *MMHelper* (<https://doi.org/10.5281/zenodo.3254394>), a publicly available custom software implemented in Python which allows the automated analysis of brightfield or phase contrast, and any associated fluorescence, images of bacteria confined in the mother machine. We show that cell data extracted via *MMHelper* from tens of thousands of individual cells imaged in brightfield are consistent with results obtained via semi-automated image analysis based on ImageJ. Furthermore, we benchmark our software capability in processing phase contrast images from other laboratories against other publicly available software. We demonstrate that *MMHelper* has over 90% detection efficiency for brightfield and phase contrast images and provides a new open-source platform for the extraction of single-bacterium data, including cell length, area, and fluorescence intensity.

Phenotypic heterogeneity is a common feature within isogenic bacterial populations^{1–3}. Cell-to-cell variations have been observed in bacterial growth rate³, virulence⁴, and resistance to stress¹. As a result, it has been suggested that such heterogeneity may allow some cells to survive within fluctuating environments^{1,5–8} and hence promote evolutionary adaptation^{9,10}. Traditional microbiological assays are based on ensemble measurements and thus unable to measure cell-to-cell differences within microbial populations. In contrast, microfluidics allows the precise manipulation of fluids at the submillimetre level¹¹ and when used in combination with microscopy can be utilised for biological assays with single-cell resolution^{12,13}. Microfluidics has already been adapted for investigating heterogeneity across multiple domains of life. For instance, Hansen *et al.* developed a protocol which enables measurement of signalling dynamics in single yeast cells¹⁴, Li *et al.* investigated heterogeneity in the migration ability of a population of lung cancer cells¹⁵, Yuan *et al.* looked at the effects of genome deletions on bacterial growth¹⁶, Pagliara *et al.* showed that embryonic stem cells exhibit auxetic properties¹⁷, and Otto *et al.* measured the mechanical deformability of single cells to identify cell sub-populations in whole blood samples¹⁸. There are a multitude of microfluidic designs and devices available for investigating single bacterial cells. One popular example is the mother machine¹⁹, which provides an ideal platform for tracking single bacterial cells over time while continuously supplying growth nutrients or compounds to be tested such as antibiotics.

Wang *et al.* designed the mother machine (MM) to allow the trapping of a single mother cell at the dead-end of each of thousands of microfluidic channels and the tracking of its daughter cells over hundreds of generations¹⁹. This tool has since been employed to investigate a variety of research questions with single-cell resolution. Tanouchi *et al.* and Kaiser *et al.* used the MM to investigate gene regulation^{20–22}. Robert *et al.* and Uphoff investigated the emergence of mutations in single cells and the dynamics of mutagenesis^{23,24}. Moolman, *et al.* utilised it to explore protein stoichiometry and dynamics²⁵ whereas Chait *et al.* used it to engineer bacterial population

¹Living Systems Institute, University of Exeter, Exeter, United Kingdom. ²Biosciences, University of Exeter, Exeter, United Kingdom. Ashley Smith and Jeremy Metz contributed equally. Correspondence and requests for materials should be addressed to J.M. (email: j.metz@exeter.ac.uk) or S.P. (email: s.pagliara@exeter.ac.uk)

behaviour²⁶. Multiple groups have used it to investigate single cell response to antibiotics^{4,27,28}, and Yang *et al.* studied bacterial adaptation under physical confinement²⁹.

Some research groups have developed software which can be used for the analysis of images of bacteria confined in the mother machine³⁰, although most still use scripts customised around their experimental and imaging set-up^{23,26,27,31}. Initially, Arnoldini, *et al.* developed *mmj*, a semi-automatic ImageJ plug-in which facilitates the analysis of mother machine images⁴. However, it is inefficient to use this semi-automated approach on thousands of images. Sachs *et al.* developed *Molyso* an unsupervised software implemented in Python³⁰. *Molyso*, provides a fast and efficient framework capable of analysing 90 GB of mother machine images in 30 min. Nonetheless, their program has limitations which prevent its use by the wider mother-machine community, including not being suitable to analyse standard brightfield images, and constraints on initial channel orientation. Another ImageJ plug-in, *MoMA*, is also available and the authors claim to achieve unprecedented accuracy in segmenting and tracking bacteria²². However, we were unable to install and run *MoMA*, on any datasets, within a reasonable (2 hour minimum) time period. Using the suggested installation method we successfully installed *MoMA* but always encountered a FIJI exception error when trying to run the application due to its dependency on Gurobi, even when running on *MoMA*'s own image set.

In order to overcome the limitations above, we introduce *MMHelper*, an analysis framework that, to the best of our knowledge, is the first fully automated program applicable to multiple imaging modalities of the mother machine. *MMHelper* is implemented as a user-friendly python module which detects bacteria confined within the MM and tracks their progeny and fate through time. These detected bacterial regions can then be used to access information on length and area as well as any accompanying fluorescence intensity data. We demonstrate that by using *MMHelper*, brightfield imaging can be used for extracting phenotypic information from individual bacteria (e.g. length, width, morphology) in the mother machine as well as phase contrast imaging; with the added value that brightfield imaging does not rely on the use of specialised optical components. Furthermore, we have recently used *MMHelper* to analyse the response to antibiotics of 11,823 single bacteria thus generating novel insight on the physiology of phenotypic variants²⁸. Therefore, we believe that the efficiency and accuracy of *MMHelper* will assist the investigation of a variety of biological questions by significantly improving the throughput and reliability of mother machine experiments.

Methods

Our image analysis pipeline can be decomposed into two core stages, detection and tracking, which are followed by the extraction of the temporal changes of single-cell parameters including length, width, area, and fluorescence intensity. After determining the imaging modality (1A), each stage is comprised of channel-centric (Fig. 1B,D) and bacteria-centric (Fig. 1C,E) sub-stages. The detection stages (Figs 1B,C and S1) take place independently of the time-point of the experiment and are shown in more detail in Fig. 2A–D and Fig. 3A–D, respectively. In comparison, the tracking stages (Fig. 1D,E) are performed relative to the previous time point (i.e. the $t = 0$ h left hand panel images are used as a reference for the tracking on the $t = 1$ h right hand panel images).

Data organisation and loading. Each image is loaded as a multi-dimensional numpy array using the scikit-image module. For experiments including fluorescence images, these arrays are split such that detection is only performed on the brightfield (or phase contrast) images. *MMHelper* can be run specifically on single images or on image time-series and it also contains a batch run mode. This mode allows the analysis of a whole folder that contains images from tens of different time points and areas of the MM. In this instance, a naming protocol is used to associate images with areas on the chip. Specifically, a string is used at the start followed by an underscore that identifies which MM area the respective image is from. After this underscore, a time stamp is used in order to sort the images in chronological order (e.g. a suitable filename for an image of area 1 of the MM acquired at 12:33:01 on the 16th October 2017 would be: "Area01_171016_123301.tiff").

Detection. The first stage of the detection process is to determine whether the image is a phase or brightfield image (Fig. 1A). We noted that the pixel intensity distributions of brightfield and phase-contrast images, obtained with similar N.A. objectives, are significantly different. Therefore, we used the skewness of the pixel intensity distribution to detect the imaging modality. As we have a large sample size in terms of pixel count (for a square image that is 1000 pixels in length: $n_{\text{pixels}} \approx 1,000^2 = 1,000,000$), we used the uncorrected expression for the skewness G_1 ³², with the samples third and second central moments of the pixel data, m_3 and m_2 respectively.

$$G_1 = \frac{m_3}{m_2^{3/2}}$$

If this equation returns G_1 as a positive value, the image is assumed to be phase contrast, whereas a negative value suggests the input image was acquired in brightfield.

After determining the imaging modality, the input image is filtered (Fig. 2A) using a gradient magnitude Sobel edge for phase contrast images or Frangi ridge filter for brightfield images³³.

The edge or ridge filtering accentuates the channel outlines, and is followed by Li's iterative minimum cross-entropy based automated thresholding³⁴ to binarize the image. This mask image is labelled using connected-component labelling, and the labelled regions are filtered based on area to remove non-channel regions.

The resulting channel-outlines are morphologically dilated to close small gaps in the outline, and the subsequent closed regions are filled using a region-filling algorithm. These inner channel regions are extracted as the difference between the outlines and the filled regions (Fig. 2B). The inner-channel perimeters are converted to pixel locations and, by determining the pixel locations that are farthest apart, channel vectors are generated. These

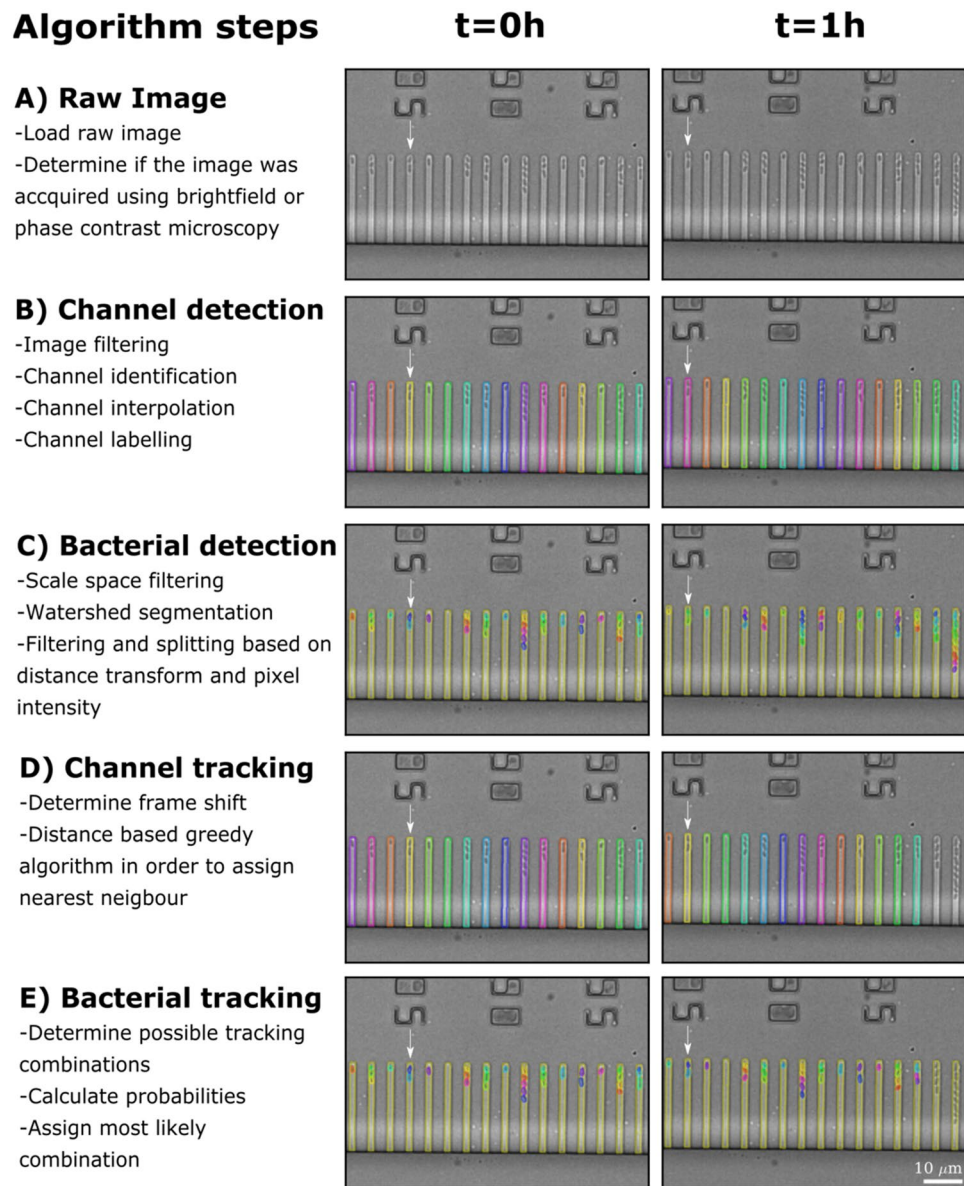


Figure 1. Overview of the analysis pipeline. The analysis pipeline is broken down into five major steps. **(A)** The imaging mode is detected, determining whether images are brightfield or phase contrast. **(B)** Channels are detected, assigned specific labels and ordered consecutively from left to right. **(C)** Bacteria are detected in each channel. **(D)** Channels are tracked throughout the image time-series. In these representative images, the mother machine device at $t = 1$ h has moved approximately $10 \mu\text{m}$ to the left with respect to $t = 0$ h, as indicated by the arrow. Our algorithm quantifies this frame shift and relabels each channel accordingly, for example the channel indicated by the arrow is recoloured in yellow. **(E)** After channel tracking, the detected bacteria in each channel are tracked accordingly and relabelled where necessary, each bacterium keeping the same unique colour through consecutive time points as indicated by the arrow.

vectors are filtered for length to select only regions in a predetermined range (default: 100–400 pixels) based on the images acquired from our typical experimental set-up, however they can be adjusted using a scale factor (see additional parameters section). The resulting vectors correspond to the long channel edges, therefore the perpendicular distance between them is also filtered to ensure that the selected channels correspond to single channels. The resulting channel regions form the basis for a subsequent interpolation stage (Fig. 2C). First, the aforementioned channel regions are analysed to determine the single channel-to-channel spacing, to allow the identification of undetected channels. Using this spacing, the positions of eventually undetected channels are interpolated from the detected channel positions. The detected average channel shape is stamped into each interpolated position. Using the channel contours, the perimeter of each detected channel can be seen in the final output images (Fig. 2D). Note that at least three channels must be detected in any given image to allow the algorithm to attempt interpolation. If two or less channels are detected the algorithm warns the user that it was unable to accurately detect channels in this image, and the frame is not considered for further detection.

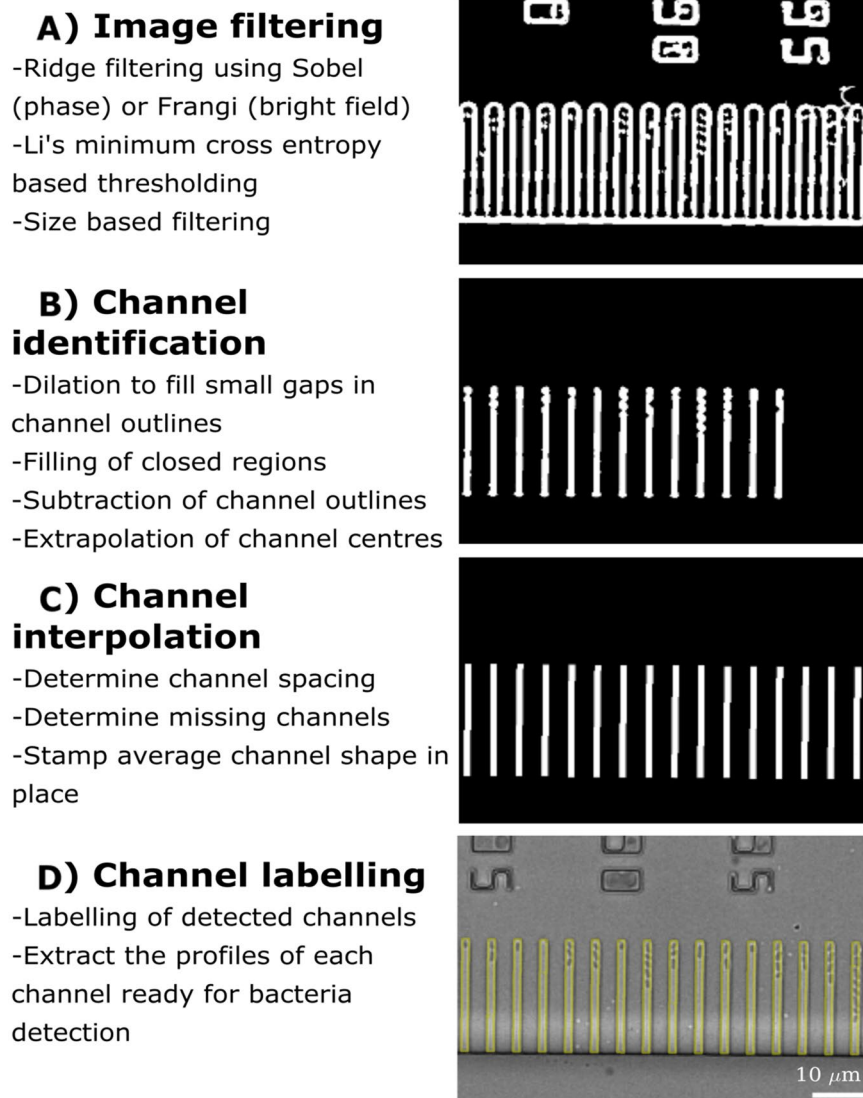


Figure 2. Pipeline for channel detection. (A) The original image is filtered (Sobel for phase images and Frangi for brightfield) followed by thresholding to identify potential ridges. These ridges are then filtered by size to leave the masks of the channels. (B) A new mask is created with the centre of each channel filled and through a simple subtraction of the previous mask with the new one, the centre of each channel is extrapolated. These masks can appear irregular in shape due to the presence of the bacteria they host. Consequently, new profiles are determined by creating vectors around the perimeter to form an average channel shape. (C) The spacing between these channels is determined and, after interpolation to determine the location of missing channels, the average channel shape is stamped in place. Noteworthy, our algorithm performs well also with images where the main channel is not horizontal resulting in slightly staggered labels. (D) A yellow contour is drawn around each label to delineate the detected channels.

The next sub-stage in detection is to detect bacteria within the channels identified from the process above. In these images, the bacteria initially appear darker than the background (Fig. 2D). Therefore, the images are inverted to allow for the use of standard algorithms to detect bright objects on dark background. To do this, the background intensity for each channel is estimated using a rolling ball filter and subtracted from its respective image³⁵ (Fig. 3A). Furthermore, by subtracting the background intensity, the watershed segmentation can remain the same for bacteria located anywhere along the channel profile (Fig. S2).

These channel images are then processed as follows: first each channel image is scale-space filtered³⁶ using a Laplace of Gaussian convolution at multiple scales, and maximum-projected along the scale axis (Fig. 3B). Using these filtered channel images, a threshold value is determined using Li's algorithm to avoid over-segmentation of empty channels. Each filtered channel image is then binarized using this threshold value and outlines generated by taking the difference between the dilation (grow) and the erosion (shrink) of the initial binary image. An initial crude region-splitting stage is included as occasionally multiple bacteria are detected as a single region, which reduces the accuracy of the region size filtering step. For this, the algorithm uses the marker-controlled Watershed

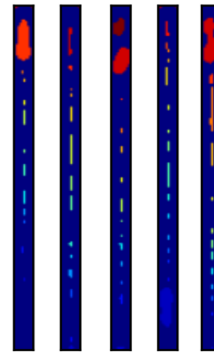
A) Image inversion

-The detection pipeline is the same for bright field or phase contrast so brightfield images are initially inverted



B) Watershed segmentation

-Scale-space filtering
-Li's minimum cross entropy based thresholding
-Marker based watershed transformation



C) Filtering and splitting

-Filter out objects smaller than a specified size
-Splitting based on distance transform and pixel intensity

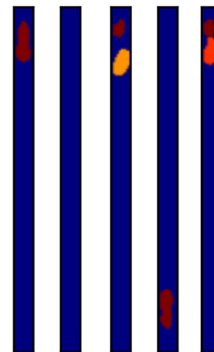


Figure 3. Pipeline for bacteria detection. (A) By using the masks for the detected channels, the corresponding original image for each channel is identified and the image inverted using background subtraction. (B) This is followed by scale space filtering and thresholding. As a result, markers are identified that can be used for a watershed transformation. (C) Each single element within each channel identified by the watershed transformation is given a unique label, represented by a different colour. The result of the watershed is filtered to remove non-bacterial particles. Bacterial splits are identified, using a combination of width and pixel intensity, and a mask of the detected bacteria produced using a combination of distance transformation and pixel intensity along the skeleton.

transform³⁷. Markers are generated from all regions greater than a predefined distance from the mask background, and used to delineate bacteria. These regions are finally filtered for width and size (Fig. 3C). Following the initial bacteria segmentation, a second dedicated bacteria-splitting stage was included to improve the segmentation quality of adjacent bacteria (Fig. 3C). The initially detected bacteria are skeletonised and “splits” identified using a combination of distance transformation and pixel intensity, with the threshold values determined using the median and median absolute deviation of all the initially detected bacteria from the original image.

Tracking. The detected channels and bacteria are tracked in two stages. First global frame shift is determined for whole images using cross-correlation based template matching³⁸. This allows channels from consecutive time-points to be matched using simple distance-based greedy assignment, which matches each point to its nearest neighbour as long as it is also the nearest neighbour to that point. To do so, channel centroid positions are extracted and channels in consecutive frames are linked if each is the nearest neighbour to the other (Fig. 1D). Once channels have been tracked in adjacent time frames, bacteria can be tracked in each channel. This proceeds according to a simple multiple-hypothesis tracking where probabilities of all possible assignments are calculated. These assignments take into account the centroid position and area of each bacterium, as well as adjustable probabilities that each bacterium remains an individual entity (no-change, Fig. 4A), or fades away from the channel

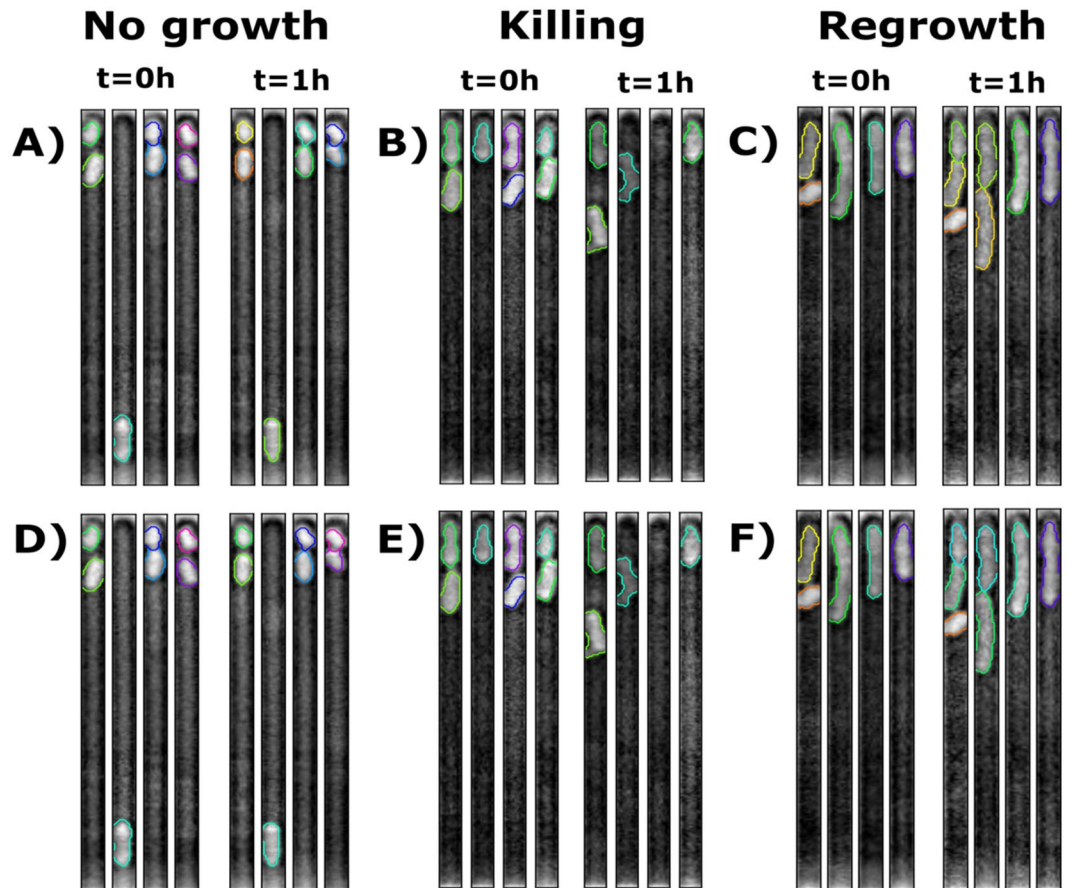


Figure 4. Overview of bacteria tracking. Individual bacteria detected in an experiment using (A) minimal medium, (B) antibiotic treatment, or (C) growth medium at $t = 0$ and at $t = 1$ h (channels at the left and right hand side of each panel, respectively). (D–F) Corresponding tracked bacteria are relabelled, where necessary (e.g. second channel from the left in D), at $t = 1$ h so that their label (i.e. contour colour) matches that at $t = 0$. When a division occurs each of the offspring is assigned a new unique label (e.g. first and second channel from the left in F).

(cell death, Fig. 4B), or gives rise to progeny (cell division, Fig. 4C). These events can occur in a number of different combinations to produce the number of bacteria detected in the current frame relative to the preceding frame ($t = 1$ h compared to $t = 0$ in Fig. 4A–C). Therefore, a list of all these possible combinations is generated and for each of these possibilities the total number of bacterial divisions that would be required is determined. A probability based on the change in area between the bacteria and its offspring is determined and normalised by the number of divisions. A second probability based on the change in centroid, is calculated taking into account that for each division the change in centroid location is expected to move by half the length of an average bacterium. Finally, the algorithm calculates the likelihood of a cell dividing, lysing, or remaining a single cell between consecutive time points. All three of these probabilities are then multiplied together to determine the overall likelihood that the given event occurred for an individual bacterium. The determined probability for each bacterium within the channel is multiplied to produce an overall probability for the respective combination of events. The resulting, most probable, combination is then used to correctly relabel each bacterium in each image (e.g. second channel from the left in Fig. 4D), with newly generated bacteria assigned a new unique label (e.g. first and second channels from the left in Fig. 4E).

Extraction of single-cell parameters. Once bacteria detection and tracking has been completed, extraction of all quantities of interest can be achieved through the detected and tracked region-based properties. Each bacterium's length, width, and area are determined using the various standardised algorithms presented via the *regionprops* function. The binary masks can then be used to extract the raw fluorescence intensity values from the corresponding fluorescence images reporting for example the activity of transcriptional reporters or the intracellular accumulation of spectrally distinct substrates. The background fluorescence is obtained from the empty areas (parts of the channels not containing detected bacteria) of each channel and subtracted from each respective bacterium's fluorescence intensity. These quantities are then saved in a csv file. We have recently used *MMHelper* to measure the temporal changes in promoter activity in 11,823 individual *Escherichia coli*²⁸. Figure 5A–C report the temporal changes in area, length and GFP fluorescence for three representative bacteria, and their progeny, growing in lysogeny broth. The fluorescence reported in Fig. 5C is the mean pixel intensity and the gradual

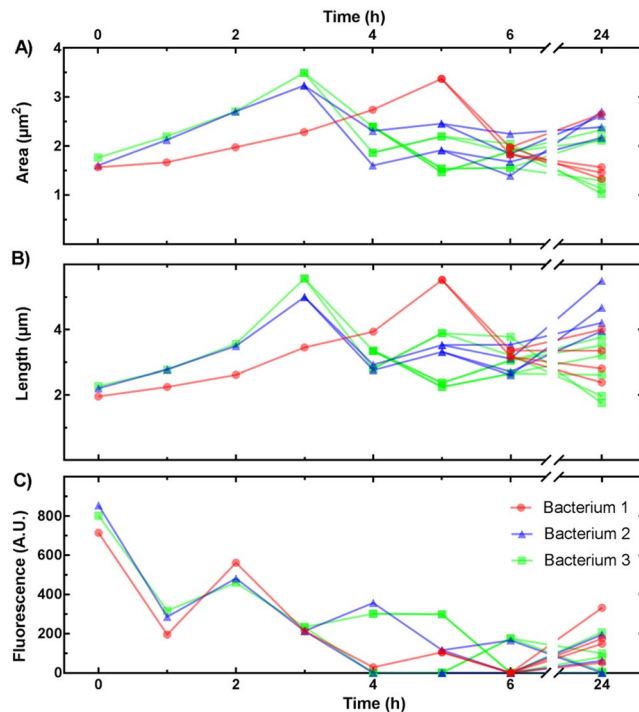


Figure 5. Dynamics in single-bacterium parameters. Temporal changes in (A) area, (B) length, and (C) GFP fluorescence for three representative bacteria, and their progeny, growing in lysogeny broth. Data bifurcations indicate bacterial divisions, e.g. bacterium 3 divided at $t = 3$ h and its daughters divided at $t = 5$ h.

decline in the fluorescence values reported is not due to photobleaching, but is a genuine proxy for the expression of the multi efflux pump *tolC* (the promoter upstream of GFP in the plasmid carried by the strain), due to the reduction of cellular stress upon continuous exposure to fresh media, similar to the profile we previously observed²⁸.

Additional parameters and module usage. *MMHelper* can be used to analyse image time series acquired with different microscopy setups (e.g. different objective magnification and numerical aperture, different cameras) by adjusting a single “Scale factor” parameter. Furthermore, the user can specify how many fluorescence image channels are acquired for each brightfield (or phase contrast) image. More information on parameters and how to adjust them will be available on the repository wiki page (<https://github.com/jmetz/mmhelper/wiki>).

Due to the 2D nature of *MMHelper*’s detection, it performs the analysis on any image orientation and there is no need for tilt correction. Furthermore, the modular nature of *MMHelper* makes it suitable for future adaptation to slightly different experimental set ups such as microchemostat devices³⁹.

Statistical comparison. In order to compare the performances of *MMHelper* and *Molyso*, we manually drew ground truth detection masks in the images using the freely available GIMP drawing program and used them to quantify three parameters: the Jaccard index, precision and recall values of the automated detection (Fig. S3). We ran both software programs on our own brightfield images, and three independent sets of phase contrast images from (i) the the Locke’s laboratory⁴⁰, (ii) the work by Sachs, *et al.* (*Molyso*)³⁰ and (iii) the work by Kaiser, *et al.* (*MoMA*)²². In order to use *Molyso* on brightfield images, we inverted these images before analysis since the authors did not develop this software for brightfield imaging. We then directly compared the respective values for each parameter, statistical significance was tested by unpaired t test with Welch’s correction, where $p \leq 0.05$ is * $p \leq 0.01$ is ** $p \leq 0.001$ is *** and $p \leq 0.0001$ is **** respectively.

Results and Discussion

We developed *MMHelper* to work on both brightfield and phase contrast images with high detection efficiency and accuracy, this also allowing accurate extraction of data from any associated fluorescence images. In order to quantify the performances of our software, we randomly selected 5 of our brightfield datasets²⁸ and analysed image time-series for 4 consecutive time-points, resulting in the analysis of 14 frames containing between 18 and 120 bacteria each. We characterised the detection efficiency as the percentage of bacteria which were detected and, from a total of 562 bacteria across all of the brightfield images, the efficiency was determined as $98 \pm 1\%$. However, in some cases one bacterium was labelled as multiple bacteria or multiple bacteria detected as an individual bacterium. In these circumstances the detection cannot be said to be accurate, therefore we termed detection accuracy as the percentage of bacteria correctly identified by a single label and calculated it to be $80 \pm 3\%$ across the 14 previously mentioned brightfield images. Furthermore, we used *MMHelper* to analyse an image dataset acquired with a phase contrast microscope in the Locke’s laboratory⁴⁰, obtaining a bacterial detection

	Pipeline	Bright field			Phase		
		Precision (%)	Recall (%)	Jaccard index (%)	Precision (%)	Recall (%)	Jaccard index (%)
Channels	<i>MMHelper</i>	77.8 ± 1.9	97.6 ± 1.4	77.2 ± 3.1	53.8 ± 0.2	99.4 ± 0.6	53.7 ± 0.3
	<i>Molyso</i>	64.3 ± 25.7*	58.9 ± 22.2*	42.1 ± 21.7*	79.9 ± 9.0	77.1 ± 9.4	64.6 ± 12.8
Bacteria	<i>MMHelper</i>	78.8 ± 14.6	76.3 ± 14.0	57.1 ± 14.1	47.3 ± 15.0	96.5 ± 3.5	43.9 ± 14.3
	<i>Molyso</i>	43.8 ± 21.7*	12.7 ± 7.9*	11.4 ± 6.5*	39.0 ± 17.1	19.5 ± 8.2	15.2 ± 7.1

Table 1. Medians and median absolute deviations of Jaccard index, precision and recall for ground truth detection for *MMHelper* and *Molyso*. **Molyso* was not specifically developed for brightfield imaging.

efficiency of $95 \pm 1\%$ and an accuracy of $65 \pm 1\%$. This demonstrates i) the capability of *MMHelper* to detect bacteria in mother machine images in both brightfield and phase contrast modalities and ii) the capability to work equally well across independent experimental setups.

For each software and each dataset we then measured three different parameters: detection precision as the overlap area between the detected and ground truth masks divided by the detection mask; detection recall as the overlap area divided by the ground truth mask^{41,42} (Fig. S3); and finally the Jaccard index, defined as the overlap area divided by the total combined area⁴². The use of precision and recall allows a comparison of the trade-off between ensuring no areas are missed (recall) and how precise the algorithm is, with the Jaccard index representing a combination of these values⁴². We compared these parameters for *MMHelper* and *Molyso* applied to the detection of 310 channels from our brightfield and Locke's phase contrast images (Fig. S4 and Table 1). The corresponding Kernel Density Estimation for channel detection precision v recall is reported in Fig. 6A for brightfield and Fig. 6B for phase contrast datasets, respectively. Noteworthy, the multi-modal distribution of density for channel detection in brightfield is probably due to small variations in the quality (e.g. focus) of images acquired, resulting in the precision values varying slightly for individual images. For instance, of the total 14 brightfield frames, the majority clustered around 0.8, one frame had a precision level of 0.9 and two frames had precision levels close to 1 (Fig. S6).

As expected, according to the Jaccard index, *MMHelper* shows significantly better channel detection than *Molyso* on the brightfield datasets ($p \leq 0.0001$, Fig. S4E), although *Molyso* performed better on the phase contrast dataset ($p \leq 0.0001$, Fig. S4B). *MMHelper* shows a channel detection recall close to 100% for both phase contrast and brightfield images as a result of the detected channels being slightly larger than the ground truth masks, and was significantly better than *Molyso* ($p \leq 0.0001$, Figs S4C and S4D). The detected channels being larger than the ground truth masks was also reflected in the precision values which were slightly lower, with *Molyso* being significantly better than *MMHelper* for phase contrast ($p \leq 0.0001$, Fig. S4B), although *MMHelper* was still significantly better for brightfield ($p \leq 0.0001$, Fig. S4A). This over-estimation, however, does not affect the level of accuracy of bacterial detection, see below, which is the ultimate aim of this pipeline. Figure 6C reports the Kernel Density Estimation obtained on the precision and recall values for 434 bacteria from brightfield images whereas Fig. 6D shows the Kernel Density Estimation measured for 494 bacteria from phase contrast images.

Secondly, we compared the Jaccard index of the *Molyso* and *MMHelper* performances in detecting channels from phase contrast images from the works by Sachs, *et al.* (*Molyso*)³⁰ and by Kaiser, *et al.* (*MoMA*)²². Surprisingly, in terms of Jaccard index channel detection *MMHelper* performed better than *Molyso* on the *Molyso* image sets ($p < 0.0001$, Fig. S5F), whereas *Molyso* performed slightly better than *MMHelper* on the *MoMA*'s dataset ($p = 0.0104$, Fig. S5E). Similar to the results on our datasets, this appeared to be a result of *MMHelper* detecting slightly larger channels than the ground truth masks. *MMHelper* performed better in terms of detection recall for both *MoMA* ($p \leq 0.0001$, Fig. S5C) and *Molyso* image sets ($p \leq 0.0001$, Fig. S5D). Finally, *Molyso* performed better than *MMHelper* in terms of detection precision on the *Molyso* ($p \leq 0.0001$, Fig. S5B) and *MoMA* image sets ($p = 0.0073$, Fig. S5A).

The next set of comparisons was done in terms of bacterial detection which is the ultimate goal of both *Molyso* and *MMHelper*. Therefore, ground truth masks were produced for bacteria allowing for the evaluation of bacterial detection precision, recall and Jaccard index for both *Molyso* and *MMHelper*. Bacteria detection is more difficult than channel detection, due to the inherent heterogeneity in bacterial shape and size within a clonal population. As a result, the levels of the three parameters are lower relative to channel detection (Table 1). However, according to the Jaccard index, *MMHelper* demonstrates superior performances compared to *Molyso* for both imaging modalities on our brightfield and Locke's lab phase contrast datasets ($p \leq 0.0001$, Figs S7E and S7F). In fact, *MMHelper* also performed significantly better in terms of recall ($p \leq 0.0001$, Fig. S7C and Fig. S7D) and precision ($p \leq 0.0001$, Fig. S7A for and $p = 0.0044$, Fig. S7B) on our brightfield and Locke's lab phase contrast datasets (Table 1). We then compared the two pipelines in detecting bacteria from the *MoMA* and *Molyso* image sets. Interestingly, according to the Jaccard index, *MMHelper* again performed better than *Molyso* on the *MoMA* dataset ($p = 0.0041$, Fig. S8E) and their own dataset ($p \leq 0.0001$, Fig. S8F). All the median values for the three parameters are listed in Table 1.

The fact that *MMHelper* outperformed *Molyso* in terms of Jaccard index for bacterial detection for all datasets further emphasises the flexibility of *MMHelper* for use on different experimental set ups as well as different bacterial species. The superior performances of *MMHelper* are probably due to the fundamental difference in the approaches to detection: the *MMHelper* algorithm is applied to the 2D images, whereas *Molyso* reduces 2D images to 1D by using line profiles and projections for channel and bacteria detection, respectively.

Finally, in order to determine the efficiency of our tracking algorithms we quantified the number of correctly tracked channels or bacteria in consecutive frames. In order to decouple tracking accuracy from detection

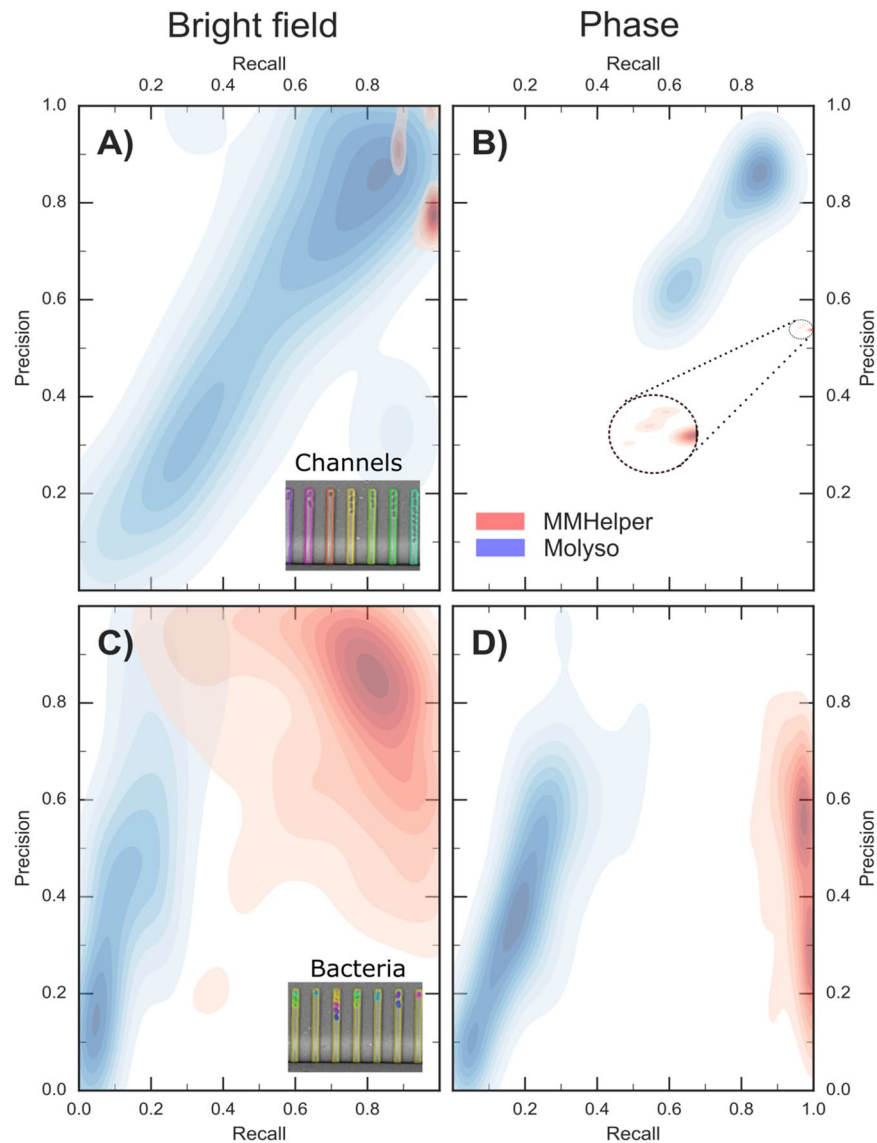


Figure 6. Comparison of *MMHelper* and *Molyso* performances. Kernel density estimation for precision and recall of channel detection from (A) brightfield and (B) phase contrast images via *MMHelper* (red) and *Molyso*³⁰ (blue). The distribution of precision and recall values obtained via *MMHelper* on phase contrast images tightly clusters around a recall value of 1 and a precision value of 0.55. Therefore, we have zoomed this area in the dashed circle to facilitate its visualisation. (C,D) Corresponding kernel density estimation for precision and recall of bacteria detection. Insets: representative images of channel (A) and bacteria (C) detection.

accuracy, we excluded from the image datasets illustrated above any channels or bacteria that were incorrectly detected. *MMHelper* returned 100% and $94 \pm 2\%$ efficiency in channel and bacteria detection on the brightfield image datasets and 100% and $67 \pm 4\%$ efficiency in channel and bacteria detection on the phase contrast image datasets.

An obvious benefit of automated image analysis is the removal of human error. In order to demonstrate the superior performances of *MMHelper*, we analysed a brightfield image and the corresponding fluorescence image both via *MMHelper* and via a semi-automated approach based on ImageJ and requiring user input. Briefly, three different users measured each bacterium length from the brightfield image by drawing a straight line through the bacterium and using the corresponding intensity plot to determine where the line crossed the edges of the bacterium thus deducting the bacterial length (Fig. S9A). They then drew a box around each bacterium to measure its area (Fig. S9B). Using this same box, the fluorescence pixel intensity was extracted from the corresponding fluorescence image (Fig. S9C). For each bacterium we calculated the mean and standard deviation of these semi-automated measurements (red shaded areas in Fig. S8) and compared these values to the ones obtained via *MMHelper* (blue circles in Fig. S9). Whereas *MMHelper* is able to accurately detect the bacterial contour, the semi-automated approach consistently overestimates the area of individual bacteria and underestimates the GFP fluorescence from single bacteria. Therefore, in order to allow a direct comparison between the values obtained

via the two approaches, Fig. S4 reports each single-bacterium value normalised to the corresponding mean of all the single-bacterium values. This allows us to demonstrate that *MMHelper* robustly and accurately extracts single-cell data with 69% of *MMHelper* measurements falling within 1 S.D. of the mean, 97% within 2 S.D., and 100% within 3 S.D. of the mean of the values obtained via the semi-automated approach (Fig. S9C).

Input images can vary in quality and magnification and the bacterial geometry can vary depending on species, phase of growth, and due to the phenotypic heterogeneity inherent in clonal populations. In order to account some of these variations, some of the input parameters for *MMHelper* can be varied accordingly. For example, tuning the scale factor accounts for changes in image magnification. Furthermore, we are also developing a graphic interface for the manual correction of *MMHelper* output, where needed, which aims to make this process both easier and more efficient.

MMHelper, to the best of our knowledge, is the only automated analysis pipeline that has been designed for the analysis of both brightfield and phase contrast images acquired with the mother machine. Some researchers use fluorescent tags in order to perform their image analysis^{24,29}, but this requires exposure to strong light sources that are known to be extrinsic damage-producing agents⁴³. Conversely, *MMHelper* allows the extraction of single-bacterium length and area measurements from brightfield or phase contrast images, allowing measurements of single-cell parameters such as growth rate and elongation time that are crucial when investigating phenomena such as ageing^{19,44,45}, bacterial susceptibility^{28,46} and cell size regulation²⁰.

When needed, fluorescence can be used as a reporter for intracellular pH, gene expression, or substrate accumulation. Therefore, *MMHelper*, will facilitate the study of mutagenesis, gene regulation, and cellular homeostasis at the single cell level. Furthermore, when current microbiological assays are performed at the population level, viable but non-culturable bacteria are overlooked. VBNC cells are a subpopulation of cells which enter a dormant state allowing them to survive otherwise lethal concentrations of antibiotics but they do not resuscitate immediately upon exposure to fresh media⁴⁷. As a result, they can be responsible for the recalcitrance of chronic infections and act as a stepping stone in the development of antibiotic resistance⁴⁷. In contrast, our high-throughput system can be used to ensure that non-growing phenotypes can be detected for example during the testing of new antimicrobials or exposure to stress. In this respect, we have recently used *MMHelper* to demonstrate that persister and viable but non culturable *E. coli* cells differentially regulate genes associated with tryptophan metabolism before exposure to ampicillin²⁸ opening new opportunities to map the detailed biochemical makeup of these clonal subpopulations.

Conclusion

MMHelper provides an automated framework for the analysis of any type of microscopy images acquired with the mother machine. This automated approach provides large amounts of data with a high level of accuracy in both a time efficient and reproducible manner. For instance, on average it would take a user approximately an hour to analyse a series of 8 consecutive images using ImageJ, whereas *MMHelper* can acquire the same information in approximately one minute, requiring only a limited amount of manual editing of the output data thanks to the high level of accuracy provided. After thoroughly testing *MMHelper* to analyse our own mother machine experiments performed on different experimental set-ups and different bacterial strains we are now making this open-source software available for all the research groups already using the mother machine around the world. Finally, we believe that, thanks to the ease of installation and use, *MMHelper* will be an incentive for researchers from a variety of scientific backgrounds to employ this powerful technology for investigating biological questions with single cell resolution.

References

- Balaban, N. Q., Merrin, J., Chait, R., Kowalik, L. & Leibler, S. Bacterial persistence as a phenotypic switch. *Science* **305**, 1622–1625 (2004).
- Nikolic, N., Barner, T. & Ackermann, M. Analysis of fluorescent reporters indicates heterogeneity in glucose uptake and utilization in clonal bacterial populations. *BMC Microbiol.* **13**, 258 (2013).
- Kotte, O., Volkmer, B., Radzikowski, J. L. & Heinemann, M. Phenotypic bistability in *Escherichia coli*'s central carbon metabolism. *Mol. Syst. Biol.* **10**, 736 (2014).
- Arnoldini, M. *et al.* Bistable expression of virulence genes in salmonella leads to the formation of an antibiotic-tolerant subpopulation. *PLoS Biol.* **12**, e1001928 (2014).
- Ackermann, M. A functional perspective on phenotypic heterogeneity in microorganisms. *Nat. Rev. Microbiol.* **13**, 497–508 (2015).
- Venturelli, O. S., Zuleta, I., Murray, R. M. & El-Samad, H. Population Diversification in a Yeast Metabolic Program Promotes Anticipation of Environmental Shifts. *PLoS Biol.* **13**, 1–24 (2015).
- Schreiber, F. *et al.* Phenotypic heterogeneity driven by nutrient limitation promotes growth in fluctuating environments. *Nat. Microbiol.* **1**, 1–7 (2016).
- Bódi, Z. *et al.* Phenotypic heterogeneity promotes adaptive evolution. *PLoS Biol.* **15**, 1–26 (2017).
- Beaumont, H. J. E., Gallie, J., Kost, C., Ferguson, G. C. & Rainey, P. B. Experimental evolution of bet hedging. *Nature* **462**, 90–93 (2009).
- New, A. M. *et al.* Different Levels of Catabolite Repression Optimize Growth in Stable and Variable Environments. *PLoS Biol.* **12**, 17–20 (2014).
- Sackmann, E. K., Fulton, A. L. & Beebe, D. J. The present and future role of microfluidics in biomedical research. *Nature* **507**, 181–189 (2014).
- Hol, F. J. H. & Dekker, C. Zooming in to see the bigger picture: Microfluidic and nanofabrication tools to study bacteria. *Science (80-)*. **346**, 1251821–1251821 (2014).
- Okumus, B., Yildiz, S. & Toprak, E. Fluidic and microfluidic tools for quantitative systems biology. *Curr. Opin. Biotechnol.* **25**, 30–38 (2014).
- Hansen, A. S., Hao, N. & O'Shea, E. K. High-throughput microfluidics to control and measure signaling dynamics in single yeast cells. *Nat. Protoc.* **10**, 1181–1197 (2015).
- Li, Y. *et al.* Cell migration microfluidics for electrotaxis-based heterogeneity study of lung cancer cells. *Biosens. Bioelectron.* **89**, 837–845 (2017).

16. Yuan, X. *et al.* Single-Cell Microfluidics to Study the Effects of Genome Deletion on Bacterial Growth Behavior. *ACS Synth. Biol.* **6**, 2219–2227 (2017).
17. Pagliara, S. *et al.* Auxetic nuclei in embryonic stem cells exiting pluripotency. *Nat Mater* **13**, 638–644 (2014).
18. Otto, O. *et al.* Real-time deformability cytometry: on-the-fly cell mechanical phenotyping. *Nat. Methods* **12**, 199 (2015).
19. Wang, P. *et al.* Robust growth of *Escherichia coli*. *Curr. Biol.* **20**, 1099–1103 (2010).
20. Tanouchi, Y. *et al.* A noisy linear map underlies oscillations in cell size and gene expression in bacteria. *Nature* **523**, 357–60 (2015).
21. Tanouchi, Y. *et al.* Long-term growth data of *Escherichia coli* at a single-cell level. *Sci. Data* **4**, 170036 (2017).
22. Kaiser, M. *et al.* Monitoring single-cell gene regulation under dynamically controllable conditions with integrated microfluidics and software. *Nat. Commun.* **9**, 212 (2018).
23. Robert, L. *et al.* Mutation dynamics and fitness effects followed in single cells. *Science (80-.)*. **359**, 1283–1286 (2018).
24. Uphoff, S. Real-time dynamics of mutagenesis reveal the chronology of DNA repair and damage tolerance responses in single cells. *Proc. Natl. Acad. Sci.* **115**, E6516–E6525 (2018).
25. Moolman, M. C. *et al.* Slow unloading leads to DNA-bound beta2-sliding clamp accumulation in live *Escherichia coli* cells. *Nat Commun* **5**, 5820 (2014).
26. Chait, R., Ruess, J., Bergmiller, T., Tkačik, G. & Guet, C. C. Shaping bacterial population behavior through computer-interfaced control of individual cells. *Nat. Commun.* **8** (2017).
27. Bergmiller, T. *et al.* Biased partitioning of the multidrug efflux pump AcrAB-TolC underlies long-lived phenotypic heterogeneity. *Science (80-.)*. **356**, 311–315 (2017).
28. Bamford, R. A. *et al.* Investigating the physiology of viable but non-culturable bacteria by microfluidics and time-lapse microscopy. *BMC Biol.* **15**, 1–12 (2017).
29. Yang, D., Jennings, A. D., Borrego, E., Retterer, S. T. & Männik, J. Analysis of factors limiting bacterial growth in PDMS mother machine devices. *Front. Microbiol.* **9**, 1–12 (2018).
30. Sachs, C. C. *et al.* Image-based single cell profiling: High-throughput processing of mother machine experiments. *PLoS One* **11**, 1–15 (2016).
31. Norman, T. M., Lord, N. D., Paulsson, J. & Losick, R. Memory and modularity in cell-fate decision making. *Nature* **503**, 481–486 (2013).
32. Zwillinger, D. & Kokoska, S. *CRC Standard Probability and Statistics Tables and Formulae*. (Chapman & Hall: New York, 2000).
33. Frangi, A. F., Niessen, W. J., Vincken, K. L. & Viergever, M. A. Multiscale vessel enhancement filtering. *Med. Image Comput. Comput. Interv.* **1496**, 130–137 (1998).
34. Li, C. H. & Lee, C. K. Minimum cross entropy thresholding. *Pattern Recognit.* **26**, 617–625 (1993).
35. Sternberg, S. Biomedical Image Processing. *Computer (Long Beach, Calif.)*. **16**, 22–34 (1983).
36. Lindeberg, T. Feature Detection with Automatic Scale Selection. *Int. J. Comput. Vis.* **30**, 79–116 (1998).
37. Vincent, L. & Soille, P. Watersheds in digital spaces: an efficient algorithm based on immersion simulations. *IEEE Trans. Pattern Anal. Mach. Intell.* **13**, 583–598 (1991).
38. Lewis, J. P. Fast Template Matching. *Vis. interface* **10**, 120–123 (1995).
39. Nobs, J. B. & Maerkl, S. J. Long-term single cell analysis of *S. pombe* on a microfluidic microchemostat array. *PLoS One* **9**, e93466 (2014).
40. Patange, O. *et al.* *Escherichia coli* can survive stress by noisy growth modulation. *Nat. Commun.* **9** (2018).
41. Tung, F., Wong, A. & Clausi, D. A. Enabling scalable spectral clustering for image segmentation. *Pattern Recognit.* **43**, 4069–4076 (2010).
42. Taha, A. A. & Hanbury, A. Metrics for evaluating 3D medical image segmentation: Analysis, selection, and tool. *BMC Med. Imaging* **15** (2015).
43. Rang, C. U., Peng, A. Y., Poon, A. F. & Chao, L. Ageing in *Escherichia coli* requires damage by an extrinsic agent. *Microbiol. (United Kingdom)* **158**, 1553–1559 (2012).
44. Rang, C. U., Peng, A. Y. & Chao, L. Temporal dynamics of bacterial aging and rejuvenation. *Curr. Biol.* **21**, 1813–1816 (2011).
45. Stewart, E. J., Madden, R., Paul, G. & Taddei, F. Aging and death in an organism that reproduces by morphologically symmetric division. *PLoS Biol.* **3**, 0295–0300 (2005).
46. Greulich, P., Scott, M., Evans, M. R. & Allen, R. J. Growth-dependent bacterial susceptibility to ribosome-targeting antibiotics. *Mol. Syst. Biol.* **11**, 796 (2015).
47. Ayrapetyan, M., Williams, T. C., Baxter, R. & Oliver, J. D. Viable but Nonculturable and Persister Cells Coexist Stochastically and Are Induced by Human Serum. **83**, 4194–4203 (2015).

Acknowledgements

We thank C. Schwall from the Locke's laboratory at the University of Cambridge for providing us with image datasets acquired on their phase contrast microscope. We thank E. Attrill and O. Goode for manually analysing images as part of the comparison process. This work was supported by a Royal Society Research Grant (RG180007), a Wellcome Trust Strategic Seed Corn Fund (WT097835/Z/11/Z), and a MRC Proximity to Discovery EXCITEME2 grant (MCPC17189) awarded to S.P. A.S. acknowledges support from the BBSRC through a SWBio-DTP studentship (BB/M009122/1). J.M. was generously supported by a Wellcome Trust Institutional Strategic Support Award (WT097835MF).

Author Contributions

S.P. developed the project and designed the research. A.S. and J.M. developed the code and implemented it in Python. A.S., J.M. and S.P. wrote the paper. All authors read and approved the final manuscript.

Additional Information

Supplementary information accompanies this paper at <https://doi.org/10.1038/s41598-019-46567-0>.

Competing Interests: The authors declare no competing interests.

Publisher's note: Springer Nature remains neutral with regard to jurisdictional claims in published maps and institutional affiliations.



Open Access This article is licensed under a Creative Commons Attribution 4.0 International License, which permits use, sharing, adaptation, distribution and reproduction in any medium or format, as long as you give appropriate credit to the original author(s) and the source, provide a link to the Creative Commons license, and indicate if changes were made. The images or other third party material in this article are included in the article's Creative Commons license, unless indicated otherwise in a credit line to the material. If material is not included in the article's Creative Commons license and your intended use is not permitted by statutory regulation or exceeds the permitted use, you will need to obtain permission directly from the copyright holder. To view a copy of this license, visit <http://creativecommons.org/licenses/by/4.0/>.

© The Author(s) 2019

4.2 Supplementary material

MMHelper: An automated framework for the analysis of microscopy images acquired with the mother machine

Ashley Smith^{1,2†}, Jeremy Metz^{1,2†*}, Stefano Pagliara^{1,2*}

¹Living Systems Institute, University of Exeter, Exeter, United Kingdom

² Biosciences, University of Exeter, Exeter, United Kingdom

†These authors contributed equally to the work

*** Correspondence:**

Stefano Pagliara

s.pagliara@exeter.ac.uk

Jeremy Metz

j.metz@exeter.ac.uk

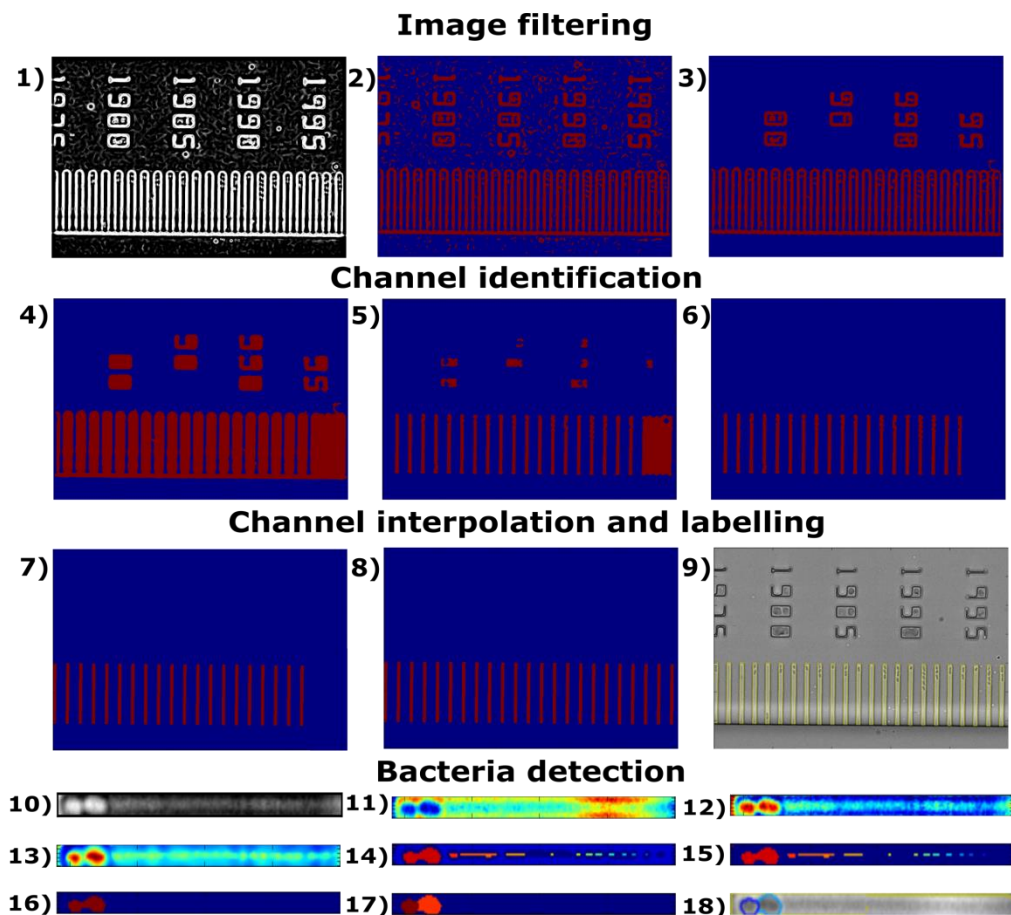


Fig. S1. Overview of the detection pipeline. The image is filtered (1) using Sobel (phase contrast) or Frangi (bright field). This is followed by thresholding (2) using Li's minimum cross entropy threshold, before finally being filtered based on size (3). The size filtered image is dilated and the gaps (channel centres filled (4). The size filtered image is then subtracted to leave only the centre of the channels (5). The channel centres are then extrapolated and only "good" channels are kept (6). An "average" shape of a channel is determined and used for each of the detected channels (7). The spacing is then determined and any missing channels "stamped" in to place (8). This final mask can then be used to extract the well profiles for bacteria detection. The final detected wells can be seen as yellow contours (9). For display purposes, images 10-18 have been rotated 90°. If the original image was acquired in bright field then it must be inverted (10). Then, in order to account for any variation in background intensity (11), the background is subtracted using a rolling ball filter (12) and then scale-space filtered (13). Using Li's minimum cross entropy based algorithm on all the channels within an image, a threshold is determined. This threshold is applied to each well individually in order to identify markers (14) for watershed segmentation (15). The result of the watershed segmentation is then

size filtered (16), before a final "splittling" algorithm is applied to their skeleton based on a combination of distance transformation and pixel intensity (17). The contours of the final labels are then plotted on the original image for visualisation purposes (18).

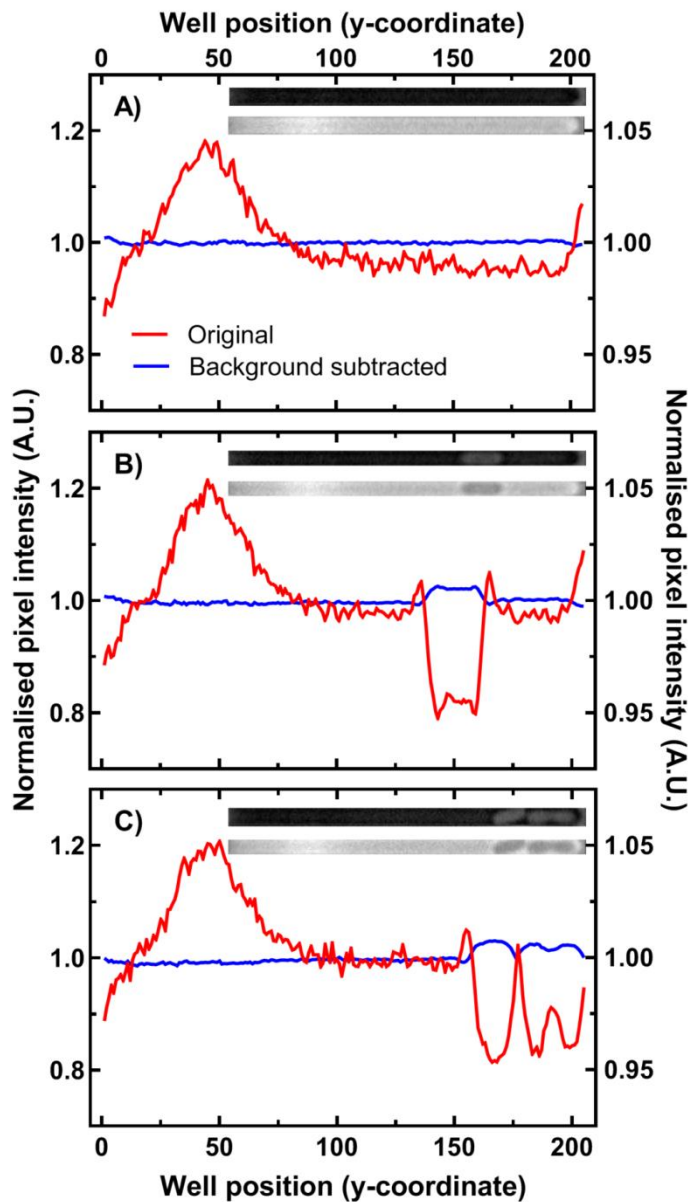


Figure S2. Comparison of channel profiles before and after background subtraction. The MMHelper pipeline uses a rolling ball filter to normalise the background profile (blue lines) to account for the changing background along the original channel profile (red lines). We measured the profile from the channel entrance ($0\mu\text{m}$) to the end of the channel ($23.5\mu\text{m}$) for a channel containing no bacteria (A), a channel with a single bacterium around the centre of the channel (B) and for a channel with multiple bacteria at one end (C) and plotted the relative intensity at each position within the channel. In all cases, the rolling ball filter removed the variation associated with the original image. It is important to note that the images were inverted prior to background subtraction, which is why we see an increase in intensity for the normalised (blue line) bacteria compared to the original (red line).



$$\text{Precision} = \frac{\text{Overlap}}{\text{Detection mask}} \quad \text{Recall} = \frac{\text{Overlap}}{\text{Ground truth mask}}$$

$$\text{Jaccard index} = \frac{\text{Overlap}}{\text{Combined area}}$$

Figure S3. Schematic illustrating our definition of detection precision and recall. Ground truth masks were drawn manually using the software GIMP and detected masks were produced from the automatic analysis pipelines. The precision value is termed as the percentage overlap area between the ground truth and detected mask divided by the total area of the detected mask. The recall value is the percentage overlap divided by the total area of the ground truth mask. Finally, the Jaccard index is determined as the overlap area divided by the total combined area.

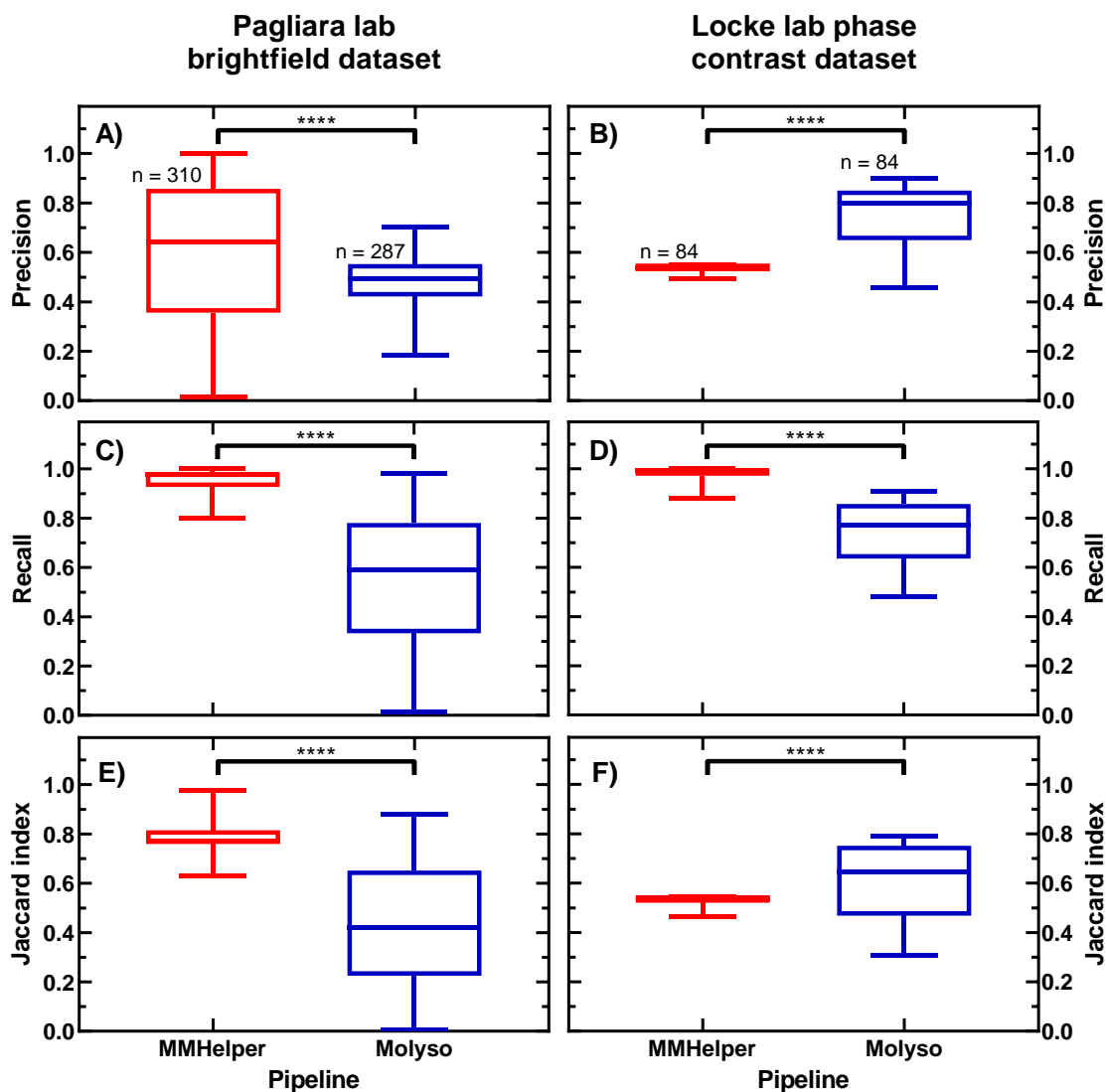


Figure S4. Comparison of channel detection in our brightfield and phase contrast datasets via MMHelper and Molyso in terms of Jaccard index, precision and recall. Using the ground truth masks manually drawn using GIMP, we determined the levels of precision and recall for the detected channels from *MMHelper* and *Molyso*, respectively. The results show that the median precision levels of *MMHelper* are approximately 0.8 for **(A)** brightfield and 0.55 % for **(B)** phase contrast images because the detected channels are consistently larger than the ground truth masks. This is reflected by the high levels of recall in both **(C)** brightfield and **(D)** phase contrast images. *Molyso*, in comparison, only out performs *MMHelper* on phase contrast precision. Finally, the Jaccard index shows that *MMHelper* was significantly better on **(E)** brightfield, but *Molyso* was significantly better for our **(F)** phase contrast

dataset. Statistical significance was determined using a Welch's correlation as described in the methods section.

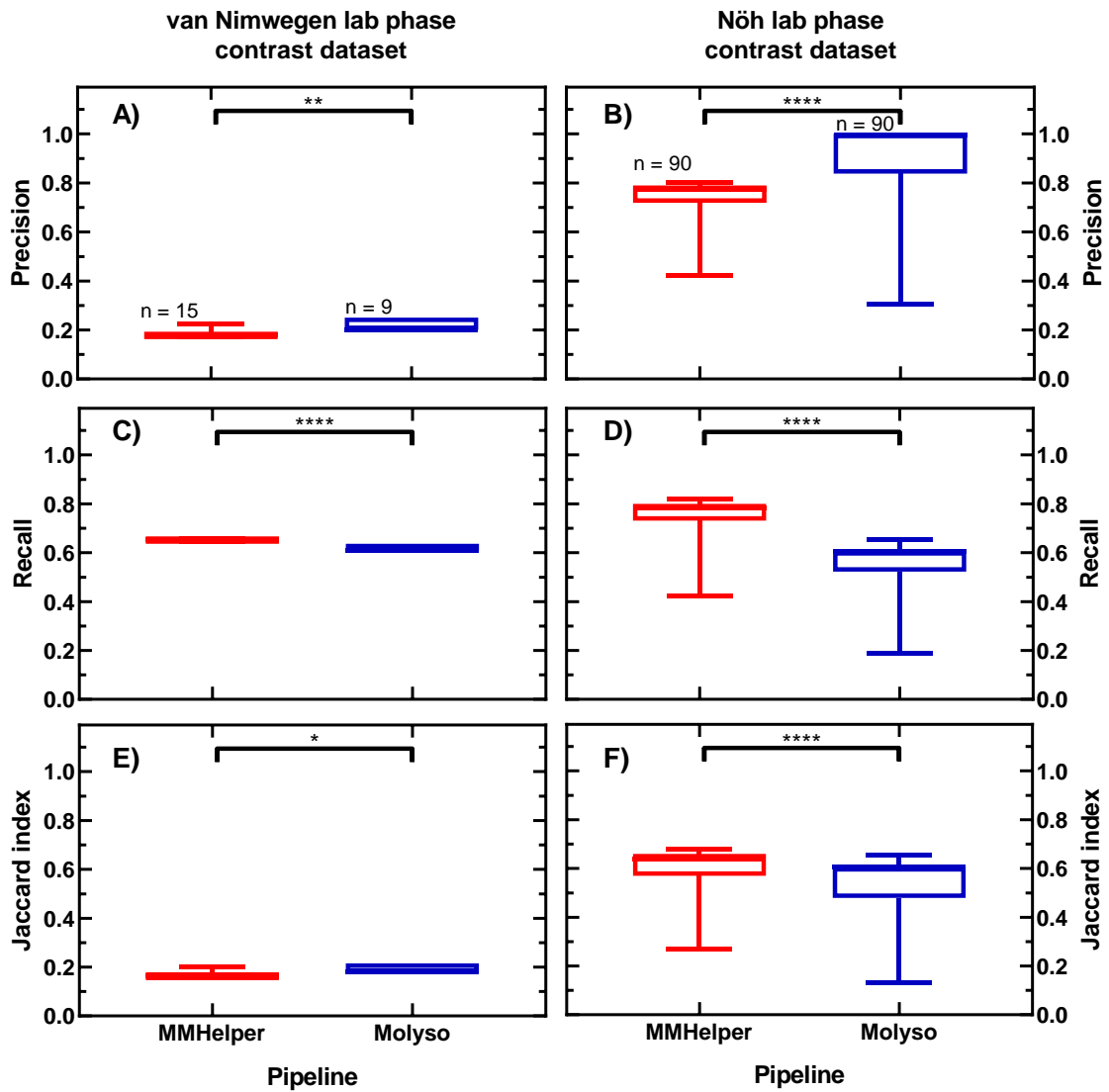


Figure S5. Comparison of channel detection in both *MoMA* and *Molyso* example phase contrast datasets via *MMHelper* and *Molyso* in terms of Jaccard Index, precision and recall. The (A) precision and (C) recall values were calculated for the *MoMA* example dataset. Similar to the (B) precision and (D) recall for *Molyso*'s dataset, *MMHelper* showed significantly better recall due to slightly larger detected channels compared to the ground truth masks, whereas *Molyso* was significantly better in terms of precision. The Jaccard index, determined by dividing the overlap of an area by the total combined area, was calculated for the channels detected in the (E) *MoMA* and (F) *Molyso* datasets, respectively. Interestingly, *Molyso* was slightly better for the *MoMA* dataset, but *MMHelper* performed significantly better on *Molyso*'s own dataset. Statistical significance was determined using a Welch's correlation as described in the methods section.

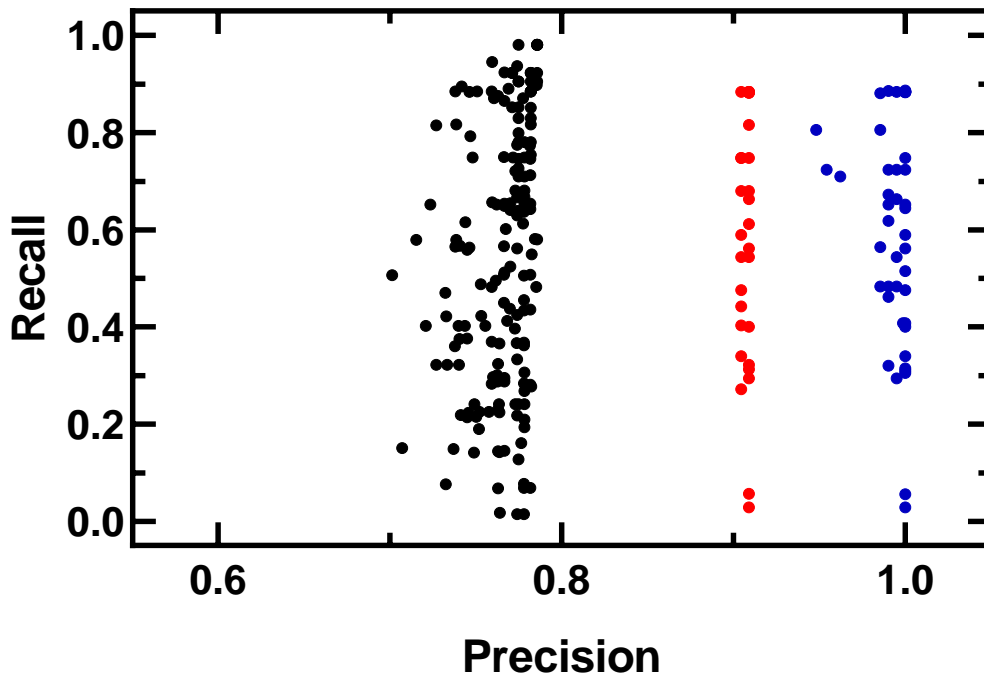


Figure S6. Scatter plot of precision and recall values for channel detection. Scatter plot of representative precision and recall values for channel detection across all 14 bright field frames. The plot clearly shows 3 different clusters of data; the majority of frames across all experiments had a precision level around 0.8, one frame had a precision level around 0.9 and two frames had a precision level around 1.0. This grouping results in the multimodal distribution in the kernel density plots.

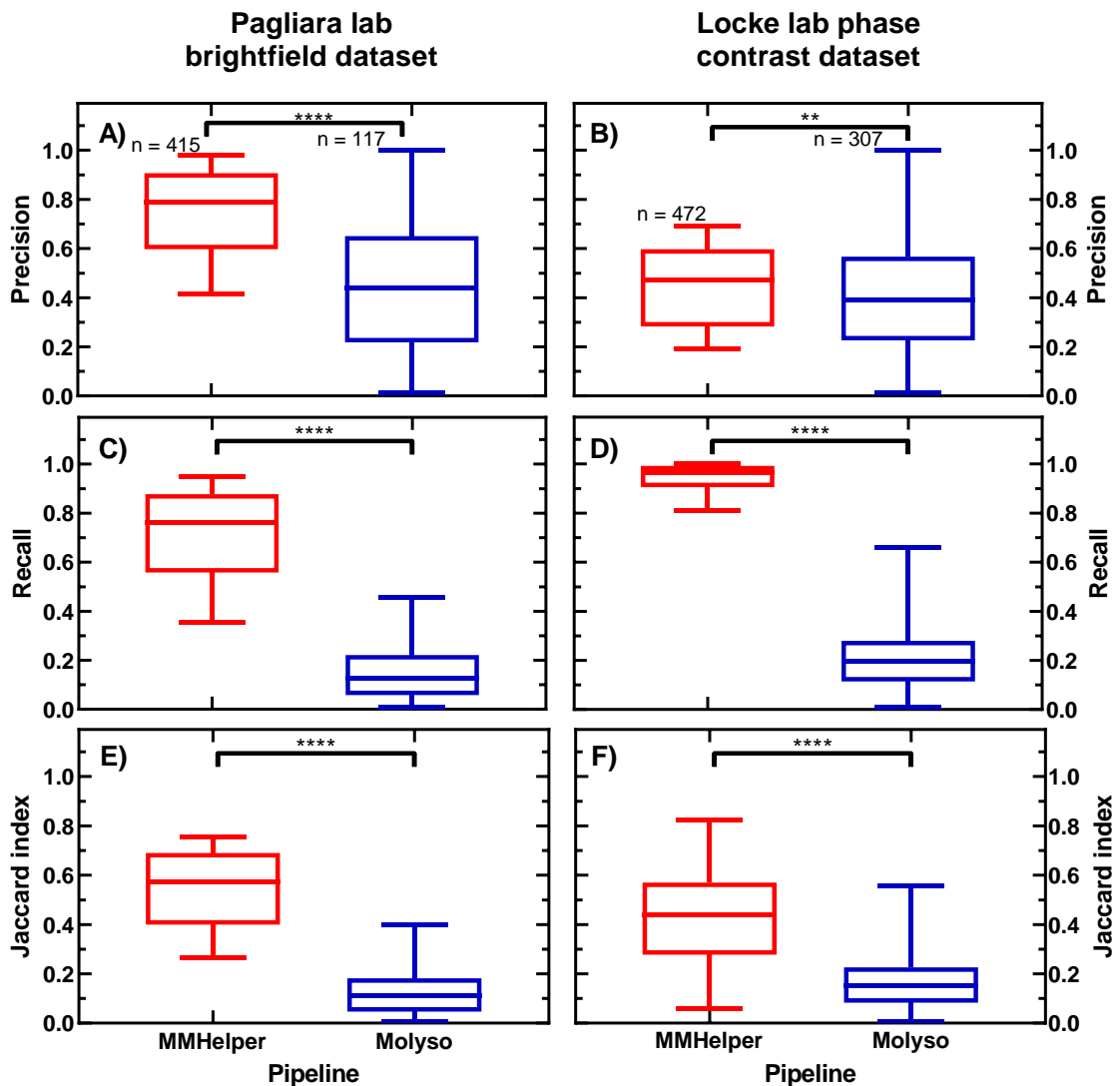


Figure S7. Comparison of bacterial detection in our brightfield and phase contrast datasets via MMHelper and Molyso in terms of Jaccard index, precision and recall. Using the ground truth masks manually drawn using GIMP, we determined the levels of precision and recall for the detected channels from *MMHelper* and *Molyso*, respectively. The results show that *MMHelper* had significantly higher precision levels for (A) brightfield and (B) phase contrast images. Similarly, *MMHelper* had significantly higher levels of recall in both (C) brightfield and (D) phase contrast images. As a result, the Jaccard index shows that *MMHelper* was again significantly better on (E) bright field and (F) phase contrast dataset. Statistical significance was determined using a Welch's correlation as described in the methods section.

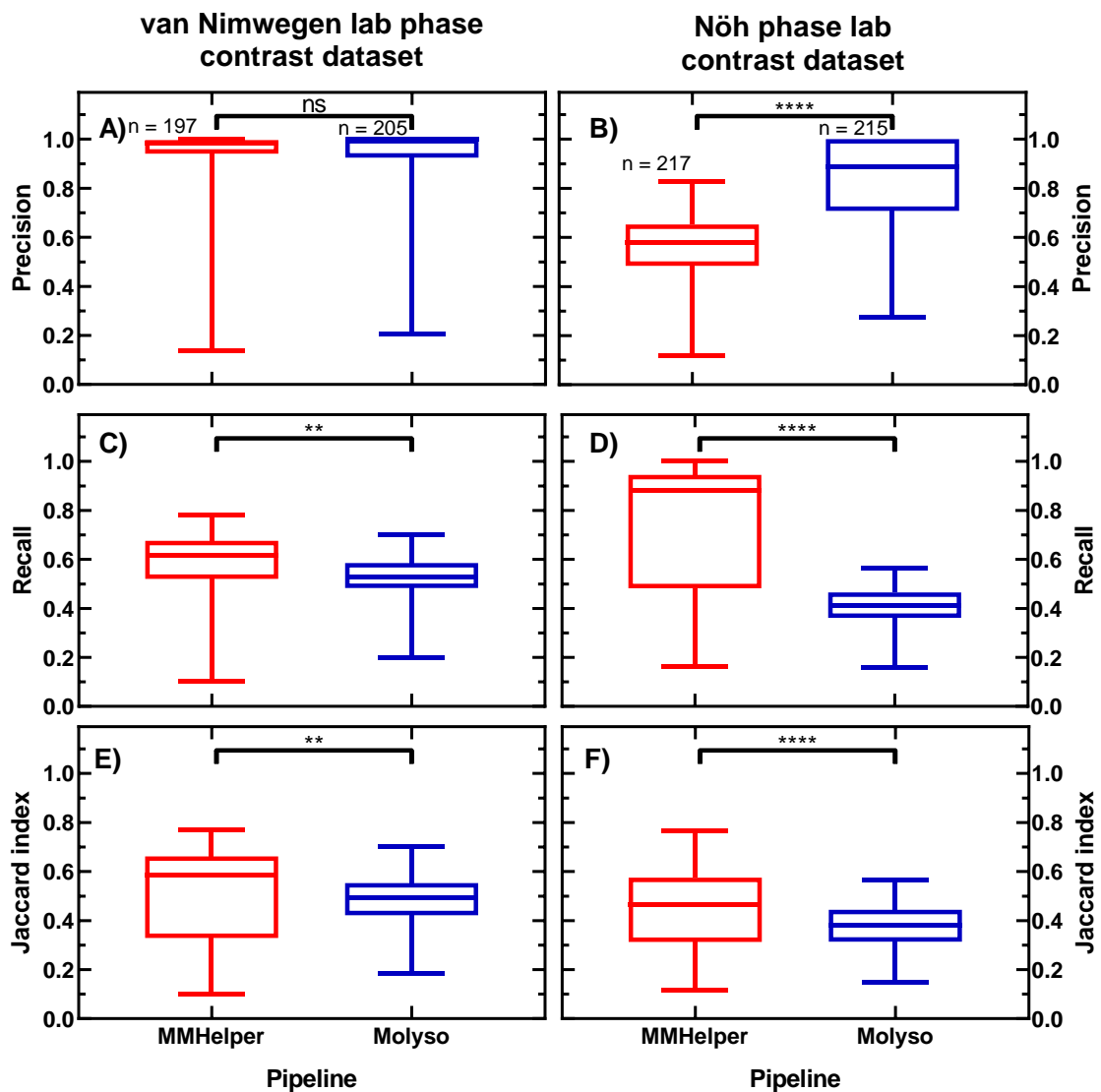


Figure S8. Comparison of bacterial detection in both *MoMA* and *Molyso* example phase contrast datasets via *MMHelper* and *Molyso* in terms of Jaccard Index, precision and recall. There was no significant difference between the (A) precision values on the *MoMA* dataset. However, *MMHelper* performed slightly better on (C) recall and therefore also with respect (E) Jaccard index. Interestingly, although *Molyso* was significantly better on its own (B) precision values, *MMHelper* outperformed it on (D) recall and (F) Jaccard index. Statistical significance was determined using a Welch's correlation as described in the methods section.

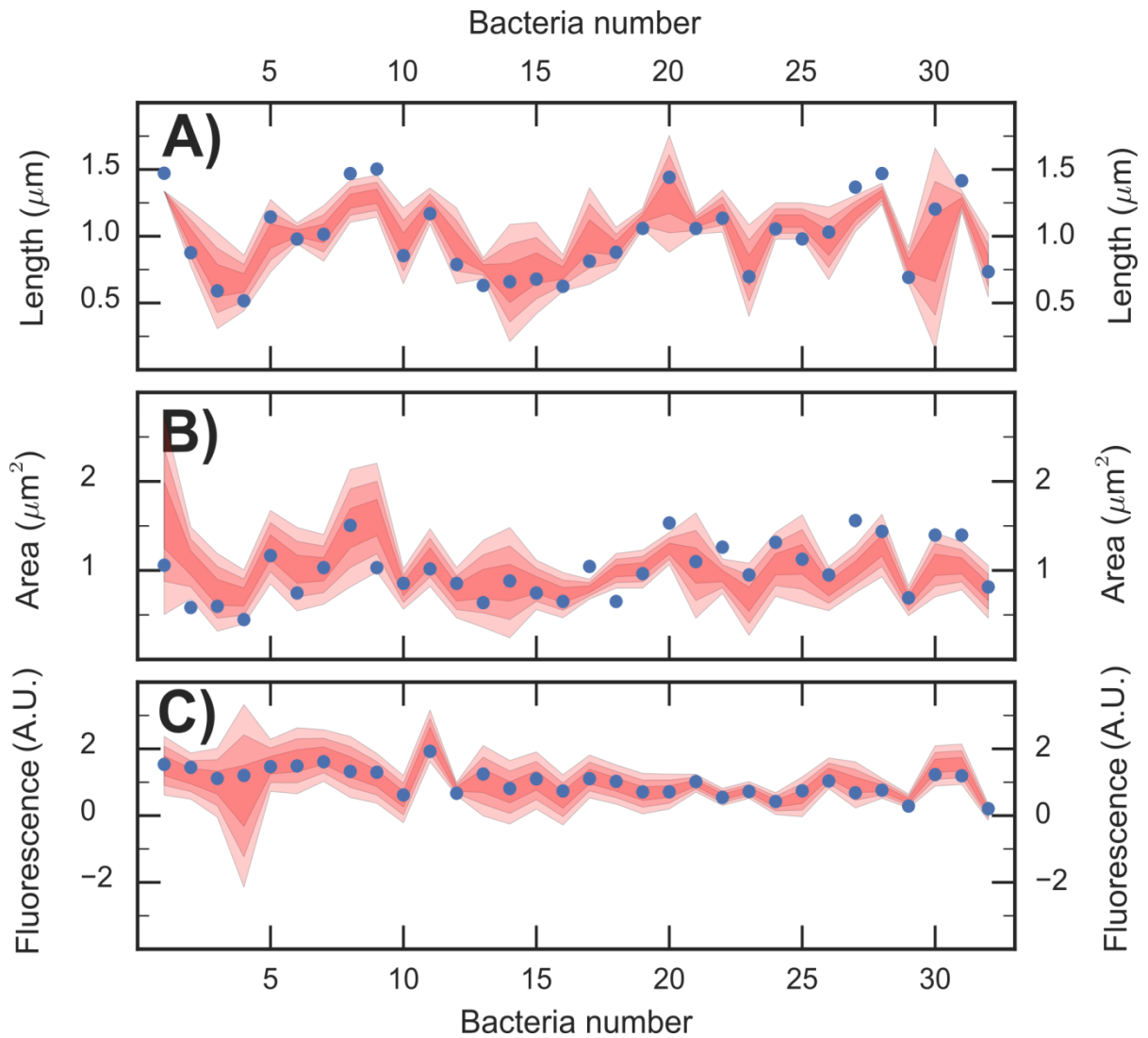


Figure S9. Comparison of single bacterium parameters obtained via *MMHelper* and a semi-automated approach requiring user input. (A) Bacterial length, **(B)** area, and **(C)** GFP fluorescence measured via *MMHelper* (blue dots) and a semi-automated method based on ImageJ and performed by three different users, the red bands indicate the mean \pm 1 S.D. (darkest red band), mean \pm 2 S.D., and mean \pm 3 S.D. (lightest red band), respectively. To account for the consistently more precise automated measurements, both the manual and automatic measurements were normalised by dividing the measurement for each bacterium by the mean of all the single-bacterium measurements.

4.3 Conclusion

In this chapter I report the development of a new automated framework for the analysis of images acquired using the microfluidic Mother Machine; *MMHelper*. *MMHelper* is the first Mother Machine specific software that is capable of being used in multiple imaging modalities and, in particular, acquired in bright field. Furthermore, as bright field microscopy does not require special optical components, *MMHelper* will make the high throughput Mother Machine technology more accessible to the research community.

Molyso is another example of a freely available platform for Mother Machine analysis, however it is designed to only detect bacteria in phase contrast¹³⁰. Using manually drawn “ground truth” masks, we were able to directly compare its performance to *MMHelper*. Although *Molyso* was better in some of the channel detections, the ultimate goal of both pipelines is bacteria detection. As expected, *MMHelper* was significantly better than *Molyso* at detecting bacteria in bright field images. However, perhaps more surprisingly, *MMHelper* significantly outperformed *Molyso*, in terms of the Jaccard index, on all bright field and phase contrasts datasets.

Outperforming other pipelines is important, but if the data collected from automated analysis is not reliable, then this becomes irrelevant. Therefore, we directly compared the measurements acquired by *MMHelper* to those determined using manual analysis on the same datasets. It is important to note that to allow the direct comparison, the two sets of measurements had to be normalised. This is a result of the automated detection producing more precise cellular contours compared to the manual analysis. However, this is actually advantageous as it allows for more accurate measurements. When comparing the extracted fluorescence intensities, 97 % of the measurements fell within 2 standard deviations of those determined using manual analysis and 100 % fell within 3 standard deviations; again highlighting the accuracy and reliability of *MMHelper*.

In order to properly quantify the efficiency and accuracy of *MMHelper* we investigated how successful the algorithm was at detecting all the bacteria within a frame. By defining efficiency as the number of bacteria successfully detected, we showed that *MMHelper* had an efficiency of 98 % and 95 % for the

bright field and phase contrast datasets, respectively. However, we realised that occasionally the algorithm would detect two bacteria as one. Therefore, we defined the percentage of single bacteria that were correctly identified as the algorithm accuracy and showed this to be 80 % and 65 % for the two respective datasets. Due to differences between individual experiments and even between time points in a single experiment, there can be substantial differences in light intensity and focus which will affect the image quality. Therefore, these accuracy and efficiency levels highlight the adaptability of the *MMHelper* algorithm.

We have already used *MMHelper* to investigate the heterogeneity in response to ampicillin for an *E. coli* population, as discussed in chapter three. Importantly, *MMHelper* was able to drastically increase the throughput of our experimental set up, something which is essential when investigating very small subpopulations such as persister and VBNC cells. Importantly, however, in this chapter we have shown that *MMHelper* is not limited to our experimental set up. In fact, we have shown it to outperform pipelines specifically developed by other research groups on their own datasets. All of this, as well as the ease of installation of *MMHelper*, makes it a readily available open source platform that can now be utilised by the wider scientific community to investigate other forms of phenotypic heterogeneity.

Chapter 5: Heterologous protein expression favours the formation of inclusion bodies in persister and sleeper *Escherichia coli*

5.1 Introduction

In chapter three I introduced a new microfluidic Mother Machine protocol that allowed for the characterisation of antibiotic response in an isogenic bacterial population. We showed that the tolerant phenotypes of antibiotic persister and VBNC (for brevity these are referred to as sleeper cells within this chapter) cells, exhibit similar characteristics prior to exposure to antibiotics but are significantly different when the extracellular environment becomes favourable once more. I then introduced an automated image analysis platform, *MMHelper*, in chapter four that allows the accurate and efficient analysis of Mother Machine images acquired in multiple imaging modalities. By combining the two we have produced a high throughput pipeline that can be used for investigating phenotypic heterogeneity in bacterial populations. In fact, during the analysis of some of the images for chapter three, we spotted an interesting visible phenotype, particularly within some of the antibiotic persister and VBNC cells; dark foci (small dark dots visible within the bacteria).

Upon reviewing the literature^{94,153,154}, we believe the dark foci we were observing were a result of protein aggregation. Protein aggregates are the accumulation of defunct proteins and their hydrophobic nature makes them difficult for the cell to break down¹¹. This results in reduced cellular resources and increased stress as the intracellular amino acid pool is depleted. A combination of mathematical modelling and experimental studies has shown that intracellular structures, such as nucleoids, cause them to be more prominent at the cellular poles^{9,10}. Furthermore, they have been linked with cellular ageing as they have been shown to accumulate at the old cell poles in mother cells⁹ which, in turn, have been shown to have lower growth than their respective daughter cells^{7,9,12}. Similarly, persisters and sleeper cells have been suggested to be in growth arrested or dormant states³⁰. On top of this,

Bergmiller *et al.* showed that old cell mother poles retain higher levels of the multidrug efflux pump AcrB-TolC during division⁷, which has been shown to result in increased antibiotic survival¹²⁷.

Antibiotic survival has also been associated with increased levels of cellular stress, one example of this is nutrient starvation, for instance amino acids⁶⁵, as discussed in detail in chapter one. Briefly, Fung *et al.* observed increases in antibiotic survival during *E. coli* growth in media lacking in different combinations of glucose and some amino acids⁶⁵. Similarly, by starving biofilms of individual amino acids, Bernier *et al.* were able to significantly increase the level of drug persistence⁶⁴. Furthermore, in chapter two, we identified several KEGG pathways associated with amino acid metabolism that were highly regulated during transitions where we also observed increases in persister fractions. Finally, in chapter three we showed that a fluorescently tagged transcriptional reporter for the pre-cursor of the *tna* operon, which is involved in the catabolism of the essential amino acid tryptophan, was significantly lower in both persisters and sleeper cells compared to their susceptible kin.

Therefore, I selected 6 transcriptional reporter strains, like the ones used in chapter three, in order to determine the relationship between the expression of exogenous proteins and the formation of protein aggregates, and how this, in turn, may affect the formation of antibiotic persister and sleeper cells. The selected genes were: the precursor of the *tna* operon, *tnaC*¹⁵⁵; the outer membrane porin, *ompC*¹⁵⁶; the protease, *lon*¹⁵⁷, the glucose specific permease, *ptsG*¹⁴; the pyruvate kinase, *pykF*²⁴ and an enzyme involved in the glyoxylate shunt, *aceB*²³. Importantly, the genes selected had either previously been linked to antibiotic survival (*tnaC*, *lon*, *ompC*) and/or are involved in cellular metabolism (*tnaC*, *ptsG*, *aceB*, *pykF*), which in turn has been linked to antibiotic survival and aggregate formation. Furthermore, in a stationary phase culture (the time point used for these assays), the genes mentioned above showed a wide range of expression (between 77 and 62837 transcriptional reads for *tnaC* and *aceB*, respectively) based on our transcriptional analysis in chapter two. As a result, each strain will have different levels of intracellular “stress” due the amount of exogenous proteins they are expressing. In the following chapter, we show that the percentage of cells within the population with visible protein aggregates increases with the level of exogenous proteins being expressed

within our transcriptional reporter strains. Furthermore, we show that these aggregates are more likely to be found in cells which exhibit the persister or sleeper phenotype. Finally, we correlate the expression of exogenous protein, and hence cellular stress, to the percentage of cells within the population that are able to survive antibiotic exposure.

5.2 Manuscript

**Ashley Smith^{1,2}, Olivia Goode^{1,2}, Rosemary Bamford^{1,2}, Zehra Kahveci^{1,2},
Georgina Glover^{1,2}, Erin Attrill^{1,2}, Alice Carr^{1,2}, Jeremy Metz^{1,2}, Stefano
Pagliara^{1,2*}**

¹Living Systems Institute, University of Exeter, Exeter, United Kingdom

² Biosciences, University of Exeter, Exeter, United Kingdom

*** Correspondence:**

Stefano Pagliara

s.pagliara@exeter.ac.uk

Abstract

Misfolded and defunct proteins move around a bacterial cell by diffusion and can accumulate into hydrophobic protein aggregates which can generate intracellular stress, for instance by depleting the cellular amino acid pool. However, as a result of their polar location within the cell, during growth these aggregates are concentrated into a small percentage of the overall population. On the other hand, a small percentage of a bacterial population can survive otherwise lethal doses of antibiotics, often as a result of reduced growth rate or exposure to stress. Here we report a strong link between antibiotic persister and sleeper (i.e. viable but non culturable) *E. coli* and the presence of protein aggregates. Specifically, the cellular stress that occurs, as a result of bacteria expressing plasmid-based transcriptional GFP reporters, increases the percentage of cells within the population that contain visible protein aggregates; with our reporter strain for *tnaC*, which expresses the lowest amount of exogenous protein, containing visible aggregates in 1.4 ± 0.2 % of cells compared to 4.4 ± 1.5 % in *aceB*, the strain expressing the most exogenous protein. Furthermore, we show that aggregate containing cells constitute on average 2.3 ± 0.2 % of the susceptible subpopulation, 47.5 ± 3.2 % of the persister subpopulation and 70.3 ± 3.4 % of the sleeper subpopulation;

supporting recent evidence that these protein aggregates play a role in the formation of persister and sleeper cells and further supports the hypothesis that these two phenotypes exist as part of one dormancy continuum.

Introduction

Cellular stress can manifest as a result of a variety of external or internal stressors; for instance increased environmental temperature or nutrient starvation¹⁵⁸. It has been documented that high levels of cellular stress favour the formation of protein aggregates, a phenomenon whereby defunct or misfolded proteins within a cell are clustered together to form largely insoluble hydrophobic aggregates^{9,10,153,159,160}. Similarly, protein aggregates have been observed in response to oxidative stress as well as cellular ageing¹⁵⁹. For instance during post mitotic ageing in *Saccharomyces cerevisiae*, Peters, *et al.* identified 480 proteins that become insoluble and aggregate¹⁶¹. In fact, such aggregates have been linked to cellular degeneration in many cellular related diseases, such as Alzheimers and Huntingtons, due to the toxicity they evoke in the cell^{9,153,159}.

In prokaryotes, aggregates have been reported to provide functional benefits, despite their cellular toxicity¹⁵³. For instance, a surface protein, protein A, induces aggregation and increases biofilm formation in *Staphylococcus aureus*¹⁶² and *tasA*, a sporulation protein in *Bacillus subtilis*, has been speculated to form oligomeric aggregates whose antibacterial properties provide *B. subtilis* with a competitive advantage for the endospore during colonisation¹⁶³. In *Escherichia coli*, protein aggregates have been shown to cause a reduction in the cellular growth rate and, within an exponentially growing bacterial population, these aggregates have been identified as a potential sign of ageing as a result of their localisation and distribution being primarily at the cellular poles^{9,164,165}. A potential reason for the polar localisation is the majority of exponentially growing bacteria having two nucleoids, non-membrane bound regions within a prokaryotic cell that contain the majority of its genetic information, approximately 500-600 nm from the cell poles, essentially dividing the bacterium into three distinct compartments; the centre and the two poles^{10,164}. After visualising the localisation of protein aggregates, Coquel *et al.*

were able to mathematically model the distribution of aggregates and show it to be a result of the nucleoids position preventing defunct proteins from being able to diffuse freely around the cellular space, particularly as these proteins aggregate and increase in size¹⁰. Lindner *et al.* elegantly showed how this intracellular distribution of defunct or misfolded proteins results in the aggregates being retained primarily at the cellular poles and in particular within the older cells of a population⁹. This is a result of biased partitioning during bacteria division⁷ whereby the nucleoid structure essentially immobilises the aggregates, resulting in polar aggregates being inherited by only one of the daughter cells¹⁰. In fact, daughter cell poles can be distinguished by their respective ages, with a new pole being generated during each round of division⁷; therefore any inherited aggregate will always be located at the old cell pole⁹. Interestingly, this mechanism, allows for the population to concentrate the aggregates into a small proportion of cells and with the toxic aggregates now removed from the majority of the healthy and fast growing population, the population as a whole can maintain a higher average growth rate^{11–13}.

As discussed above, aggregates of defunct or misfolded proteins are not homogeneously distributed within a clonal microbial population. Furthermore, the biased partitioning towards old-pole daughter cells compared to new-pole daughter cells is not restricted to protein aggregates. Bergmiller *et al.* investigated phenotypic heterogeneity in *E. coli* as a result of polar cell envelope localisation⁷. For instance, they discuss how formation of supramolecular islands restricts the diffusion of outer membrane proteins and they show how this results in the main efflux pump (AcrAB-TolC) being biasedly partitioned towards the old-pole in *E. coli*⁷. They then show how this results in old-pole daughter having increased efflux activity relative to new-pole daughter cells⁷; a trait which has been linked to antibiotic persistence^{127,166}. In fact, phenotypic heterogeneity is present across all domains of life, for example substantial cell-to-cell differences have been reported in the expression of virulence related genes in a fungal pathogen *Candida glabrata*², in chromatin condensation states in human tumour cell lines⁵² and in metabolic activity in bacteria^{14,15}. Such heterogeneity often arises in response to fluctuations in the extracellular environment with subpopulations experiencing more “stress” than their isogenic kin^{60,61,160,167}.

Interestingly, heterogeneity within an isogenic population, particularly with respect to growth rate, nutrient stress and cellular toxicity, has been linked to the ability of small subpopulations to survive exposure to otherwise lethal doses of antibiotics in a phenomenon known as antibiotic persistence^{22,23,30,81,168}. In fact, a consequence of the aggregation of defunct and misfolded proteins is for the amino acid pool within that particular cell to be depleted¹¹, triggering the stringent response and subsequent production of (p)ppGpp, which has previously been associated with persister and sleeper cells^{60,62,64,169}. Although the above suggests a potential link between protein aggregates and antibiotic survival, only as recently as 2018 did Pu *et al.* first reported how ATP-dependent “aggresome”, a collection of endogenous protein aggregates, formation can regulate cellular dormancy and in turn the development of persister and sleeper (i.e. viable but non culturable) *E. coli*⁹⁴. However, they report the aggregates they investigated were caused by ATP depletion and claim they are different from toxic protein aggregates formed from misfolded proteins⁹⁴. Furthermore, they claim that aggregates formed as a result of the expression of exogenous proteins, such as the ones discussed in this report, do not show the same relationship with persister or sleeper cells⁹⁴. Mortier *et al.* induced the expression of a fluorescent protein, mCerulean3, resulting in the formation of fluorescent protein aggregates, they could then follow the disaggregation, as a result of chaperone systems such as DnaKJE, by observing how the fluorescently tagged proteins diffused throughout the cell¹⁶⁰. Furthermore, some of these now soluble fluorescent proteins were passed to the daughter cells during cellular division, resulting in a decrease in the level of fluorescence after each division¹⁶⁰. Interestingly, by using a genetic mutant, $\Delta dnaK$, which prevented disaggregation, Mortier *et al.* were able to abolish the observed decrease in fluorescence upon cell division so that the fluorescent protein aggregates were retained by the old pole daughters upon cell division.

Based on the above, there is evidence to show that protein aggregation can be a sign of cellular stress and may play a role in the formation of antibiotic persister and sleeper cells. Therefore, we hypothesised that by perturbing the level of intracellular stress (via the control of the production of exogenous proteins), we can manipulate the occurrence of protein aggregates within an *E.*

coli population. Furthermore, we hypothesised that the level of intracellular stress has an impact on the efficacy of treatment with antibiotics, ampicillin in this study. Therefore in order to manipulate the level of intracellular stress we used a collection of *E. coli* BW25113 transcriptional reporter strains¹⁷⁰. For each gene, we could then use the transcript reads we previously reported¹⁷¹ to predict the additional cellular stress being exerted on the cell as a result of exogenous protein expression. Therefore by using strains with varying levels of fluorescence and transcriptional activity (as a proxy for cellular stress), we took our previously reported protocol that allows the detection and temporal tracking of single bacterium in a microfluidic device¹⁶⁶ to investigate the relationship between intracellular stress, protein aggregation and antibiotic efficacy. We found that the percentage of cells within the population containing one or more visible aggregates increased with the expression of exogenous proteins, i.e. intracellular stress, and that these cells were more likely to survive exposure to ampicillin. Taken together our data suggest that intracellular stress favours both protein aggregation and the formation of antibiotic persister cells that have been linked to the recalcitrance of chronic infections and development of antibiotic resistance^{33,38,46}.

Materials and Methods

Strains and culturing

tnaC, *pykF*, *ptsG*, *lon*, *aceB* and *ompC* reporter strains from the *E. coli* MG1655 transcriptional reporter library¹⁷⁰ were purchased from Dharmacon (GE Healthcare). The plasmids were then extracted and transformed into chemically competent *E. coli* BW25113 strain, as this was the strain used for our previously reported transcriptomic analysis¹⁷¹, which was also purchased from Dharmacon (GE Healthcare). Overnight cultures were prepared by picking a single colony of *E. coli* BW25113 from a streak plate and growing it in 200 ml fresh LB medium (10 g/L tryptone, 5 g/L yeast extract, and 10 g/L NaCl, Melford) on a shaking incubator at 200 rpm at 37 °C for 17 hours. For pH assays, a parental strain harbouring pBAD TOPO-mCherry-pHluorin vector (Invitrogen) were kindly provided by the Summers group, Cambridge. Cultures were grown as above but

with additional chloramphenicol (25 µg/mL) supplementation for plasmid maintenance and arabinose (5 µg/mL) to induce the pBAD promoter.

Microfluidic device fabrication

The original mould of the mother machine microfluidic device was kindly provided by S. Jun⁸, whereas a detailed methodology for replicating and handling this device has been reported elsewhere¹⁶⁶. Briefly, each microfluidic device was made by pouring a 9:1 (base:curing agent) polydimethylsiloxane (PDMS, Dow Corning) mixture onto the mould and curing it at 70 °C for 2 hours. The PDMS was then peeled from the mould, access holes for the fluidic tubing was punched and the PDMS chip was then irreversibly bonded to a glass coverslip as previously reported¹⁷². To prevent cell adhesion to the device surfaces, 2 µl of a 50 mg/ml BSA solution was injected into the device and the device was incubated for one hour at 37 °C.

Microfluidic assay

An overnight culture was grown as described above. 10 ml of this overnight culture was centrifuged in a falcon tube (10 minutes at 3000 x g and 20 °C). The supernatant was filtered twice (Medical Millex-GS Filter, 0.22 µm, Millipore Corp.) to extract spent LB. This spent LB was then used to re-suspend the bacteria to an O.D. of 50 at 595 nm. This highly concentrated bacterial suspension was then injected into the BSA functionalised microfluidic device and incubated at 37 °C for approximately 20 minutes or until the bacteria had sufficiently (approximately 2 bacteria per channel) entered the side channels. Fluorinated ethylene propylene (FEP) tubing (1/32" _0.0008") were connected to the pre-punched inlet and outlet holes of the device and connected to a flow-rate measuring device (Flow Unit S, Fluigent, Paris, France) and a waste collection cylinder, respectively. At the end of the incubation period, the device was mounted onto an inverted microscope (IX73 Olympus, Tokyo, Japan), the flow rate pump was controlled using MAESFLO software (Fluigent) and spent LB used to wash excess bacteria from the main channel using spent LB at 300 µL/h for 8 minutes. During this time window, the initial bright field and fluorescence images were acquired for between 50 and 67 imaging areas (each

area containing 23 lateral channels each hosting between one and three bacteria) of the microfluidic device, in order to image approximately 2000 bacteria. All images were acquired using a 60x, 1.2 N.A. objective (UPLSAPO60XW, Olympus) and a sCMOS camera (Zyla 4.2, Andor, Belfast, UK). For the acquisition of fluorescence images the bacteria were exposed to the blue excitation band of a broad-spectrum LED (CoolLED pE300white, Andover, UK). The light intensity and exposure time were adjusted in order to maximise the signal to noise ratio; FITC filter with LED light intensity set at 20 % and exposure of 0.03s for *tnaC*, *pykF* and *aceB*, 20 % and 0.05s for *ptsG* and *ompC*, and 60 % and 0.05s exposure for *lon*.

After acquiring the initial images, spent LB was changed to fresh LB containing ampicillin at 25xMIC ($125 \mu\text{g ml}^{-1}$) and flowed through at 300 $\mu\text{L/h}$ for 8 minutes before being reduced to 100 $\mu\text{L/h}$ for 3 hours, with images being taken hourly. After 3 hours, the medium was changed again to fresh LB medium and images continued to be taken on an hourly basis for a further 3 hours. As a result, during the first day of the assay, images were acquired prior to antibiotic exposure, for 3 hours during exposure to antibiotics and then for 3 hours after exposure. This allowed us to determine the phenotype of each cell in response to antibiotics and then extract its initial level of fluorescence. The chip was left overnight, with fresh LB continuing flowing at 50 $\mu\text{L/h}$ and more images acquired the next morning after 21 hours of total regrowth. Finally, propidium iodide (PI, Thermo Fisher Scientific) was used to perform live/dead staining and one last set of images acquired in bright field and fluorescence using the TRITC filter (100% green LED intensity and 0.01s exposure). The entire assay was carried out at room temperature.

Intracellular pH determination

In order to measure the pH of each individual cell, we used arabinose to constitutively express a fused fluorescent protein in a parental strain harbouring pBAD TOPO-mCherry-pHluorin vector. As the expression of mCherry can be used to normalise by copy number, the ratio between the pH sensitive GFP (pHluorin) and mCherry can then be used to determine intracellular pH. We applied the previously described microfluidic assay to identify persister and

VBNC cells prior to antibiotic exposure on this pH reporter strain. Once we determined each cell's phenotype in response to antibiotic, we then extracted the GFP/mCherry fluorescence ratio. These ratios could then be converted to a pH value based on a known standard curve (Supp. Fig. S1).

Briefly, we exposed the pH reporter strain to 50 μ M Carbonyl cyanide m-chlorophenyl hydrazone (CCCP) at 300 μ L/h for 8 minutes and then at 100 μ L/h for 20 minutes. The exposure to CCCP results in disruption of the cellular membrane and allows the intracellular pH to equalise to the pH of the medium. We then flowed PBS with differing pH levels (pH 6.5, 7.0, 7.5 and 8.0, respectively) through the device one at a time at 300 μ L/h for 8 minutes and then 100 μ L/h for 20 minutes. We acquired images of mCherry (TRITC filter, 5 % green LED intensity and 0.03s exposure) and GFP (FITC filter, 20 % LED intensity and 0.03s exposure) at each pH and extracted the fluorescence intensity (see image and data analysis section below). The ratio of GFP to mCherry could then be determined for each cell and the mean ratio used to generate a standard curve (Supp. Fig. S1) when plotted against the known pH.

Image and data analysis

Image analysis was performed using our custom Python module (*MMHelper*) to extract cellular fluorescence intensities¹⁷³. All data reported in GraphPad Prism 7 represent mean and standard error of the mean of at least biological triplicates. Statistical significance was tested by unpaired t-test with Welch's correction or two tailed Pearson's correlation, respectively.

Aggregates were clearly visible in mother machine images acquired in bright field. However, in order to ensure there was no human bias we randomly selected five bacteria that we had scored by eye as containing at least one or more visible aggregates and five cells we scored by eye as not containing a visible aggregate for each strain, respectively (Supp. Fig. S2). We then investigated the bright field pixel intensity for the cell profiles to quantitatively validate these cells were correctly identified as containing visible aggregates (Supp. Fig. S2). Briefly, using ImageJ we then drew a 5-pixel wide line along the length of the bacterium and extracted the brightness profile. As the aggregates

are primarily located at the poles, we then took the 10 most central pixels for each bacterium and used the average greyscale value to estimate a baseline value. This baseline was then subtracted and, as aggregates are visible as dark foci with lower pixel intensities, the brightness determined as the sum of at least three consecutive negative values. This allowed for the exclusion of the centre of the bacterium as well as any spurious signal (less than 3 consecutive negative or positive values) ^{174,175}. The results showed that for all cells with aggregates a trough in cumulative pixel intensity of between -545.6 and -1778.9 was visible across all strains (red dashed line figure S2), whereas the cumulative intensity for cells without aggregates remained relatively constant throughout (black dashed line figure S2).

Statistical analysis

For comparisons of fluorescence intensities between antibiotic susceptible, persister and sleeper cells, respectively, statistical significance was tested using GraphPad Prism 8 by unpaired t test with Welch's correction. Pearson's correlation, where r signifies the linear dependence of the variables (between -1 and 1), was used to investigate the relationship between different variables; log values were used for transcript reads. In both analyses $p \leq 0.05$ is *, $p \leq 0.01$ is **, $p \leq 0.001$ is *** and $p \leq 0.0001$ is ****, respectively.

Results

Cellular stress favours protein aggregation

Based on literature reports, protein aggregates have been shown to include aggregations of defunct or misfolded proteins^{153,154}. In this study, in the absence of external stressors, such as heat shock, we observed no aggregates in the wild type parental strain for a stationary phase *E. coli* culture after 17 h of growth in LB media (the conditions used throughout this report). Although these results are consistent with previous reports for wild type *E. coli*, it is conceivable that these protein aggregates are still present in the parental strain but do not reach sizes which allow them to be visible¹⁷⁵.

We used the expression of exogenous protein, as a result of fluorescence based transcriptional reporters (see methods), in order to introduce a well-controlled cellular stress. Therefore, based on the evidence that protein aggregation can occur as a result of heterologous protein expression¹⁵⁴, we hypothesised that the proportion of cells with visible aggregates within a population would increase with the expression of the gene being reported. With that in mind, we used microfluidics-microscopy (see Methods) to investigate the proportion of cells containing aggregates among populations of six different *E. coli* transcriptional reporter strains; *tnaC*, *pykF*, *ptsG*, *lon*, *aceB* and *ompC*¹⁷⁰. We selected these strains because the associated genes cover a range of three orders of magnitude in transcript levels (from 78±18 for *tnaC* to 62,837 ± 10,090 for *aceB*, Fig.1) in a stationary phase *E. coli* culture after 17 h of growth in LB media¹⁷¹ that is the inoculum injected in our microfluidic device. Furthermore, some of these genes have been previously associated with antibiotic efficacy. Specifically, *tnaC* is the precursor of the *tna* operon that catabolises tryptophan into pyruvate, ammonia and indole, and has been linked to antibiotic persistence^{35,83,88,166}. *pykF* is a pyruvate kinase and has been linked to bacterial adaptation into different growth phenotypes, growing and non-growing, upon nutrient starvation²³. *ptsG* is a glucose transporter which has been linked to heterogeneity in cellular metabolism¹⁴. *lon* is a protease whose involvement in persistence has been the centre of some debate¹⁵⁷. *aceB* is involved in the glyoxylate shunt during growth on acetate²³, which has previously been linked with changes in phenotypic heterogeneity^{14,171}. *ompC* is one of the major outer membrane porins that allow β -lactams, such as ampicillin, to diffuse into the cell¹⁷⁶. Figure 1 clearly shows a significant positive correlation ($r = 0.99$, $p < 0.0001$ ****) between the measured number of transcriptional reads for each gene and the percentage of cells containing one or more aggregates that are visible using bright field microscopy in the corresponding reporter strain with a maximum of 4.40±1.50 % bacteria containing aggregates for *aceB* that exhibited the highest number of transcript reads (62,837±10,090).

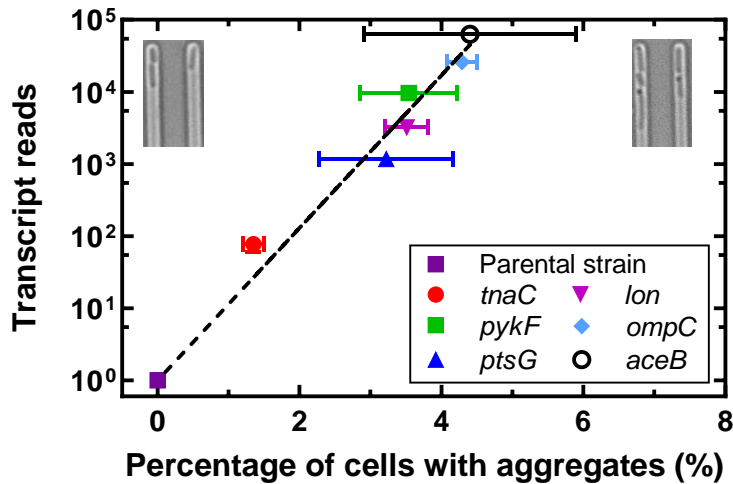


Figure 1. The percentage of cells containing aggregates within a population correlates with the expression of exogenous proteins. Aggregates were clearly visible as dark foci using bright field microscopy (top right inset) and by a clear decrease in pixel intensity when analysing their cellular profile (see Supplementary Figure S1). We quantified the number of cells containing one or more protein aggregates across our 6 reporter strains and the parental wild type *E. coli* strain, comparing this to the number of transcriptional reads from an overnight (17h growth in LB media) stationary phase culture for each respective gene (Smith, *Frontiers in Microbiology*, 2018). We found the percentage of cells containing one or more aggregates was 1.4 ± 0.2 % in *tnaC* ($n = 8273$), 3.5 ± 0.7 % in *pykF* ($n = 8480$), 3.2 ± 1.0 % in *ptsG* ($n = 8141$), 3.5 ± 0.3 % in *lon* ($n = 6854$), 4.3 ± 0.2 % in *ompC* ($n = 3159$) and 4.4 ± 1.5 % in *aceB* ($n = 5867$), respectively. Interestingly, when we performed a linear regression (black dashed line) this showed a significant ($r = 0.99$, $p < 0.0001$ ****) positive correlation determined using Pearsons correlation in GraphPad Prism. Whereby as the number of transcriptional reads increased, and therefore the additional expression of exogenous proteins, as did the percentage of cells containing one or more aggregates within the population. It is important to note, that the parental strain expressed no exogenous proteins and also displayed no aggregates (top left inset) so is located at the origin. Although some error bars are hidden by data points, all data points and error bars are representative of the mean and SEM of 3 biological replicate.

Bacteria containing aggregates have a lower GFP fluorescence than aggregate-free bacteria

For each reporter strain we then use our microfluidics-microscopy assay to measure and compare the GFP fluorescence of bacteria with no visible aggregates after 17 h of growth in LB media (Fig. 2; red boxes) and the corresponding bacteria displaying one or more aggregates (Fig. 2, blue boxes). The results showed that bacteria with aggregates displayed significantly lower fluorescence ($p < 0.0001$ ****) on average compared to the control cells in all of our reporter strains (Fig. 2). For instance, by dividing the mean fluorescence of cells without aggregates by the mean fluorescence of cells without visible aggregates, we determined that cells without aggregates were on average 1.29 ± 0.03 times more fluorescent for *ptsG*, 1.58 ± 0.08 for *lon*, 2.82 ± 0.08 for *ompC*, 4.89 ± 0.08 for *pykF*, 6.40 ± 0.09 for *aceB* and 9.80 ± 0.13 for *tnaC*, respectively.

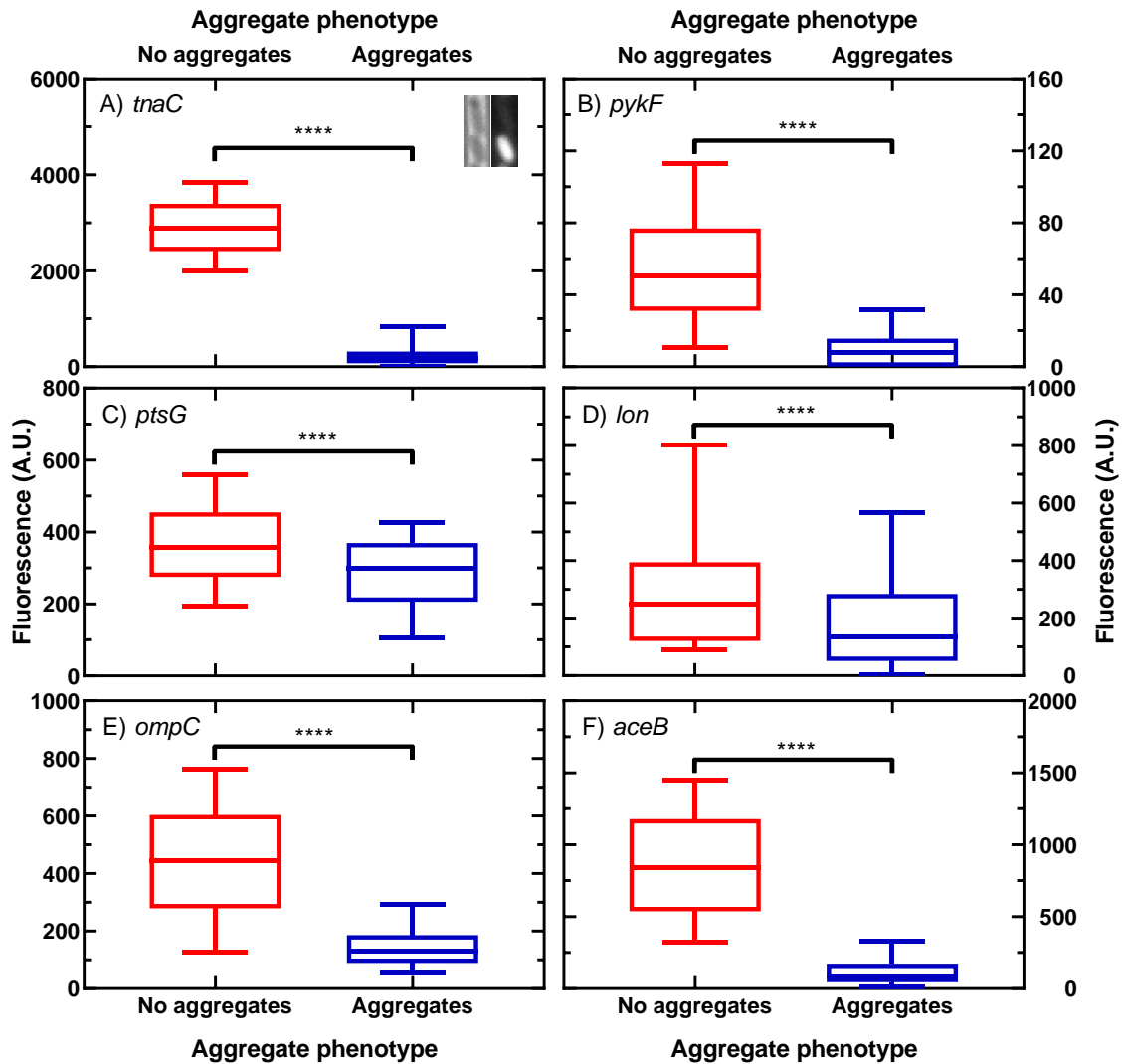


Figure 2. Cells with aggregates have significantly lower fluorescence than cells without aggregates. We split the bacterial populations into two phenotypes depending on if the cells contained visible aggregates (top bacteria in the inset in panel A) or not (bottom bacteria in the inset in panel A) using the same datasets as figure 2. We then compared the initial fluorescence intensities (a stationary phase culture after 17h of growth in LB) for the two subpopulations and found that bacteria containing aggregates (blue boxes) had significantly lower ($p < 0.0001$ ****) fluorescence than those that had no visible aggregates (red boxes) in all 6 of our reporter strains. Images were acquired after exposing bacteria to the blue excitation band of a broad-spectrum LED. The light intensity and exposure time were adjusted in order to maximise the signal to noise ratio; FITC filter with LED light intensity set at 20 % and exposure of 0.03s for *tnaC*, *pykF* and *aceB*, 20 % and 0.05s for *ptsG* and *ompC*, and 60 % and 0.05s

exposure for *lon*. Boxes represent the median and quartile range of each sub-population, with whiskers showing the 10th and 90th percentile range. Statistical significance was determined in GraphPad Prism using unpaired t test with Welch's correction.

Persister and sleeper cells are more likely to contain protein aggregates

Besides distinguishing between bacteria with or without protein aggregates at the beginning of the experiment (i.e. after 17 h of growth in LB media), our microfluidics-microscopy assay also allows us to dose the bacteria with an antibiotic, ampicillin in this study, and determine whether each bacteria is susceptible to the drug or can survive it by regrowing after drug removal, i.e. persister bacteria, or by remaining viable but non culturable after drug removal, i.e. sleeper cells. These combined capabilities allowed us to determine that the proportion of bacteria containing one or more aggregates prior to exposure to the antibiotic was significantly higher in the bacteria which were found to be persister or sleeper cells by the end of the microfluidics-microscopy experiment (Fig. 3). In fact, on average the susceptible sub-populations for all 6 investigated reporter strains contained (2.3±0.2)% bacteria with visible aggregates before antibiotic exposure (Fig. 3; Susceptible). In comparison, on average the persister and sleeper sub-populations for all 6 investigated reporter strains contained (47.5±3.2)% and (70.3±3.4)% bacteria with visible aggregates before antibiotic exposure, respectively (Fig. 3; Persister and Sleeper). Specifically, in only the *ompC* (Fig. 3; blue diamonds) strain (11.3±1.3 %) did less than 30 % of the persister sub population have clearly visible aggregates, with the *tnaC* strain (Fig. 3; red circles) having the highest occurrence of bacteria with aggregates (75.2±6.3)% and the average across all strains being. Visible aggregates were even more prevalent in the sleeper subpopulations, with the lowest occurrence being in the *ompC* strain ((44.4±11.1)%, Fig. 3, blue diamonds)), the maximum in the *aceB* strain ((81.3 ± 4.1)%, Fig. 3, black hollow circles). In all of the strains except *tnaC*, the percentage of cells with visible aggregates was greater for the sleeper subpopulation compared to the persister subpopulation.

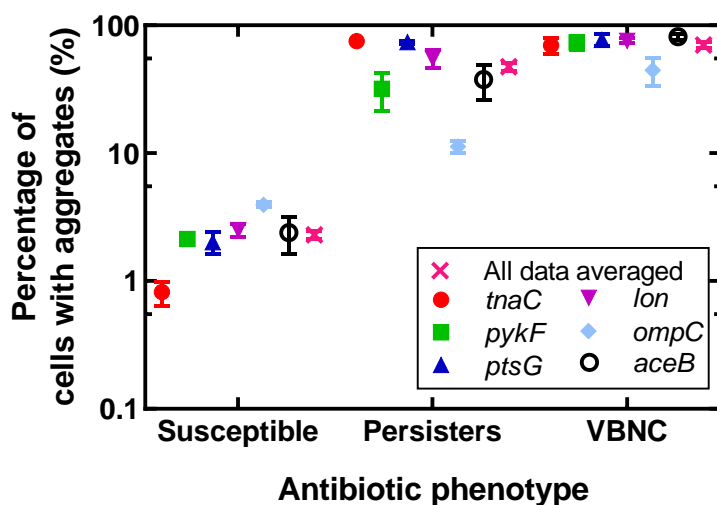


Figure 3. Sleeper and persister cells are more likely to contain aggregates.

Using the same datasets from figure 2 and 3, we split the bacterial populations into three different phenotypes depending on their response to antibiotics (see Figure 1). We then determined the percentage of cells within each of these subpopulations that contained visible aggregates. The results clearly show that less than 5 % of susceptible cells contained aggregates in each of our 6 strains. In comparison, the tolerant subpopulations (persister and sleeper) had considerably higher percentage of cells with visible aggregates. In fact, when we calculated the mean and SEM values for each phenotype across all the strains (pink cross), on average $2.3 \pm 0.2\%$ of susceptible cells contained one or more aggregates, compared to $47.5 \pm 3.2\%$ and $70.3 \pm 3.4\%$ for the persister and sleeper sub populations, respectively. Interestingly, there was no significant correlation between the percentage of cells containing aggregates within each phenotype and the number of transcriptional reads (data not shown). Although some error bars are hidden by data points, data points for each strain represent the mean and SEM of 3 biological replicate.

Cellular stress correlates with percentage of persister but not sleeper bacteria

As expected susceptible cells made up the majority of the population in all of the strains, with *tnaC* ($99.2 \pm 0.1\%$) having the highest proportion and *ompC*

(97.8±0.1)% having the lowest proportion of susceptible bacteria, respectively. Accordingly, also the percentage of the persister and sleeper subpopulations, varied depending on the strain, with two of the strains, *tnaC* and *ptsG*, having a higher percentage of sleeper bacteria, whereas the remaining four strains had a higher percentage of persister cells (Fig. 3). Therefore, we investigated if the relative distribution of the tolerant phenotypes was also a reflection of cellular stress. However, when we plotted the initial transcripts against each of the respective surviving phenotype percentages (Fig. 4A and 4B) we found a statistically significant correlation between log transcript reads and persister percentage ($r = 0.75$, $p = 0.05$, Fig. 4A) but no correlation with sleeper percentage ($r = 0.57$, $p = 0.18$, Fig. 4B), suggesting that the amount of cellular stress plays a role in the formation of persister bacteria.

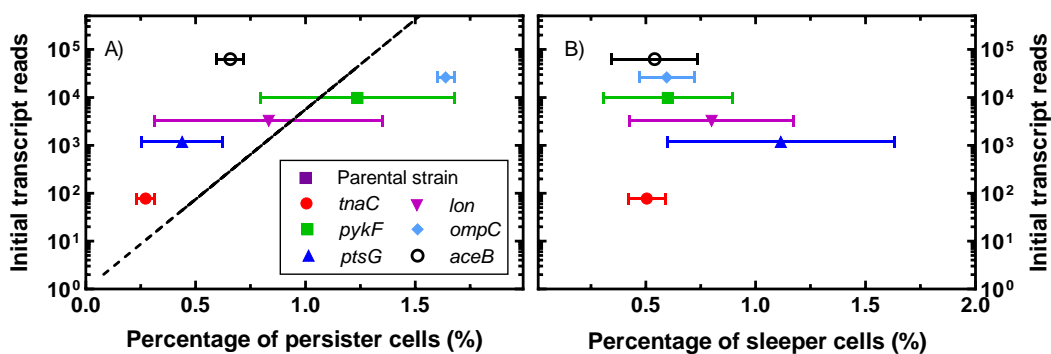


Figure 4. The distribution of tolerant phenotypes is correlated to the level of transcriptional stress. We split the tolerant cells into two sub phenotypes depending on their ability to resuscitate upon removal of antibiotic (see figure 1). We took the initial transcript reads for 6 reporter strains of stationary phase *E. coli* (Smith, *Frontiers in Microbiology*, 2018), as in figure 2, and then plotted it against the percentage of persister cells (A) and sleeper cells (B) within the entire population. We then performed a linear regression (represented by the dashed black line) and the results show that using Pearsons correlation the number of transcriptional reads significantly correlates ($r = 0.76$, $p = 0.0483$ *) with the distribution of persister cells (A). In comparison, sleeper cells (C) appeared to show a negative correlation, although this was not significant. All data points and error bars are representative of the mean and SEM of 3 biological replicate.

Protein aggregates are more basic than the rest of the cell

We then investigated bacterial pH both at the whole cell level and at the level of the protein aggregates. In order to do so, we used pHluorin, a plasmid based fluorescent report of cellular pH¹⁷⁷. We extracted fluorescence intensities for both mCherry and GFP for the visible protein aggregates and the rest of the cell, respectively (see methods). We then determined the ratio of GFP to mCherry and used this to determine the pH intensity based on a standard curve (Supp. fig. 2). Interestingly, we found that protein aggregates were significantly more basic than the rest of the cell in all of the antibiotic phenotypes (Fig. 5). Briefly, the pH for susceptible cells was 6.93 ± 0.02 for the whole cell but 7.23 ± 0.04 for the protein aggregates ($p < 0.0001$ ****, $n = 30$), for persister cells the whole cell pH was 6.96 ± 0.04 and 7.17 ± 0.08 for protein aggregates ($p = 0.012$ *, $n = 30$), and for sleeper cells the whole cell pH was 7.02 ± 0.04 compared to 7.23 ± 0.05 for protein aggregates ($p = 0.023$ *, $n = 30$).

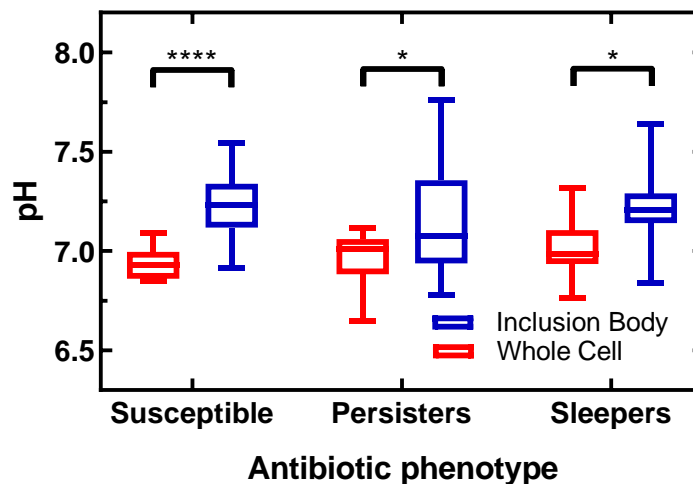


Figure 5. Dark foci have significantly higher pH than the rest of the cell.

We used a fluorescence based pH reporter and performed the microfluidic antibiotic susceptibility assay described in the methods section. We then categorised the bacteria based on their susceptibility to the antibiotic ampicillin (figure 1). We determined the ratio of mCherry fluorescence, used to normalise the fused protein copy number, against the fluorescence of the pH sensitive pHluorin GFP. Once the ratios had been calculated we were then able to

extrapolate the pH value based on the pre-determined standard curve (supplementary figure 2). We used this method to determine the pH of the dark foci (blue boxes), that can be assumed to be protein aggregations, and found them to be significantly lower than the remainder of the cell (red boxes) in 20 cells for all 3 antibiotic response phenotypes; $p < 0.0001$ **** for susceptible, $p = 0.0271$ for persisters * and $p = 0.0062$ ** for sleepers. Boxes represent the median and quartile range of each sub-population, with whiskers showing the 10th and 90th percentile range. Statistical significance was determined in GraphPad Prism using unpaired t test with Welch's correction.

Discussion

Protein aggregates have been observed with fluorescence based microscopy using fluorescently tagged chaperones^{9,10}. However, there is the possibility that the formation of aggregates in these circumstances is a result of the damage that comes from exposure to the strong light sources used to excite the fluorescence proteins or simply by limiting cellular resources as a result of the expression of these exogenous fluorescent proteins¹⁷⁸. This fluorescent tagging has been required, as to the best of our knowledge, only two papers have reported observing aggregates in *E. coli* cells in the absence of fluorescence probes to facilitate aggregate visualisation^{10,94}. However, only one of these was using bright field microscopy⁹⁴ and the other only observed using them using phase contrast after growing single cells in LB medium for 32 hours in a mother machine device (>150 generations)¹⁰. Carrio *et al.* used a strain of *E. coli* with a deletion mutation for the protease La and introduced a plasmid that expressed the model chimeric protein VP1LAC; resulting in reduced proteolytic activity and favouring the generation of large protein aggregates in almost all bacteria¹⁵⁴. Although we did not observe aggregates in the *E. coli* BW25113 parental strain, it is still conceivable that these aggregates are present but are simply not large enough to be observed without the use of fluorescent probes¹⁷⁵. However, we did observe aggregates in *E. coli* BW25113 strains with plasmid-mediated expression of heterologous GFP (see Methods). We found that there was a variety in the occurrence of these aggregates depending on the expression of the gene being reported and hence of the GFP

being produced. This variation shows a significant positive correlation with the number of transcriptional reads of the gene in question and hence the level of added stress the cell is under (Fig. 1). Importantly, the aggregates we observed in our reporter strains were only dark foci in bright field and not fluorescent foci, further supporting the idea that these were aggregates of defunct proteins rather than of actively fluorescent GFP.

Aggregates are known to form as a result of intracellular stress or toxicity and are formed by the clustering of multiple defunct proteins into hydrophobic bundles of protein¹¹. The hydrophobic nature makes them difficult to be then broken down by proteases and their respective chaperones¹¹. As a result, they often grow gradually in size and result in a steady depletion of the amino acid pool^{10,11}. We propose this is the result of what is essentially a negative feedback loop (Supp. Fig. S3); whereby an increase in cellular stress (i.e. the expression of the exogenous protein GFP in our study) results in depletion of the amino acid pool, that in turn increases the amount of defunct proteins which aggregate and further decrease the amino acid pool (Supp. Fig. S3). On top of this, biased partitioning during division results in aggregates being concentrated in the old-pole daughter cells, resulting in a gradual reduction in the growth rate of the older cells within the population^{9,10}. Therefore, we also propose that the above illustrated negative feedback loop results in the level of dormancy increasing within cells with increased cellular stress, resulting in them moving towards the persister and sleeper states (Supp. Fig. S3). Furthermore, as a result of biased partitioning, we propose that this process is more prominent in the old-pole daughter cells within a population. This would explain why we record a higher proportion of cells with protein aggregates in the persister subpopulation compared to the susceptible subpopulation and more still in the sleeper subpopulation (Fig. 3). This tentative explanation is supported by the fact that cells containing aggregates show significantly lower fluorescence (Fig. 2) and by the work by Bergmiller, *et al.* showing that biased partitioning of AcrAB-TolC, a multi drug efflux pump, results in old-pole daughter cells showing higher levels of efflux activity⁷. Furthermore, Govers *et al.* showed that cells inheriting an aggregate formed as a result of proteotoxic stress had a fitness advantage, relative to their isogenic kin, when exposed to a subsequent stress¹⁵⁸. Finally, a series of studies showed that pre-stressed bacterial populations have a higher

proportion of bacteria surviving antibiotic treatment^{35,61,63,64,179}. For instance, Leung and Lévesque showed that alongside oxidative stress, heat shock and nutrient limiting conditions, persister levels to ofloxacin could be increased in *S. mutans* in response to acidic pH⁵⁵. Similarly, Pu *et al.* showed that increasing cytoplasmic acidity correlated with formation of protein aggregates, although was not the singular reason⁹⁴. Furthermore, Pu *et al.* only looked at the pH of the whole cell and how this correlated with the number of cells containing aggregates within the population⁹⁴. Importantly, when we used the plasmid encoded fluorescent pH reporter pHluorin¹⁷⁷, the pH of our bacteria was consistent with those reported by Pu, *et al.*⁹⁴ (data not shown). However, when we investigate the pH of the dark foci separately from the remainder of the cell, we found that dark foci were significantly more basic than the rest of the cell (Fig. 5). Furthermore, as the pH strain we used consists of a mCherry-pHluorin translational fusion protein controlled by the arabinose inducible pBAD promoter¹⁸⁰, the bacteria in this strain were constitutively expressing exogenous proteins throughout the assays; this was reflected in the percentage of cells containing visible aggregates (59.3 ± 0.3 %). We therefore predicted that, based on our hypothesis (Supp. Fig. S3), that we should observe a relatively high percentage of cells surviving antibiotic exposure in the pH strain. As expected, the proportion of persister and sleeper cells (4.3 ± 0.7 % combined) was higher in this strain than in any of the transcriptional reporter strains (*ompC* strain had the highest at 2.23 ± 0.13 % combined), further supporting our hypothesis (Supp. Fig. S3).

Conclusion

We showed that in a stationary phase culture of *E. coli*, protein aggregates are not visible in the parental strain in the absence of external stressors. In contrast, we reported that when using fluorescence based transcriptional reporters, the expression of exogenous proteins (which reflects the expression of the gene being reported) positively correlates with the percentage of cells within the population containing one or more visible aggregates. Furthermore, we show that a higher percentage of cells within the persister and sleeper subpopulations contained one or more visible aggregates compared to their susceptible kin and that the pH of the aggregates is more alkaline when compared to that of the

entire cell. Taken together these findings shed new light on the nature and function of protein aggregates, a phenomenon that is being recognised to be ubiquitous in biology and that could have profound consequences on drug treatment.

Acknowledgements

This work was supported by a Royal Society Research Grant, a Wellcome Trust Strategic Seed Corn Fund and a Start up Grant from the University of Exeter awarded to SP. AS acknowledges support from the BBSRC through a SWBio-DTP studentship. OG acknowledges support from the University of Exeter and DSTL for funding through a studentship. ZK acknowledges The Gordon and Betty Moore Foundation for their support through the grant GBMF5514. EA acknowledges the MRC and the DSTL for their support through a studentship. G.G. was supported by an EPSRC DTP PhD studentship (EP/M506527/1). JM was generously supported by a Wellcome Trust Institutional Strategic Support Award (WT097835MF).

Author contributions

A.S., O.G., R.B., Z.K., G.G., E.A., A.C. performed the experiments; A.S. analysed the data; A.S. and J.M. wrote the image analysis code; A.S. and S.P. wrote the paper.

5.3 Supplementary figures

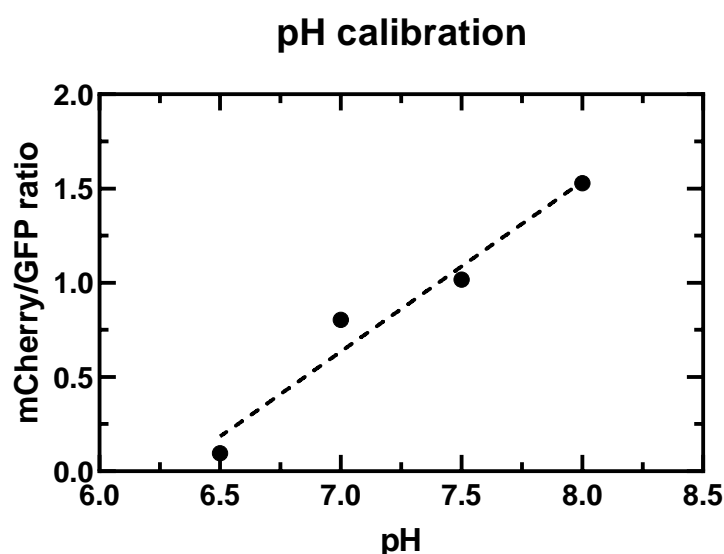


Figure S1. Standard curve for pH analysis. We used an *E. coli* strain which contained a plasmid encoded fused translational protein mCherry-pHluorin to investigate intracellular pH. As the fused protein allows mCherry fluorescence to be normalised by protein copy number whilst the pHluorin (GFP) is pH sensitive, the mCherry/GFP ratio allows cellular pH to be determined. However, in order to do this, a standard curve is required to convert the ratio to pH. We used Carbonyl cyanide m-chlorophenyl hydrazine (CCCP) to disrupt the cellular membrane of *E. coli* cells within the microfluidic mother machine. We then exposed the bacteria to PBS with varying pH concentrations. We acquired images of mCherry (TRITC filter, 5 % green LED intensity and 0.03s exposure) and GFP (FITC filter, 20 % LED intensity and 0.03s exposure) and used *MMHelper* (Smith, *Scientific Reports*, 2019) to analyse 30 bacteria for each pH. The ratio of mCherry to GFP was then plotted against the known pH and a linear regression used to produce the above standard curve (dashed black line). Data points are mean and SEM of 30 cells for each pH value, error bars are included but are too small to be visible for all data points.

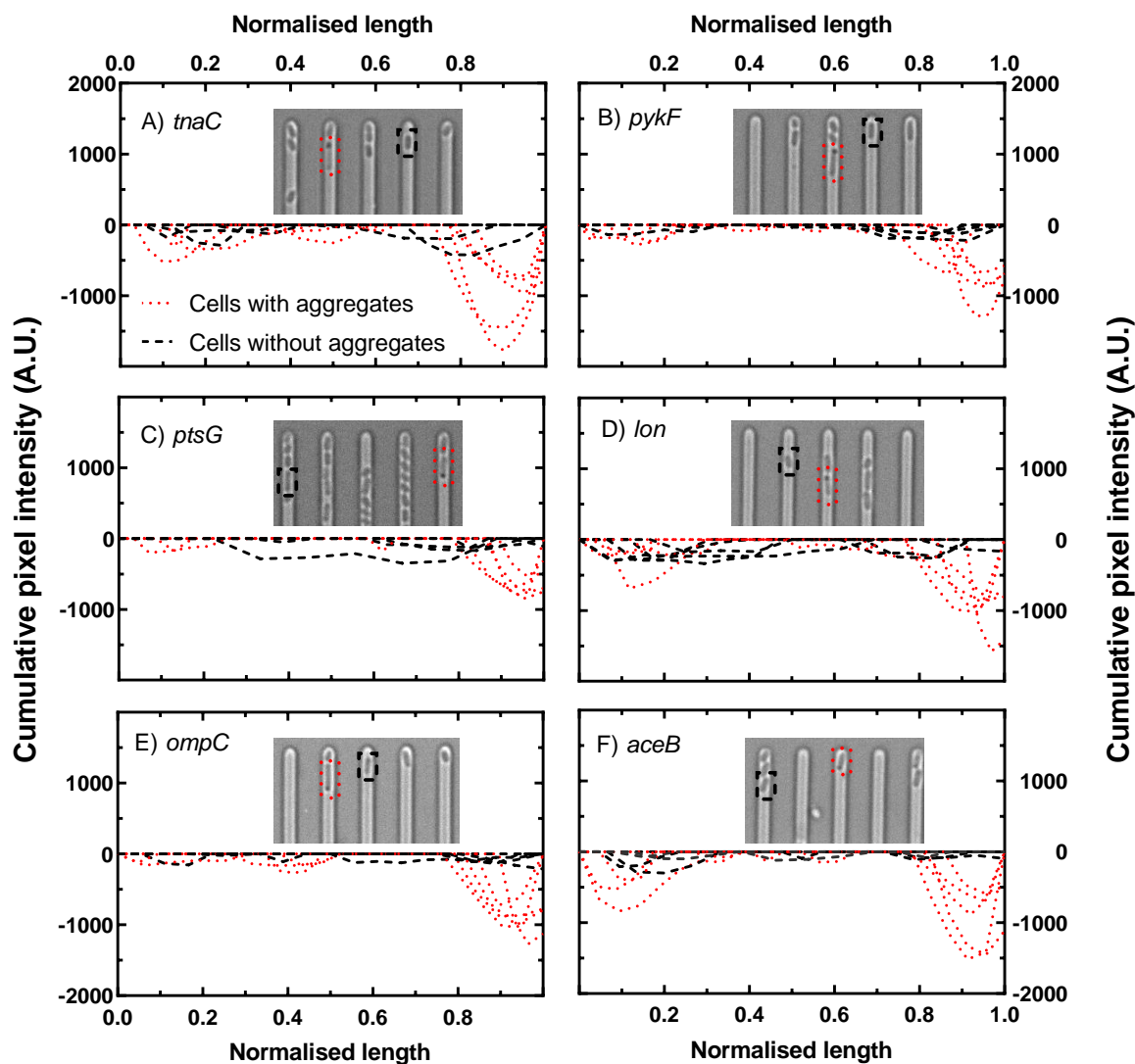


Figure S2. Quantitative validation of our approach for visually scoring cells containing protein aggregates. Using ImageJ we drew a 5 pixel wide line along the length of a bacterium and extracted the bright field intensity. We determined the background as the average intensity of the 10 centre most pixels and subtracted this from the remaining pixels. Moving along the length of the bacterium, if 3 or more consecutive values were negative (due to aggregates being dark foci – see cells with aggregates in insets) then the newly calculated background-subtracted intensities were added together else they were set to 0. We then randomly selected 5 cells that we scored as containing a protein aggregate by visual inspection (red dashed lines) and 5 cells that we scored as not containing a protein aggregate by visual inspection (black dashed line) from each biological replicate experiment and plotted their bright field profiles against normalised length of the cell for each of the 6 reporter strains;

tnaC (A), *pykF* (B), *ptsG* (C), *lon* (D), *ompC* (E) and *aceB* (F). The resulting profiles clearly show that for all cells with aggregates a cumulative decrease in pixel intensity of at least 500 A.U is visible (red dashed lines) compared to the cells without aggregates (black dashed lines) which remain relatively constant throughout. Insets show a representative image of a cell with aggregates (red dashed line) and cell without aggregates (black dashed line) for each respective strain.

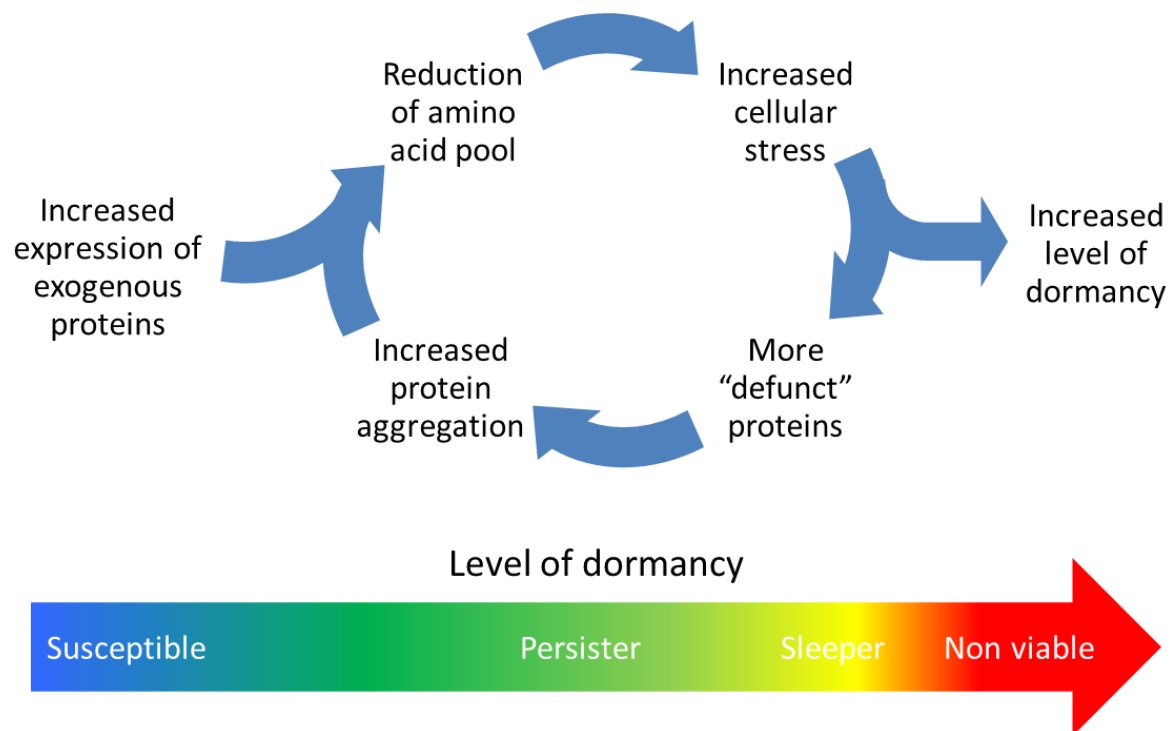


Figure S3. Increase in reporter strain expression levels result in an increase in protein aggregation, cellular stress and level of cellular dormancy. We propose a snowball effect for the formation of intracellular protein aggregates; whereby an increase in cellular stress results in the production of more non-viable proteins, these defunct proteins then aggregate and reduce the cellular amino acid pool, further increasing the level of cellular stress. We hypothesise that if the expression of a plasmid based fluorescent reporter is increased then this will result in a reduced amino acid pool, triggering the above cycle and increasing the snowball effect. Crucially, an increased level of cellular stress will result in an increased level of cellular dormancy and, as a result, the cells response to antibiotic exposure. This is consistent with the proposed dormancy continuum; whereby persister cells, cells that survive antibiotic exposure and are able to begin regrowth upon exposure to fresh nutrients, are more dormant than their susceptible kin, but are less dormant than sleeper cells, cells that require long and specific treatment to resuscitate after antibiotic exposure. However, we propose that there is a “sweet spot” on the continuum that allows sleeper cells to form; where the cells are more dormant than persister cells but have not sustained enough cellular damage to become non-viable.

5.4 Conclusion

In this chapter I used the previously discussed high throughput protocol (chapters three and four, respectively) to investigate the relationship between the expression of plasmid based transcriptional reporters and the formation of visible protein aggregates. Furthermore, I investigated how the resulting additional stress that is applied to the cell affects the distribution of antibiotic tolerant phenotypes; persister and sleeper cells.

In this paper, I determined the percentage of cells with visible protein aggregates in multiple *E. coli* strains that contained plasmid based transcriptional reporters. The genes chosen had either been previously linked to the persister or sleeper state, or were shown to be highly regulated using the transcriptomic based approach I discussed in chapter two. Importantly, these genes also exhibited a wide range of expression levels based on our results in chapter two, which allowed for the testing of our hypothesis. Therefore, I was able to use the expression of exogenous protein for each respective gene as a proxy for additional cellular stress. Using this approach, I showed that as the level of additional cellular stress increased, as did the proportion of cells within the population that exhibit visible protein aggregates.

As discussed in this paper and in chapter one, protein aggregation causes a reduction in the cellular amino acid pool. As a result, the additional stress may also manifest as nutrient exhaustion, particularly with respect to amino acids. Therefore, given that metabolic stress has been linked to dormancy and the formation of persister and VBNC cells, we hypothesised that the added intracellular stress of the reporter strains may also affect the percentage of antibiotic persister and sleeper cells within the population. Using the same experimental data, I was able to categorise individual bacterium based on their antibiotic response. Interestingly, I found that as the levels of additional stress increased, a significant correlation could be observed with the total number of cells that survived antibiotic exposure. However, when investigated individually, I found that the correlation was also positive compared to the persister percentage, but showed no correlation with respect to the sleeper percentage. One potential explanation could be the existence of a “sweet spot” for the formation of sleeper cells, whereby too little stress they exhibit persister or

susceptible phenotypes but too much stress and they experience cell death and become unviable prior to antibiotic exposure.

Protein aggregates have been linked to cellular diseases¹⁵³ and aggregates that form as a result of cellular stress provided a fitness advantage to future lineages¹⁵⁸. Therefore, based on our results and the fact aggregates have also been linked to cellular ageing^{9,10}, we propose that cellular ageing within bacterial populations may be a memory mechanism by which the older cells within a population have a survival advantage during future exposure to exogenous stress, such as antibiotics; providing an exciting avenue for future research.

Chapter 6: Conclusions and Outlook

6.1 Population level transcriptome and the need for single cell analysis

In chapter two, we characterised the extracellular environment, in terms of pH and sugar availability, for a growing planktonic population of *E. coli*. Alongside this, we utilised antibiotic persister cell formation as a proxy to identify temporal phases where there was substantial changes in population heterogeneity. Furthermore, throughout this growth cycle we also investigated the population level transcriptome and identified highly regulated genes and pathways that coincided with these temporal phases. Therefore, this comprehensive dataset provides, for the first time, a series of well-defined time points, medium composition and potential pathways for further single cell analysis. In fact, we carried forward some of the genes identified within chapter two for single cell analysis during chapters three and five, respectively. On top of this, we investigated the transcriptomic dataset reported in chapter two for highly regulated genes and pathways during specific temporal windows. However, the dataset is freely available and there remains scope for further analysis. For instance, as *E. coli* is a commonly used model organism, the transcriptomic data could be used to support a wide range of experiments.

Interestingly, we found the temporal phases where there were substantial changes in persister formation and, hence, population heterogeneity, were different depending on the type of antimicrobial used. Additionally, the temporal windows changed if these antimicrobials were supplied alongside fresh nutrients. However, the transcriptomic data which we acquired was reflective of the population mean and not necessarily of the persister populations themselves; highlighting the importance of further investigating population heterogeneity at the single cell level.

Although persister cells had previously been investigated using microfluidics, to the best of my knowledge, prior to this thesis, no one had utilised microfluidics to investigate the VBNC phenotype. Therefore, the main aim of this thesis was to develop a high throughput microfluidic pipeline that would allow us to simultaneously investigate both persister and VBNC cells that are produced in

response to antibiotics within isogenic bacterial populations. This is particularly important, due to the hypothesis that they are part of one physiological continuum.

To this end, I introduced our newly developed protocol in chapter three that utilised the pre-existing mother machine microfluidic device. This protocol is the first of its kind that allows the investigation of both VBNC and persister cells before, during and after exposure to antibiotics.

6.2 The dormancy continuum and cellular ageing

In chapter three we showed that, in the three strains used in the study, VBNC and persister cells showed no significant difference prior to drug exposure, supporting the hypothesis that they are part of one physiological continuum. In fact, the two phenotypes also showed similar fluorescence levels throughout antibiotic exposure, with the only obvious variation being in the reporter strain for the glucose specific permease, *ptsG*. In this strain, the average fluorescence of the VBNC population decreased faster and to a lower final level than *tnaC*; suggesting VBNC cells are more dormant than their persister kin. Similarly, after regrowth in the reporter strain for the multi drug efflux pump, *tolC*, the average fluorescence of the VBNC population was significantly higher than that of the persister population. This suggests that the VBNC population are potentially more damaged than persister cells and perhaps this is the reason they exhibit a higher level of dormancy.

As a result, I investigated the relationship between persister cells, VBNC cells and cellular stress in chapter five. Using the expression of exogenous protein as a proxy, I showed that the combined fraction of VBNC and persister cells within a population increased with in an increase in cellular stress. Interestingly, when persister and VBNC cells were considered separately, a positive correlation was also observed between cellular stress and the persister fraction but there was no correlation with the VBNC fraction. This lack of correlation for the VBNC population suggests that perhaps a “sweet spot” exists, where the level of cellular stress is high enough that the cell enters the VBNC state but is not sufficient to cause cell death. Furthermore, in chapter five, I also identified that an increase in cellular stress correlated with an increase in the number of visible

protein aggregations within the population. Using this information, I investigated how these aggregates were distributed in persister and VBNC cells. I found that protein aggregates were rarely visible (on average 2.30 ± 0.16 %) in susceptible cells across all 6 of the reporter strains used in the study but were significantly higher in both the persister and VBNC populations, respectively; suggesting cells that survived antibiotic exposure were more stressed prior to antibiotic exposure than their susceptible kin. Adding to this, in all of the strains except *tnaC*, the percentage of cells with visible protein aggregates was higher in the VBNC population than the persister population. However, in *tnaC*, although the mean was greater in the persister population, it fell within the SEM range for the VBNC population. The fact that visible protein aggregates were more prominent in the VBNC population compared to the persister population, suggests that VBNC cells are more stressed than their persister kin prior to antibiotic exposure. Therefore we have provided further evidence that suggests VBNC cells are more stressed than their persister counterparts prior to antibiotic exposure and hypothesised the existence of a “sweet spot” with respect to cellular stress in which VBNC cells are able to form.

On top of this, as discussed in chapter one and chapter five, protein aggregates have been suggested to be a sign of cellular ageing and reduced cellular growth rate, therefore it would be interesting to determine if VBNC and persister cells are the older cells within a population. In fact, the combination of the microfluidic protocol and *MMHelper* that I introduced in chapter three and four, respectively, would prove an excellent platform for investigating this. The age of individual cells could be determined by growing an isogenic bacterial population in the mother machine device for an extended period of time prior to antibiotic exposure. Then, by using the protocol discussed in chapter three, it would be possible to identify persister and VBNC cells and hence the relationship between cellular age and antibiotic survival.

6.3 Identification of potential biomarkers

Using the high throughput approach discussed in chapters three and four, we were able to identify that both persister and VBNC cells exhibited significantly lower fluorescence in a plasmid based reporter strain of the *tna* operon

precursor, *tnaC*. As a result, in chapter three, we proposed that this is a potential biomarker that would allow the isolation and further analysis of persister and VBNC cells, prior to antibiotic exposure.

The strain identified as potential biomarkers, *tnaC*, could now be used to isolate and investigate persister and VBNC cells using fluorescence activated cell sorting and transcriptional analysis. As mentioned above, all three of these strains were significantly different for both persister and VBNC cells with respect to their susceptible kin; however they were not significantly different from each other. Therefore, further screening is required in order to identify biomarkers that show significant difference between persisters and VBNC cells; this would then allow for this approach to be used to investigate the differences between persister and VBNC cells and help decipher the structure of the proposed physiological continuum.

Development of a mathematical model to identify candidate genes for analysis in the mother machine has the potential to increase the throughput of this screening process. A potential solution to this would be through the analysis of fluorescence data for a bacterial population collected using a flow cytometer. The first step would be to take the reporter strains that we have analysed in the Mother Machine that showed significant difference between subpopulations (i.e. *tnaC*) and acquire flow cytometer data for their fluorescence. Then, by identifying small “peaks” in the fluorescence histograms we could attempt to correlate these to the subpopulation size and relative fluorescence for our respective antibiotic response phenotypes. Once a working model has been developed, it could be used to rapidly screen flow cytometer data on hundreds of genes to try and identify any which may contain similar significantly different subpopulations.

As mentioned above, identification of these biomarkers is essential in allowing the further analysis and comparison of the three phenotypes (susceptible, persisters and VBNC) before exposure to antibiotics. One potential method for this would be by isolating the subpopulations based on the fluorescence biomarker using Fluorescence Activated Cell Sorting (FACS) and performing transcriptomic analysis. A similar approach was used by Shah, *et al.* in 2006 when they sorted cells based on a transcriptional ribosomal reporter, after they

showed that dim cells consisted of a higher proportion of persister cells³⁴. However, even though the persister fraction was higher, the dim cell population was still less than 40% persisters. Therefore, an important step of any isolation protocol would be to separately perform a survival assay on the isolated population to confirm a high proportion of the cells (i.e. > 80 %) were persister or VBNC cells, respectively. This would help to ensure any transcriptomic data is a more accurate reflection of the persister or VBNC phenotype.

6.4 Adaptability of the protocol

Throughout this thesis I have emphasised the capability of the microfluidic protocol we introduced in chapter three and chapter four for investigating antibiotic persister and VBNC cells. Due to the nature of the protocol and the fact that *MMHelper* (reported in chapter four) can be used for both bright field and phase contrast images, a wide variety of information can be gathered from an individual experiment. For instance, in chapter five I used information from the accompanying bright field images to identify cells that contained protein aggregates. Furthermore, another key attribute of *MMHelper* not requiring fluorescence for detection is that it allows the fluorescent channels to be utilised for reporting of biological factors; such as the transcriptional reporters used in chapter three and five, respectively. In fact, the number of fluorescent channels can be specified in *MMHelper* to allow the investigation of multiple fluorescent reporters simultaneously.

6.4.1 Potential for investigating cellular pH

In chapter five I used transcriptional activity as a proxy for cellular stress and showed it can be directly linked to an increase in the size of persister and VBNC subpopulations. Furthermore, in chapter two I identified temporal windows in the growth cycle of an *E. coli* population where the fraction of persister cells increased in response to antibiotics. Alongside this I showed that there were changes with respect to the nutritional environment and pH during the same temporal window; which was supported by changes in the population level expression of genes involved in metabolism. As a result, I investigated some of these genes using the single cell microfluidic pipeline developed in chapter

three and four, respectively. However, my analysis was limited to genes involved in metabolism, but the role of cellular pH in antibiotic survival has yet to be investigated.

In chapter five I reported that cells that contained protein aggregates were significantly more likely to be persisters or VBNC cells. We then used a bacterial strain containing an intracellular pH reporter, pHluorin, to show how protein aggregates had significantly more basic pH compared to the rest of the cells; further indicating the role of pH in the formation of persisters in VBNC cells. Therefore, we are currently using this reporter strain along with the protocol I introduced in chapter three to investigate the cellular pH of cells before, during and after treatment, to determine if cellular pH is different for susceptible, persister and VBNC cells, respectively. Additionally, *MMHelper* can be used to analyse the multiple fluorescent channels which are required for pHluorin to provide an accurate pH measurement.

6.5 Future development of the protocol and microfluidic setup

In this thesis we introduced a high throughput protocol for investigating persisters and VBNC cells simultaneously before, during and after exposure to antibiotics. In order to image the bacteria at sufficient time intervals, in this case every hour, the manual approach to taking the images meant we were limited to investigating approximately 2000-3000 bacteria per experiment. Therefore, we would need a persister fraction of approximately 0.005 in order to gain sufficient persisters to make a significant comparison. As a result, the single cell results we discussed with respect to fluorescent biomarkers and visible protein aggregates are only a reflection of the population at stationary phase (after 17h of growth), when the fraction of persister cells in the population is at its highest (see chapter 2). It is important in the future to perform a similar assay on bacteria during different stages of the growth cycle, however this would require a further increase in throughput.

One way in which the throughput could be further increased would be to increase the regularity of channels within the microfluidic device, resulting in more channels, and hence more bacteria, per image. However this would still probably not produce a sufficient increase. Therefore, perhaps the best option

would be to automate the image acquiring set up. In fact, due to the modular nature of *MMHelper* several of its functions would be perfectly suited to help achieve this goal. For instance, by acquiring images in the z-direction, the detection algorithm for the channels could be used to quickly filter out any that would fail and help to narrow down the correct z-setting to provide the best focus. Furthermore, the detection of the main channel and side channels could be used to extract information on any drift in the y-direction to ensure the channels always stayed central in the field of view. Interestingly, automation of imaging would not only lend itself to increasing the amount of bacteria being imaged, but would also allow an increase in how regularly images could be acquired, particularly between 6 and 24 hours. Furthermore, *MMHelper* could potentially be integrated in to the automation so the results become almost instant.

As mentioned above, one way to improve the throughput would be to increase the number of channels within the device. However, perhaps a better option would be to have two devices “interlinked”; a second upside down Mother Machine on the same chip with the channels in between the first Mother Machine – although this would not directly improve the throughput of an individual experiment, it would allow for a more direct comparison between control and experimental assays by ensuring the environmental conditions of the chip (i.e. temperature) are the same.

6.6 Future development of *MMHelper*

MMhelper is not simply limited to our microfluidic protocol, for instance I showed in chapter four that it can be used to analyse images acquired in multiple imaging modalities as well as in a variety of mother machine devices and experimental set ups. In fact, within chapter four I use *MMHelper* to analyse 4 bright field datasets and 3 phase contrast data sets. Furthermore, of these 7 different data sets, 3 of them had slightly different mother machine designs with respect to the shape of their channels and one contained a different bacterial strain; this again providing different detection challenges for *MMHelper*. Despite this, *MMHelper* outperformed the only other fully automated python software, *Molyso*, with respect to bacteria detection in all of the available datasets,

including the example dataset provide by the authors of *Molyso* themselves. Adding to this, to date *MMHelper* remains the only freely available fully automated image analysis tool for Mother Machine images acquired in bright field.

As discussed above, *MMHelper* has been developed as an automated image analysis tool for Mother Machine images and has been shown to be the most efficient and accurate freely available tool for the academic community. However, an important feature of *MMhelper* that is easy to overlook, is the modular nature of the pipeline, which could easily be adapted for the analysis of images acquired in other microfluidic devices, for example microfluidic chemostat devices.

It is also important to remember that software development is a continuous process. Therefore, further changes and improvements to the algorithm maybe required for further releases. Furthermore, although *MMHelper* was shown to outperform other available analysis tools, it is still not 100 % accurate due to the variation between individual cells, with respect to cell shape, and differences in experimental setups both within a lab and between labs. In fact, it is unlikely that *MMHelper*, or any other automated platform, will very be 100 % accurate. One way to counteract this would be to develop the software to allow interactive editing of the detection results.

6.7 Concluding remarks

To summarise, in this thesis I have presented a newly developed high throughput microfluidic protocol for investigating phenotypic heterogeneity, in particular with respect to antibiotic response, in isogenic microbial populations; including the only freely available Mother Machine image analysis pipeline that is capable of analysing images acquired in multiple imaging modalities. Using transcriptomic analysis I then determined highly regulated genes and pathways in temporal windows in which the persister fraction was enriched and used the previously mentioned microfluidic protocol to investigate the role of these genes during the formation of persister and VBNC cells. The results of these experiments suggest that the fluorescence levels of some of the strains can be used as biomarkers for isolation of VBNC and persister cells prior to antibiotic

exposure; paving the way for further analysis of these important phenotypes. Finally, I then used the protocol to look at the relationship between persisters and VBNC cells, finding that protein aggregates were more prominent in the persister and VBNC cells compared to their susceptible kin. Furthermore, we have proposed a negative feedback loop that results in the formation of protein aggregates and how this may, in turn, affect the formation of persister and sleeper cells.

Bibliography

1. Frank, S. A. & Rosner, M. R. Nonheritable Cellular Variability Accelerates the Evolutionary Processes of Cancer. *PLoS Biol.* **10**, e1001296 (2012).
2. Halliwell, S. C., Smith, M. C. A., Muston, P., Holland, S. L. & Avery, S. V. Heterogeneous expression of the virulence-related adhesin Epa1 between individual cells and strains of the pathogen *Candida glabrata*. *Eukaryot. Cell* **11**, 141–50 (2012).
3. Bubendorfer, S., Koltai, M., Rossmann, F., Sourjik, V. & Thormann, K. M. Secondary bacterial flagellar system improves bacterial spreading by increasing the directional persistence of swimming. *Proc. Natl. Acad. Sci.* **111**, 11485 LP – 11490 (2014).
4. Chai, Y., Chu, F., Kolter, R. & Losick, R. Bistability and biofilm formation in *Bacillus subtilis*. *Mol. Microbiol.* **67**, 254–263 (2008).
5. Anetzberger, C., Pirch, T. & Jung, K. Heterogeneity in quorum sensing-regulated bioluminescence of *Vibrio harveyi*. *Mol. Microbiol.* **73**, 267–277 (2009).
6. Süel, G. M., Kulkarni, R. P., Dworkin, J., Garcia-ojalvo, J. & Elowitz, M. B. Tunability and Noise Dependence in Differentiation Dynamics. *Science (80-.)*. **315**, 1716–1720 (2007).
7. Bergmiller, T. *et al.* Biased partitioning of the multidrug efflux pump AcrAB-TolC underlies long-lived phenotypic heterogeneity. *Science (80-.)*. **356**, 311–315 (2017).
8. Wang, P. *et al.* Robust growth of *Escherichia coli*. *Curr. Biol.* **20**, 1099–1103 (2010).
9. Lindner, A. B., Madden, R., Demarez, A., Stewart, E. J. & Taddei, F. Asymmetric segregation of protein aggregates is associated with cellular aging and rejuvenation. *Proc. Natl. Acad. Sci.* **105**, 3076–3081 (2008).
10. Coquel, A. *et al.* Localization of Protein Aggregation in *Escherichia coli* Is Governed by Diffusion and Nucleoid Macromolecular Crowding Effect. *PLoS Comput. Biol.* **9**, e1003038 (2013).
11. Rokney, A. *et al.* *E. coli* Transports Aggregated Proteins to the Poles by a Specific and Energy-Dependent Process. *J. Mol. Biol.* **392**, 589–601

- (2009).
12. Koleva, K. Z. & Hellweger, F. L. From protein damage to cell aging to population fitness in *E. coli* : Insights from a multi-level agent-based model. *Ecol. Modell.* **301**, 62–71 (2015).
 13. Chao, L., Rang, C. U., Proenca, A. M. & Chao, J. U. Asymmetrical Damage Partitioning in Bacteria : A Model for the Evolution of Stochasticity , Determinism , and Genetic Assimilation. *PLOS Comput. Biol.* **12**, 1–17 (2016).
 14. Nikolic, N., Barner, T. & Ackermann, M. Analysis of fluorescent reporters indicates heterogeneity in glucose uptake and utilization in clonal bacterial populations. *BMC Microbiol.* **13**, 258 (2013).
 15. Şimşek, E. & Kim, M. The emergence of metabolic heterogeneity and diverse growth responses in isogenic bacterial cells. *ISME J.* **12**, 1199–1209 (2018).
 16. Schreiber, F. *et al.* Phenotypic heterogeneity driven by nutrient limitation promotes growth in fluctuating environments. *Nat. Microbiol.* **1**, 1–7 (2016).
 17. Veening, J. W. *et al.* Transient heterogeneity in extracellular protease production by *Bacillus subtilis*. *Mol. Syst. Biol.* **4**, 1–15 (2008).
 18. Beaumont, H. J. E., Gallie, J., Kost, C., Ferguson, G. C. & Rainey, P. B. Experimental evolution of bet hedging. *Nature* **462**, 90–93 (2009).
 19. Solopova, A. *et al.* Bet-hedging during bacterial diauxic shift. *Proc. Natl. Acad. Sci.* **111**, 7427–7432 (2014).
 20. Verstraeten, N. *et al.* O₂ and Membrane Depolarization Are Part of a Microbial Bet-Hedging Strategy that Leads to Antibiotic Tolerance. *Mol. Cell* **59**, 9–21 (2015).
 21. Van den Bergh, B. *et al.* Frequency of antibiotic application drives rapid evolutionary adaptation of *Escherichia coli* persistence. *Nat. Microbiol.* **1**, 16020 (2016).
 22. Lidstrom, M. E. & Konopka, M. C. The role of physiological heterogeneity in microbial population behavior. *Nat. Chem. Biol.* **6**, 705–712 (2010).
 23. Kotte, O., Volkmer, B., Radzikowski, J. L. & Heinemann, M. Phenotypic bistability in *Escherichia coli*'s central carbon metabolism. *Mol. Syst. Biol.* **10**, 736 (2014).
 24. Kotte, O., Zaugg, J. B. & Heinemann, M. Bacterial adaptation through

- distributed sensing of metabolic fluxes. *Mol. Syst. Biol.* **6**, 1–9 (2010).
25. Acar, M., Mettetal, J. T. & Oudenaarden, A. Van. Stochastic switching as a survival strategy in fluctuating environments. *Science* **40**, 471–475 (2008).
 26. Heerden, J. H. Van *et al.* Lost in Transition : Start-Up of Glycolysis Yields Subpopulations on Nongrowing Cells. *Science (80-.)*. **343**, (2014).
 27. Bódi, Z. *et al.* Phenotypic heterogeneity promotes adaptive evolution. *PLoS Biol.* **15**, 1–26 (2017).
 28. Becskei, A. & Serrano, L. Engineering stability in gene networks by autoregulation. *Nature* **405**, 590–593 (2000).
 29. Smits, W. K., Kuipers, O. P. & Veening, J. Phenotypic variation in bacteria : the role of feedback regulation. *Nat. Rev. Microbiol.* **4**, 259–271 (2006).
 30. Balaban, N. Q., Merrin, J., Chait, R., Kowalik, L. & Leibler, S. Bacterial persistence as a phenotypic switch. *Science* **305**, 1622–1625 (2004).
 31. Lewis, K. Persister cells, dormancy and infectious disease. *Nat. Rev. Microbiol.* **5**, 48–56 (2007).
 32. Lewis, K. Persister cells. *Annu. Rev. Microbiol.* **64**, 357–372 (2010).
 33. Keren, I., Shah, D., Spoering, A., Kaldalu, N. & Lewis, K. Specialized Persister Cells and the Mechanism of Multidrug Tolerance in *Escherichia coli*. *J. Bacteriol.* **186**, 8172–8180 (2004).
 34. Shah, D. *et al.* Persisters: a distinct physiological state of *E. coli*. *BMC Microbiol.* **6**, 53 (2006).
 35. Vega, N. M., Allison, K. R., Khalil, A. S. & Collins, J. J. Signaling-mediated bacterial persister formation. *Nat. Chem. Biol.* **8**, 431–3 (2012).
 36. Ayrapetyan, M., Williams, T. C. & Oliver, J. D. Bridging the gap between viable but non-culturable and antibiotic persistent bacteria. *Trends Microbiol.* **23**, 7–13 (2015).
 37. Ayrapetyan, M., Williams, T. C., Baxter, R. & Oliver, J. D. Viable but nonculturable and persister cells coexist stochastically and are induced by human serum. *Infect. Immun.* **83**, 4194–4203 (2015).
 38. Levin-Reisman, I. *et al.* Antibiotic tolerance facilitates the evolution of resistance. *Science (80-.)*. **355**, 1–10 (2017).
 39. Aslam, B. *et al.* Antibiotic resistance : a rundown of a global crisis. *Infect. Drug Resist.* **11**, 1645–1658 (2018).
 40. Van Boeckel, T. P., Brower, C., Gilbert, M., Grenfell, B. T. & Levin, S. A.

- Global trends in antimicrobial use in food animals. *Proc. Natl. Acad. Sci.* **112**, 5649–5654 (2015).
41. Hobby, G. L., Meyer, K. & Chaffee, E. Observations on the Mechanism of Action of Penicillin. *Proc. Soc. Exp. Biol. Med.* **50**, 281–285 (1942).
 42. Bigger, J. Treatment of staphylococcal infections with penicillin by intermittent sterilisation. *Lancet* **244**, 497–500 (1944).
 43. Balaban, N. Q. *et al.* Definitions and guidelines for research on antibiotic persistence. *Nat. Rev. Microbiol.* **17**, 441–448 (2019).
 44. Ayrapetyan, M., Williams, T. & Oliver, J. D. Relationship between the Viable but Nonculturable State and Antibiotic Persister Cells. *J. Bacteriol.* **200**, (2018).
 45. Orman, M. A., Henry, T. C., Decoste, C. J. & Brynildsen, M. P. Analyzing persister physiology with fluorescence-activated cell sorting. *Methods Mol. Biol.* **1333**, 83–100 (2016).
 46. Mulcahy, L. R., Burns, J. L., Lory, S. & Lewis, K. Emergence of *Pseudomonas aeruginosa* strains producing high levels of persister cells in patients with cystic fibrosis. *J. Bacteriol.* **192**, 6191–6199 (2010).
 47. LaFleur, M. D., Kumamoto, C. A. & Lewis, K. *Candida albicans* biofilms produce antifungal-tolerant persister cells. *Antimicrob. Agents Chemother.* **50**, 3839–3846 (2006).
 48. Wuyts, J., Van Dijck, P. & Holtappels, M. Fungal persister cells : The basis for recalcitrant infections? *PLoS Pathog.* **14**, e1007301 (2018).
 49. Bojsen, R., Regen, B., Gresham, D. & Folkesson, A. A common mechanism involving the TORC1 pathway can lead to amphotericin B-persistence in biofilm and planktonic *Saccharomyces cerevisiae* populations. *Sci. Rep.* **6**, 1–10 (2016).
 50. LaCrue, A. N., Scheel, M., Kennedy, K., Kumar, N. & Kyle, D. E. Effects of artesunate on parasite recrudescence and dormancy in the rodent malaria model *Plasmodium vinckei*. *PLoS One* **6**, e26689–e26689 (2011).
 51. Hangauer, M. J. *et al.* Drug-tolerant persister cancer cells are vulnerable to GPX4 inhibition. *Nature* **551**, 247–250 (2017).
 52. Sharma, S. V. *et al.* A Chromatin-Mediated Reversible Drug-Tolerant State in Cancer Cell Subpopulations. *Cell* **141**, 69–80 (2010).
 53. Shan, Y., Lazinski, D., Rowe, S., Camilli, A., L. K. Genetic Basis of Persister Tolerance to Aminoglycosides in *Escherichia Coli*. *MBio* **6**, 1–10 (2015).

54. Windels, E. M. *et al.* Bacterial persistence promotes the evolution of antibiotic resistance by increasing survival and mutation rates. *ISME J.* **13**, 1239–1251 (2019).
55. Leung, V. & Lévesque, C. M. A stress-inducible quorum-sensing peptide mediates the formation of persister cells with noninherited multidrug tolerance. *J. Bacteriol.* **194**, 2265–2274 (2012).
56. Radzikowski, J. L. *et al.* Bacterial persistence is an active σ S stress response to metabolic flux limitation. *Mol. Syst. Biol.* **12**, 882 (2016).
57. Cohen, N. R., Lobritz, M. A. & Collins, J. J. Microbial Persistence and the Road to Drug Resistance. *Cell Host Microbe* **13**, 632–642 (2013).
58. Petrosino, J. F., Galhardo, R. S., Morales, L. D. & Rosenberg, S. M. Stress-induced β -lactam antibiotic resistance mutation and sequences of stationary-phase mutations in the Escherichia coli chromosome. *J. Bacteriol.* **191**, 5881–5889 (2009).
59. Nguyen, D. *et al.* Active Starvation Responses Mediate Antibiotic Tolerance in Biofilms and Nutrient-Limited Bacteria. *Science (80-.)*. **334**, 982–986 (2011).
60. Amato, S. M. & Brynildsen, M. P. Persister Heterogeneity Arising from a Single Metabolic Stress. *Curr. Biol.* **25**, 2090–8 (2015).
61. Wu, Y., Vulić, M., Keren, I. & Lewis, K. Role of Oxidative Stress in Persister Tolerance. *Antimicrob. Agents Chemother.* **56**, 4922–4926 (2012).
62. Amato, S. M. & Brynildsen, M. P. Nutrient transitions are a source of persisters in Escherichia coli biofilms. *PLoS One* **9**, 1–9 (2014).
63. Amato, S. M., Orman, M. a & Brynildsen, M. P. Metabolic control of persister formation in Escherichia coli. *Mol. Cell* **50**, 475–87 (2013).
64. Bernier, S. P. *et al.* Starvation, Together with the SOS Response, Mediates High Biofilm-Specific Tolerance to the Fluoroquinolone Ofloxacin. *PLoS Genet.* **9**, e1003144 (2013).
65. Fung, D. K. C., Chan, E. W. C., Chin, M. L. & Chan, R. C. Y. Delineation of a bacterial starvation stress response network which can mediate antibiotic tolerance development. *Antimicrob. Agents Chemother.* **54**, 1082–1093 (2010).
66. Dörr, T., Vulić, M. & Lewis, K. Ciprofloxacin causes persister formation by inducing the TisB toxin in Escherichia coli. *PLoS Biol.* **8**, 29–35 (2010).

67. Möker, N., Dean, C. R. & Tao, J. *Pseudomonas aeruginosa* increases formation of multidrug-tolerant persister cells in response to quorum-sensing signaling molecules. *J. Bacteriol.* **192**, 1946–1955 (2010).
68. Lewis, K. Persister Cells: Molecular Mechanisms Related to Antibiotic Tolerance. in *Antibiotic Resistance* (ed. Coates, A. R. M.) 121–133 (Springer-Verlag, 2012).
69. Spoering, A. & Lewis, K. Biofilms and Planktonic Cells of *Pseudomonas aeruginosa* Have Similar Resistance to Killing by Antimicrobials. *J. Bacteriol.* **183**, 6746–6751 (2001).
70. Hansen, S., Lewis, K. & Vulić, M. Role of global regulators and nucleotide metabolism in antibiotic tolerance in *Escherichia coli*. *Antimicrob. Agents Chemother.* **52**, 2718–2726 (2008).
71. Gefen, O. & Balaban, N. Q. The importance of being persistent: Heterogeneity of bacterial populations under antibiotic stress: Review article. *FEMS Microbiol. Rev.* **33**, 704–717 (2009).
72. Cabral, D. J., Wurster, J. I. & Belenky, P. Antibiotic persistence as a metabolic adaptation: Stress, metabolism, the host, and new directions. *Pharmaceuticals* **11**, (2018).
73. Moyed, H. S. & Bertrand, K. P. Newly Recognized Gene of *Escherichia coli* K-12 That Affects Frequency of Persistence After Inhibition of Murein Synthesis. *J. Bacteriol.* **155**, 768–775 (1983).
74. LaFleur, M. D., Qi, Q. & Lewis, K. Patients with long-term oral carriage harbor high-persister mutants of *Candida albicans*. *Antimicrob. Agents Chemother.* **54**, 39–44 (2010).
75. Keren, I., Shah, D., Spoering, A., Kaldalu, N. & Lewis, K. Specialized Persister Cells and the Mechanism of Multidrug Tolerance in *Escherichia coli* Specialized Persister Cells and the Mechanism of Multidrug Tolerance in *Escherichia coli*. *J. Bacteriol.* **186**, 8172–8180 (2004).
76. Wu, N. *et al.* Ranking of persister genes in the same *Escherichia coli* genetic background demonstrates varying importance of individual persister genes in tolerance to different antibiotics. *Front. Microbiol.* **6**, 1–11 (2015).
77. Mechler, L. *et al.* A novel point mutation promotes growth phase-dependent daptomycin tolerance in *Staphylococcus aureus*. *Antimicrob. Agents Chemother.* **59**, 5366–5376 (2015).

78. Varik, V., Raquel, S., Oliveira, A., Hauryliuk, V. & Tenson, T. Composition of the outgrowth medium modulates wake-up kinetics and ampicillin sensitivity of stringent and relaxed *Escherichia coli*. *Nat. Publ. Gr.* 1–10 (2016). doi:10.1038/srep22308
79. Keren, I., Kaldalu, N., Spoering, A., Wang, Y. & Lewis, K. Persister cells and tolerance to antimicrobials. *FEMS Microbiol. Lett.* **230**, 13–18 (2004).
80. Allison, K. R., Brynildsen, M. P. & Collins, J. J. Metabolite-enabled eradication of bacterial persisters by aminoglycosides. *Nature* **473**, 216–220 (2011).
81. Maisonneuve, E. & Gerdes, K. Molecular mechanisms underlying bacterial persisters. *Cell* **157**, 539–548 (2014).
82. Lee, J., Jayaraman, A. & Wood, T. K. Indole is an inter-species biofilm signal mediated by SdiA. *BMC Microbiol.* **7**, 1–15 (2007).
83. Vega, N. M., Allison, K. R., Samuels, A. N., Klempner, M. S. & Collins, J. J. *Salmonella typhimurium* intercepts *Escherichia coli* signaling to enhance antibiotic tolerance. *Proc. Natl. Acad. Sci. U. S. A.* **110**, 14420–14425 (2013).
84. Gaimster, H., Cama, J., Hernández-Ainsa, S., Keyser, U. F. & Summers, D. K. The indole pulse: A new perspective on indole signalling in *Escherichia coli*. *PLoS One* **9**, e93168 (2014).
85. Gaimster, H. & Summers, D. Regulation of indole signalling during the transition of *E. coli* from exponential to stationary phase. *PLoS One* **10**, 4–5 (2015).
86. Lacour, S. & Landini, P. S -Dependent Gene Expression at the Onset of Stationary Phase in *Escherichia coli* : Function of S -Dependent Genes and Identification of Their Promoter Sequences. *Society* **186**, 7186–7195 (2004).
87. Chant, E. L. & Summers, D. K. Indole signalling contributes to the stable maintenance of *Escherichia coli* multicopy plasmids. *Mol. Microbiol.* **63**, 35–43 (2007).
88. Hu, Y., Kwan, B. W., Osbourne, D. O., Benedik, M. J. & Wood, T. K. Toxin YafQ increases persister cell formation by reducing indole signalling. *Environ. Microbiol.* **17**, 1275–1285 (2015).
89. Lee, J.-H., Kim, Y.-G., Gwon, G., Wood, T. K. & Lee, J. Halogenated indoles eradicate bacterial persister cells and biofilms. *AMB Express* **6**,

- 123 (2016).
90. Li, L., Mendis, N., Trigui, H., Oliver, J. D. & Faucher, S. P. The importance of the viable but non-culturable state in human bacterial pathogens. *Front. Microbiol.* **5**, 1–1 (2014).
 91. Mishra, A., Taneja, N. & Sharma, M. Viability kinetics , induction , resuscitation and quantitative real-time polymerase chain reaction analyses of viable but nonculturable *Vibrio cholerae* O1 in freshwater microcosm. *J. Appl. Microbiol.* **112**, 945–953 (2012).
 92. Boaretti, M., Lleò, M., Bonato, B., Signoretto, C. & Canepari, P. Involvement of *rpoS* in the survival of *Escherichia coli* in the viable but non-culturable state. *Environ. Microbiol.* **5**, 986–996 (2003).
 93. Korch, S. B. & Hill, T. M. Ectopic Overexpression of Wild-Type and Mutant *hipA* Genes in *Escherichia coli* : Effects on Macromolecular Synthesis and Persister Formation. *J. Bacteriol.* **188**, 3826–3836 (2006).
 94. Pu, Y. *et al.* ATP-Dependent Dynamic Protein Aggregation Regulates Bacterial Dormancy Depth Critical for Antibiotic Tolerance. *Mol. Cell* 143–156 (2018). doi:10.1016/j.molcel.2018.10.022
 95. Grote, J., Krysciak, D. & Streit, W. R. Phenotypic Heterogeneity, a Phenomenon That May Explain Why Quorum Sensing Does Not Always Result in Truly Homogenous Cell Behavior. *Appl. Environ. Microbiol.* **81**, 5280–5289 (2015).
 96. Kiviet, D. J. *et al.* Stochasticity of metabolism and growth at the single-cell level. *Nature* **514**, 376–379 (2014).
 97. Elowitz, M., Levine, a, Siggia, E. & Swain, P. Stochastic gene expression in a single cell. *Science (80-.)*. **297**, 1183–6 (2002).
 98. Ackermann, M. A functional perspective on phenotypic heterogeneity in microorganisms. *Nat. Rev. Microbiol.* **13**, 497–508 (2015).
 99. Single-cell microbiology. *Nat. Biotechnol.* **34**, 1077 (2016).
 100. Silander, O. K. *et al.* A genome-wide analysis of promoter-mediated phenotypic noise in *Escherichia coli*. *PLoS Genet.* **8**, (2012).
 101. Chait, R., Ruess, J., Bergmiller, T., Tkačik, G. & Guet, C. C. Shaping bacterial population behavior through computer-interfaced control of individual cells. *Nat. Commun.* **8**, (2017).
 102. Cama, J., Chimerel, C., Pagliara, S., Javer, a & Keyser, U. F. A label-free microfluidic assay to quantitatively study antibiotic diffusion through lipid

- membranes. *Lab Chip* **14**, 2303–8 (2014).
103. Ahmed, T., Shimizu, S. & Stocker, R. Microfluidics for bacterial chemotaxis. *Integr. Biol.* **2**, 604–629 (2010).
 104. Li, Y. *et al.* Cell migration microfluidics for electrotaxis-based heterogeneity study of lung cancer cells. *Biosens. Bioelectron.* **89**, 837–845 (2017).
 105. Kaiser, M. *et al.* Monitoring single-cell gene regulation under dynamically controllable conditions with integrated microfluidics and software. *Nat. Commun.* **9**, 212 (2018).
 106. Sackmann, E. K., Fulton, A. L. & Beebe, D. J. The present and future role of microfluidics in biomedical research. *Nature* **507**, 181–189 (2014).
 107. Duffy, D. C., McDonald, J. C., Schueller, O. J. A. & Whitesides, G. M. Rapid Prototyping of Microfluidic Systems in Poly(dimethylsiloxane). *Anal. Chem.* **70**, 4974–4984 (1998).
 108. Pagliara, S. *et al.* Auxetic nuclei in embryonic stem cells exiting pluripotency. *Nat Mater* **13**, 638–644 (2014).
 109. Nobs, J. B. & Maerkl, S. J. Long-term single cell analysis of *S. pombe* on a microfluidic microchemostat array. *PLoS One* **9**, e93466 (2014).
 110. Yu, S. *et al.* Subdiffusion of loci and cytoplasmic particles are different in compressed *Escherichia coli* cells. *Commun. Biol.* **1**, (2018).
 111. Qiang, L. *et al.* A novel anti *Candida albicans* drug screening system based on high-throughput microfluidic chips. *Sci. Rep.* **9**, 8087 (2019).
 112. Wessel, A. K., Hmelo, L., Parsek, M. R. & Whiteley, M. Going local: technologies for exploring bacterial microenvironments. *Nat. Rev. Microbiol.* **11**, 337–348 (2014).
 113. Park, S. *et al.* Motion to Form a Quorum. *Science (80-.)*. **301**, 188 (2003).
 114. Cho, H. *et al.* Self-Organization in High-Density Bacterial Colonies : Efficient Crowd Control. *PLoS Biol.* **5**, e302 (2007).
 115. Mao, H., Cremer, P. S. & Manson, M. D. A sensitive, versatile microfluidic assay for bacterial chemotaxis. *Proc. Natl. Acad. Sci. U. S. A.* **100**, 5449–5454 (2003).
 116. Stocker, R., Seymour, J. R., Samadani, A., Hunt, D. E. & Polz, M. F. Rapid chemotactic response enables marine bacteria to exploit ephemeral microscale nutrient patches. *Proc. Natl. Acad. Sci.* **105**, 4209 LP – 4214 (2008).

117. Elfving, A., LeMarc, Y., Baranyi, J. & Ballagi, A. Observing Growth and Division of Large Numbers of Individual Bacteria by Image Analysis. *Appl. Environ. Microbiol.* **70**, 675–678 (2004).
118. Long, Z. *et al.* Microfluidic chemostat for measuring single cell dynamics in bacteria. *Lab Chip* **13**, 947–954 (2013).
119. Choi, J. *et al.* Rapid antibiotic susceptibility testing by tracking single cell growth in a microfluidic agarose channel system. *Lab Chip* **13**, 280–287 (2013).
120. Norman, T. M., Lord, N. D., Paulsson, J. & Losick, R. Memory and modularity in cell-fate decision making. *Nature* **503**, 481–486 (2013).
121. Uphoff, S. Real-time dynamics of mutagenesis reveal the chronology of DNA repair and damage tolerance responses in single cells. *Proc. Natl. Acad. Sci.* **115**, E6516–E6525 (2018).
122. Robert, L. *et al.* Mutation dynamics and fitness effects followed in single cells. *Science (80-.).* **359**, 1283–1286 (2018).
123. Moolman, M. C. *et al.* Slow unloading leads to DNA-bound beta2-sliding clamp accumulation in live *Escherichia coli* cells. *Nat Commun* **5**, 5820 (2014).
124. Arnoldini, M. *et al.* Bistable expression of virulence genes in salmonella leads to the formation of an antibiotic-tolerant subpopulation. *PLoS Biol.* **12**, e1001928 (2014).
125. Gefen, O., Gabay, C., Mumcuoglu, M., Engel, G. & Balaban, N. Q. Single-cell protein induction dynamics reveals a period of vulnerability to antibiotics in persister bacteria. *Proc. Natl. Acad. Sci.* **105**, 6145–6149 (2008).
126. Pu, Y. *et al.* Enhanced Efflux Activity Facilitates Drug Tolerance in Dormant Bacterial Cells. *Mol. Cell* **62**, 284–294 (2016).
127. Pu, Y. *et al.* Enhanced Efflux Activity Facilitates Drug Tolerance in Dormant Bacterial Cells Article Enhanced Efflux Activity Facilitates Drug Tolerance in Dormant Bacterial Cells. 284–294 (2016).
doi:10.1016/j.molcel.2016.03.035
128. Irimia, D. & Toner, M. Spontaneous migration of cancer cells under conditions of mechanical confinement. *Integr. Biol. (Camb).* **1**, 506–512 (2009).
129. Perlman, Z. E. *et al.* Multidimensional Drug Profiling By Automated

- Microscopy. *Science (80-.)*. **306**, 1194 LP – 1198 (2004).
130. Sachs, C. C. *et al.* Image-based single cell profiling: High-throughput processing of mother machine experiments. *PLoS One* **11**, 1–15 (2016).
 131. Yang, D., Jennings, A. D., Borrego, E., Retterer, S. T. & Männik, J. Analysis of factors limiting bacterial growth in PDMS mother machine devices. *Front. Microbiol.* **9**, 1–12 (2018).
 132. Taheri-Araghi, S. *et al.* Cell-size control and homeostasis in bacteria. *Curr. Biol.* **25**, 385–391 (2015).
 133. Grant, M. A. A., Waclaw, B., Allen, R. J. & Cicuta, P. The role of mechanical forces in the planar-to-bulk transition in growing *Escherichia coli* microcolonies. *J. R. Soc. Interface* **11**, (2014).
 134. Abramoff, M. D., Magalhães, P. J. & Ram, S. J. Image Processing with ImageJ. *Biophotonics Int.* **11**, 36–42 (2004).
 135. Ducret, A., Quardokus, E. M. & Brun, Y. V. MicrobeJ, a tool for high throughput bacterial cell detection and quantitative analysis. *Nat. Microbiol.* **1**, 16077 (2016).
 136. Haugan, M. S., Charbon, G., Frimodt-Møller, N. & Løbner-Olesen, A. Chromosome replication as a measure of bacterial growth rate during *Escherichia coli* infection in the mouse peritonitis model. *Sci. Rep.* **8**, 14961 (2018).
 137. Carpenter, A. E. *et al.* CellProfiler: image analysis software for identifying and quantifying cell phenotypes. *Genome Biol.* **7**, R100–R100 (2006).
 138. Rees, P., Wills, J. W., Brown, M. R., Barnes, C. M. & Summers, H. D. The origin of heterogeneous nanoparticle uptake by cells. *Nat. Commun.* **10**, 2341 (2019).
 139. Inamine, H. *et al.* Spatiotemporally Heterogeneous Population Dynamics of Gut Bacteria Inferred from Fecal Time Series Data. *MBio* **9**, e01453-17 (2018).
 140. Zilionis, R. *et al.* Single-cell barcoding and sequencing using droplet microfluidics. *Nat. Protoc.* **12**, 44–73 (2017).
 141. Yuan, X. *et al.* Single-Cell Microfluidics to Study the Effects of Genome Deletion on Bacterial Growth Behavior. *ACS Synth. Biol.* **6**, 2219–2227 (2017).
 142. Pu, Y., Ke, Y. & Bai, F. Active efflux in dormant bacterial cells – New insights into antibiotic persistence. *Drug Resist. Updat.* **30**, 7–14 (2017).

143. Levin, B. R. & Rozen, D. E. Non-inherited antibiotic resistance. *Nat. Rev. Microbiol.* **4**, 556–562 (2006).
144. Hayes, E. T. *et al.* Oxygen limitation modulates pH regulation of catabolism and hydrogenases, multidrug transporters, and envelope composition in *Escherichia coli* K-12. *BMC Microbiol.* **6**, 89 (2006).
145. Bergholz, T. M. *et al.* Global transcriptional response of *Escherichia coli* O157:H7 to growth transitions in glucose minimal medium. *BMC Microbiol.* **7**, 1–27 (2007).
146. Baev, M. V., Baev, D., Radek, A. J. & Campbell, J. W. Growth of *Escherichia coli* MG1655 on LB medium: Determining metabolic strategy with transcriptional microarrays. *Appl. Microbiol. Biotechnol.* **71**, 323–328 (2006).
147. Losen, M., Frölich, B., Pohl, M. & Büchs, J. Effect of oxygen limitation and medium composition on *Escherichia coli* fermentation in shake-flask cultures. *Biotechnol. Prog.* **20**, 1062–1068 (2004).
148. Nyström, T. Nonculturable bacteria: programmed survival forms or cells at death's door? *BioEssays* **25**, 204–211 (2003).
149. Oliver, J. D. Recent findings on the viable but nonculturable state in pathogenic bacteria. *FEMS Microbiol. Rev.* **34**, 415–425 (2010).
150. Mali, S. *et al.* A Proteomic Signature of Dormancy in the Actinobacterium *Micrococcus luteus*. *J. Bacteriol.* **199**, e00206-17 (2017).
151. Hansen, A. S., Hao, N. & OShea, E. K. High-throughput microfluidics to control and measure signaling dynamics in single yeast cells. *Nat. Protoc.* **10**, 1181–1197 (2015).
152. Jug, F. *et al.* Optimal Joint Segmentation and Tracking of *Escherichia Coli* in the Mother Machine. *Bayesian Graph. Model. Biomed. Imaging* 25–36 (2014). doi:10.1007/978-3-319-12289-2
153. Bednarska, N. G., Schymkowitz, J., Rousseau, F. & Van Eldere, J. Protein aggregation in bacteria: The thin boundary between functionality and toxicity. *Microbiology* **159**, 1795–1806 (2013).
154. Carrió, M. M., Corchero, J. L. & Villaverde, A. Dynamics of in vivo protein aggregation: Building inclusion bodies in recombinant bacteria. *FEMS Microbiol. Lett.* **169**, 9–15 (1998).

155. Konan, K. V. & Yanofsky, C. Regulation of the *Escherichia coli* *tna* operon: Nascent leader peptide control at the *tnaC* stop codon. *J. Bacteriol.* **179**, 1774–1779 (1997).
156. Jaffe, A., Chabbert, Y. A. & Semonin, O. Role of porin proteins OmpF and OmpC in the permeation of β -lactams. *Antimicrob. Agents Chemother.* **22**, 942–948 (1982).
157. Wood, T. K. Combatting bacterial persister cells. *Biotechnol. Bioeng.* n/a-n/a (2015). doi:10.1002/bit.25721
158. Govers, S. K., Mortier, J., Adam, A. & Aertsen, A. *Protein aggregates encode epigenetic memory of stressful encounters in individual Escherichia coli cells.* *PLOS Biology* **16**, (2018).
159. Weids, A. J., Ibstedt, S., Tamás, M. J. & Grant, C. M. Distinct stress conditions result in aggregation of proteins with similar properties. *Sci. Rep.* **6**, 24554 (2016).
160. Mortier, J., Tadesse, W., Govers, S. K. & Aertsen, A. Stress-induced protein aggregates shape population heterogeneity in bacteria. *Current Genetics* **65**, 865–869 (2019).
161. Peters, T. W. *et al.* Tor1 regulates protein solubility in *Saccharomyces cerevisiae*. *Mol. Biol. Cell* **23**, 4679–4688 (2012).
162. Merino, N. *et al.* Protein A-Mediated Multicellular Behavior in *Staphylococcus aureus*. *J. Bacteriol.* **191**, 832 LP – 843 (2009).
163. Stöver, A. G. & Driks, A. Secretion, localization, and antibacterial activity of TasA, a *Bacillus subtilis* spore-associated protein. *J. Bacteriol.* **181**, 1664–1672 (1999).
164. Winkler, J. *et al.* Quantitative and spatio-temporal features of protein aggregation in *Escherichia coli* and consequences on protein quality control and cellular ageing. *EMBO J.* **29**, 910–923 (2010).
165. Stewart, E. J., Madden, R., Paul, G. & Taddei, F. Aging and death in an organism that reproduces by morphologically symmetric division. *PLoS Biol.* **3**, 0295–0300 (2005).
166. Bamford, R. A. *et al.* Investigating the physiology of viable but non-culturable bacteria by microfluidics and time-lapse microscopy. *BMC Biol.* **15**, 1–12 (2017).
167. Holland, S. L., Reader, T., Dyer, P. S. & Avery, S. V. Phenotypic heterogeneity is a selected trait in natural yeast populations subject to

- environmental stress. *Environ. Microbiol.* **16**, 1729–1740 (2014).
168. Germain, E., Castro-roa, D., Zenkin, N. & Gerdes, K. Molecular Mechanism of Bacterial Persistence by HipA. *Mol. Cell* **52**, 248–254 (2013).
169. Starosta, A. L., Lassak, J., Jung, K. & Wilson, D. N. The bacterial translation stress response. *FEMS Microbiol. Rev.* **38**, 1172–1201 (2014).
170. Zaslaver, A. *et al.* A comprehensive library of fluorescent transcriptional reporters for Escherichia coli. *Nat. Methods* **3**, 623–628 (2006).
171. Smith, A. *et al.* The culture environment influences both gene regulation and phenotypic heterogeneity in Escherichia coli. *Front. Microbiol.* **9**, 1739 (2018).
172. Pagliara, S., Chimere, C., Langford, R., Aarts, D. G. A. L. & Keyser, U. F. Parallel sub-micrometre channels with different dimensions for laser scattering detection. *Lab Chip* **11**, 3365–3368 (2011).
173. Smith, A., Metz, J. & Pagliara, S. MMHelper: An automated framework for the analysis of microscopy images acquired with the mother machine. *Sci. Rep.* **9**, 10123 (2019).
174. Pagliara, S., Dettmer, S. L. & Keyser, U. F. Channel-Facilitated Diffusion Boosted by Particle Binding at the Channel Entrance. *Phys. Rev. Lett.* **113**, 48102 (2014).
175. Lapinska, U., Glover, G., Capilla-Lasheras, P., Young, A. & Pagliara, S. Bacterial ageing in the absence of external stressors. *Philos. Trans. B* (2019). doi:10.1098/rstb.2018.0442
176. Ziervogel, Brigitte. Roux, B. The Binding of Antibiotics in OmpF Porin. *Structure* **21**, 76–87 (2013).
177. Miesenböck, G., De Angelis, D. A. & Rothman, J. E. Visualizing secretion and synaptic transmission with pH-sensitive green fluorescent proteins. *Nature* **394**, 192–195 (1998).
178. Rang, C. U., Peng, A. Y., Poon, A. F. & Chao, L. Ageing in Escherichia coli requires damage by an extrinsic agent. *Microbiol. (United Kingdom)* **158**, 1553–1559 (2012).
179. Helaine, S. *et al.* Internalization of Salmonella by Macrophages Induces Formation of Nonreplicating Persisters. *Science (80-.)*. **343**, 204–208 (2014).
180. Zarkan, A. *et al.* Indole Pulse Signalling Regulates the Cytoplasmic pH of

E. coli in a Memory-Like Manner. *Sci. Rep.* **9**, 3868 (2019).